

UC Berkeley

UC Berkeley Electronic Theses and Dissertations

Title

An Improved Chemical Mechanism for Photochemical Air Quality Modeling

Permalink

<https://escholarship.org/uc/item/1r14r44k>

Author

Shearer, Sharon

Publication Date

2013

Peer reviewed|Thesis/dissertation

An Improved Chemical Mechanism for Photochemical Air Quality Modeling

By

Sharon Michelle Shearer

A dissertation submitted in partial satisfaction of the
requirements for the degree of

Doctor of Philosophy

In

Engineering – Civil and Environmental Engineering

in the

Graduate Division

of the

University of California, Berkeley

Committee in charge:

Professor Robert A Harley, Chair

Professor William W Nazaroff

Professor John CH Chiang

Fall 2013

An Improved Chemical Mechanism for Photochemical Air Quality Modeling

© 2013

by Sharon Michelle Shearer

Abstract

An Improved Chemical Mechanism for Photochemical Air Quality Modeling

By

Sharon Michelle Shearer

Doctor of Philosophy in Engineering - Civil and Environmental Engineering

University of California, Berkeley

Professor Robert A Harley, Chair

Tropospheric ozone, an air pollutant and greenhouse gas, is a hazard to both human health and ecosystems. Health-based ozone standards are regularly exceeded in many regions of the world. Controlling ozone formation is a challenge for scientists and policy makers due to the non-linear dependence of ozone on its precursors, namely nitrogen oxides (NO_x) and volatile organic compounds (VOC). Photochemical air quality modeling is one of the primary tools used to assess the effectiveness of strategies intended to control ozone formation. Air quality model predictions are sensitive to meteorological and emission inputs, as well as the description of atmospheric chemistry embodied in the chemical mechanism. Typical chemical mechanisms describe the reactants, reaction rates, and product yields for each of hundreds of individual chemical reactions that take place in the atmosphere.

The Statewide Air Pollution Research Center (SAPRC) mechanism developed by Dr. William Carter at UC Riverside is a chemically accurate, but also computationally intensive, example of a chemical mechanism used to describe the dynamics of photochemically-formed air pollutants. This mechanism is widely used for air quality research and planning at urban and regional scales. The first step in my research was to assess the effects of using a new version (SAPRC07) of this mechanism in place of an outdated earlier version (SAPRC99). This assessment was done using an Eulerian photochemical air quality model known as the Community Multiscale Air Quality model or CMAQ, applied to the prediction of air quality in Central California under polluted summertime conditions. Domain-wide reductions in predicted ozone were found using the newer mechanism as compared with SAPRC99, with larger ozone reductions collocated spatially and temporally with higher ozone concentrations. Underprediction of peak ozone was already evident using the older (SAPRC99) mechanism, and this bias increased with the new mechanism.

In order to understand the reasons for the changes in predicted ozone, first-order sensitivity coefficients using both mechanisms were calculated with respect to important rate coefficients. Among the more important revisions to the mechanism is a ~20% increase in the rate of the chain-terminating reaction $\text{OH} \cdot + \text{NO}_2 \rightarrow \text{HNO}_3$. This revision in SAPRC07 was a dominant contributor to overall decreases (relative to SAPRC99) of up to 25 ppb in peak predicted ozone concentrations in the San Joaquin Valley. Other significant revisions include the rate coefficient for the reaction $\text{O}_3 + \text{NO} \rightarrow \text{NO}_2 + \text{O}_2$ and the photolysis rate for the reaction $\text{NO}_2 + h\nu \rightarrow \text{NO} +$

O3P, but these changes were found to exert offsetting effects with ozone responses of similar magnitude acting in opposite directions.

A reassessment of ozone sensitivity to changes in precursor emissions shows that the updated mechanism has a response to VOC emissions that is stronger than that of SAPRC99, indicating more ozone reduction potential associated with VOC emission controls. With the exception of the Bay Area, the newer mechanism drives the model predictions more toward a NO_x disbenefit regime, where moderate NO_x emission reductions (by 20%) lead to local increases in ozone in the near field. An unexpected finding was that use of a condensed and computationally efficient version of SAPRC07 known as CS07A contributed substantially to the decreases in predicted ozone levels mentioned above. For this reason, a less condensed mechanism (SAPRC07A) is used in further research presented in this dissertation, with a resulting increase in computational demand necessary for model simulations. Additionally a recent study (Mollner et al., 2010) recommends a lower value for the reaction rate coefficient for OH· + NO₂ → HNO₃ that I have implemented as a revision to SAPRC07A.

The many hundreds of individual anthropogenic VOC emitted into the atmosphere are primarily represented in the SAPRC mechanism using lumped species groups. Species are separated into groups based on their reaction mechanism and rate coefficient, and surrogate species are used to represent the reactions of all VOC assigned to each lumped group. The existing surrogate species mixtures defining the chemistry of the lumped groups were developed by Carter based on speciated measurements of ambient hydrocarbon concentrations, but these data were collected in the mid-1980s. Reformulation of fuels and consumer products, and control measures that have altered the total amounts of VOC emitted by various source categories, have substantially changed the concentrations and relative abundances of many individual VOC present in the atmosphere. The next step in my research was to develop updated lumped species definitions using emission inventories and source category-related VOC speciation profiles. The resulting lumped species definitions created in this dissertation are up-to-date and simpler, but still represent 95% of the total moles of species assigned to each lumped group. Most of the inventory-based lumped VOC definitions now align better with ambient VOC measurements compared to the existing lumped species definitions in SAPRC99 and SAPRC07. The updated definitions result in lower rate coefficients for most lumped VOC + OH· reactions, that reflect the effects of emission control measures that have required reformulation to reduce the reactivity of VOC mixtures used in fuels and consumer products. In the air quality model, the new surrogate species definitions result in slightly lower peak ozone concentrations, as much as a 1.8 ppb reduction in hourly maximum ozone concentration in some cases.

Consistent with current practice in other mechanisms, the SAPRC mechanism describes the atmospheric oxidation of VOC using temperature-independent parameters that specify branching in peroxy radical + NO reactions between NO to NO₂ conversion and organic nitrate-forming channels. Additional temperature-independent parameters are used to describe the fate of alkoxy radicals: reaction with O₂, isomerization, and decomposition. In reality, the branching ratios for these pathways depend on temperature. The final major element of my research, needed to reproduce more accurately the spatial, diurnal, and day-to-day differences in air quality that are driven in part by differences in temperature, is development of a new version of the mechanism that captures the missing temperature dependencies of alkoxy and peroxy radical reactions.

Organic nitrate formation, which decreases with temperature, competes with NO to NO₂ conversion and hence inhibits production of ozone locally. Alkoxy radical decomposition competes with isomerization, resulting in increased aldehyde yields and decreased ketone yields with increasing temperature. This drives the resulting VOC oxidation products toward a more reactive mix at higher temperatures. The VOC oxidation product yields for the existing SAPRC mechanism are all specified for T = 300 K, and do not vary with temperature. Changes in predicted organic nitrate, aldehyde, and ketone concentrations follow as expected with inclusion of these missing temperature dependencies in the mechanism, as do subsequent changes in predicted ozone. Variations in predicted ozone linked to temperature differences are further enhanced with the additional inclusion of temperature-dependent evaporative VOC emissions. However, predicted ozone is not very sensitive to these mechanism changes, the largest changes were in the maximum hourly ozone (up to $\sim\pm 1.5$ pbb).

Temperatures in California are predicted to rise by 1 to 4°C throughout the state of California by 2050 relative to year 2000. In studying the effects of climate change on air quality, it is important to describe correctly the temperature dependence of relevant atmospheric chemistry. The effect of using the temperature-dependent VOC reaction mechanism developed as part of this research is assessed for a future climate change scenario. Compared to previous assessments, use of the revised chemical mechanism indicates a slightly increased potential penalty from climate change with respect to ozone air quality in central California.

Acknowledgements

I owe a sincere debt of gratitude to the many colleagues, mentors, friends, and family who have helped me along this path. First and foremost, I'd like to thank the faculty at UC Berkeley for the guidance and support throughout my graduate studies. My advisor, Rob Harley, has provided invaluable advice in helping direct my research toward providing meaningful scientific contributions. He has offered thoughtful direction, insightful reviews, continued encouragement, and patience throughout my research. I am also grateful for the contributions and guidance of Bill Nazaroff, who continued to provide a fresh perspective on my work, with both broad and detailed inspection of my research and findings at various points along the way. I also thank Tina Chow, Jim Hunt, and John Chiang, who have served as members of my exam and dissertation committees.

Many colleagues have helped with my education and the research presented in this dissertation. I would like to thank Ling Jin and Nancy Brown at Lawrence Berkeley National Lab for their assistance and research collaboration. I owe a big thanks to Shaheen Tonse who offered early support in my understanding of 3-D air quality modeling. Much of my research builds on the work of others, and I particularly would like to thank Bill Carter of UC Riverside for the helpful discussions regarding implementation of the SAPRC07 mechanism, Alison Steiner of University of Michigan for assistance with climate change perturbations, and Golam Sarwar of the USEPA for assistance in setting up a CMAQ box model for mechanism testing.

I am grateful to the National Science Foundation and the Environmental Protection Agency for financial support during my graduate studies.

I was greatly inspired by the instruction and mentorship of my professors at the University of Texas at Austin - Richard Corsi, Lynn Katz, Kerry Kinney, Kara Kockelman, and Desmond Lawler. I am so appreciative of the wonderful coursework and all of the opportunities I had as a student at UT. I also learned a great deal (while having lots of fun in the lab) from Jennifer Woertz at UT and Elmira Kujundzic at CU Boulder.

It was harder than I ever expected to move away from my loving family in Texas to Berkeley, California. I am thankful for my parents, Bill and Dianne Shearer, who instilled a love of learning and appreciation of nature, and Debbie and Keith Jones, who never let me take myself too seriously and always provided encouragement. My grandmother and late grandfather, Ann and Darrell Hazel, have always believed in my ability to accomplish anything. I acquired a great mother-in-law while at Berkeley, Susan Hansen, who helped out in any way she could along the way.

I feel very lucky to have made lifelong friendships in the Airheads group during my time at Berkeley - George Ban-Weiss, Seema Bhangar, Bev Coleman, Ling Jin, Dev Millstein, Nasim Mullen, and Arman Shehabi. I have so many great and funny memories of our times together,

and hope we have many more! Seema, I wish we could share an office forever.

Ali Bond, a fellow graduate student, and Megan Daniels, a former graduate student, offered me all kinds of support through my last year of dissertation writing that I am truly grateful for. A big thanks to all of my other dear friends and family for believing in me and putting up with me - Erica, Heidi, Jenny, Jeremy, Luke, Matt, Patrick, Lauren, Rohit, Greg, Ted, Issabella, Ben, Inga, Kate, Colin, Jake, Brook, Carla, Chris, Tanner, Nikki, Edgardo, Deanna, Tim, Ashley, Lisa, Matt, Hannah, Jared, Cristie, Shaun, Taylor, Xander, Shyanne, Aunt Kel and Greg, Aunt Tina, Great Aunt Mare, and Grandma Myrna. Truly the greatest thing to come out of my time at UC Berkeley was meeting my husband, Aren Hansen. I am so lucky to have his love and support.

Table of Contents

Acknowledgements.....	i
List of Figures.....	v
List of Tables.....	vi
Chapter 1: Introduction.....	1
1.1 Motivation.....	1
1.2 Air quality modeling.....	4
1.3 Atmospheric chemical mechanisms for air quality models.....	4
1.4 Research objectives.....	8
1.5 Dissertation overview.....	8
Chapter 2: Implementation and assessment of an updated chemical mechanism in an air quality model.....	10
2.1 Introduction.....	10
2.1.1 SAPRC07 chemical mechanism.....	10
2.1.2 Comparison of SAPRC07 and other mechanisms in air quality modeling.....	13
2.1.3 Research objective.....	14
2.2 Methods.....	15
2.3 Results and discussion.....	18
2.3.1 Ozone.....	18
2.3.2 Individual reaction rate coefficient updates and mechanism condensation.....	24
2.3.3 Emission sensitivity.....	27
2.3.4 Responses to climate change-sensitive parameters.....	29
2.4 Conclusions.....	35
Chapter 3: Revised VOC lumping strategy.....	37
3.1 Introduction.....	37
3.1.1 Motivation.....	37
3.1.2 VOC reactivity.....	37
3.2 Methods.....	38
3.2.1 Revised chemical mechanism overview.....	38
3.2.2 Air quality modeling.....	41
3.2.3 VOC emissions.....	43
3.2.4 New model species.....	56
3.2.5 Lumped species definitions.....	57
3.2.6 Air quality model simulations.....	61
3.2.7 OH-reactivity.....	61
3.3 Results.....	62
3.3.1 Revised emissions and rate parameters.....	62

3.3.2	Ozone model results for Episode 1 (E1)	66
3.3.3	Episode 2 (E2) results	70
3.3.4	VOC concentration and OH-reactivity analysis	71
3.4	Discussion	73
Chapter 4:	Improved representation of the temperature dependence of VOC oxidation reactions for air quality modeling	75
4.1	Introduction	75
4.1.1	Motivation	75
4.1.2	Background	78
4.2	Methods	82
4.2.1	Temperature-dependent VOC oxidation products	82
4.2.2	SAPRC mechanism	90
4.2.3	Air quality model	93
4.2.4	Temperature-dependent emissions	94
4.2.5	Air quality model simulations	95
4.2.6	Ambient measurements: NO ₂ , NO _x , and ozone	96
4.3	Results	97
4.3.1	Chemical mechanism	97
4.3.2	Organic nitrate	104
4.3.3	Secondary VOC	113
4.3.4	Ozone air quality	119
4.3.5	Ozone air quality in 2050	122
4.4	Discussion	126
Chapter 5:	Conclusions	128
5.1	Summary of research findings	128
5.2	Recommendation for future research	130
References		132
Appendix		147

List of Figures

Figure 1-1. Schematic of the reactions involved in ozone production	5
Figure 1-2. VOC degradation schematic	6
Figure 2-1. Central California AQM domain	16
Figure 2-2. Temperature and predicted ozone using SAPRC99. Change in predicted ground-level ozone when CS07A is used in place of SAPRC99	19
Figure 2-3A. Diurnal variations in observed and predicted ozone concentrations for E1	20
Figure 2-3B. Diurnal variations in observed and predicted ozone concentrations for E2	21
Figure 2-4. Chemical mechanism and reaction rate coefficient AQM sensitivity	26
Figure 2-5A. VOC and NO _x sensitivity using SAPRC99 vs CS07A, Episode 1	28
Figure 2-5B. VOC and NO _x sensitivity using SAPRC99 vs CS07A, Episode 2	29
Figure 2-6. Effects of individual climate-change related perturbations on ozone air quality	33
Figure 2-7. Ozone response to the combined climate change perturbation (temperature, humidity, and biogenic VOC) using SAPRC99 and CS07A mechanisms	35
Figure 3-1. Map of air quality modeling domain	42
Figure 3-2. VOC emission maps (mol/s)	45
Figure 3-3. Lumped VOC emission time series (mol/s)	50
Figure 3-4. Temperature dependent VOC + OH [•] reaction rate coefficients	60
Figure 3-5. VOC + OH [•] reaction rate coefficients (Alkanes)	64
Figure 3-6. VOC + OH [•] reaction rate coefficients (Olefins and Aromatics)	65
Figure 3-7. Temperature, default ozone concentrations, and the ozone response for Revised mechanism (E1)	68
Figure 3-8. Ozone response due to step-wise changes made to the SAPRC07 mechanism	69
Figure 3-9. Temperature, default ozone concentrations, and the ozone response for Revised mechanism (E2)	71
Figure 3-10. Percent contribution to R _{OH, total} for the Default and Revised mechanisms	73
Figure 4-1: Schematic for VOC degradation in the atmosphere	77
Figure 4-2. n-Butane degradation schematic	80
Figure 4-3. Central California model domain outlined with red box	96
Figure 4-4. Nitrate yield for VOC of different carbon number	99
Figure 4-5. Atmospheric reactions for 2-butoxy radical in the presence of NO	100
Figure 4-6. Dependence of reaction rate coefficients for 2-butoxy radical on temperature.	101
Figure 4-7. Atmospheric reactions for 1-butoxy radical in the presence of NO	102

Figure 4-8. Temperature-dependent reaction rate coefficients for 1-butoxy radical	103
Figure 4-9. Temperature, RONO ₂ concentration, and the change in RONO ₂ concentration with use of the SCT mechanism	105
Figure 4-10. Pollutant concentrations (ppb) at Granite Bay for Julian day 209	108
Figure 4-11 Pollutant concentrations (ppb) at Granite Bay	110
Figure 4-12 Pollutant concentrations (ppb) at Blodgett Forest.....	111
Figure 4-13. Nitrate formation rates attributed to different reactions (ppb/day)	112
Figure 4-14 Change in aldehyde concentration with use of the SCT mechanism	114
Figure 4-15 Change in aldehyde concentration due to use of temperature-dependent evaporative emissions.....	115
Figure 4-16. Change in ketone concentration with use of the SCT mechanism	117
Figure 4-17. Change in ketone concentration due to use of temperature-dependent evaporative emissions.....	118
Figure 4-18. Temperature, O ₃ concentration, and the change in O ₃ concentration with use of the SCT mechanism.....	120
Figure 4-19. Change in O ₃ concentration due to use of temperature-dependent evaporative emissions.....	121
Figure 4-20. Temperature and water vapor perturbations for the year 2050, JD209 at 4 pm.....	123
Figure 4-21. Biogenic and anthropogenic emission perturbations for the year 2050 at 4 pm.....	125
Figure 4-22. Change in O ₃ from 2000 to 2050	126
Figure A-1. Map of central California counties.....	147

List of Tables

Table 2-1. SAPRC mechanism comparison.....	10
Table 2-2. SAPRC VOC representation	12
Table 2-3. Estimated ozone response.....	13
Table 2-4. AQM boundary conditions	18
Table 2-5. Ozone concentrations and responses at four sites	23
Table 2-6. AMQ ozone performance statistics	24
Table 3-1. Compounds and weighting factors used to represent ALK3.....	40
Table 3-2. Descriptions of SAPRC07A VOC categories	44
Table 3-3. Compounds and weighting factors used to derive parameters for lumped species.....	47

Table 3-4. Total organic gas (TOG) and reactive organic gas (ROG) emissions by emission category.....	51
Table 3-5. Gasoline-related VOC emission speciation (ALK3 and ALK4).....	53
Table 3-6. Example VOC emission speciation for two categories.....	55
Table 3-7. Reactions and rate parameters for new species.....	57
Table 3-8. Weighting factors used to derive parameters for SAPR07A lumped species – Comparison with measurements.....	58
Table 3-9. Redistribution of emissions from Default to Revised.....	63
Table 3-10. Reactions, rate parameters, and percent increase in reaction rate coefficient for updated lumped species.....	66
Table 3-11. Comparison of Default and Revised OH-reactivity statistics.....	72
Table 4-1. Temperature-dependent structure activity relationship.....	84
Table 4-2. Substituent factor parameters for VOC.....	85
Table 4-3. Mechanism and SAR parameters for OH [•] addition to alkenes.....	86
Table 4-4. Temperature-dependent structure activity relationship.....	88
Table 4-5. Parameter used for estimating alkoxy radical decomposition rate.....	90
Table 4-6. Reactions in which temperature-dependent products are included.....	91
Table 4-7. Species added to SAPRC07 to account for organic nitrate.....	93
Table 4-8. Stoichiometric coefficients for n-butane + OH [•] reaction.....	98
Table 4-9. Difference in stoichiometric coefficients due to temperature increase.....	104
Table 4-10. Selected nitrate descriptors for six central California sites and two days.....	107
Table 4-11. Emission scaling factors by county for 2050 anthropogenic emissions relative to year 2000.....	124
Table A-1. County level VOC emissions, tons organic gas (TOG) from year 2000 CARB emission estimates.....	148
Table A-2. VOC weight percent in gasoline, separated by SAPRC07 species.....	150
Table A-3. Redistribution of area emissions from SAPRC07 to SCCOS, motor vehicle redistribution has the same multipliers for each county.....	158

Chapter 1: Introduction

1.1 Motivation

Anthropogenic air pollution has been a part of the human experience since the advent of fire. There is evidence of urban air pollution events, resulting from both wood and coal burning, as early as the medieval times (Brimblecombe, 1987; Ausset et al., 1998). The most extreme and deadly air pollution events in more recent times, the Meuse Valley of Belgium Fog in 1930 (Nemery et al., 2001) and Fog of London of 1952 (Wilkins, 1954) were the result stagnant winter meteorology and dense sources of emissions, primarily from coal combustion (Bell and Davis, 2001). However, the 1940s brought a new type of pollution, causing eye and throat irritation and low visibility, to warm and sunny Los Angeles, California (Brienes, 1976). Termed “smog”, these air pollution episodes also began to cause visible crop damage and rapid rubber deterioration. Using these attributes, Haagen-Smit determined that anthropogenic ozone was a major constituent of smog that resulted from emissions of nitrogen oxides (NO_x) and volatile organic compounds (VOC) in the presence of sunlight (Haagen-Smit, 1952; Haagen-Smit and Fox, 1954).

In the decades since Haagen-Smit’s discovery, the effects of ozone on health and the environment have been a major focus of air quality research. Evidence of ozone as a respiratory irritant was documented in a laboratory setting as early as 1851 (Shönbein, 1851). The identification of ozone as a major component of photochemical smog, and the recognition of photochemical smog in many other areas in the world, has led to further developments in health effects research. Through ozone exposure in controlled laboratory experiments, respiratory effects, including airway and pulmonary inflammation and lung function decrements, have been documented (Aris et al., 1993; Devlin et al., 2012). Blomberg et al. (1999) find that respiratory inflammation presents with ozone exposure even in cases where lung function decrements do not occur. Epidemiological studies have provided additional evidence of ozone health effects. The first study performed with a focus on photochemical smog found that oxidant level was correlated with a decrease in athletic performance in high-school cross-country races (Wayne et al., 1967). Other acute effects of ozone exposure determined by epidemiology are summarized in Thurston and Ito (1999), and include decreases in lung function, exacerbation of respiratory disease such as asthma, increase in hospital admission, and excess mortality. More recently, Bell et al. (2006) found that any anthropogenic increase in ozone contributes to risk of premature mortality, indicating that even regions with ozone concentrations “below air quality regulatory standards should not be misinterpreted as safe for human health.” Recent research correlates ozone exposure to healthy human subjects with an increase in their markers of vascular inflammation, which gives insight into the possible mechanism through which ozone exposure causes excess mortality (Devlin et al., 2012). These studies suggest that efforts to reduce ozone to levels below regulatory standards, based on health effects determined in direct exposure studies, would be beneficial for human health.

Crop damage, an ecological symptom of smog used by Haagen-Smit to identify ozone as its major component, has also evolved into a field of study, motivated by food security issues and economic loss. Ozone is taken up by vegetation through gas-exchange pores (stomata) and reacts

with plant cells causing oxidative stress. This can lead to plant damage and decreased crop yields through a number of potential mechanisms, including decreased photosynthetic carbon assimilation (Reich and Amundson, 1985; Ainsworth et al., 2012). Estimates for the year 2000 show that ozone caused crop yield losses of wheat ranging between 7% and 12%, and that, globally, total reduction in crop yields (wheat, soybean, corn, and rice) resulted in economic losses estimated between \$14 and \$26 billion dollars (Van Dingenen et al., 2009). Crop yield estimates for the year 2030 show that losses are expected to worsen throughout much of the developing world (Van Dingenen et al., 2009.)

In addition to reducing crop yields, elevated ozone decreases photosynthesis for many tree species (Wittig et al., 2007). Forests are important sinks for atmospheric carbon dioxide (CO₂). Experimental evidence suggests that any increase in ozone causes a reduction in biomass accumulation, and thus a decrease in carbon fixing ability (Wittig et al., 2009). At 40 and 97 parts per billion (ppb) ozone, as compared to 17 ppb ozone, biomass accumulation is reduced by 7% and 17% respectively (Wittig et al., 2009) The earliest ozone measurements, from late 19th century in Europe, show yearly average ozone around 10 ppb with little variation throughout the year (Volz and Kley, 1988; Anfossi et al., 1991). Vingarzan (2004) shows that background ozone has likely doubled since pre-industrial times, and using IPCC emission scenarios predict that background concentrations could reach 42 to 84 ppb by 2100 dependent on emission scenario. However, ozone concentrations in many forested areas are already additionally elevated above background concentrations due to upwind emissions. Four of 12 US National Parks had years in the late 1990s with average ozone concentrations over 40 ppb (Vingarzan, 2004).

Sitch et al. (2007) define the CO₂ that remains in the atmosphere due to ozone-suppressed land-carbon sinks “indirect radiative forcing” due to ozone. The “indirect radiative forcing” is estimated to be equivalent in magnitude to the direct radiative forcing caused by tropospheric ozone increase relative to the pre-industrial atmosphere. Tropospheric ozone is the third strongest greenhouse gas (behind CO₂ and methane), and accounts for 10% of contribution to increased radiative forcing from a pre-industrial atmosphere (IPCC, 2007). The increase in radiative forcing is the driver of global warming (IPCC, 2007). Direct and indirect ozone radiative forcings are predicted to at least double, and possibly triple, by the year 2100 (Sitch et al., 2007), which emphasizes the role ozone control should play in climate change mitigation.

Early air pollution legislation in the 1950s and 60s in the United States involved federal funding of air pollution research, but left responsibility to create control measures in the hands of state and local governments (Wark et al., 1998). However, by the late 1960s, smog episodes had spread beyond Los Angeles, with episodes reported in San Francisco, Miami, Chicago, New York, Philadelphia, and Houston (Dewey, 2000). The lack of progress in reducing ozone and other air pollutants by local agencies, led to the Clean Air Act Amendments of 1970 which included the setting of National Ambient Air Quality Standards (NAAQS), the first federal health-based air quality standards (Portney and Stavins, 2000). The current standard for ozone is 75 ppb over an 8-hour averaging time. A location is considered out of compliance when the three-year average of the annual fourth-highest daily 8-hour concentration exceeds 75 ppb (USEPA, 2012). A previous 120 ppb 1-hour standard is in place as an “anti-backsliding measure” in some areas, “not to be exceeded more than once per year” (USEPA, 2012). While

ozone reductions below these standards could be beneficial for human health, food-security, and global warming mitigation, many areas in the US are still out of compliance with the NAAQS.

The American Lung Association (2012) reports that from 2009 to 2012 at least 38% of people (119.3 million) in the US live in counties where ozone levels exceed the NAAQS; the number may be higher because not all counties are monitored. Arguably, California still has the worst ozone problem in the US, 16 of the 25 counties with the worst ozone pollution are in California (American Lung Association, 2012), covering most of southern California and the Central Valley. California is the most populous state, 2005 data show almost half of the 36 million inhabitants reside in southern California, and 30% reside in the Central Valley, where population is also rapidly increasing (Kotkin and Frey, 2007). Ozone induced crop damage is also a major concern for the Central Valley, the country's most productive agricultural region (USDA-NASS, 2009).

Controlling ozone has proven to be challenging for California and many other regions of the world, both urban and rural. The basics of ozone formation are well understood (Atkinson, 2000), but predicting and controlling ozone formation is a challenge due to its complex non-linear dependence on its precursors, NO_x and VOC. Ozone- NO_x -VOC sensitivity studies show that under certain conditions reducing NO_x can increase ozone formation, and for a different set of conditions reducing VOC could have no effect on ozone (Sillman, 1999). For instance, while both NO_x and VOC have decreased in most areas by more than 40% from 1980 to 2008, a study investigating ozone concentration at 27 sites across the US found that almost 30% of sites did not see any significant reduction in 8-hour ozone NAAQS measurements (LeFohn et al., 2010). This is likely attributable to ozone- NO_x -VOC sensitivity; relevant atmospheric chemistry is further described in section 1.3.

Additionally, meteorological variables have a large role in the formation, transport, and accumulation of ozone. The most extreme ozone events are correlated with meteorological stagnation events, characterized by high-pressure systems that result in low winds (Logan, 1989; Jacob et al., 1993). Ozone has also been shown to have a strong correlation with elevated temperatures (Cardelino and Chameides, 1990; Sillman and Samson, 1995; Camalier et al., 2007; Bloomer et al., 2009). A smog chamber allows study of the temperature variable alone, and the rate of ozone formation was found to increase with increasing temperature (Carter et al., 1979). A box modeling study allows inclusion of other meteorological variables and attributes ozone increases mainly to increases in temperature-dependent photochemical rate constants (Sillman and Samson, 1995). However, water vapor, biogenic emissions, and anthropogenic emissions were also determined to play a role in increasing ozone (Sillman and Samson, 1995; Steiner et al., 2010). Ozone dependence on these meteorological variables is particularly interesting in the context of determining pollution responses to climate change.

As a requirement of the Clean Air Act amendments of 1990, US states with areas that do not comply with the ozone NAAQS are required to develop a State Implementation Plan (SIP) to show that standards will be met by a specific deadline, given suitable reductions in precursor emissions (USEPA, 2013). The SIP must include 3-D photochemical air quality modeling results to ensure that relevant atmospheric chemistry and meteorological effects on ozone have been

taken into account in demonstrating future attainment of the ozone NAAQS (Georgopoulos, 1995).

1.2 Air quality modeling

Air quality modeling is an important tool for both regulatory purposes and for advancing scientific understanding of the atmosphere. Eulerian photochemical air quality models (AQM) determine pollutant concentrations by solving numerically the atmospheric diffusion equation for a coupled system of chemical species ($i=1, 2, 3, \dots, N$):

$$\frac{\partial C_i}{\partial t} = -\nabla \cdot (\mathbf{u}C_i) + \nabla \cdot (\mathbf{K} \cdot \nabla C_i) + R_i + E_i \quad (\text{E1.1})$$

where C_i is species concentration, \mathbf{u} is the wind velocity vector, \mathbf{K} is the eddy diffusivity tensor, R is the net rate of chemical production, and E is the emission rate. Once initial and boundary conditions have been specified (including dry deposition for the ground-level cells in the model), the resulting system of equations can be solved numerically (McRae et al., 1982).

The research in this dissertation uses the Community Multiscale Air Quality model (CMAQ; Byun and Schere, 2006). CMAQ requires input data that include emission and meteorological fields. An off-line meteorological model is used separately to provide wind vectors, eddy diffusivity, temperature, water vapor content, and other relevant meteorological variables by hour of the day, resolved to a 3-D grid system superimposed on the region of interest. Russell and Dennis (2000) found strong evidence in a major literature review that uncertainties in the emission and meteorological input fields are the major source of uncertainty in predicted ozone.

Ozone predictions are also known to be sensitive to the AQM initial conditions, boundary conditions, chemical reactions, and reaction rates (Russell and Dennis, 2000; Hanna et al., 2001). Rates of formation and destruction of relevant atmospheric species are calculated during AQM simulations using an atmospheric chemical mechanism. The focus of research presented in this dissertation centers around the chemical mechanism.

1.3 Atmospheric chemical mechanisms for air quality models

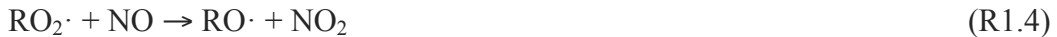
Atmospheric chemistry is described in air quality models using a chemical mechanism, which mathematically describes atmospheric reaction rates as a function of temperature, light intensity, and reactant species concentrations. Many different chemical mechanism choices are available, but the basic ozone formation reactions are well understood and represented using the same chemical reactions across mechanisms. Ozone formation is initiated by photolysis of nitrogen dioxide (NO_2), which separates the molecule into nitrogen oxide (NO) and a free oxygen (O) atom. An N_2 or O_2 molecule (where $\text{N}_2 + \text{O}_2 = \text{M}$) is needed to stabilize a collision between O and O_2 to result in ozone (O_3) formation. O_3 is subsequently destroyed by reaction with NO, which regenerates NO_2 . This set of reactions (R1.1-1.3) is termed the primary photolytic cycle:





NO_x emissions in an otherwise clean atmosphere will not result in the elevated levels of ozone often recorded, but the addition of volatile organic compounds (VOC) emissions lead to a set of oxidation reactions that can increase ozone accumulation, by converting NO to NO₂ without consuming ozone molecules in the process.

Figure 1-1 shows the cycle created by the primary photolytic reactions on the left, and the schematic on the right shows the mechanism by which ozone accumulates. VOC oxidation leads to formation of peroxy radicals (RO₂·) and the hydroperoxy radical (HO₂·) that cause NO to NO₂ conversion without O₃ loss:



In general, high VOC/NO_x ratios result in NO_x-limited conditions. In these conditions, ozone formation is controlled by the amount of NO that can participate in the RO₂· + NO reactions. Low VOC/NO_x ratios generally indicate a VOC sensitive regime. The abundance of NO_x leads to an increase in the rate of nitric acid (HNO₃) formation, reaction (R1.5), as well as local ozone suppression by titration — reaction (R1.3). Therefore, a decrease in NO_x in these conditions will slow reactions (R1.3) and (R1.5), which can lead to increased ozone.

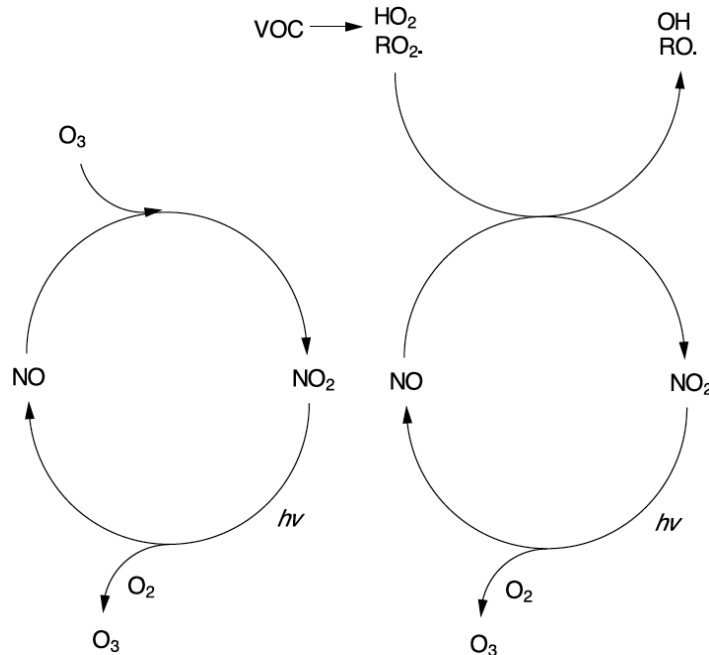


Figure 1-1. Schematic of the reactions involved in ozone production

Ozone production (left and right cycles), accumulation (right), and destruction (left); figure adapted from Atkinson (2000).

Thousands of VOC species, from both anthropogenic and biogenic sources, are emitted to the atmosphere. The sheer number of VOC, as well as the variety and complexity of their oxidation reactions, pose a major challenge for regional air quality modeling. Figure 1-2 shows the VOC oxidation schematic. The figure shows that OH[•] oxidation (O₃, NO₃, and photolysis reactions are also important for some VOC) forms an alkyl or substituted alkyl radical (R[•]). R[•] reacts rapidly with O₂ to form a peroxy radical (RO₂[•]). Reactions on the left side of the RO₂[•] cycle: RO₂[•] reaction with HO₂ and RO₂[•] self- or cross-reactions may become significant for low-NO_x conditions. Reaction with NO₂ leads to a peroxyxynitrate (ROONO₂[•]), which will thermally decompose at lower-tropospheric temperatures (Atkinson, 2000), and thus most are not included in chemical mechanisms. The right side of the cycle shows the pathway that allows reaction of RO₂[•] with NO. This reaction leads to formation of an organic nitrate (RONO₂; alkyl or substituted alkyl nitrate) or an alkoxy radical (RO[•]) and NO₂. RONO₂ formation competes with the NO to NO₂ conversion that allows ozone accumulation described in Figure 1-1. The alkoxy radical, RO[•], may react with oxygen, isomerize, or decompose, leading to different products that can re-enter the VOC oxidation cycle.

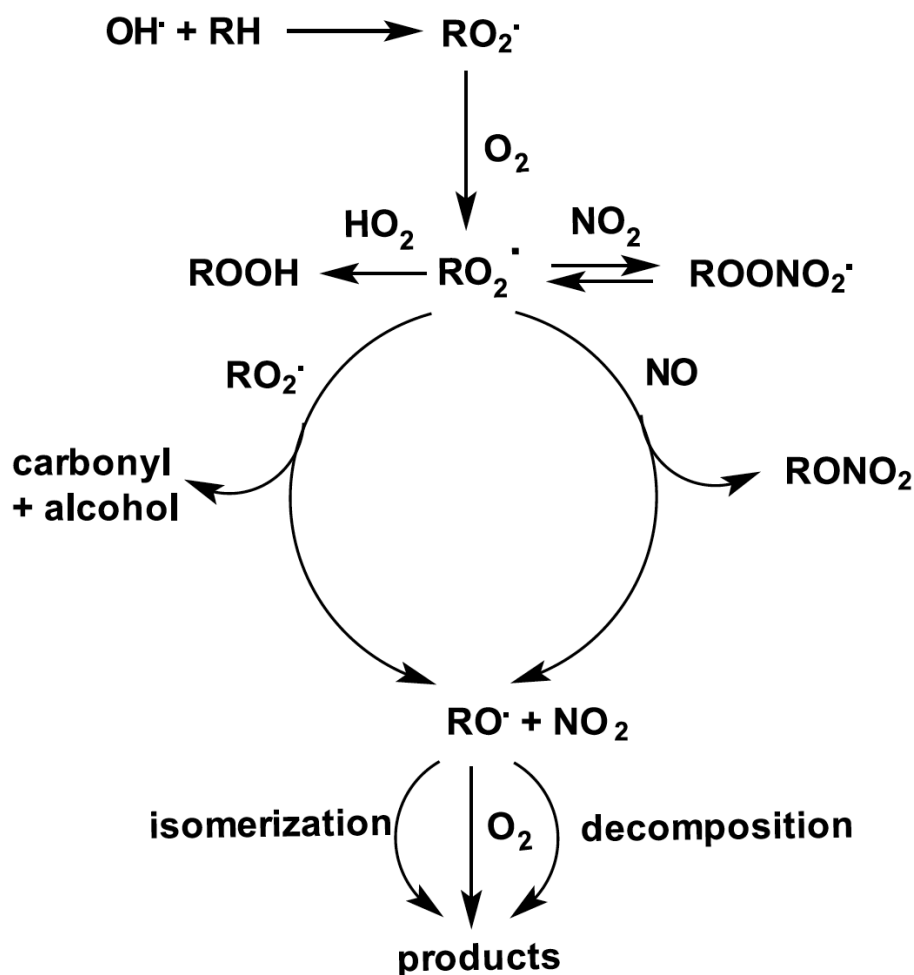


Figure 1-2. VOC degradation schematic
Adapted from Atkinson (2000).

Treatment of VOC and their oxidation reactions is the main difference among existing atmospheric chemical mechanisms. There are chemical mechanisms that attempt to describe each VOC and almost every step in VOC oxidation such as the NCAR Master Mechanism (Madronich and Calvert, 1990) and the Master Chemical Mechanism (MCM; Saunders et al., 2003). For example, the Master Chemical Mechanism includes explicit reactions for 125 primary VOC and their many associated oxidation products, resulting in a mechanism with 12,737 reactions. The chemical mechanism is generally the most computationally intensive part of an air quality model, and the very detailed master mechanisms are not a practical choice for most 3-dimensional modeling studies. These detailed mechanisms are mainly used for box and Lagrangian model studies where the number of computational cells is small. Due to the innumerable possible combinations of $\text{RO}_2 + \text{RO}_2$ reactions involving different parent hydrocarbons (RH), even the MCM simplifies the representation of the reactions of the product species (Saunders et al, 2003). More practical mechanisms intended for use in regional and global atmospheric chemistry and transport models are simplified further, as described below.

Two methods are commonly used to condense mechanisms for use in regional AQMs. The first is the “lumped structure” approach, where the chemical bonds of the VOCs are lumped by bond type and reactions are developed for each type. For example, most single-bonded carbon atoms are lumped into one group independent of the class of VOC they are in. This approach is used for most species in the Carbon Bond Mechanism (Yarwood et al., 2005). The other method is the “lumped molecule” approach in which representation of VOC oxidation in the atmosphere is condensed in two ways. First, the set of reactions for each VOC is reduced to one reaction by removing the intermediate radical chemistry. Then, the VOC that behave similarly in the atmosphere are lumped together. The reactions for the lumped molecules are described by a surrogate species, which is a specific compound or a hypothetical compound developed to represent the species in the lumped group of VOCs. This approach is used in the RACM chemical mechanism (Stockwell et al., 1997; Goliff et al., 2013) and in the versions of SAPRC (Carter, 2010a,b) appropriate for airshed modeling. As compared to the Carbon Bond Mechanism, the lumped molecule approach results in a more detailed chemical mechanism with a larger number of species and reactions, but is better suited to applications where chemical accuracy is important (Carter, 2010a).

Many AQM studies include investigations involving the associated chemical mechanism. Major updates of the SAPRC mechanism have occurred twice in the roughly 20 years since its original development, and other mechanisms are updated on a similar time scale. Air quality model performance reassessment is generally studied by comparing model results with the updated and prior version of a chemical mechanism (Lucken et al., 2007; Sarwar et al., 2008; Cai et al., 2011; Li et al., 2012). One evaluation of the latest SAPRC mechanism has been performed (Cai et al., 2011), but multiple versions of the mechanism with different levels of VOC condensation were made available (Carter, 2010b). Similarly designed studies allow comparison of AQM performance with the use of different chemical mechanisms, and have been the focus of many studies (Jimenez et al., 2003; Luecken et al., 2008; Faraji et al., 2008; Chen et al., 2010; Sarwar et al., 2013).

Mechanism evaluation and development outside of those included in the major updates is less common, but is increasing in practice. For example, the prevalence of isoprene emissions and the

potential for increased emissions under climate change conditions, has led to many studies focused on the representation of isoprene chemistry in the AQM (Horowitz et al., 2007; Paulot et al., 2009; Stavrou et al., 2010; Peeters and Müller, 2010; Crouse et al., 2011). In one instance, the isoprene mechanism was tuned such that the model predictions of isoprene oxidation products more closely matched measurement data (Perring et al., 2009). Isoprene is represented as an explicit species in most chemical mechanism allowing mechanism changes to be implemented with relative ease.

Due to the nature of anthropogenic VOC mechanism development (extensive lumping and widely used mechanisms tightly controlled by a few senior researchers), new research findings have been difficult to incorporate. Additionally, time constraints associated with the most recent SAPRC mechanism development effort did not allow for updating the composition of VOC lumped species groups (Carter, 2009). The lumped species group definitions were developed in the mid-1980s based on data from 29 urban areas across the United States. One box model study has been performed in which a few olefins, those that dominate the reactivity of the mostly industrial emissions in Southeast Texas, are removed from the lumped species groups and represented explicitly but the lumped species definitions are otherwise unchanged (Heo et al., 2010). Heo et al. (2010) find that this more accurate VOC representation improves ozone predictions in their box model. Regional air quality model sensitivity to the VOC lumped group definitions has never been studied. Furthermore, known temperature dependencies of competing reaction pathways of VOC oxidation products have long been ignored in the SAPRC mechanism.

1.4 Research objectives

Steps are taken to implement a major chemical mechanism update in an AQM, and then improve the representation of VOC in a lumped atmospheric reaction mechanism. More realistic and contemporary definitions of lumped species properties are developed as part of this dissertation. Then, missing effects of temperature on VOC oxidation are included in the mechanism; specifically the product yields of $RO\cdot$ and $RO_2\cdot$ radicals are determined as a function of temperature. Air quality modeling studies are used to investigate the effects of the chemical mechanism improvements on predicted concentrations of ozone and other relevant air pollutants, their sensitivity to precursor emissions, and sensitivity to perturbations in climate-sensitive variables such as temperature, water vapor, and biogenic VOC emission rates.

1.5 Dissertation overview

The research presented in this dissertation describes development of a new VOC reaction mechanism that is more descriptive of the real atmosphere, specifically in terms of the mix of VOC that is represented, and the temperature-dependence of key reaction steps. Particular emphasis is placed on the effects of the improved mechanism on ozone sensitivity to VOC and NO_x emissions as well as climate change variables.

Chapter 2 describes the implementation in CMAQ of a major update of the SAPRC mechanism. The effects of using the new mechanism are evaluated under summertime conditions for central California. The mechanism sensitivity to individual reaction rate coefficient changes are ranked.

Differences in ozone sensitivity to changes in VOC and NO_x emissions, as well as changes in climate-related variables are explored.

In Chapter 3, emission speciation for important VOC sources and county-level emission inventories are utilized to update obsolete lumped VOC species definitions in the SAPRC mechanism that are based on old and incomplete ambient data from the 1980s. Ethanol and higher alcohols were assigned their own categories in the revised mechanism, due to large fuel-related increases in emissions of these species in recent years. The revised lumped species definitions are compared with recent atmospheric VOC measurements. The change in VOC reactivity in the AQM is determined, and resulting effects on ozone formation are assessed. The revised lumped species definitions are also a necessary enabling step for later steps in this research.

In Chapter 4, VOC oxidation product yields are updated by implementing a recent structure-activity relationship for alkoxy radical (RO[•]) reactions. Additionally, the AQM is altered to allow temperature-dependent product yields for VOC oxidation products, including RONO₂ formation and RO[•] reaction via O₂, isomerization, and thermal decomposition. Understanding the effect of temperature on air quality is potentially important everywhere owing to spatial and temporal temperature variations. This issue is also centrally relevant to studies of the effects of climate change on air quality, with current models likely to underrepresent the responsiveness of the real atmosphere to systematic changes in temperature. The new mechanism allows for an accurate accounting of organic nitrate, a collection of product species that weren't possible to study with the existing SAPRC mechanism. The modeling approach developed in this dissertation also allows for easier manipulation of the reaction mechanism. The lumped species can be changed in modeling areas that have different VOC emission speciation, and new data on reaction rates for peroxy and alkoxy radicals are also easily incorporated. Changes in VOC, RNO₃, and O₃ output using the new mechanism are evaluated in central California.

Additionally, Chapter 4 considers the effects of future climate change in 2050 on air quality, using the new chemical mechanism described above. The effectiveness of future emission reduction strategies are investigated, as well as effects of increased temperature, water vapor, and biogenic VOC emissions due to global warming.

In Chapter 5, a summary of major research findings is presented. Additional recommendations for areas of further research are discussed.

Chapter 2: Implementation and assessment of an updated chemical mechanism in an air quality model

Reproduced in part from:

Shearer SM, Harley RA, Jin L, Brown NJ, 2011. Comparison of SAPRC99 and SAPRC07 mechanisms in photochemical modeling for central California. *Atmospheric Environment* **46**, 205-216, (doi:10.1016/j.atmosenv.2011.09.079), with permission from Elsevier.

2.1 Introduction

2.1.1 SAPRC07 chemical mechanism

The SAPRC atmospheric chemical mechanisms (Carter, 2000) have been widely used in air quality research and air quality planning and control strategy development. SAPRC07 (Carter, 2010a,b,c), an update of the SAPRC99 mechanism, has recently been published. Various versions of the SAPRC07 mechanism appropriate for 3-dimensional air quality modeling have been developed and mechanism details are summarized in Table 2-1 with SAPRC99 for comparison. Prior to SAPRC07 releases of the SAPRC mechanism only included one mechanism appropriate for regional air quality modeling. Updates consistent among the SAPRC07 versions include an improved method for representing aromatic ring fragmentation products and their reactions, optional chlorine chemistry, and numerous changes to individual rate coefficients.

Table 2-1. SAPRC mechanism comparison

Number of species and reactions in each mechanism, smaller mechanisms are more computationally efficient.

Version ^a	Number		VOC	
	Species	Reactions	Explicit	Lumped
SAPRC99	72	214	22	23
SAPRC07A	70	218	21	23
CS07A ^b	47	140	9	16
SAPRC07B	104	275	21	23
SAPRC07C	104	511	21	23

^aInformation presented for SAPRC07 mechanisms does not include chlorine chemistry

^bCondensed version of SAPRC07A (Carter 2010b)

The most directly evolved version from SAPRC99 is SAPRC07A, which includes updates to reactions and reaction rate coefficients, but preserves the general structure and chemical operator approach of SAPRC99. CS07A, a new, more condensed mechanism, is derived from SAPRC07A, but is much more computationally efficient due to reduced numbers of species and

reactions. The SAPRC07B and SAPRC07C implementations utilize a new chemical operator approach developed to allow for more accurate representation of peroxy radical (RO_2^\cdot) chemistry, specifically the $\text{RO}_2^\cdot + \text{RO}_2^\cdot$ and $\text{RO}_2^\cdot + \text{HO}_2^\cdot$ reactions that are important under low NO_x conditions, and whose products are thought to be important contributors to secondary organic aerosol (Carter, 2010a). SAPRC07B is Carter's implementation of the new chemical operator approach, but it is not directly compatible with current air quality modeling software platforms that do not support variable parameter rate coefficients as are used to describe the rates of peroxy radical reactions. To implement this approach in the Community Multiscale Air Quality model (CMAQ; Byun and Schere, 2006), additional species and many additional reactions had to be added to the mechanism, resulting in SAPRC07C with 119 species and 602 reactions. Cai et al. (2011) found that use of SAPRC07C doubled CMAQ simulation computational time as compared to SAPRC99, making it unlikely to be used widely for ozone modeling given the SAPRC07A and CS07A alternatives. However, it will likely be an important option for secondary organic aerosol modeling until variable parameter rate coefficients, and thus SAPRC07B, are supported by CMAQ.

The chemical solver is among the most computationally intensive parts of an air quality model (Dabdub and Seinfeld, 1994; Tonse and Brown, 2007), and therefore reductions in the numbers of species and reactions included in a chemical mechanism can speed model calculations significantly. The performance of CS07A, the only SAPRC mechanism that is computationally competitive with the widely used Carbon Bond mechanism, and has not previously been implemented in a 3-D AQM, is the focus of this chapter.

In creating CS07A, Carter (2010c) explored economies in the representation of atmospheric chemistry stepwise in a 0-dimensional model, with a goal of keeping changes in ozone predictions small relative to the more detailed SAPRC07 mechanisms. Table 1 of Carter (2010c) documents the stepwise condensations applied to SARPC07A to create CS07A. To condense the mechanism, Carter (2010c) used a smaller number of lumped species to represent low reactivity VOC such as alkanes and ketones. Other organic species were combined on a case-by-case basis after checking that their lumping did not have a large effect on box model simulated ozone concentrations. A summary of VOC lumping strategies (Carter, 2010c) for the speciated VOC emissions used in this study is presented in Table 2-2 for SAPRC99, SAPRC07A, and CS07A. Note that in CS07A, ALK4 was modified by Carter (2010c) to represent both the ALK4 and ALK5 emissions. All other lumped VOC species were unchanged, and reactivity weighting was used to combine species into the CS07A mechanism. Further condensation of the mechanism was achieved by reducing the level of detail included in aromatic and isoprene oxidation mechanisms by lumping of reactions and related product species and by removing a model species for aromatic aldehydes (Carter, 2010c). The resulting CS07A mechanism has 47 species and 140 reactions, roughly two-thirds the size of SAPRC07A and SAPRC99.

Table 2-2. SAPRC VOC representation

Representation of VOC in different versions of the SAPRC mechanism.

Species	SAPRC99 ^a	SAPRC07A ^a	CS07A ^a
Methanol	MEOH	MEOH	0.288 ALK3
Acetylene	ALK2	ACYE	0.308 ALK3
Alkanes, 200 < kOH ^b < 500	ALK1	ALK1	0.132 ALK3
Alkanes, 500 < kOH < 2500	ALK2	ALK2	0.334 ALK3
Alkanes, 2500 < kOH < 5000	ALK3	ALK3	ALK3
Alkanes, 5000 < kOH < 10,000	ALK4	ALK4	ALK4
Alkanes, kOH > 10,000	ALK5	ALK5	1.0 ALK4
Benzene	0.295 ARO1	BENZ	0.045 ARO1+0.154 CRES
Aromatics, kOH < 20,000	ARO1	ARO1	ARO1
Aromatics, kOH > 20,000	ARO2	ARO2	ARO2
Alkenes, kOH < 70,000	OLE1	OLE1	OLE1
Alkenes, kOH > 70,000	OLE2	OLE2	OLE2
Ethene	ETHENE	ETHE	ETHE
Isoprene	ISOPRENE	ISOP	ISOP
Terpenes	TERP	TERP	TERP
Formaldehyde	HCHO	HCHO	HCHO
Acetaldehyde	CCHO	CCHO	CCHO
Lumped C3+ Aldehydes	RCHO	RCHO	RCHO
Aromatic Aldehydes	BALD	BALD	<i>removed</i>
Acetone	ACET	ACET	0.071 PRD2
Ketones, kOH < 7300	MEK	MEK	0.369 PRD2
Ketones, kOH > 7300	PROD2	PRD2	PRD2
Phenols	PHEN	1.0 CRES	1.0 CRES
Cresols	CRES	CRES	CRES
Glyoxal	GLY	GLY	0.582 MGLY+0.016 AFG1
Methyl Glyoxal	MGLY	MGLY	MGLY

^aA number in front of a species represents reactivity weighted lumping of the species^bkOH [=] ppm⁻¹ min⁻¹

Each of the SAPRC07 mechanisms incorporates rate coefficient updates based on recent IUPAC (2006) and NASA (2006) chemical data panel evaluations. Carter (2010b) states that the modification to the rate coefficient of the reaction $\text{OH} \cdot + \text{NO}_2 \rightarrow \text{HNO}_3$ (e.g., ~20% increase at 298 K and 1 atm) may be the most important single change. A study performed for southern California ranked ozone sensitivity coefficients to emissions and rate coefficients (Martien and Harley, 2006). The ozone sensitivity to the $\text{OH} \cdot + \text{NO}_2 \rightarrow \text{HNO}_3$ rate coefficient was among the largest of the rate coefficient ozone sensitivities, with sensitivity coefficients of similar magnitude as those for emissions of VOC and NO_x . Although ozone formation and accumulation

is the result of complex chemistry, an increase in the rate of this reaction is expected to result in lower ozone concentrations compared to SAPRC99 due to the consistently negative ozone sensitivity coefficients to this rate coefficient, as determined in the aforementioned study (Martien and Harley, 2006). However, the effect could be offset by other changes in SAPRC07, some of which are expected to raise modeled ozone levels. For example, SAPRC07 incorporates an 8% increase in NO₂ photolysis rates (that would lead to increased ozone production). Also, some uncertain reaction rates and product yields were adjusted to tune the mechanism to match environmental chamber data (Carter, 2010b). Table 2-3 shows relevant SAPRC07 reactions and percentage change in rate coefficients at three atmospherically relevant temperatures.

Table 2-3. Estimated ozone response

Reactions where the SAPRC07 rate coefficient changed by more than 5% and ozone sensitivity to the rate coefficient is significant.

SAPRC07 Reaction	Reaction Rate Coefficient Change at given temperature and 1 atm (SAPRC07-SAPRC99)/SAPRC99			S-N Ozone Sensitivity ^a (ppb)	Estimated Ozone Response ^b (ppb)
	275K	300K	315K		
OH + NO ₂ = HNO ₃	13.0%	18.8%	24.3%	-49.6	-9.3
O ₃ + NO = NO ₂ + O ₂	5.6%	8.1%	10.3%	-35.6	-2.9
PAN = MECO ₃ + NO ₂	-10.4%	-11.0%	-11.7%	8.1	-0.9
O ₁ D + M = O ₃ P + M	14.5%	14.4%	14.4%	-29.1	-4.2
O ₁ D + H ₂ O = 2OH	-8.5%	-9.5%	-10.4%	29.1	-2.8
MECO ₃ + NO ₂ = PAN	-9.8%	-10.6%	-11.4%	-8.8	0.9
HO ₂ + NO = OH + NO ₂	5.9%	5.9%	5.9%	9.8	0.6
HCHO + hν = 2HO ₂ + CO ^c		19.0%		18.8	3.6
NO ₂ + hν = NO + O ₃ P ^c		8.0%		39.2	3.1

^aFrom Martien and Harley (2006): Semi-Normalized Sensitivities for Rubidoux 8-hour peak Ozone

^bEstimated Ozone Response at 300K = (Rate Coefficient Change)*(Ozone Sensitivity)

^cPhotolysis rate increase reported by Carter (2010a)

2.1.2 Comparison of SAPRC07 and other mechanisms in air quality modeling

To date, few studies have been published comparing SAPRC07 use in AQMs to other mechanisms. A version of SAPRC07 has been compared to SAPRC99 and three other chemical mechanisms in a zero-dimensional box model, with rate coefficients for all mechanisms updated according to NASA (2006), to determine differences in OH[•] and HO₂ concentrations due to chemical mechanism structure alone (Chen et al., 2010). Cai et al. (2011) investigated the effects of using the extended SAPRC07C in air quality modeling for all of California. They found that ozone predictions were generally lower using SAPRC07C in place of SAPRC99, with the magnitude of the ozone decreases tending to be largest in polluted regions that were out of compliance with health-based air quality standards. These high-ozone regions also showed

reductions in radical and NO_x concentrations, pointing to the importance of the increase in OH + NO₂ reaction rate in SAPRC07 (Cai et al., 2011).

SAPRC99 has been compared with the commonly used Carbon Bond mechanisms, CB4 (Gery et al., 1989) and CB05 (Yarwood et al., 2005), in 3-dimensional air quality modeling studies. SAPRC99 resulted in consistently higher ozone concentrations than CB4 (Faraji et al., 2008; Luecken et al., 2008) and, although to a lesser extent, than CB05 (Luecken et al., 2008). The SAPRC99 mechanism simulation runtime was 40% to 50% longer than for CB4, depending on domain size (Luecken et al., 2008), but use of CS07A in place of SAPRC99 should significantly decrease the disparity in simulation time.

2.1.3 Research objective

As the SAPRC99 mechanism has been used extensively in prior air quality planning and research, it is important to understand differences in air quality model predictions between SAPRC99 and SAPRC07. The condensed mechanism (CS07A) was developed to replace SAPRC99, featuring a representation of the more current understanding of atmospheric chemistry, as well as improved computational efficiency for regional modeling in which ozone prediction is the primary interest (Carter, 2010c). The main objective of the study reported in this chapter is to implement and then evaluate the effects of using CS07A in predicting air quality in central California, as compared to SAPRC99. Doing so significantly extends the scope of published comparisons as CS07A has thus far only been examined in Carter's box model (Carter, 2010c). Contributions to overall changes in ozone concentrations are quantified individually for the most important revisions that were made in updating the mechanism. The contribution to differences in ozone concentration changes due to mechanism condensation from SAPRC07A to CS07A is also quantified.

Ozone responses to emission changes are important to understand in designing effective control strategies, as ozone formation depends nonlinearly on emissions of VOC and NO_x precursors. It is of particular interest to identify regions that exhibit NO_x disbenefit (VOC-sensitivity), where NO_x emission reductions could cause an increase in ozone concentrations. Emission sensitivity studies using the SAPRC99 mechanism have been carried out in California using both the brute force method (Marr et al., 2002) and the direct decoupled method (Jin et al., 2008). Marr et al. (2002) found that, as of 1990, the Bay Area and its immediate downwind areas were VOC-sensitive, while the more rural Central Valley was largely NO_x sensitive for 1-hour ozone levels. Jin et al. found for a more recent year (2000), that, in addition to the Bay Area, urban centers in the Central Valley were also VOC-sensitive for 8-hour ozone. Note that there are differences in both the base year and the ozone metric being analyzed between these studies. Also note that results are highly dependent on the reaction rate of $\text{OH} + \text{NO}_2 \rightarrow \text{HNO}_3$. Further results of sensitivity analysis are reported in this chapter to illuminate how updating the mechanism to CS07A alters ozone sensitivity to anthropogenic VOC and NO_x emissions as compared to SAPRC99.

As discussed in Chapter 1, another relevant issue for central California is how air quality could be affected by climate change. Weaver et al. (2009) assimilate ozone responses due to climate change from five global and seven regional AQMs. The models consistently predict that ozone

concentrations will increase over a substantial portion of the continental US. Steiner et al. (2006) studied ozone responses to climate-sensitive variables (assuming a doubling of atmospheric CO₂) using the SAPRC99 chemical mechanism. A similar analysis is presented in this chapter using an updated chemical mechanism. Ozone responses to temperature, relative humidity, and biogenic emissions are examined to update the assessment of possible climate change impacts on air quality in California.

2.2 Methods

Air quality model simulations were performed using the Community Multiscale Air Quality (CMAQ version 4.6) modeling system (Byun and Schere, 2006), implementing both the SAPRC99 and CS07A chemical mechanisms. While the CS07A mechanism had not been integrated into CMAQ, Carter provided data files, (<http://www.engr.ucr.edu/~carter/SAPRC/files.htm>) which were used to update CMAQ to work with the CS07A mechanism. The central California modeling domain used in this study is indicated by the red dotted lines in Figure 2-1. Typical wind patterns in this region include a daytime sea breeze that is funneled through the Carquinez Strait, which provides a break in the coastal mountains to the north and south. The flow then splits to the north and flows into the Sacramento Valley and to the south into the San Joaquin Valley, carrying ozone and its precursors from the heavily populated San Francisco Bay area to downwind areas.



Figure 2-1. Central California AQM domain

Map of central California showing the 384 km × 468 km air quality model domain as the inner red rectangle

Model simulations were performed on a 96×117 grid with 4 km horizontal resolution, and 27 vertical layers extending from the surface to 100 mb, or approximately 17 km above sea level. Output from a mesoscale meteorological model (MM5; Grell et al., 1995), which has been described in detail elsewhere (Michelson et al., 2010; Jin et al., 2010), drives the air quality model simulations. Hourly emission estimates for each day of the week from motor vehicle, point, and area sources were compiled by the California Air Resources Board (CARB). Biogenic emissions were estimated using the Biogenic Emission Inventory Geographic Information System (Scott and Benjamin, 2003) that takes into account temperature, sunlight intensity, and green leaf biomass as a function of plant species. Further description of relevant anthropogenic emissions is available elsewhere (Harley et al., 2006; Jin et al., 2010). CS07A emissions were remapped from the SAPRC99 emission lumping scheme using the information given in Table 2-2.

Lateral boundary conditions and initial conditions are also based on previous studies (Jin et al., 2008; Jin et al., 2010). All model lateral boundary concentrations were held constant over time. Most model species boundary concentrations are also vertically constant, although the western inflow boundary condition for ozone varies vertically according to ozonesonde observations performed in California by Newchurch et al. (2003). Northern, eastern, and southern (primarily outflow) boundary concentrations are all the same for each model species, while the western boundary conditions are generally set to lower values to represent clean background conditions that prevail over the Pacific Ocean. Boundary conditions for select species are presented in Table 2-4. For initial conditions, surface observations are used when available, or clean background values otherwise. Harley et al. (2006) determined that within 50 hours of simulation time (for the domain shown in Figure 2-1), ozone concentrations do not retain memory of the initial conditions. Spin-up for the model results presented here was 72 hours, minimizing effects of uncertainties due to initial conditions.

Two Monday to Wednesday simulations were conducted for conditions that were observed during summer 2000. I focus on weekday periods to avoid confounding effects from weekday-weekend emission differences. July 24 to 26 had above average temperatures and ozone levels, and July 31 to August 2 had even higher temperatures and more stagnant conditions, which also resulted in elevated ozone levels. The two time periods are evaluated separately to determine if there are differing model responses to emissions and mechanism updates due to meteorological effects. Results are presented in maps showing concentration distributions at 3 pm PST, an hour when ozone concentrations are at a peak in many locations in the domain. In addition to considering peak ozone levels, it is also of interest to consider effects on 8-hour maximum ozone concentrations (the highest running 8-hour average over a day), which are also thought to be more closely linked to adverse health effects (World Health Organization, 2000) than peak ozone concentrations. Average 8-hour maximum ozone concentration results are presented in tables for specific sites.

Table 2-4. AQM boundary conditions

Boundary conditions for select SAPRC species, table recreated from Jin et al. (2008; Supplementary Information)

SAPRC Species	Clean Western Boundary (ppb)	N/E/S Boundary (ppb)
CO	120	200
NO	0.01	0.05
NO2	0.03	1
PAN	0.15	0.005
PAN2	0.02	0
O3 at sfc	22	40
O3 at 1km	44	48
O3 at 2km	60	60
O3 at 3km	60	60
HCHO	0.3	2
CCHO	0.15	0.456
ACET	0.89	1
ALK1	1.06	10
ALK2	0.13	2.5
ARO1	0.019	0.35
ARO2	0	0.25
ISOP	0	0.1
OLE1	0	0.5
OLE2	0	0.2

2.3 Results and discussion

2.3.1 Ozone

Ground-level weekday average temperatures, ozone concentrations for SAPRC99, and ozone differences (CS07A–SAPRC99) at 3 pm PST are presented in Figure 2-2 for both the July episode (E1), and July/August episode (E2). The third panel for each time period shows mostly negative values, indicating that using CS07A in place of SAPRC99 resulted in lower predicted ozone levels in almost all areas of the domain. Larger ozone decreases were generally collocated with the areas with higher temperatures and higher ozone concentrations. Ozone concentrations were generally higher during E2 than E1 due to meteorological differences: higher temperatures and more stagnant conditions were conducive to more ozone production and accumulation. During E1, large differences (more than 10 ppb) in ozone predictions were confined to the Sacramento and San Joaquin Valleys where temperatures were highest, while during the warmer E2, large ozone differences were also seen in the San Francisco Bay Area. For E1, the largest hourly ozone difference was 17 ppb; the corresponding largest difference for E2 was 25 ppb, near Fresno in both cases. In parts of the Sacramento Valley ozone concentrations were lower during E2, and the difference between mechanisms also decreased. The Sacramento Valley is close to the northern boundary of the domain, and although the boundary is dominated by outflow, Harley et al. (2006) examined pollutant fluxes and found occasional inflow. Given the Sacramento Valley's proximity to a more polluted boundary (northern) of the study domain, and

the intermittent existence of inflow conditions at this boundary, this area should be most sensitive to uncertainties in boundary conditions.

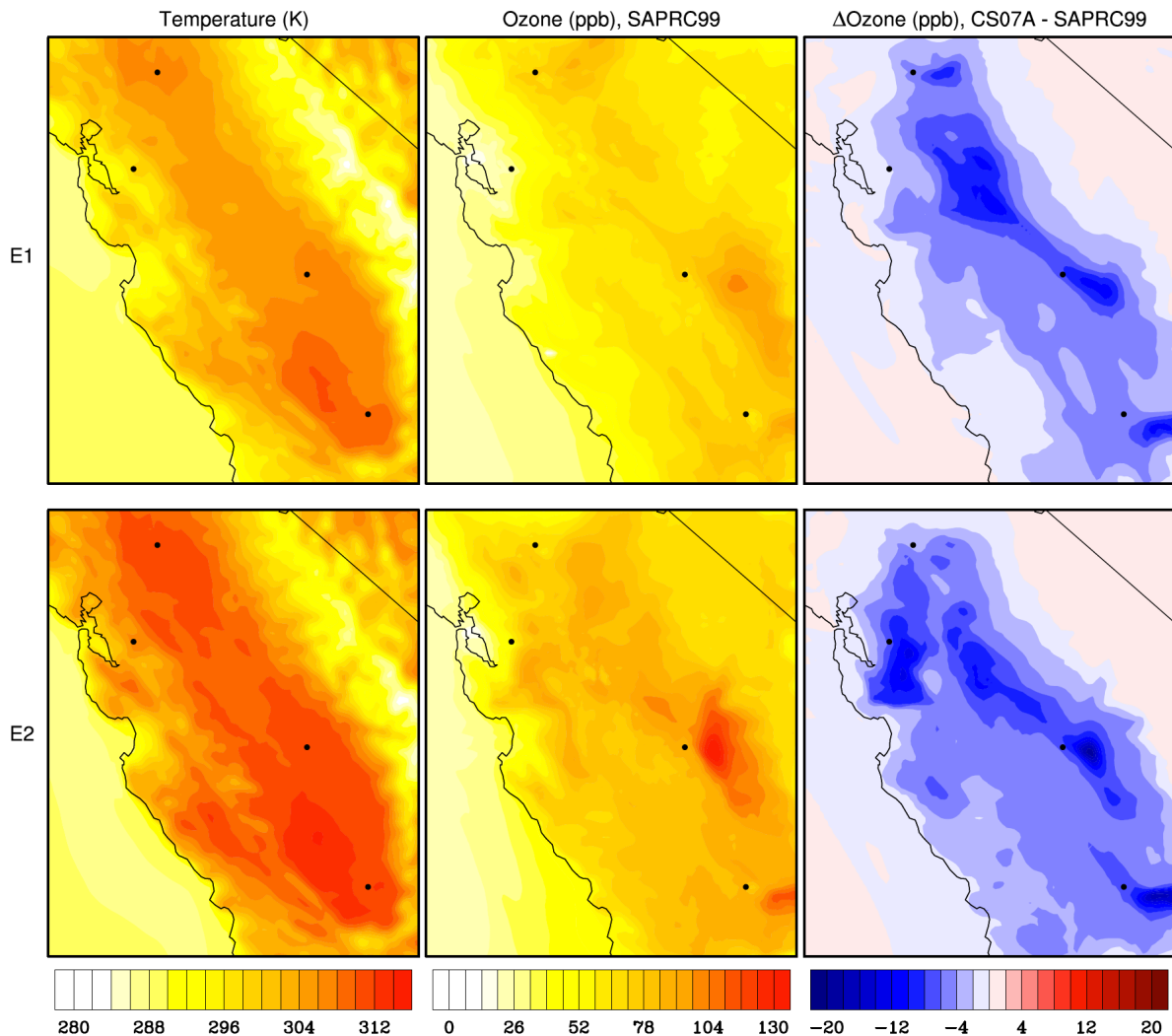


Figure 2-2. Temperature and predicted ozone using SAPRC99. Change in predicted ground-level ozone when CS07A is used in place of SAPRC99

Blue color indicates a decrease in predicted ozone. The top row shows Episode 1 (July), and the bottom row shows analogous plots for Episode 2 (late July/early August) when temperatures were especially high. All values are 3-day weekday averages at 3 pm during the summer 2000 simulations.

CS07A ozone, SAPRC99 ozone, and ground-level ozone observation time series for four typically high-ozone sites (Livermore, Sacramento, Fresno, and Bakersfield, see Figure 2-1) are shown in Figures 2-3A and 2-3B. Ozone concentrations predicted using CS07A never exceed SAPRC99 levels at these sites during either episode. The timing of peak ozone matches between mechanisms, and the largest differences occur at the peak ozone hour for all sites and days. The

hourly ozone observations shown in Figures 2-3A and 2-3B, for these and many other sites, were collected as part of the Central California Ozone Study (Fujita et al., 2005).

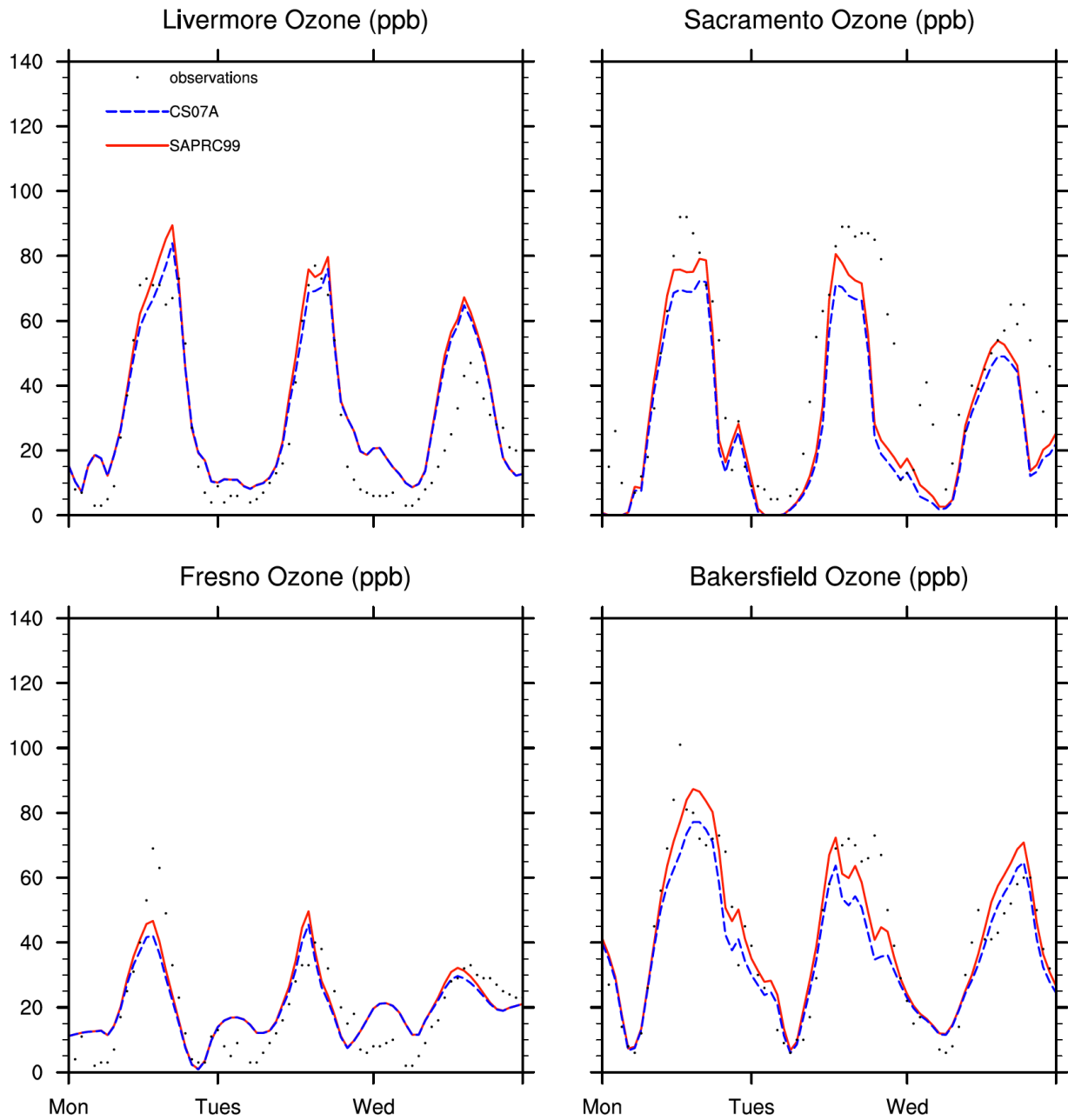


Figure 2-3A. Diurnal variations in observed and predicted ozone concentrations for E1

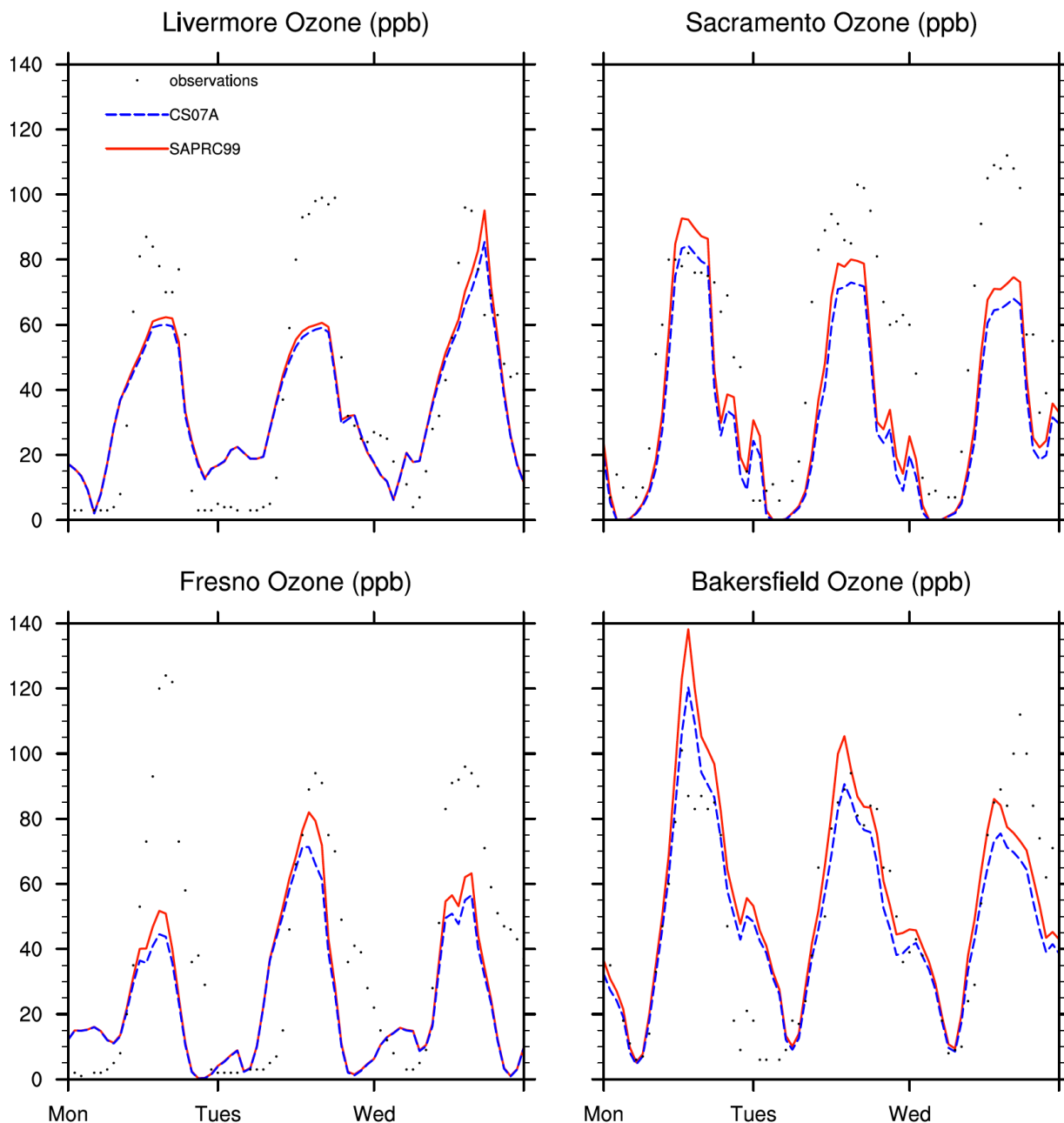


Figure 2-3B. Diurnal variations in observed and predicted ozone concentrations for E2

Underprediction of peak ozone levels is a common problem in air quality modeling, and updating the chemical mechanism to CS07A increased the magnitude of this problem. Note that other large sources of uncertainty in the model that may also contribute to ozone underprediction include emission inputs and meteorological fields (Jin et al., 2010). In both episodes, the number of site-days with ozone measurements that switched from an overprediction to an underprediction of the peak 1-hour ozone increased by about 10% with the use of CS07A. Also,

the magnitude of the underpredictions increased at about 95% of the sites in both episodes. The sites and days used for model evaluation are limited to those with a 1-hour maximum observed ozone concentration of 60 ppb or higher, as the model generally overpredicts ozone at lower concentrations as shown in Jin et al. (2010). Three hundred and seventy three site-days met the criteria over the 6 days studied.

Table 2-5 shows both observed and predicted weekday 8-hour maximum ozone concentrations at the same four sites mentioned above. As expected, use of CS07A leads to lower predicted ozone concentrations. The percentage change in predicted ozone in updating to CS07A from SAPRC99 in Livermore and Sacramento are small compared to Fresno and Bakersfield. SAPRC99 underpredicts at 5 out of the 8 sites and episodes analyzed, and CS07A underpredicts at 7 out of the 8.

Relevant mean normalized model performance statistics are presented in Table 2-6. Note that the previously mentioned observational cutoff of 60 ppb ozone was employed in calculating all of these model performance statistics. The magnitudes of domain-wide normalized bias and gross error for hourly ozone, peak 1-hour ozone, and peak 8-hour ozone all increase with use of CS07A for both episodes.

Table 2-5. Ozone concentrations and responses at four sites

8-hour maximum concentrations (in ppb) and ozone differences at four central California sites.

		Livermore		Sacramento		Fresno		Bakersfield	
		E1	E2	E1	E2	E1	E2	E1	E2
Base Case Prediction ^a	Observed	35.4	83.4	54.4	80.3	66.6	86.7	73.6	90.5
	SAPRC99	32.7	52.8	63.7	61.4	66.9	90.8	62.1	72.0
	SAPRC07A	31.3	49.5	62.2	60.6	62.5	84.1	59.1	67.8
	CS07A	30.3	47.6	59.9	58.7	59.1	80.5	56.4	64.8
20% AVOC Emission Reduction	SAPRC99	-0.9	-2.9	-1.0	-0.5	-2.7	-5.1	-1.9	-2.3
	CS07A	-1.0	-3.0	-1.4	-0.7	-3.4	-5.9	-2.5	-2.8
20% NO _x Emission Reduction	SAPRC99	2.54	5.8	-0.99	-1.03	2.3	2.7	1.0	0.6
	CS07A	2.49	5.6	-0.2	-0.5	3.6	4.3	1.7	1.4
Temperature Perturbation	SAPRC99	0.4	1.0	1.5	0.9	1.7	2.3	1.1	1.2
	CS07A	0.3	0.5	1.2	0.5	1.13	1.10	0.7	0.4
Water Vapor Perturbation	SAPRC99	0.5	1.0	0.29	-0.09	1.0	0.6	0.03	-0.4
	CS07A	0.3	0.6	0.34	-0.11	0.9	0.2	0.00	-0.7
Biogenic Emission Perturbation	SAPRC99	0.37	1.3	0.8	0.22	1.1	2.49	0.79	1.1
	CS07A	0.39	1.2	1.1	0.18	1.2	2.50	0.84	1.0
Combined Climate Simulation	SAPRC99	1.3	3.5	2.8	1.1	3.9	5.5	2.1	2.0
	CS07A	1.0	2.8	2.7	0.9	3.3	4.6	1.6	1.3

^a Base case reported as 8-hour averages, all other values reported as the difference relative to the base case

Relevant mean normalized model performance statistics are presented in Table 2-6. Note that the previously mentioned observational cutoff of 60 ppb ozone was employed in calculating all of these model performance statistics. The magnitudes of domain-wide normalized bias and gross error for hourly ozone, peak 1-hour ozone, and peak 8-hour ozone all increase with use of CS07A for both episodes.

Table 2-6. AMQ ozone performance statistics
Mean performance statistics for central California domain.

	Version	N. Bias ^a		N. Gross Error ^b	
		E1	E2	E1	E2
Hourly Ozone	SAPRC99	-13%	-18%	18%	23%
	CS07A	-15%	-19%	21%	26%
1-hour peak ozone	SAPRC99	-7%	-12%	15%	19%
	CS07A	-14%	-18%	17%	21%
8-hour peak ozone	SAPRC99	-7%	-8%	12%	18%
	CS07A	-13%	-14%	15%	19%

$$^a \text{Normalized Bias} = \frac{1}{N} \sum_{i=1}^N \left(\frac{C_{\text{model},i} - C_{\text{obs},i}}{C_{\text{obs},i}} \right) \quad \text{for } i, \text{ where } C_{\text{obs},i} > 60 \text{ ppb}$$

$$^b \text{Normalized Gross Error} = \frac{1}{N} \sum_{i=1}^N \left| \frac{C_{\text{model},i} - C_{\text{obs},i}}{C_{\text{obs},i}} \right| \quad \text{for } i, \text{ where } C_{\text{obs},i} > 60 \text{ ppb}$$

2.3.2 Individual reaction rate coefficient updates and mechanism condensation

It is expected that the increase in the OH + NO₂ rate coefficient is an important contributor to lower ozone predictions that result from using any version of SAPRC07 (Carter, 2010a). However, many other changes were made as part of the mechanism update. The effects on model predictions of changes to specific individual rate coefficients using CS07A are considered here, but rate coefficient changes are common to all versions of SAPRC07. The effect that mechanism condensation from SAPRC07A to CS07A had on ozone predictions is also examined.

To study rate coefficient changes, the condensed CS07A mechanism is used as the base, and individual rate coefficients are changed back to their values as defined in the older SAPRC99 mechanism. Multiple rate coefficients were studied, and the air quality responses to these changes were computed and analyzed one at a time. Reactions were selected for study by considering the percent change in rate coefficients between SAPRC07 and SAPRC99, combined with ozone sensitivities to the rate coefficient, k . The semi-normalized 8-hour ozone

sensitivities, $k_i \frac{\partial [O_3]}{\partial [k_i]}$, were determined for sites in southern California by Martien and Harley

(2006) for each SAPRC99 reaction, i , using the adjoint method, allowing comparison regardless of the rate coefficient units. The Rubidoux sensitivity coefficients are shown in the second to last column in Table 2-3, and while this is not ideal as sensitivity coefficients depend on local emissions and environmental conditions, these are the only extensive rate coefficient ozone sensitivities reported in the literature. All reactions are considered for which Martien and Harley (2006) report a rate coefficient sensitivity from SAPRC99 to SAPRC07 of 5% or greater at 300

K and standard pressure. Table 2-3 shows the resulting reactions and their relevant data. The last column is a first-order estimate of the expected ozone response, the product of the percent change in the rate coefficient and the semi-normalized ozone sensitivity coefficient.

The overall change in predicted ozone concentrations caused by switching from SAPRC99 to CS07A, along with the change in ozone attributable to using the condensed CS07A mechanism in place of SAPRC07A, and the model response to each of the rate coefficient updates that were considered individually are all shown in Figure 2-4. The percent change in each rate coefficient at 300 K is shown in parentheses along with individual reactions that were perturbed. Results presented are 8-hour maxima for E1 (top) and E2 (bottom).

Condensing the mechanism from SAPRC07A to CS07A and increasing the $\text{OH} \cdot + \text{NO}_2$ rate coefficient were responsible for the largest contributions to the decrease in predicted ozone. As previously mentioned, the expected effect of the increase in this rate coefficient was a decrease in ozone concentration. However, the ozone decrease due to mechanism condensation was unexpected. In Carter's zero-dimensional model, the condensation of SAPRC07A to CS07A, had the effect of slightly increasing maximum ozone concentration (Carter, 2010c), so the decrease it caused in ozone concentration in the 3-dimensional model is surprising. As discussed in the introduction, many changes were made in condensing the mechanism; so further study is necessary to explain this result.

Other changes in SAPRC07 include increasing the NO_2 photolysis rate because of changes in recommended absorption cross sections and quantum yields, but this effect was offset by an increase in the $\text{O}_3 + \text{NO}$ reaction rate, and hence there was little net effect on predicted ozone levels. Another reaction pair where revisions were made in SAPRC07 involves PAN formation and thermal decomposition. Ozone responses to these two changes were much smaller, and again had opposite and almost equal, offsetting effects.

Reactions of electronically excited oxygen atoms $\text{O}(^1\text{D})$ with air molecules (M) and water vapor have competing effects on OH radical formation. The reaction rate with M to form $\text{O}(^3\text{P})$ was increased and the reaction rate with H_2O was decreased in SAPRC07, with both changes leading to decreased OH radical formation. The resulting ozone response to decreased $\text{OH} \cdot$ formation varied based on the chemical regime of the site. The predicted 8-hour ozone averages decrease for both episodes, E1 and E2, at Livermore and Fresno, whereas at Bakersfield, increases are predicted for both episodes. In mostly VOC limited regions (Livermore and Fresno), decreasing $\text{OH} \cdot$ concentration slows VOC oxidation that, in turn, suppresses ozone formation. In NO_x limited regions (e.g. Bakersfield) increased NO_x availability as a result of lower $\text{OH} \cdot$ lead to an increase in predicted ozone.

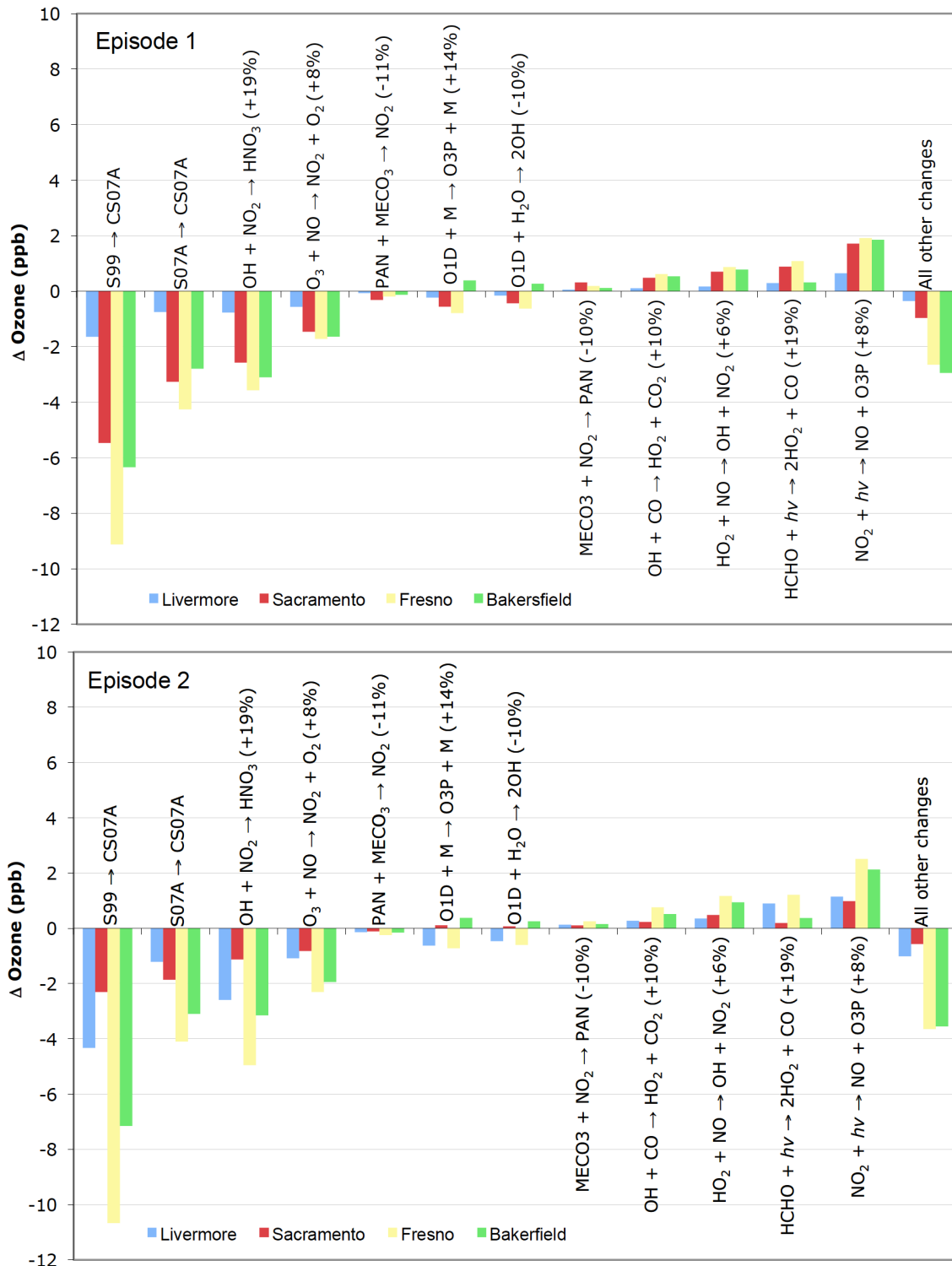


Figure 2-4. Chemical mechanism and reaction rate coefficient AQM sensitivity
 Changes in 8-hour maximum predicted ozone concentrations at 4 Central California sites due to using different chemical mechanisms (at left: S99→CS07A and S07A→CS07A), and due to separate updating of individual reaction rate coefficients (relative changes to each rate coefficient shown in parentheses). All values are 3-day weekday averages during the summer 2000 simulations.

For most of the reaction rate coefficients, Episode 2 showed ozone responses greater in magnitude but similar in direction, with the exception of the directional response to $O(^1D)$ reactions in Sacramento, indicating a shift in chemical regime as compared to E1. Again, condensation of the mechanism from SAPRC07A to CS07A and the increase in the $OH + NO_2$ rate coefficient appear to be the most important factors in lowering ozone concentrations predicted using CS07A, as compared to SAPRC99.

This analysis allows a comparison of the relative importance of individual rate coefficient revisions and mechanism condensation, but other potentially important variables that contribute to simulation differences are not considered. Other CS07A updates that may contribute to ozone differences include the new aromatic hydrocarbon oxidation mechanism, other unstudied rate coefficient changes, and product yield changes. Also, interactions within the mechanism and between the mechanism and other model inputs may differ and can also affect ozone predictions.

2.3.3 Emission sensitivity

A key policy-relevant issue relating to the new mechanism is whether predicted air quality responses to changes in anthropogenic emissions differ with respect to SAPRC99. To examine this matter, first all anthropogenic VOC emissions model species were perturbed, including lumped species (e.g., the lumped alkanes), by reducing values by 20% in all model grid cells at all times. Similarly, an emission file was created with NO_x emissions reduced by 20%; forest fire emissions were not included or perturbed in any of the emission files. Maps showing ozone responses to separate 20% reductions in anthropogenic VOC and NO_x emissions are presented in Figures 2-5A (E1) and 2-5B (E2). Eight-hour ozone sensitivities to these emission changes are summarized in Table 2-5 for both episodes. Modeled ozone is seen to decrease everywhere in response to VOC emission reductions (see first two columns in the top row of Figures 2-5A and 2-5B). Reducing VOC emissions in the higher-ozone episode E2 results in larger ozone reductions. Use of CS07A leads to a larger ozone reduction than SAPRC99 for both episodes, as can be seen in the last column and top row of Figure 2-5A and 2-5B, which shows the differences between the ozone responses. With both mechanisms, NO_x emission reductions lead to localized areas of NO_x disbenefit, as can be seen in the first two columns in the bottom row of the figures. This increase in ozone concentrations in response to decreased NO_x emissions occurs at VOC-limited sites, most notably the Bay Area, and to a lesser degree near the Fresno and Bakersfield city centers.

Use of CS07A has very little effect on ozone response to emission reductions in the Bay Area, compared to predictions made using SAPRC99, but shifts the rest of the domain toward more VOC-limited conditions, as indicated by the positive values in the difference between the ozone responses (see Table 2-5 and last column, bottom row of Figures 2-5A and 2-5B). The shift toward VOC-limited conditions is results in a slight increase in magnitude and spatial extent of the NO_x disbenefit region outside of the Bay Area for both episodes. Note that the CS07A mechanism is more sensitive than SAPRC99 to emissions changes on an absolute basis in the highest ozone regions of the San Joaquin Valley even though predicted ozone concentrations are lower. NO_x disbenefit is less widespread in the modeling domain for E1 than for E2. Use of CS07A also slightly increases the spatial extent of NO_x disbenefit in E1 compared with SAPRC99. Although generally smaller in magnitude, directionally E1 results are the same as E2 at the four sites studied. Cai et al. (2011) found a similar ozone response pattern to emissions in

comparing SAPRC07C to SAPRC99, and speculate that the NO_x disbenefit regions expand due to lower OH radical concentration.

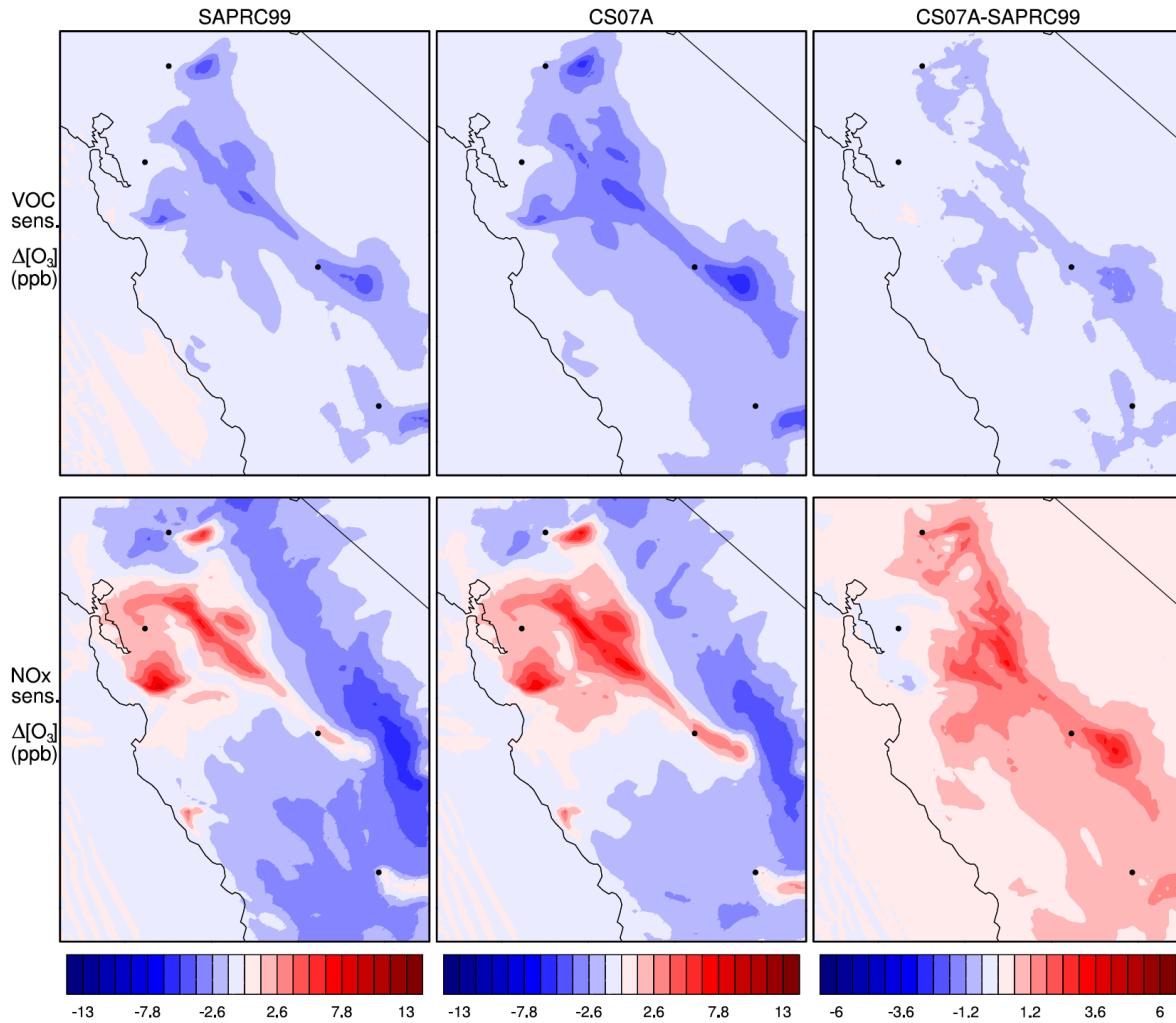


Figure 2-5A. VOC and NO_x sensitivity using SAPRC99 vs CS07A, Episode 1

Effects of emissions perturbations on ozone air quality. The first row shows the ozone response to 20% reduction in VOC emission, and the second row shows the ozone response to 20% reduction in NO_x emissions. The last panel shows the difference in response to the same perturbations between mechanisms. Weekday 3 pm E1 averages.

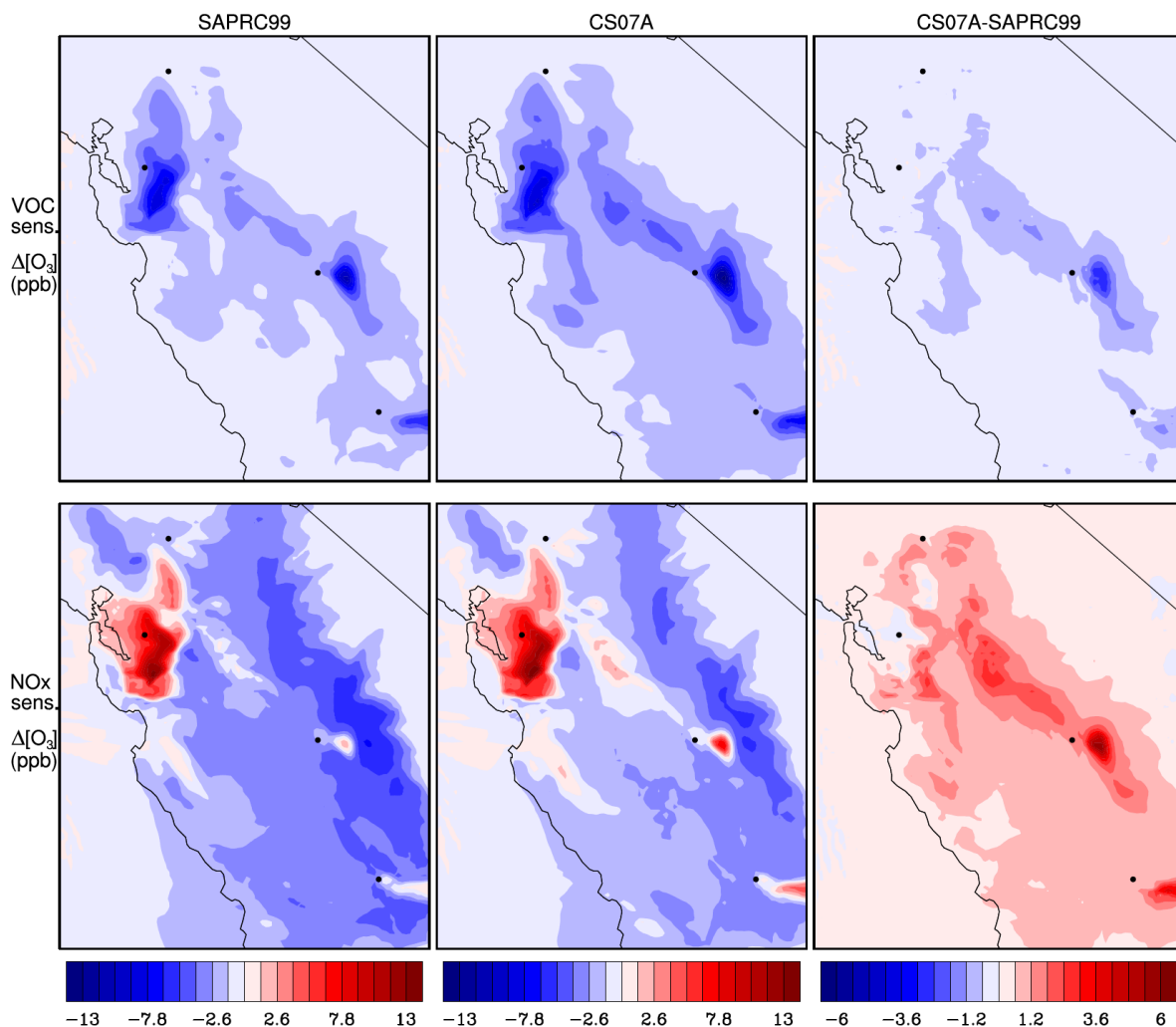


Figure 2-5B. VOC and NO_x sensitivity using SAPRC99 vs CS07A, Episode 2

Effects of emissions perturbations on ozone air quality. The first row shows the ozone response to 20% reduction in VOC emission, and the second row shows the ozone response to 20% reduction in NO_x emissions. The last panel shows the difference in response to the same perturbations between mechanisms. Weekday 3 pm E2 averages.

2.3.4 Responses to climate change-sensitive parameters

Steiner et al. (2006) have considered the effects of climate change-related perturbations on air quality in central California. Here, the effects of the same perturbations to temperature, water vapor, and biogenic VOC emissions are evaluated using the newer CS07A mechanism instead of SAPRC99. Air quality effects of a combined simulation including all three of the above perturbations were also evaluated.

The temperature perturbations were derived from downscaled effects of an assumed doubling of atmospheric CO₂ (Snyder et al., 2002). The temperature increase is larger inland than along the coast. The perturbation is applied at all time steps as in Steiner et al. (2006). Although first studied independently to isolate the effect of each variable on ozone concentration in the air

quality model, water vapor and biogenic VOC emission perturbations were developed based on the same temperature perturbation.

The capacity of air to hold water vapor increases with increasing temperature, and the potential increase in water vapor can be estimated using the water vapor mixing ratio (q), atmospheric pressure (P), and temperature (T) from the meteorological model, as well as the temperature perturbation described above. First the vapor pressure (e) is calculated for each grid cell:

$$e = \frac{qP}{\varepsilon + (1-\varepsilon)q} \quad (\text{E2.1})$$

where $\varepsilon = (\text{Molecular Weight}_{\text{H}_2\text{O}} / \text{Molecular Weight}_{\text{dry air}}) = (18 \text{ g/mol}) / (29 \text{ g/mol}) = 0.62$.

Relative humidity assumed to be unchanged at the perturbed (increased) temperature, and is calculated using:

$$RH = \frac{e_1}{e_{\text{sat}}(T_1)} = \frac{e_2}{e_{\text{sat}}(T_2)} \quad (\text{E2.2})$$

where e_{sat} is the saturation vapor pressure, calculated using the approximate solution presented in Hartman (1994):

$$e_{\text{sat}}(T) = 6.11 \cdot \exp\left[\frac{L}{R_v} \left(\frac{1}{273} - \frac{1}{T}\right)\right] \quad (\text{E2.3})$$

where e_{sat} is in millibars, L is the latent heat of vaporization ($2.5 \times 10^6 \text{ J/kg}$), and R_v is the gas constant for vapor (461 J/K/kg). After calculating e_{sat} for each temperature, e_2 can be solved using Equation (2), and finally Equation (1) is rearranged to solve for q at the new vapor pressure, e . The meteorological input file is updated with the increased water vapor mixing ratios.

Terpene emissions are expected to increase exponentially, while isoprene emissions increase exponentially until 303 K, and continue to increase until a maximum emission rate is reached at 313 K (Guenther et al., 1993). Guenther et al. (1993) developed a model for biogenic isoprene emissions as a function of a temperature (T) for cases in which emissions, I_S , have been previously defined at temperature T_S . The estimate for isoprene emissions (I) is shown below in equation (E2.4),

$$I = I_S \left(\frac{\exp\left(\frac{C_{T1}(T-T_S)}{RT_S T}\right)}{1 + \exp\left(\frac{C_{T2}(T-T_M)}{RT_S T}\right)} \right) \quad (\text{E2.4})$$

where R is the gas constant (8.314 J/K/mol), and C_{T1} (=95,000 J/mol), C_{T2} (=230,000 J/mol), and T_M (=314 K) are empirical coefficients defined in Guenther et al. (1993). Similarly, Guenther et al. (1993) develop a temperature-dependent terpene emission equation:

$$Terp = Terp_s \cdot \exp[\beta(T - T_s)] \quad (E2.5)$$

where $Terp_s$ is the emission rate at defined temperature, T_s , and β (=0.065) is an experimentally determined coefficient. The climate change-related perturbations to air quality model input data, and ozone responses to these perturbations are shown in Figure 2-6. Results that are shown are the weekday 3 pm average for E2, which is the same episode studied by Steiner et al. (2006). The 8-hour maximum ozone results for both episodes are shown in Table 2-5.

Temperature

Temperature affects ozone concentration through its effect on rate coefficients. Predicted ozone response to the temperature perturbation using CS07A is shown in the first column and the bottom row of Figure 2-6. Both mechanisms show the expected increase in ozone with higher temperature; the largest increases are in areas with elevated ozone in the base case. Use of CS07A gives a weaker response to temperature perturbations over the entire domain. The 8-hour maximum ozone responses to the temperature perturbation are shown in Table 2-5 for both episodes. With higher base case temperatures (the late July/early August period E2 was hotter), the ozone response to temperature perturbations using CS07A was weaker as compared to the SAPRC99 response. This weaker dependence can be explained in part by the $OH^\cdot + NO_2$ rate coefficient, which decreases with increasing temperature, and shows a larger relative difference between SAPRC99 and CS07A as temperature increases. The percentage change for this rate coefficient is shown in Table 2-3 for three different temperatures. Compared to SAPRC99, in the newer mechanism the $OH^\cdot + NO_2$ rate coefficient increases by values ranging from 8% at 275 K to 24% at 315 K. The more rapid $OH^\cdot + NO_2$ reaction in CS07A suppresses ozone formation, and this effect becomes stronger at higher temperatures.

Water vapor

Water vapor is a greenhouse gas. The increase due to temperature increases causes a positive global warming feedback (Hartmann 1994). Steiner et al. (2006) found this increase in water vapor to cause increases in ozone as well. Increasing water vapor leads to an increase in OH^\cdot production via the $O(1D) + H_2O$ reaction. The CS07A and SAPRC99 model runs with perturbed water vapor are similar spatially and in agreement with Steiner et al. (2006). The CS07A model response is shown in Figure 2-6. In areas with high NO_x and VOC emissions (generally urban areas), increased reactivity (via OH^\cdot production) has the effect of increasing ozone due to NO to NO_2 conversions that occur as a result of VOC oxidation (see middle column, bottom row of Figure 2-6). Steiner et al. (2006) propose that decreases in predicted ozone in the less populated southern and eastern portions of the modeling domain in response to higher water vapor result from increased HO_x radicals and peroxide production in these NO_x -limited regions. Another possibility in some locations is that the additional OH^\cdot could be directly scavenging ozone.

In updating to SAPRC07, the rate coefficient for $O(^1D) + H_2O$ was decreased, and the response to that change was discussed previously and can be seen in Figure 2-4. In SAPRC99 this rate coefficient was independent of temperature, but the newer mechanisms now include temperature dependence. The revised rate coefficient is lower than in SAPRC99 at atmospherically relevant temperatures, ranging from a 16% decrease at 275 K to a 6% decrease at 315 K (see Table 2-3). As expected, due to the lower rate coefficient, most locations show a slightly weaker response to the water vapor perturbation (column 2 of Figure 2-6) using CS07A.

Table 2-5 shows that ozone at Livermore and Fresno increases in response to the water vapor increase, and the magnitude of the increase is less for CS07A as expected in these consistently VOC-limited regions. In Bakersfield there is almost no response during E1, and for Sacramento and Bakersfield there is a negative ozone response to the increase in water vapor during E2. Both of these sites are located near the boundary between positive and negative ozone responses to humidity changes shown in Figure 2-6. At such locations the sign of the ozone response can vary depending on time of day and advection effects.

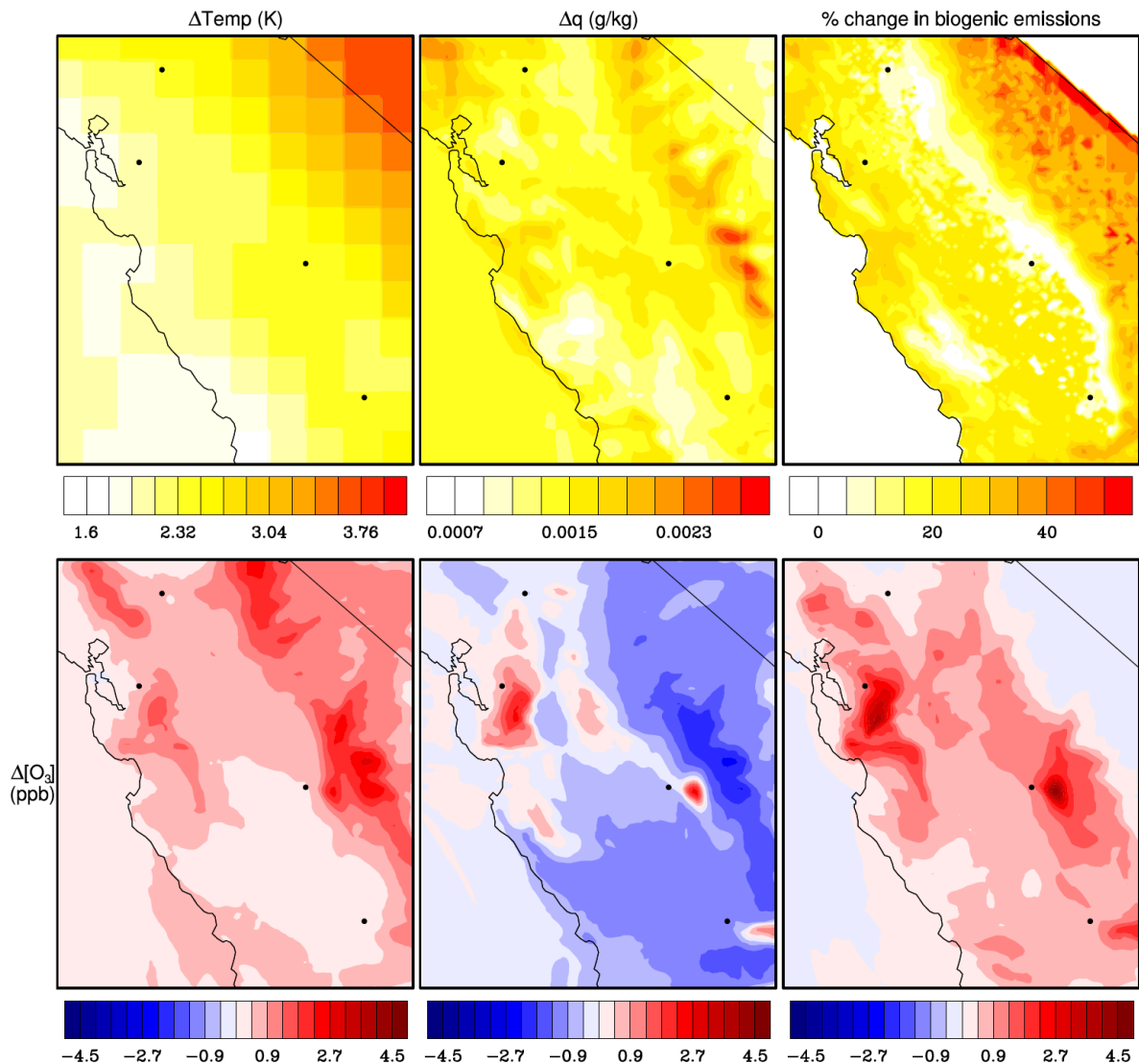


Figure 2-6. Effects of individual climate-change related perturbations on ozone air quality

The first row shows the magnitude of perturbations to temperature, absolute humidity, and biogenic VOC emissions. The second row shows ozone responses to each perturbation using CS07A. Red color indicates higher predicted ozone concentrations in response to variable perturbation. Weekday 3 pm E2 averages.

Biogenic VOC emissions

Increases in biogenic emissions of isoprene and terpenes result in higher ozone throughout the domain (see CS07A ozone response in the third column of Figure 2-6). Note that the lower the initial temperature, the larger the biogenic VOC emission perturbation. The difference in ozone response between SAPRC99 and CS07A is small. Table 2-5 shows that CS07A has a slightly stronger response than SAPRC99 to an increase in biogenic emissions for the cooler E1 at all sites, while the response is similar or slightly lower for the warmer E2. This was the only perturbation that resulted in different direction responses for the mechanism update between episodes at the same site.

The isoprene reactions were unchanged in CS07A, but changes to reactions involving products of isoprene oxidation can affect ozone concentrations. The photolysis rate of formaldehyde (HCHO) to give 2 HO₂ radicals + CO was increased by 19% in SAPRC07, and the positive ozone response is shown in Figure 2-4. The effects of changes in terpene reactions are less clear, because terpene oxidation product yields are tuned to match environmental chamber results. Terpene oxidation products include formaldehyde and lumped higher aldehydes (RCHO). The rate coefficient of the RCHO + OH· reaction was modified to include temperature dependence, and this reaction is now slightly slower at relevant atmospheric temperatures (differences range from 0.1% at 275 K to 5% at 315 K). This update has offsetting effects on ozone concentrations compared to the effects of revisions to the HCHO + *hν* rate coefficient. In any case, changes in ozone sensitivity to biogenic VOC emissions between mechanisms are small for both episodes.

Combined effects of climate-related perturbations

The combined climate simulation considers the aggregate effect of temperature, water vapor, and biogenic VOC emission perturbations together in one simulation. The ozone responses are presented for E2 in Figure 2-7 for both SAPRC99 and CS07A mechanisms. The results are similar, but a difference in response to the same perturbation between mechanisms (shown in the third column of Figure 2-7) shows that CS07A predicts slightly less ozone increase, on the order of 1 ppb difference in peak ozone at high-ozone locations for E1, and 1.5 ppb for E2. This result represents a noticeable downward revision in the assessment of climate change impacts since the ozone increases predicted by Steiner et al. (2006) for the combined climate simulation using SAPRC99 were on the order of 10 ppb.

Although a combined-climate simulation is considered here, note that the simulation is based on the available meteorological model with perturbations, and there are climate change parameters overlooked by the analysis that would require a new MM5 simulation driven by a regional climate model with an appropriate increase in atmospheric CO₂ (2×CO₂). These parameters include planetary boundary layer height and wind speed, both of which can affect ozone concentrations, but were held constant in the simulations presented in this chapter.

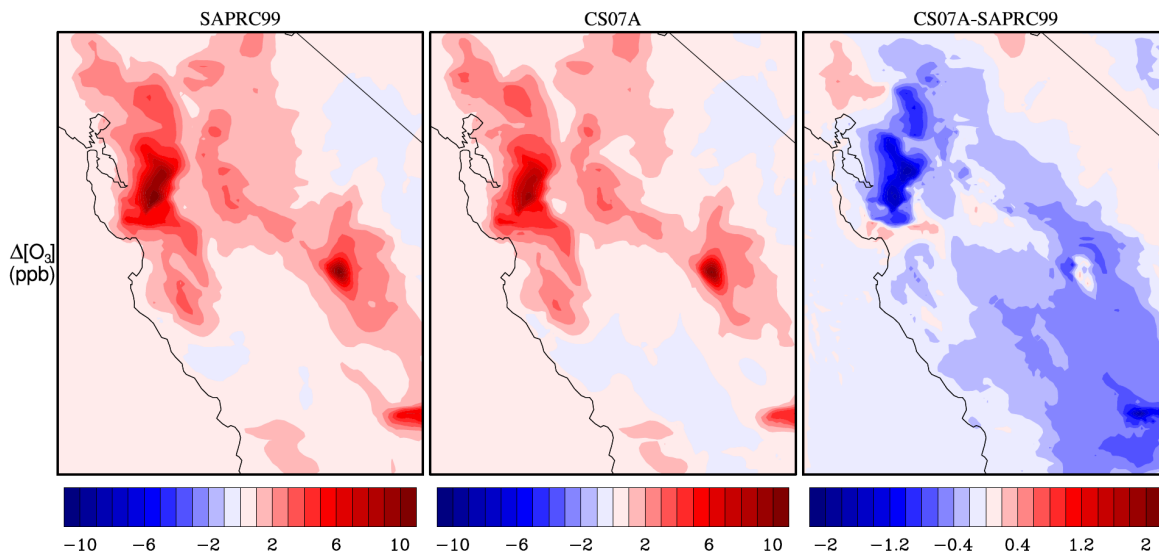


Figure 2-7. Ozone response to the combined climate change perturbation (temperature, humidity, and biogenic VOC) using SAPRC99 and CS07A mechanisms

The first two panels show mostly increases in ozone due to the climate change perturbations applied to AQM using SAPRC99 and CS07A. The last panel shows the difference in response to the same perturbation between mechanisms, with lower ozone sensitivity apparent in CS07A. Weekday 3 pm E2 averages.

2.4 Conclusions

In this chapter, the effects of using an updated chemical mechanism in a 3-D photochemical air quality model were evaluated for two air-pollution episodes modeled in central California. Predicted ozone concentrations were compared between CMAQ model simulations using a condensed version of the updated SAPRC07 mechanism (CS07A) and the earlier SAPRC99. The updated mechanism resulted in lower predicted ozone concentrations at all locations, and larger negative bias in peak ozone predictions. The degraded model performance in predicting ozone does not imply that the SAPRC07 mechanism is inferior to SAPRC99. Air quality modeling involves many other uncertainties such as boundary conditions, emissions, and meteorology that affect ozone concentrations and could serve as sources of compensating error in model predictions.

The increased $OH + NO_2$ reaction rate coefficient in the updated mechanism appears to be responsible for a considerable fraction of the decreases in ozone concentrations seen here, based on a systematic comparison between SAPRC99 and CS07A. It is important to note that there is still considerable uncertainty associated with the $OH + NO_2$ rate coefficient. After publication of the SAPRC07 mechanisms, Mollner et al. (2010) reported new rate coefficient parameters for this reaction, lowering the rate coefficient by 13% at 300 K and 1 atm as compared to the NASA (2006) recommended parameters used in SAPRC07. Use of these reaction rate parameters resulted in widespread increases in ozone concentrations, of up to 7 ppb, in a recently published (2010) southern California air quality model simulation (Mollner et al., 2010). The latest NASA (2011) chemical kinetics data evaluation cites the Mollner et al. study, but ultimately the recommended rate coefficient parameters from the 2006 evaluation are not altered. As this rate coefficient has been shown to be of great importance in air quality simulations, more precise and

accurate knowledge of the rate of the $\text{OH} \cdot + \text{NO}_2$ reaction rate is needed to increase confidence in air quality model predictions.

In general, ozone predictions developed using the newer CS07A mechanism were found to be slightly more sensitive to changes in both VOC and NO_x emissions at high-ozone sites than the ozone predictions determined with SAPRC99. The CS07A ozone predictions showed less sensitivity to the climate-related parameters, temperature and water vapor, and similar sensitivity to the biogenic VOC emissions as compared to SAPRC99. A combined climate simulation using the CS07A mechanism resulted in a smaller ozone response as compared to using SAPRC99.

The effect of condensing the updated mechanism was evaluated by comparing SAPRC07A with CS07A. The use of the condensed mechanism resulted in larger changes in predicted ozone concentrations than expected. Further study is needed to resolve the cause of the unexpected sign and magnitude of the ozone differences in the central California model domain. For the simulations in the following chapters, the more explicit SARPC07A is used as the base mechanism. Additionally, the Mollner et al. (2006) $\text{OH} \cdot + \text{NO}_2 \rightarrow \text{HNO}_3$ rate coefficient is implemented, allowing ozone predictions similar to those modeled using SAPRC99.

Chapter 3: Revised VOC lumping strategy

3.1 Introduction

3.1.1 Motivation

As discussed in Chapter 1, NO_x and VOC emitted into the atmosphere participate in complex chemical reactions that can result in elevated levels of tropospheric ozone, other oxidants, and particulate matter. These emissions are a critically important input for regional air quality models for studying ozone formation and transport. Direct NO_x emissions come from many sources but consist of just two compounds: nitric oxide (NO) and nitrogen dioxide (NO_2). In contrast, VOC emissions include thousands of different anthropogenic and biogenic compounds. Most individual VOC are not typically represented individually in air quality models due to the high computational burden associated with chemistry solvers that scales with the total number of species being tracked in the mechanism. As a result, most reaction mechanisms used for air quality modeling combine a large number of VOC into a much smaller number of lumped groups.

For example, in the SAPRC07A chemical mechanism (Carter, 2010c), there are 16 explicitly represented VOC, and all others are represented using 22 lumped model species. The reaction of each lumped model species is described by a surrogate species, either a specific compound or a mixture of compounds, that is used to represent the atmospheric chemistry of all compounds assigned to the lumped VOC group.

SAPRC07A and other mechanisms used for regional air quality modeling are fixed-parameter mechanisms, in which the compounds and weighting factors used to derive the reaction parameters for the lumped model species are pre-defined. The SAPRC07A mechanism has the same lumped species definitions as its predecessor, SAPRC99. Lumped species definitions were developed by Jeffries et al. (1989) based on measurements of VOC concentration in ambient air in 29 urban areas in the mid-1980s (Lonneman, 1986). The fixed-parameter SAPRC mechanism is widely used in both regulatory and research-oriented air quality modeling studies. A literature search does not reveal any air quality modeling studies in which the SAPRC lumped species definitions have been altered. The objective of the work presented in this chapter is to update the lumped VOC species definitions using a central California emission inventory and VOC emission speciation data. The new lumped VOC species definitions are compared to morning VOC measurements where available. The SARPC07A mechanism is updated with the revised lumped species, and air quality model simulations are performed to study the effect on predicted ozone concentrations. The specific steps taken to update the chemical mechanism, as well as the motivation for these changes, are presented below after a brief discussion of VOC reactivity.

3.1.2 VOC reactivity

Modeling is a useful tool for evaluating emissions reduction strategies and their effectiveness for ozone abatement. Early VOC-based control strategies involve limiting total VOC emissions on a

mass basis. However, each VOC can affect ozone formation differently, and a specific compound's ozone-forming potential is often referred to as its reactivity. Avery (2006) describes an interesting example of a proposed mass-based regulation for VOC emissions from varnish that would have almost doubled the ozone-forming potential of the regulated product, highlighting the importance of reactivity considerations in control strategy design.

The reactivity of a VOC is based on kinetic, mechanistic, and environmental factors (Carter, 1994). Reactivity depends heavily on reaction kinetics, i.e., the rate at which the VOC reacts in the atmosphere. For most VOC, reaction with the hydroxyl radical (OH[•]) is the dominant sink, but in some cases (e.g., aldehydes, alkenes, and aromatics), photolysis, reaction with NO₃ radicals, and reaction with ozone can be important as well (Atkinson, 2000). The mechanistic reactivity of an emitted VOC captures effects related to reactivity of the oxidation products formed after initial reaction with OH radical. Other components of mechanistic reactivity include the effect of VOC reaction on radical levels, and the number of NO to NO₂ conversions that occur for each molecule of VOC that reacts. Environmental factors include ambient VOC/NO_x ratio, sunlight, temperature, and water vapor concentration (Carter, 1994).

A widely used reactivity metric is OH-reactivity, which captures only kinetic effects on VOC reactivity. This metric is useful in comparing VOC reactivity between model simulations (Jeffries and Tonnesen, 1994; Tonse et al., 2008), and in comparing simulated VOC reactivity to reactivity calculated from VOC measurements (Steiner et al., 2008; Velasco et al., 2007). OH-reactivity can be calculated for any species that reacts with the OH radical, and thus is not limited to VOC. Incremental reactivity (IR; Carter, 1994) is a more comprehensive metric for VOC that captures mechanistic as well as kinetic effects on reactivity. The most commonly used maximum incremental reactivity (MIR) scale is calculated by adjusting NO_x levels to achieve maximum sensitivity of ozone to incremental additions of VOC in the base mixture.

3.2 Methods

3.2.1 Revised chemical mechanism overview

The base SAPRC07A mechanism is referred to as the Default mechanism throughout this chapter, while the mechanism developed in the chapter to more accurately describe VOC emissions is referred to as the Revised mechanism.

Lumped model species are defined based on molecular properties. VOC are first sorted by class, such as alkane, olefin, aromatic, aldehyde, and terpene. In most cases, each broad class is further partitioned into subgroupings based on VOC reaction rates with OH[•] (k_{OH}). Specific surrogate compounds are chosen to represent reactions of each lumped species group. The reaction rate coefficients and oxidation product yields for the lumped group are calculated as a suitably weighted average of corresponding values for a few of the main compounds assigned to the lumped group. The representation of many other compounds assigned to the same lumped group is therefore approximate, but still aims to be representative both in terms of reaction rate and atmospheric oxidation mechanism for all of the individual VOC that are lumped together.

Well-documented changes to anthropogenic VOC emissions that have occurred over the last several decades include reformulations of gasoline and efforts to reduce reactivity in solvent-

borne products (e.g. aerosol coatings regulation implemented by CARB). Changes that cannot be modeled accurately using existing lumped species definitions include an increase in use of oxygenated and polar molecules in fuels and solvents, as well as changes in the molecular weight ranges and structures of the hydrocarbons used in fuels. In this chapter, the lumped species definitions are updated to reflect changes in the composition of VOC emissions that have occurred since the 1980s.

Alcohol, amine, and ester emissions are lumped together with alkanes in the SAPRC mechanism according to their k_{OH} values, but were not used in defining the properties of the lumped alkane species. The first step in developing an improved reaction mechanism in this work was to create new lumped groups to represent these species and to track them separately from alkanes. The next step was to update all the lumped species definitions using contemporary VOC emission inventory data, speciated to the level of emissions of individual organic compounds. Finally, the method by which reaction parameters are determined was refined in order to describe the temperature dependence of the oxidation product yields more accurately. Details concerning these three steps are presented below.

Add new model species to the chemical mechanism

The emissions of oxygenated species (e.g., ethanol, methyl tert-butyl ether (MTBE), and various organic co-solvents associated with water-based surface coatings), which are lumped with alkanes in the Default mechanism, fixed-parameter SAPRC mechanism, have become a more significant part of the emission inventory. The blending of oxygenates such as ethanol and MTBE in gasoline has increased significantly since the 1980s (Renewable Fuel Association, 2010; USEPA, 2008) as a method to reduce exhaust emissions that contribute to photochemical smog. MTBE and ethanol use have followed different trajectories over time; use of MTBE in California was banned after 2002, due to concerns about groundwater contamination. Therefore these two oxygenates are tracked explicitly and separately in the Revised chemical mechanism. Another significant change in VOC emissions since the 1980s has been a large increase in organic co-solvent emissions associated with the use of water-based architectural coatings. This coincided with a decrease in use of oil-based solvents (CARB, 2005). With this shift comes an increase in alcohol, ester, and glycol ether co-solvents used in water-based coatings (CARB, 2005). Additionally, propyl acetate and amine emissions from animal waste, an important part of the emission inventory in agricultural areas, are by default lumped with alkanes. To represent these constituents more accurately, three new explicit VOC (ethanol, MTBE, and propyl acetate), and two new lumped groups (other oxygenated VOC and amines) were created. These changes to the mechanism facilitate model-observation comparisons of alkanes, since many of the oxygenated species are not routinely measured.

Table 3-1. Compounds and weighting factors used to represent ALK3

Default ALK3 speciation and five most prevalent compounds represented by ALK3 in year 2000 CARB emission inventory for SAPRC07 mechanism.

Default ALK3 emission representation		Emissions from ARB inventory categorized as ALK3	
n-butane	68%	ethanol	44%
isobutane	30%	MTBE	24%
2,2-dimethyl butane	2%	n-butane	12%
		propyl acetate	8%
		isobutane	5%

An illustrative example of the prevalence of oxygenated species can be seen in the ALK3 lumped species, which in the fixed-parameter mechanism, is used to represent reactions of alkanes, alcohols, and amines with k_{OH} between 2.5×10^3 and 5.0×10^3 ppm⁻¹ min⁻¹. ALK3 reactions are represented using the three most abundant alkanes assigned to the lumped group. Their individual reaction rate and oxidation product yield parameters are weighted by prevalence as determined from 1980s vintage data. Table 3-1 shows the fixed parameter, or Default, representation of ALK3 emissions compared to the mix of ALK3-assigned VOC emissions from a more recent CARB inventory. While the existing ALK3 definition is a relatively good approximation for the alkanes that are assigned to this lumped group, the emitted VOC classified as ALK3 are dominated by oxygenates. Similarly, the predominant ALK5 emissions are amines that are not included among the list of compounds that were used to define the reaction properties of the lumped group.

Update lumped species definitions

After oxygenates and amines were removed from the lumped alkane groups, new definitions were created for all of the major lumped model species (alkanes, olefins, and aromatics). Large changes in VOC emissions have occurred since the 1980s, in the absolute emissions and in the relative importance of various sources, as well as in the detailed chemical composition or speciation of the emissions. VOC emissions from gasoline-related transportation have decreased in magnitude, but increased in proportion, from 17% in 1985 to 28% of overall emissions in 2000 (see Table 3-4 in CARB, 2009a). This indicates that motor vehicle emissions should be a more important part of the lumped species definitions than in the fixed-parameter SAPRC mechanism. The decrease in vehicle-related VOC emissions is due mainly to implementation of California's low-emission vehicle and reformulated gasoline (RFG) program in the 1990s.

Phase 1 RFG requirements included a cap on Reid vapor pressure (RVP) to reduce evaporative emissions, mandatory addition of deposit-control additives, and the removal of lead from gasoline (CARB, 1990). Phase 2 RFG required further RVP reductions, as well as imposing limits on sulfur, benzene, total aromatics, total olefins, and fuel oxygen content. In addition to expected changes in liquid gasoline composition, Kirchstetter et al. (1999) report that the fuel changes also significantly altered the speciation of evaporative and tailpipe VOC emissions.

Subsequent fuel regulations required the phase-out of MTBE from gasoline by the end of 2002 due to concerns about contamination of groundwater (CARB, 2000). Ethanol replaced MTBE in gasoline, but use of ethanol in fuel was not yet widespread in the summer of 2000. Similar though less far-reaching programs to reformulate gasoline have been implemented in ozone non-attainment areas throughout the US. Furthermore, various federal mandates have required increased blending of ethanol in gasoline nationwide.

Because lumped species assignments are defined based on ranges of values for k_{OH} , many of the major changes in emission speciation and reactivity over time are captured in the fixed parameter version of the mechanism simply from redistribution of VOC emissions to different lumped groups (e.g., increased alkane and decreased aromatic content in gasoline). However, other changes such as increased blending of ethanol and highly branched alkanes (e.g., 2,2,4-trimethylpentane) in gasoline cannot be modeled using existing versions of the SAPRC mechanism.

The updated lumped species definitions are compared with Sacramento data for the year 2000 summer described by Steiner et al. (2008) from the Photochemical Assessment Monitoring Stations (PAMS) network. The 3-hour average data (5-8 am) from morning samples are used to ensure that the ambient VOC composition is well aligned with fresh emissions. Additional comparisons are made with VOC measurements made at Granite Bay, a suburb of Sacramento, in the summer of 2001 (Rubin et al., 2006), and early fall in Los Angeles in 1995 (Fujita et al., 1997).

3.2.2 Air quality modeling

The effects of the above changes to the representation of VOC in the chemical mechanism were analyzed in a step-wise fashion using a 3-D air quality model applied to central California. The main objective is to determine how Revised lumped VOC species definitions affect predicted ozone concentrations. An analysis of OH-reactivity was conducted to assist in interpreting the ozone response to the chemical mechanism revisions.

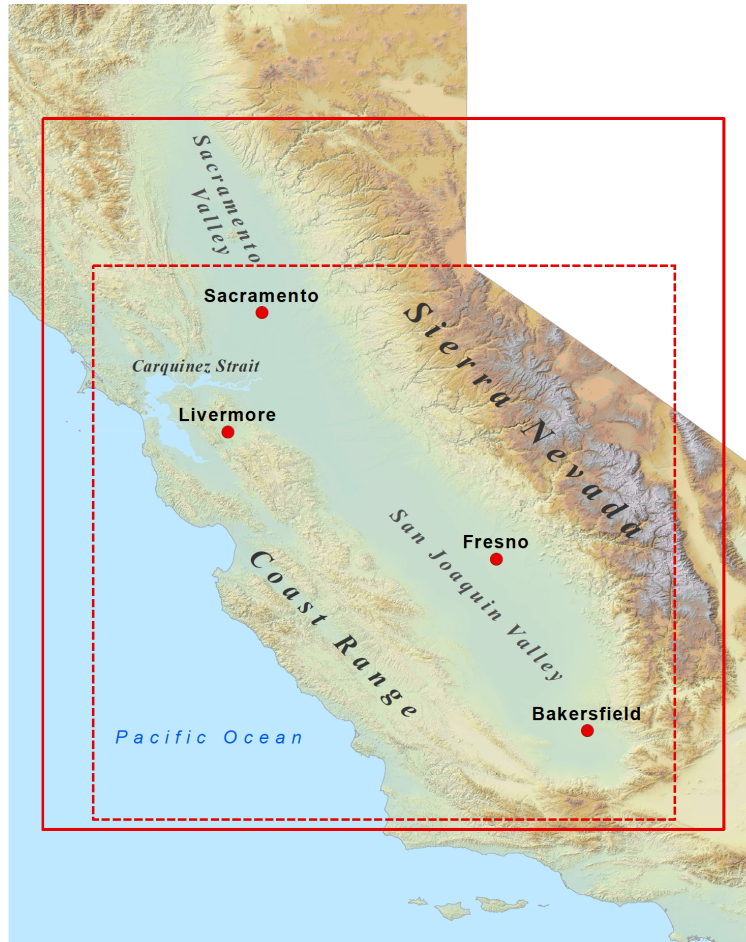


Figure 3-1. Map of air quality modeling domain

Domain used in this study outlined in solid red; previously used smaller modeling domain from Chapter 2 outlined with dotted red lines.

The air quality model used in this research is CMAQ, as in Chapter 2, with standard and modified versions of the SAPRC07A chemical mechanism. The model domain for the simulations presented in this and subsequent chapters is similar to the domain used in Chapter 2, but has been expanded to the north to reduce the effects of boundary condition uncertainties in high-ozone areas of the Sacramento Valley. The new 110×150 grid has 4-km horizontal resolution and is shown as a solid red rectangle in Figure 3-1. The red dotted rectangle shown in the same figure outlines the previously used smaller modeling domain from Chapter 2. To keep computational time reasonable for this larger modeling domain, vertical layers were reduced from 27 to 17 by combining the highest model layers, while maintaining fine vertical resolution near the ground where most of the emissions occur.

3.2.3 VOC emissions

The SAPRC07A chemical mechanism used in this analysis was the version that had the least condensed representation for VOC species that is still appropriate for regional ozone modeling. A list of VOC species defined in SAPRC07A and short descriptions are presented in Table 3-2. The shaded species in the table are those that were added to the mechanism as described above. The aldehyde and other oxygenated VOC categories have been separated from the anthropogenic and biogenic emission categories because these species are present in the atmosphere due both to primary emissions (anthropogenic and/or biogenic), and as oxidation products of primary VOC emissions. Therefore, altering lumped species definitions based only on emissions data is not appropriate.

Table 3-2. Descriptions of SAPRC07A VOC categories

Shaded species are new for the Revised mechanism; emissions are lumped with alkanes in the Default mechanism.

SAPRC category	Description	Species representation ¹
Primary Anthropogenic (AVOC)		
ACYE	Acetylene	--
BENZ	Benzene	--
ETHE	Ethene	--
CH4	Methane	--
ALK1	Non-aromatic alkanes, $1.36\text{e-}13 < k_{OH}^2 < 3.41\text{e-}13$	Ethane
ALK2	Non-aromatic alkanes, $3.41\text{e-}13 < k_{OH} < 1.70\text{e-}12$	Propane
ALK3	Non-aromatic alkanes, $1.70\text{e-}12 < k_{OH} < 3.41\text{e-}12$	*
ALK4	Non-aromatic alkanes, $3.41\text{e-}12 < k_{OH} < 6.81\text{e-}12$	*
ALK5	Non-aromatic alkanes, $k_{OH} > 6.81\text{e-}12$	*
OLE1	Alkenes (other than ethene), $k_{OH} < 4.77\text{e-}11$	*
OLE2	Alkenes, $k_{OH} > 4.77\text{e-}11$	*
ARO1	Aromatics, $k_{OH} < 1.36\text{e-}11$	*
ARO2	Aromatics, $k_{OH} > 1.36\text{e-}11$	*
AMIN	Lumped Amines	*
Biogenic (BVOC)		
ISOP	Isoprene	--
TERP	Terpenes	*
Aldehydes (ALD)		
GLY	Glyoxal	--
MGLY	Methyl glyoxal	--
HCHO	Formaldehyde	--
CCHO	Acetaldehyde	--
RCHO	Lumped C3+ aldehydes	Propionaldehyde
BALD	Aromatic aldehydes	Benzaldehyde
Other Oxygenated (OXVOC)		
ACET	Acetone	--
MEOH	Methanol	--
ETOH	Ethanol	--
UPOH	Lumped C3+ alcohols	*
PACET	Propyl acetate	--
MTBE	Methyl tert-butyl ether	--
MVK	Methyl vinyl ketone	--
MACR	Methacrolein	--
CRES	Phenols and cresols	o-Cresol
MEK	Ketones, $k_{OH} < 5\text{e}12$	Methyl ethyl ketone
PRD2	Ketones, $k_{OH} > 5\text{e}12$	*

¹ "--" indicates explicit species, "*" indicates that a mixture of compounds represents species

² $k_{OH} = [\text{cm}^3 \text{ molecule}^{-1} \text{ s}^{-1}]$

Speciated emissions of VOC and other pollutants, resolved by grid cell and time of day, were available from previous modeling efforts (Jin et al., 2010). These were updated (respecified) to match the level of chemical resolution in SAPRC07A as described in Chapter 2. The spatial distribution of primary anthropogenic, biogenic, aldehydes, and other oxygenated VOC, are presented in Figure 3-2. Anthropogenic emissions are concentrated in urban areas and along heavily traveled roadways, while biogenic emissions are mainly in the Sierra Nevada and coastal mountain ranges. The direct aldehyde emissions are mostly anthropogenic, while the other oxygenated category emissions have a large biogenic component due to acetone and methanol emissions from vegetation.

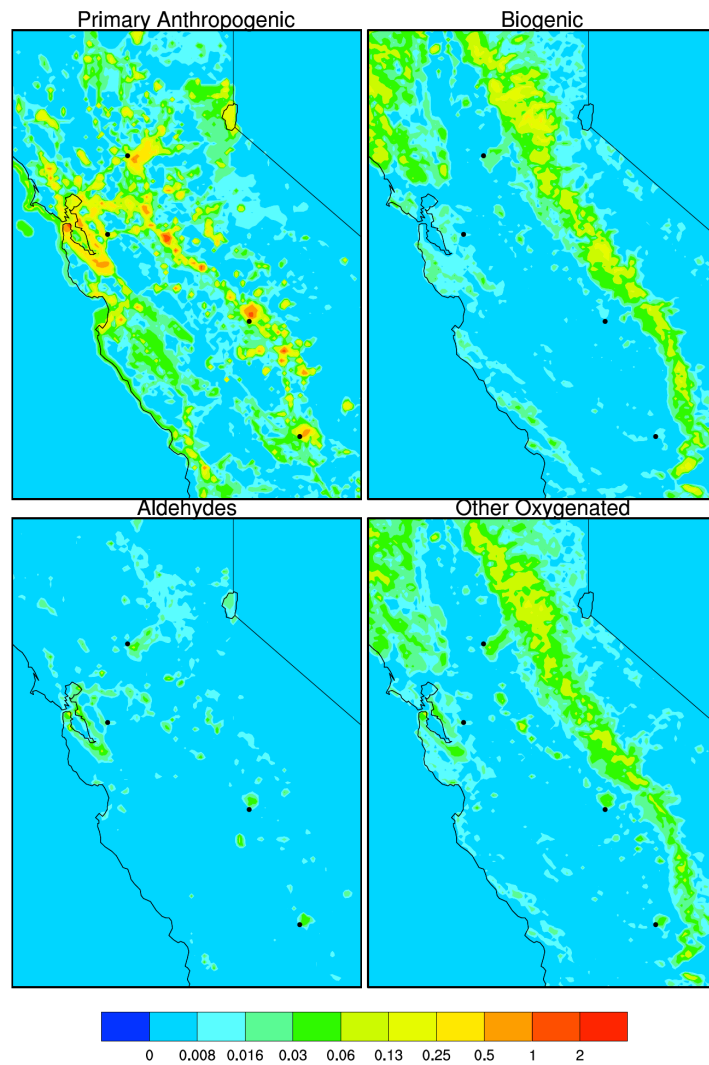


Figure 3-2. VOC emission maps (mol/s)
Weekday 8 am average, note scale on label bar is not linear.

The focus of this work is on anthropogenic VOC, as the goal is to update lumped species definitions based on current emissions data. For the anthropogenic emissions, it was verified that ALK1 and ALK2 species are dominated (over 99% by mole fraction) by ethane and propane, respectively. No changes to existing definitions were made for these species. New lumped species definitions were developed for the more reactive alkanes (ALK3, ALK4, and ALK5), olefins (OLE1 and OLE2), and aromatics (ARO1 and ARO2). New organic species were added to limit the species assigned to the ALK1-ALK5 lumped groups to hydrocarbons only. Table 3-3 shows the compounds and weighting factors used to define the surrogate species in the Default SAPRC07A mechanism, as well as the weighting factors for the Revised mechanism developed in this research. These changes are described further in the following sections.

Table 3-3. Compounds and weighting factors used to derive parameters for lumped species

Both Default and Revised mechanism definitions shown. Shaded compounds are not tracked separately in the Default SAPRC07A mechanism (Carter, 2010a).

Group & Compound	Default Molar Fraction	Revised Molar Fraction	Group & Compound	Default Molar Fraction	Revised Molar Fraction
<u>ALK3</u>			<u>ALK5</u>		
n-Butane	68%	59%	2,4-Dimethylhexane	12%	5.9%
Isobutane	30%	30%	n-Decane	11%	--
2,2-Dimethylbutane	2%	11%	3-Methylhexane	11%	13%
			2,3-Dimethylpentane	6.7%	10%
<u>ALK4</u>			2-Methylheptane	6.0%	3.9%
Isopentane	43%	41%	4-Methylheptane	6.0%	--
n-Pentane	18%	12%	2,4-Dimethylheptane	5.1%	--
2-Methylpentane	10%	10%	2,6-Dimethyloctane	4.7%	--
3-Methylpentane	7.4%	6.4%	Methylcyclohexane	4.4%	8.3%
2,4-Dimethylpentane	4.7%	--	n-Nonane	4.4%	--
Methylcyclopentane	4.6%	7.0%	n-Octane	4.4%	8.9%
n-Hexane	3.7%	7.8%	Cyclohexane	4.1%	15%
n-Heptane	3.4%	--	2-Methylnonane	3.3%	--
2,3-Dimethylbutane	3.1%	4.9%	2-Methylhexane	3.1%	14%
Cyclopentane	2.0%	2.3%	2-Methyloctane	2.5%	--
1,1-Dimethylcyclopentane	0.1%	--	4-Methyloctane	2.5%	--
2,2,4-Trimethylpentane	--	8.1%	n-Dodecane	1.9%	--
<u>UPOH</u>			4-Methylnonane	1.4%	--
Isopropyl alcohol	--	79%	Ethylcyclohexane	1.1%	--
Ethylene glycol	--	7%	n-Undecane	1.0%	--
Propylene glycol	--	8%	3,6-Dimethyldecane	1.0%	--
Ethanolamine	--	6%	2,6-Dimethylnonane	0.5%	--
<u>AMIN</u>			3-Methylundecane	0.5%	--
Ethylamine	--	63%	5-Methylundecane	0.5%	--
Trimethylamine	--	37%	3-Methyldecane	0.3%	--
			4-Methyldecane	0.3%	--
			1,2-Dimethylcyclopentane	0.1%	--
			Ethylcyclopentane	0.1%	--
			n-Tridecane	0.09%	--
			3,6-Dimethylundecane	0.03%	--
			3-Methyldodecane	0.02%	--
			5-Methyldodecane	0.02%	--
			Hexadecane	--	8.3%
			1,3-Dimethylcyclopentane	--	5.5%
			3-Methylheptane	--	4.2%
			1,3-Dimethylcyclohexane	--	3.0%

Table 3-3. (continued)

Group & Compound	Default Molar Fraction	Revised Molar Fraction	Group & Compound	Default Molar Fraction	Revised Molar Fraction
<u>OLE1</u>			<u>ARO1</u>		
Propene	29%	81%	Toluene	75%	81%
1-Hexene	24%	1%	Ethylbenzene	10%	10%
1-Butene	12%	9%	C11 Monosubstituted benzenes	5%	--
1-Pentene	11%	5%	n-Propylbenzene	4%	3%
1-Heptene	11%	--	C10 Monosubstituted benzenes	3%	--
1-Nonene	4.8%	--	Isopropylbenzene	2%	1%
3-Methyl-1-butene	3.0%	4%	t-Butylbenzene	1%	5%
1-Octene	2.2%	--	C12 Monosubstituted benzenes	0.2%	--
1-Undecene	1.8%	--			
1-Decene	0.9%	--			
<u>OLE2</u>			<u>ARO2</u>		
Cis-2-pentene	14%	4%	m-Xylene	13%	21%
Trans-2-pentene	14%	7%	p-Xylene	13%	21%
Trans-2-butene	11%	4%	o-Xylene	11%	13%
Isobutene	10%	46%	1,2,3-Trimethylbenzene	9%	4%
Cis-2-butene	9%	3%	1,3,5-Trimethylbenzene	9%	4%
2-Methyl-1-butene	8%	7%	1,2,4-C10 Trisubstituted benzenes	6%	--
1,3-Butadiene	6%	10%	m-Ethyltoluene	5%	12%
2-Methyl-2-butene	5%	14%	o-Ethyltoluene	5%	6%
Cis-2-hexene	5%	--	p-Ethyltoluene	5%	7%
Trans-2-hexene	5%	--	1,2,4-Trimethylbenzene	5%	12%
Trans-3-heptene	4%	--	1,2,3-C10 Trisubstituted benzenes	4%	--
Trans-4-nonene	2%	--	1,3,5-C10 Trisubstituted benzenes	2%	--
Trans-4-octene	2%	--	1-Methyl-4-Isopropylbenzene	2%	--
Trans-2-heptene	2%	--	m-C10 Disubstituted benzenes	2%	--
Trans-5-undecene	2%	--	o-C10 Disubstituted benzenes	2%	--
Cyclohexene	2%	--	p-C10 Disubstituted benzenes	2%	--
Trans-4-decene	0.9%	--	m-C11 Disubstituted benzenes	0.4%	--
Cyclopentene	--	5%	1,3,5-C12 Trisubstituted benzenes	0.3%	--
			m-C12 Disubstituted benzenes	0.2%	--
			p-C12 Disubstituted benzenes	0.2%	--
			1,2,4-C11 Trisubstituted benzenes	0.2%	--
			1,2,3-C11 Trisubstituted benzenes	0.2%	--
			1,3,5-C11 Trisubstituted benzenes	0.2%	--
			1,2,4-C12 Trisubstituted benzenes	0.1%	--
			1,2,3-C12 Trisubstituted benzenes	0.1%	--
			o-C11 Disubstituted benzenes	0.1%	--
			p-C11 Disubstituted benzenes	0.1%	--
			o-C12 Disubstituted benzenes	0.1%	--

Emission estimates used in this study were available by major source category, which included motor vehicle, area, point, and biogenic sources. An example of a weekly time series of the domain-wide sum of the alkanes, olefins, and aromatics are shown by emission category in Figure 3-3. Day of week differences are apparent in the motor vehicle, area, and point source categories; these differences do not vary from week to week. The domain-wide sum of the point source category is taken to be the same from week to week, but emissions may be lofted to different heights depending on day- and location-specific meteorology. The biogenic source category is the only category that is different each day and from week to week, with differences due to temperature, light intensity, and moisture. Motor vehicle and area source categories contribute an order of magnitude more emissions to alkane, aromatic, and olefin (OLE1-2, group does not include isoprene and terpenes) than point or biogenic sources, so only emissions from these sources were considered in creating new lumped species definitions.

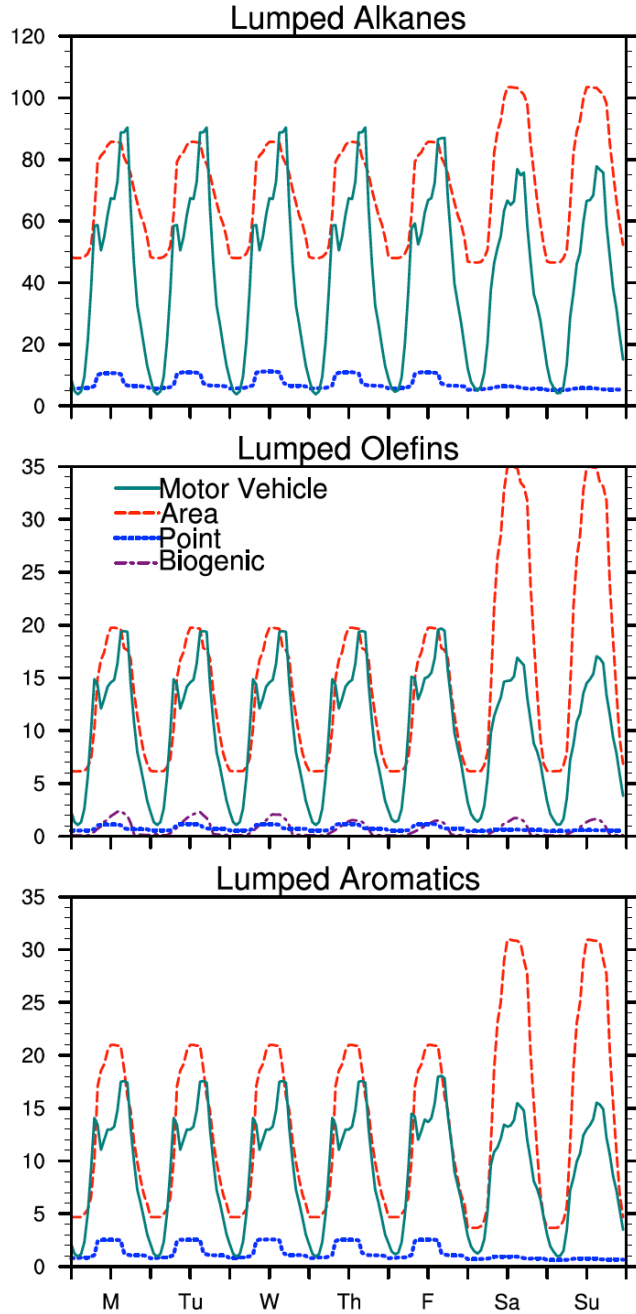


Figure 3-3. Lumped VOC emission time series (mol/s)

Lumped alkanes (ALK3+ALK4+ALK5), olefins (OLE1+OLE2), and aromatics (ARO1+ARO2). Sum over the model domain shown in Figure 3-1 is presented. Source of data is the Default CARB provided AQM emissions.

Detailed county-wide and air basin-wide VOC emission estimates are available (CARB, 2009b). These data are presented in terms of both total organic gas (TOG) and reactive organic gas (ROG) emissions by category in tons per day. ROG excludes emissions of methane, and various other low-reactivity organics, which makes ROG more closely aligned to the lumped groups of interest in this research. However, TOG emissions estimates are used in this analysis, as

emission speciation profiles include all organics including the low-reactivity molecules. Using TOG emissions and appropriate speciation profiles for motor vehicle and area source emissions, new recipes (assigned species and their relative abundances) were developed for many of the lumped model species in the SAPRC07A mechanism.

Table 3-4 shows organic gas emissions for the San Francisco Bay (SFB) area and the San Joaquin Valley (SJV) air basins. These basins are responsible for most of the emissions in the central California study domain. A map showing the counties in the modeling domain is shown in the Appendix (Figure A-1), and the more detailed county level data can be found in Table A-1. Emissions from gasoline-powered motor vehicles are the largest anthropogenic source of ROG. Gasoline-related emissions from off-road mobile sources are included with area source rather than on-road vehicle emissions; inclusion of off-road gasoline engine emissions further strengthens the conclusion about the dominance of gasoline-related sources of VOC emissions.

Table 3-4. Total organic gas (TOG) and reactive organic gas (ROG) emissions by emission category.

Tons per day (year 2000 daily average) from anthropogenic sources estimated by CARB (2009b). Data at county level for entire domain presented in Table A-1 in the Appendix.

Emission Category	Emission File	Air Basin			
		San Francisco Bay		San Joaquin Valley	
		TOG	ROG	TOG	ROG
On-Road Gasoline	MV	236.4	218.2	123.7	114.5
Off-Road Gasoline	Area	106.0	95.6	75.1	67.3
Diesel	MV	4.8	4.3	18.6	16.4
Consumer Products	Area	100.4	46.6	49.0	22.7
Animal Waste Decomposition	Area	65.7	5.3	747.7	59.8
Architectural Coatings - Oil Based	Area	12.2	11.7	5.9	5.7
Architectural Coatings - Water Based	Area	8.3	8.3	4.0	4.0
Consumer Aerosols	Area	6.0	4.2	2.8	2.0
Thinning & Cleanup Solvents	Area	3.4	3.3	1.6	1.6
Non-Methyl Bromide Pesticides	Area	0.8	0.8	20.9	20.9
Methyl Bromide Pesticides	Area	0.3	0.3	4.3	4.3

Motor vehicle emissions

In central California as of 2000, on-road mobile emissions accounted for 30% of all ROG emissions. Mobile emissions are primarily gasoline-related, accounting for 85% of motor vehicle ROG emissions in the domain, with the remainder attributed to diesel engine emissions. Gasoline related ROG emissions are comprised of tailpipe exhaust, evaporative emissions (headspace vapor emissions), and liquid emissions due to leaks in the fuel system and spillage at service stations. Rubin et al. (2006) found, by chemical mass balance, that headspace vapor emissions accounted for 17% by weight of gasoline-related motor vehicle emissions on average in the Sacramento area during summer 2001, with variation from day to day depending on ambient temperature. This number is in good agreement with an earlier study, which concluded that 14%

of gasoline-related emissions were evaporative, and 18% were from liquid gasoline (Fujita et al., 1995). For this study, definition of lumped VOC species proceeded from an assumed mix of 17% of emissions coming from headspace vapors as per the more recent study, 18% from liquid gasoline, and the remaining 65% of gasoline-related emissions due to exhaust. Each of these categories has a different speciation profile. Headspace vapor emissions are enriched in lower molecular weight VOC as compared to liquid gasoline. Vapor pressure increases with decreasing size for VOC with similar structure, so the ratio of evaporative to liquid sources increases as molecular weight decreases. Exhaust emissions of VOC include both unburned fuel and fuel-derived hydrocarbon fragments and partially oxidized products (e.g., ethane, ethene, acetylene, propene, formaldehyde), many of which are not present in liquid gasoline.

In order to create new lumped VOC definitions, gasoline speciation data collected closest to the year 2000 from within the model domain were used to represent VOC speciation for each category of gasoline-related emissions: liquid, evaporative, and tailpipe. Rubin et al. (2006) report the sales-weighted average composition of gasoline collected from the service stations of five major brands in the Sacramento area in the summer of 2001. The liquid gasoline was analyzed by gas chromatography, specifics of which can be found in Kirchstetter et al. (1999). At that time, one refiner used ethanol as the gasoline oxygenate and four others used MTBE. With the liquid gasoline data, Rubin et al. (2006) calculated the corresponding average headspace vapor speciation using the vapor-liquid equilibrium theory; details of the methodology are presented in Harley et al. (2000).

Kirchstetter et al. (1999) found a linear relationship between weight fractions of many alkanes in exhaust emissions and liquid gasoline. This result proves useful for detailed study of alkane speciation in vehicle exhaust, as emission studies typically do not include as complete a list of VOC species in the measurements. However, due to the eventual lumping of species present in gasoline in smaller amounts with other compounds that are more abundant, use of exhaust data from the Caldecott Tunnel studies results in a similar speciation in the case of the alkanes. To represent tailpipe exhaust emissions, data from more recent Caldecott Tunnel studies (Harley and Kean, 2004) were used, allowing for a consistent methodology for all alkane, olefin, and aromatic lumped species. The tunnel data correlate well with tailpipe speciation determined via dynamometer testing of vehicles running on California phase 2 reformulated gasoline (Schauer et al., 1999).

The gasoline VOC were sorted into SAPRC07A lumped species groups to define new surrogate species mixtures to represent the atmospheric chemistry of each lumped group. Compounds from the ALK3 and ALK4 categories and their corresponding weight fractions are shown in Table 3-5, sorted from most to least prevalent in liquid gasoline. The entire list of gasoline-related VOC is presented in Table A-2 (see Appendix). ALK3 is the only lumped species in which some of the most prevalent VOC emissions, MTBE and ethanol, are not used at all in defining the lumped species properties, since these oxygenates are now tracked separately in the Revised mechanism. Other prevalent gasoline species not used in the lumped alkane definitions include ethanol, 2,2,4-trimethyl pentane, 1,3-dimethylcyclopentane, 3-methylheptane, 1,3-dimethylcyclohexane, and cyclopentene.

Table 3-5. Gasoline-related VOC emission speciation (ALK3 and ALK4)

Original data from Harley and Kean (2004). All species are shown in Table A-2 in the Appendix.

Group & Compound	Class	Sacramento	Sacramento	Caldecott	Caldecott
		2001	2001	1999	2001
		Liquid Gasoline	Headspace Vapors	Tunnel Emissions	Tunnel Emissions
ALK3		wt %	wt %	wt %	wt %
MTBE	ether	10.57	15.97	3.74	3.79
2,2-Dimethylbutane	branched	0.96	1.81	1.56	0.9
Butane	straight	0.89	8.90	1.68	1.43
Ethanol	alcohol	0.86	1.22	--	--
2-Methylpropane	branched	0.17	2.43	0.22	0.29
2,2-Dimethylpentane	branched	0.11	0.08	--	--
3,3-Dimethylpentane	branched	0.11	0.06	--	--
ALK4					
2-Methylbutane	branched	7.51	29.82	10.72	8.55
2-Methylpentane	branched	3.55	4.68	3.04	4.14
Pentane	straight	2.83	8.52	2.85	2.72
Methylcyclopentane	cyclic	2.76	2.40	--	--
3-Methylpentane	branched	2.19	2.59	2.43	2.26
2,2,4-Trimethylpentane	branched	1.93	0.65	3.54	2.75
Hexane	straight	1.90	1.82	1.45	1.32
Heptane	straight	1.61	0.51	0.98	0.8
2,3-dimethylbutane	branched	1.14	1.64	--	--
2,3,3-Trimethylpentane	branched	0.97	0.18	--	--
2,3,4-Trimethylpentane	branched	0.95	0.18	1.58	1.07
2,4-Dimethylpentane	branched	0.73	0.48	--	--
Cyclopentane	cyclic	0.52	0.98	0.52	0.76
2,2,5-Trimethylhexane	branched	0.38	0.05	--	--
1,1,3-Trimethylcyclopentane	cyclic	0.14	0.04	--	--
2,2,3-Trimethylpentane	branched	0.11	0.03	--	--
2,4,4-Trimethylhexane	branched	0.08	0.01	--	--
3,3-Dimethylhexane	branched	0.06	0.01	--	--
2,2-Dimethylhexane	branched	0.05	0.01	--	--
3,3-Dimethylheptane	branched	0.04	0.00	--	--
2,2,3-Trimethylbutane	branched	0.04	0.02	--	--
2,2,3-Trimethylhexane	branched	0.03	0.00	--	--
4,4-Dimethylheptane	branched	0.02	0.00	--	--
2,2-Dimethylheptane	branched	0.02	0.00	--	--
1,1,2-Trimethylcyclopentane	cyclic	0.006	0.00	--	--
1,1-Dimethylcyclopentane	cyclic	0.002	0.00	0.67	0.98

Compounds representing diesel fuel are also missing from the lumped species definitions. Less information is available regarding the speciation of diesel emissions. For this analysis an assumption was made that liquid emissions from diesel are the same proportion as from gasoline, 18%, and the other 82% are exhaust emissions. Evaporation emissions from diesel fuel are trivial due to the low vapor pressure of diesel fuel and much lower sales volumes compared to gasoline. Liquid fuel and exhaust speciation profiles were obtained from a dynamometer study of emissions from medium duty diesel trucks (Schauer et al., 2002). Over 60% of the resolvable compounds in diesel fuel by weight are straight long chain alkanes (Schauer et al., 2002), with a median carbon number of 16 (Chevron Products Co., 1998; Schauer et al., 2002); all diesel fuel n-alkanes are represented with hexadecane (C₁₆H₃₄) in the Revised mechanism. The ALK5 species, in which hexadecane and the other long-chain alkanes are lumped, is the only category significantly altered by including diesel emissions, because many of the other prevalent ROG emissions in diesel exhaust (ethene, acetylene, formaldehyde, and acetaldehyde) are already explicitly represented in SAPRC07A. More recent work using vacuum-ultraviolet single-photon ionization mass spectrometry determined that the unresolved compounds in diesel fuel are mostly branched and cyclic alkanes, although straight chain alkanes still predominate (Isaacman et al., 2012).

Area source emissions

In the model domain, off-road gasoline-related emissions account for almost 50% of the area source ROG emissions. These emissions were represented with the same speciation developed in the previous section for on-road motor vehicle emissions. Other large sources of ROG emissions are consumer product, pesticide, and animal waste decomposition emissions. While consumer products are the highest non-gasoline VOC emission source in the SF Bay area, animal waste decomposition, primarily from dairy cattle, and pesticide emissions dominate in the SJV. This is expected as the SF Bay area is heavily urbanized with little agricultural activity, while in contrast the SJV is a highly productive agricultural region.

Consumer product emissions inventoried by CARB include 138 sub-category sources, each with its own organic speciation profile (CARB, 2010). Examples of important consumer product categories include hair spray, multipurpose solvents, rubbing alcohol, general-purpose cleaners, and automotive windshield washer fluids. A speciation profile was created for consumer products, using an emissions-weighted average of the most important sources, accounting for over 80% of consumer product ROG emissions. The resulting speciation profile with associated distribution by lumped species groups is presented in Table 3-6; only the top 20 individual species are shown; however, 171 species were included in the analysis. Notice that pseudo-species such as “mineral oil” and “hydrocarbon propellant” are shown, and these are mixtures that have already been speciated using SAPRC07A (emitdb.xls, available at <http://www.engr.ucr.edu/~carter/emitdb/>). The simpler case is hydrocarbon propellant, of which 6.7% is assumed to be dimethyl ether assigned to ALK1, and remainder is propane, which is assigned to ALK2. A composite speciation profile for consumer product aerosol sprays, which contains 15 sub-categories of emissions, was created following the same methodology.

Table 3-6. Example VOC emission speciation for two categories

Estimates speciation from CARB year 2000 estimates (available at: www.arb.ca.gov/ei/speciate/speciate.htm)
 Shaded species indicate the lumping category changes with the update to the emissions use with the Revised mechanism.

Category & Species	Wt %	Mol Wt	Default	Revised
Consumer Products				
Mineral oil	20.3	110.1	Further Speciation	Further Speciation
Ethanol	16.3	46.1	ALK3	ETOH
Isopropyl alcohol	8.1	60.1	ALK4	UPOH
Methyl alcohol	5.7	32.0	MEOH	MEOH
Acetone	4.5	58.1	ACET	ACET
Volatile methyl siloxanes	4.4	296.6	NROG	NROG
Dichloromethane	3.7	84.9	ALK1	ALK1
2-Butoxyethanol	3.3	118.2	ALK5	UPOH
Isobutane	3.2	58.1	ALK3	ALK3
Toluene	2.3	92.1	ARO1	ARO1
p-Dichlorobenzene	2.3	147.0	ARO2	ARO2
Perchloroethylene	2.2	165.8	ALK1	ALK1
Ethanolamine	2.0	61.1	ALK5	UPOH
Propane	2.0	44.1	ALK2	ALK2
Isomers of xylene	1.6	106.2	ARO2	ARO2
n-Hexane	1.3	86.2	ALK4	ALK4
Pine oil	1.1	142.8	TERP	TERP
n-Butane	0.8	58.1	ALK3	ALK3
Hydrocarbon propellant (LPG)	0.8	44.1	Further Speciation	Further Speciation
n-Heptane	0.8	100.2	ALK4	ALK4
Animal Waste Decomposition				
Methane	70	16.0	CH4	CH4
Trimethylamine	1	59.1	ALK5	AMIN
Ethylamine	1	45.1	ALK5	AMIN
Isopropyl alcohol	2	60.1	ALK4	UPOH
Propyl acetate	2	102.1	ALK3	PACET
Ethanol	2	46.1	ALK3	ETOH
Ethane	20	30.1	ALK1	ALK1
Acetone	2	58.1	ACET	ACET

For animal waste decomposition, pesticides, and the rest of the major area source emission categories (water-based surface coatings, oil-based coatings, thinning and cleanup solvents), speciation profiles available from CARB (www.arb.ca.gov/ei/speciate/speciate.htm) were used directly. The speciation profile for livestock waste decomposition, which includes the smallest number of species, and the associated SAPRC07A species are presented in Table 3-6 as an example. The speciation profiles have been created by CARB for statewide modeling efforts.

As mentioned in the introduction to this chapter, MTBE and ethanol are not included in the Default recipe for ALK3, although they represent a large fraction of the gasoline-related VOC emissions assigned to ALK3 in the base mechanism. There are also important species emitted by area sources that are not represented in the definition of lumped alkane species groups. These include ethanol and propyl acetate (ALK3), isopropyl alcohol (ALK4), and trimethylamine and ethylamine (ALK5). The resolution in all cases was to lump these species separately from the alkanes using new lumped species groupings.

3.2.4 New model species

Significant non-alkane emissions, which in the Default SAPRC07 mechanism are lumped along with alkanes, include MTBE, ethanol (ETOH), propyl acetate (PACET), lumped higher alcohols and glycols (UPOH), and lumped amine species (AMIN). These species are now modeled using separated lumped groups in the Revised mechanism developed here. The reactions added to the chemical mechanism and their associated rate parameters were derived from highly explicit mechanisms used for VOC reactivity assessment in box model simulations (Carter, 2010a). The lumped species definitions were determined as described in the following section. The new reactions and associated rate parameters are shown in Table 3-7.

Table 3-7. Reactions and rate parameters for new species

Reaction & Products	Rate Parameters			
	k(300) ^{a,b}	A ^b	E _a /R ^c	b
ETOH + OH = .95*HO2 + .05*RO2R + .081*HCHO + .96*CCHO	3.21E-12	5.49E-13	-530	2
MTBE + OH = .743*RO2R + .162*MEO2 + .016*TBUO + .381*R2O2 + .078*RO2N + .234*HCHO + .024*ACET + .719*MEK + .007*PRD2	2.95E-12	5.89E-13	-483	2
PACET + OH = .44*RO2R + .494*RCO3 + .548*R2O2 + .066*RO2N + .012*CO + .001*HCHO + .041*CCHO + .05*RCHO + .348*MEK + .497*AACD + .009*PACD + .002*MGLY	3.40E-12	3.40E-12	--	--
AMIN + OH = .306*HO2 + .694*RO2R + PRD2	3.41E-11	3.41E-11	--	--
AMIN + O3 = RO2R + OH + PRD2	2.91E-18	2.91E-18	--	--
AMIN + NO3 = .32*HO2 + .68*RO2R + HNO3 + PRD2	1.37E-13	1.37E-13	--	--
UPOH + OH = .902*HO2 + .097*RO2R + .074*HCHO + 0.105*CCHO + 0.029*RCHO + 0.732*ACET + 0.049*MEK + 0.049*PRD2	9.05E-12	6.91E-12	-81	--

$$^a k(T) = A \cdot (T/300)^B \cdot e^{-(E_a/RT)}$$

^bUnits of k(300) and A are [cm³ molec⁻¹ s⁻¹]

^cUnits of E_a/R are [K]

3.2.5 Lumped species definitions

After removing non-alkane emissions from the lumped alkane groups, motor vehicle and area source emission estimates were combined with corresponding speciation profiles to create new lumped species definitions for the ALK3-5, OLE1-2, ARO1-2 categories. The updated list of representative compounds and weighting factors was shown in Table 3-3 alongside the Default values; Table 3-8 shows the new weighting factors with the composition of VOC measurements made for three times and locations. Where measured data are available, agreement is clearly better than the Default in most cases. While presented for completeness, some problems were identified in the PAMS network data. The PAMS network does not measure the OLE2 species that are found to account for the largest percentage of emissions. Additionally, the PAMS agreement for the ALK5 and ARO1 species is particularly bad. Brown and Main (2002) found for the PAMS data in year 2000 and 2001, there was a problem with misidentification of the 2-methylheptane and toluene species. This problem in the data may contribute to the poor agreement between the Revised mechanism ALK5 and ARO1 species definitions and PAMS measurements. Additionally, Brown and Main (2002) found a gas chromatograph calibration problem that lead to falsely high concentrations of decane and undecane, species also lumped in ALK5, in some of the PAMS network data.

Table 3-8. Weighting factors used to derive parameters for SAPR07A lumped species – Comparison with measurements

Values calculated on a molar basis. Species without values (–) were not measured in the particular network.

Group & Compound	Revised Fraction	PAMS^a 2000	Sacramento^b 2001	Los Angeles^c 1995
ALK3				
n-Butane	59%	56%	--	65%
Isobutane	30%	36%	--	32%
2,2-Dimethylbutane	11%	8%	--	3%
ALK4				
Isopentane	41%	39%	46%	34%
n-Pentane	12%	14%	18%	18%
2-Methylpentane	10%	15%	24%	12%
n-Hexane	8%	--	--	6%
2,2,4-Trimethylpentane	8%	7%	8%	7%
Methylcyclopentane	7%	9%	--	9%
3-Methylpentane	6%	7%	--	7%
2,3-Dimethylbutane	5%	4%	--	3%
Cyclopentane	2%	3%	3%	2%
2,4-Dimethylpentane	--	2%	--	2%
ALK5				
Cyclohexane	15%	7%	--	9%
2-Methylhexane	14%	6%	--	12%
3-Methylhexane	13%	8%	--	17%
2,3-Dimethylpentane	10%	4%	--	12%
n-Octane	9%	3%	--	5%
Methylcyclohexane	8%	6%	--	16%
Hexadecane	8%	--	--	--
2,4-Dimethylhexane	6%	--	--	--
1,3-Dimethylcyclopentane	6%	--	--	--
2-Methylheptane	4%	32%	--	5%
3-Methylheptane	4%	3%	--	4%
1,3-Dimethylcyclohexane	3%	--	--	--
2,3,4-Trimethylpentane	--	--	--	5%
n-Decane	--	3%	--	13%
n-Heptane	--	7%	--	--
n-Nonane	--	2%	--	3%
n-Undecane	--	18%	--	--

^a original data described in Steiner et al. (2008)

^b original data described in Rubin et al. (2006)

^c original data described in Fujita et al. (1997)

Table 3-8. (continued)

Group & Compound	Revised Fraction	PAMS^a 2000	Sacramento^b 2001	Los Angeles^c 1995
<u>OLE1</u>				
Propene	81%	80%	80%	80%
1-Butene	9%	11%	8%	10%
1-Pentene	5%	9%	9%	7%
3-Methyl-1-butene	4%	--	4%	3%
1-Hexene	1%	--	--	--
<u>OLE2</u>				
Isobutene	46%	--	49%	46%
2-Methyl-2-butene	14%	--	16%	14%
1,3-Butadiene	10%	--	--	--
2-Methyl-1-butene	7%	--	12%	--
Trans-2-pentene	7%	23%	11%	11%
Cyclopentene	5%	--	2%	4%
Cis-2-pentene	4%	22%	5%	6%
Trans-2-butene	4%	28%	6%	7%
Cis-2-butene	3%	26%	--	6%
Cis-2-hexene	--	--	--	2%
Trans-2-hexene	--	--	--	6%
<u>ARO1</u>				
Toluene	81%	31%	86%	83%
Ethylbenzene	10%	45%	14%	12%
t-Butylbenzene	5%	--	--	--
n-Propylbenzene	3%	17%	--	3%
Isopropylbenzene	1%	8%	--	2%
<u>ARO2</u>				
m-Xylene	21%	34%	48%	24%
p-Xylene	21%	34%	27%	24%
o-Xylene	13%	6%	25%	18%
1,2,4-Trimethylbenzene	12%	2%	--	26%
m-Ethyltoluene	12%	--	--	--
p-Ethyltoluene	7%	1%	--	--
o-Ethyltoluene	6%	4%	--	--
1,2,3-Trimethylbenzene	4%	3%	--	--
1,3,5-Trimethylbenzene	4%	16%	--	8%

^aoriginal data described in Steiner et al. (2008)

^boriginal data described in Rubin et al. (2006)

^coriginal data described in Fujita et al. (1997)

The OH· reaction rate coefficients of alkanes have been found to increase with temperature (Atkinson, 1986), and the detailed SAPRC VOC species reaction rate parameters reflect this positive temperature dependence. In contrast, the method by which reaction parameters were defined for the lumped alkane species in SAPRC07 results in an incorrect negative temperature dependence for reactions of ALK3, ALK4, and ALK5. Figure 3-4 illustrates the negative temperature dependence of the Default ALK3 reaction (ALK3_D) as compared to the explicit species from which the lumped species is derived. Reaction parameters for all the lumped species were revised to describe correctly the actual temperature dependence of these reactions.

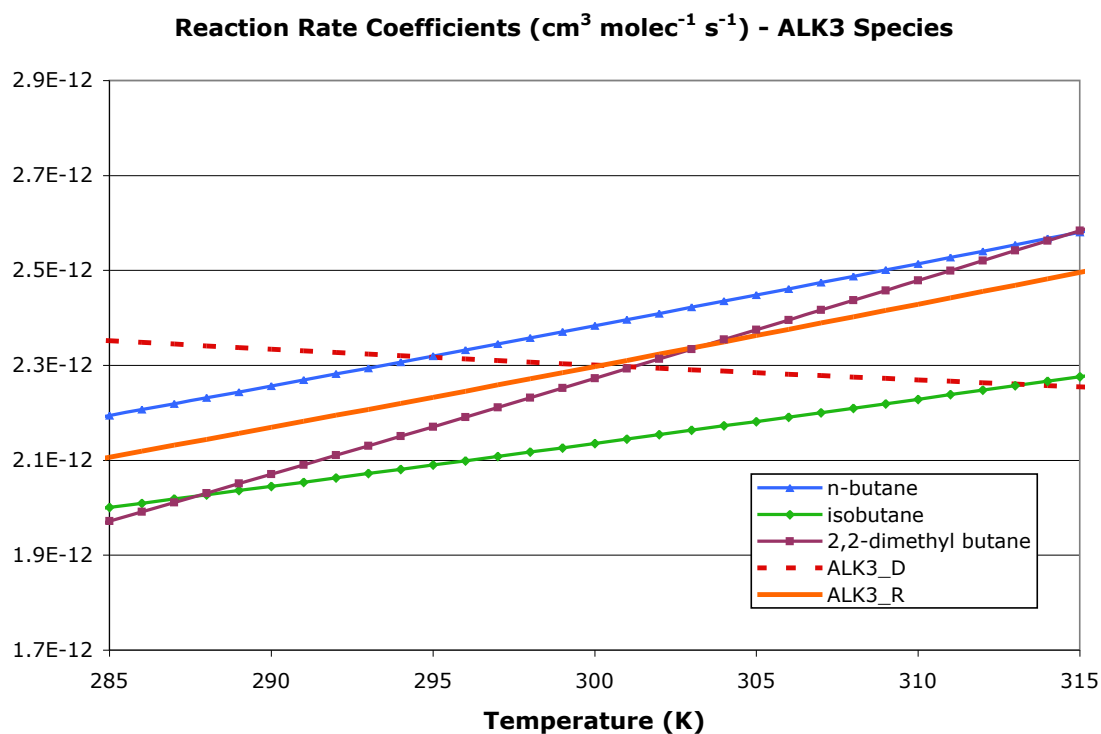


Figure 3-4. Temperature dependent VOC + OH· reaction rate coefficients

ALK3 is a weighted average of the explicit species. Revised ALK3 (ALK3_R) reaction rate parameters allow a better fit of reaction rate coefficient temperature dependence.

With the weighting factors, average product species and derived rate parameters, A and E_a , were calculated from estimates available for over 700 individual VOC in the most highly detailed version of the SAPRC07 mechanism used for reactivity assessment. The rate parameters are used to describe the temperature-dependent reaction rate coefficients using the Arrhenius expression of the form,

$$k(T) = A \times \exp\left(\frac{-E_a}{RT}\right) \quad (\text{E3.1})$$

where the units of $k(T)$ and A are cm³ molec⁻¹ sec⁻¹ and the units of E_a/R are K. In defining rate parameters for SAPRC07A, Carter calculated a weighted average activation energy for each

lumped species. However, in each of the lumped alkane groups, some of the species that define the groups have a temperature-dependent pre-exponential factor for reaction with OH[•] that can be calculated using,

$$A = A_0 \left(\frac{T}{300} \right)^b \quad (\text{E3.2})$$

Because this is not consistent for all species in the lumped group definitions, to determine the new rate parameters, a weighted average reaction rate coefficient for a wide range of atmospheric temperatures was calculated. From a graph of weighted average $\ln k$ versus $1/T$, the slope and y-intercept of a linear fit give the new lumped rate parameters: the slope corresponds to $-E_a/R$, and the y-intercept is the pre-exponential factor A . This updated method is used to calculate each of the lumped VOC species reaction rate parameters in the Revised mechanism.

3.2.6 Air quality model simulations

As previously mentioned, the Default mechanism in the simulations is SAPRC07A, with the OH[•] + NO₂ → HNO₃ reaction rate coefficient updated as described by Mollner et al. (2010). Simulations are performed in this chapter to determine if updating from the Default to the Revised mechanism changes ozone predictions in an air quality model in a significant way. Changes to the emission speciation and lumped species definitions described above in sections 3.2.4 and 3.2.5 were applied in a step-wise fashion to assess the effect of these changes separately. First, all the new species, MTBE, ETOH, PACET, UPOH, and AMIN, were separated from the lumped alkane emissions with which they were previously binned, and added and tracked separately in the Revised chemical mechanism. Next, the rate coefficients and reaction products of the lumped alkanes were altered according to their updated definitions. Further air quality model simulations were performed after additionally altering the lumped olefin species, and again after altering the lumped aromatic species definitions. The last model simulation encompasses all the changes to the chemical mechanism described above.

The CMAQ model was used to simulate air quality in central California. Following a 72-hour model spin-up period, step-wise model simulations are run for 3 days encompassing Episode 1 (E1; Tuesday, July 25 to Thursday July 27, 2000), as described in Chapter 2. Only the model simulations with Default SAPRC07A and final Revised mechanism were considered for Episode 2 (E2; Monday, July 31 to Wednesday, August 2, 2000).

3.2.7 OH-reactivity

OH-reactivity values are calculated for NO₂, CO, CH₄, and each of the VOC species tracked in the model. Integrated reaction rates (IRR) are calculated by CMAQ using process analysis (Jeffries and Tonnesen, 1994; Tonse et al., 2008). Integrated loss rates of OH[•] due to reaction with each species, i , are calculated by integrating over each model time step using the following equation,

$$OH_{loss,i}(t + \Delta t) = OH_{loss,i}(t) + \int_t^{t+\Delta t} k_{i+OH} [OH][i] dt \quad (\text{E3.3})$$

where OH_{loss} is the IRR of the species i and k_{i+OH} is the reaction rate coefficient. Model output is produced at hourly intervals, giving results in units of [ppb/hour]. The OH-reactivity (R_{OH}) of a species, i , is given by the equation,

$$R_{OH,i} = \frac{OH_{loss,i}}{[OH]}, \quad (E3.4)$$

with results in units of s^{-1} . Total reactivity, $R_{OH, total}$, is representative of the reactivity of the atmosphere and can be calculated by adding the values of $R_{OH,i}$ for each species:

$$R_{OH,total} = \frac{\sum_{i=1,n} OH_{loss,i}}{[OH]} \quad (E3.5)$$

where n is the total number of species that react with the OH radical.

3.3 Results

3.3.1 Revised emissions and rate parameters

Emission files were altered to include the new species, MTBE, ETOH, PACET, UPOH, and AMIN. Motor vehicle ALK3 emissions were redistributed: 44% of ALK3 emissions moved to MTBE and 12% to ETOH emissions. For area source emissions, MTBE and ETOH are also important due to off-road gasoline engines and related emissions. Ethanol is also prevalent in area source emissions due to its high percentage in emissions from animal waste decomposition (25% of ROG by weight) and pesticides (17% of ROG by weight excluding methyl bromide). Ethanol is also present in smaller percentages in emissions from use of consumer products, solvent and waterborne architectural coatings, and thinning and cleanup solvents. Propyl acetate (PACET) and lumped amine (AMIN) are prevalent species in emissions from animal waste decomposition. The lumped UPOH species is largely isopropyl alcohol, which is a component in all the area source emission speciation profiles except methyl-bromide containing pesticides. Ethylene glycol and propylene glycol also contribute significantly to the lumped species UPOH, with the remainder of UPOH emissions due to about 50 other species present in small amounts.

A summary of area source emissions from the SF Bay area and SJV is presented in Table 3-9 (county-level results are presented in Table A-3 in the Appendix). A large percentage of emissions from ALK3 motor vehicle (MV) and area emission files are moved to the MTBE and ETOH species for the Revised mechanism. Emissions that originate almost solely from animal waste decomposition (PACET and AMIN) result in a much higher multiplier in the SJV than for the SF Bay area. Removing non-alkanes from the lumped alkane groups allows for a more readily scalable spatial representation of these emissions. Clear separation of agricultural and motor vehicle emissions is desirable since effects of control measures on these sources will differ.

Table 3-9. Redistribution of emissions from Default to Revised

Percentage of each Default species (by emission type) that is moved to a new species for the Revised emissions. Motor vehicle (MV) emission percentage redistributions are the same for each county. All emission files are altered at county level, but values shown for the SFB and SJV air basins for illustrative purposes. County-level detail presented in Table A-3 the Appendix.

New Emission Category	Emission File	Air Basin Average Multiplier (%*species)	
		SFB	SJV
MTBE	MV	46.3*ALK3	46.3*ALK3
ETOH	MV	11.5*ALK3	11.5*ALK3
MTBE	Area	13.3*ALK3	4.2*ALK3
ETOH	Area	55.9*ALK3	65.8*ALK3
PACET	Area	2.7*ALK3	18.8*ALK3
AMIN	Area	10.3*ALK5	72.3*ALK5
UPOH	Area	25.3*ALK4+51.2*ALK5	61.9*ALK4+14.8*ALK5

An example of the temperature-dependent reaction rate coefficient (Revised and Default fits) is presented in Figure 3-6 for three lumped alkane species. The default activation energy chosen for ALK3 does not correctly represent the temperature dependence of the reaction rate coefficient, but using the method described above, alkane reaction rate parameters were adjusted and correspond to the expectation of increasing alkane reaction rates at higher temperatures. The reaction rate coefficients for the new species, MTBE, ETOH, PACET, and UPOH, are also plotted with the alkane species (with the exception of AMIN which has a much higher reaction rate coefficient). The updated alkane reaction rate coefficients are all lower than the corresponding default SAPRC07A coefficients for temperatures below 300 K. The updated ALK3 rate coefficient is lower than the default reaction rate coefficient for temperatures below 300 K, and higher for temperatures above 300. The updated ALK4 and ALK5 rate coefficients show similar trends, but cross from lower to higher at different temperatures. The new species MTBE, ETOH, and PACET have higher kinetic reactivity than the ALK3 group that was originally used to represent their reactions. UPOH is composed of emissions originally lumped with the ALK4 and ALK5 groups, and the kinetic reactivity is similar in magnitude to that of ALK5. The reaction rate coefficient for AMIN is $3.4 \times 10^{-11} \text{ cm}^3 \text{ molec}^{-1} \text{ sec}^{-1}$, and the temperature-dependent rate parameters have not been determined.

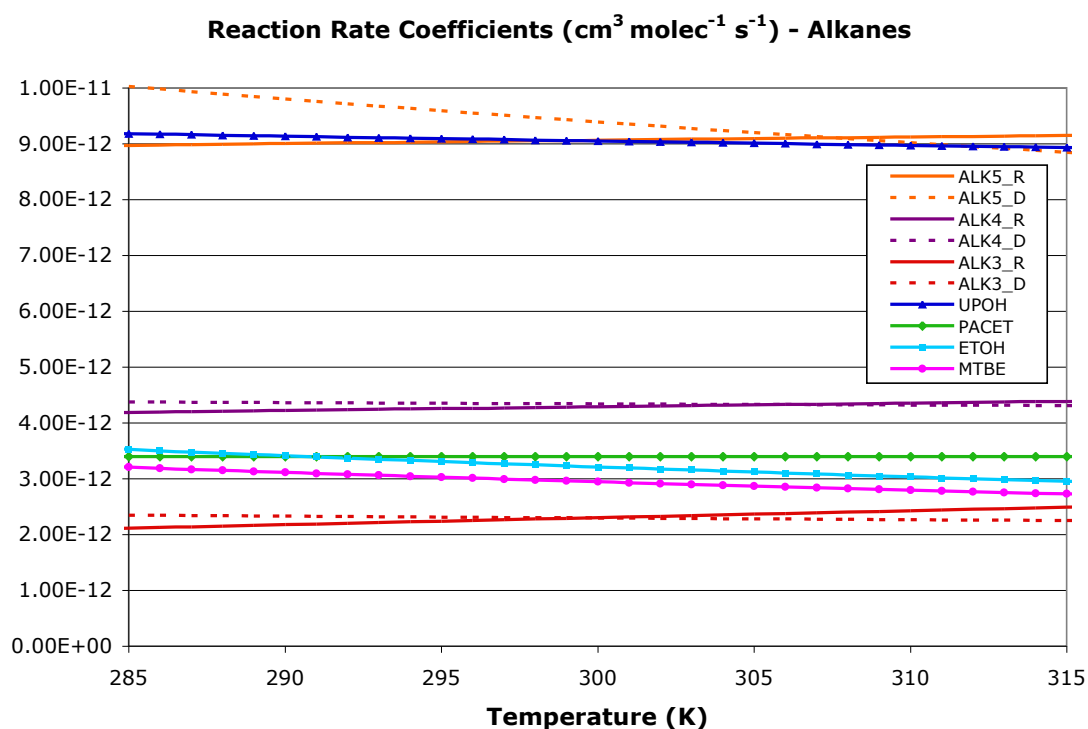


Figure 3-5. VOC + OH· reaction rate coefficients (Alkanes)

Solid lines show Revised while the dashed lines show the default. Species added to the Revised mechanism, whose emissions were removed from the lumped ALK species are also presented on this plot.

The updated temperature-dependent rate coefficients for the lumped olefin and aromatic reactions with OH·, along with the default reaction rate coefficients are presented in Figure 3-6. In all instances, the updated rate coefficients are lower than the default values. Temperature dependence has been introduced into the ARO1 reaction rate coefficient. In general there is little information available on the temperature dependence of reaction rate coefficients for most aromatics, but ARO1 is primarily toluene for which temperature-dependent reaction rate data have been acquired. The updated reactions and rate coefficient parameters are summarized in Table 3-10.

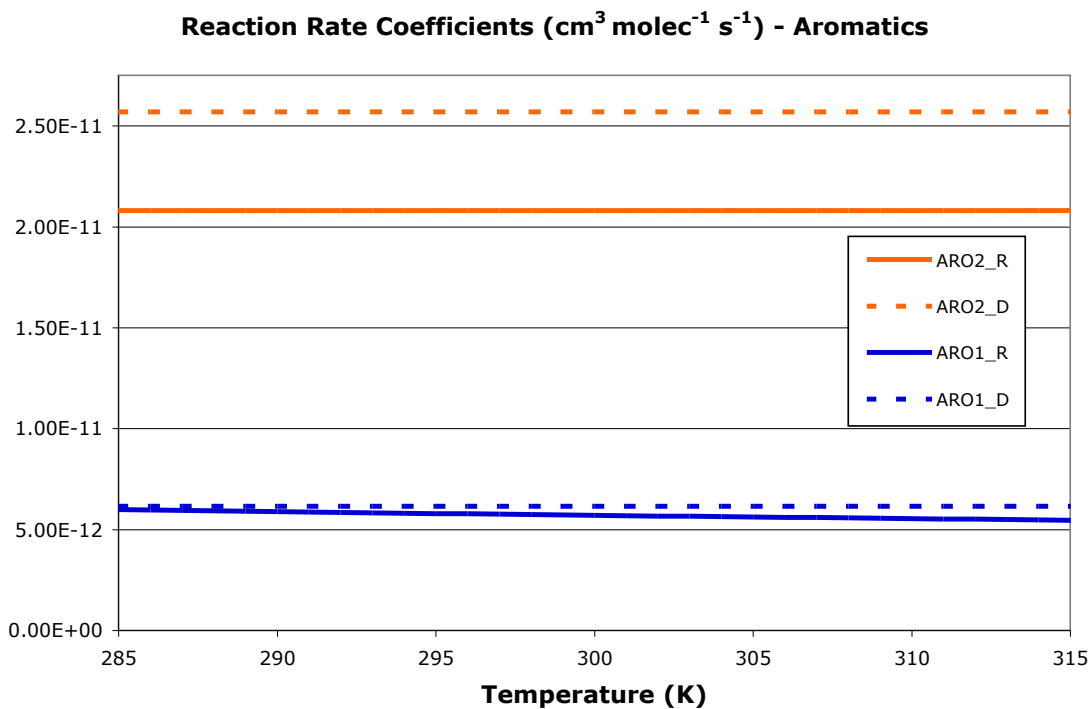
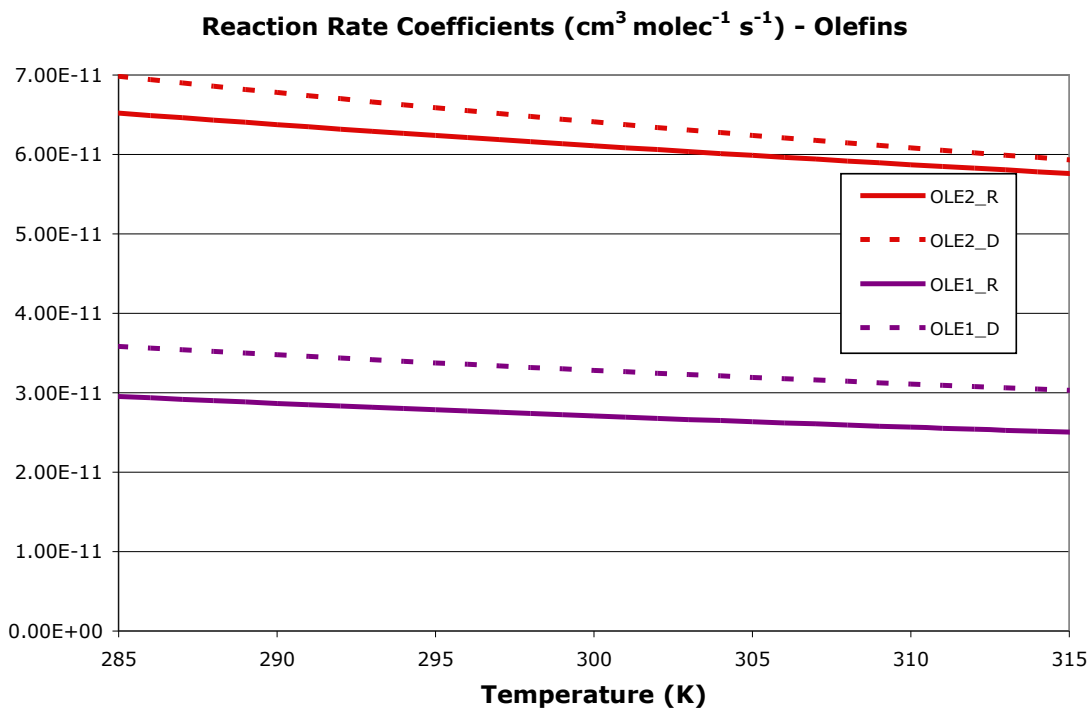


Figure 3-6. VOC + OH· reaction rate coefficients (Olefins and Aromatics)
 Solid lines show Revised while the dashed lines show the Default.

Table 3-10. Reactions, rate parameters, and percent increase in reaction rate coefficient for updated lumped species

Reaction & Products	% change at 300 K	Rate Parameters		
		k(300) ^{a,b}	A ^b	E _a /R ^c
ALK3 + OH = 0.635 RO2R + 0.286 TBUO + 0.078 RO2N + 0.666 R2O2 + 0.046 HCHO + 0.450 CCHO + 0.120 RCHO + 0.043 ACET + 0.286 MEK + 0.001 MEO2	0.3	2.30E-12	1.18E-11	490
ALK4 + OH = 0.795*RO2R + 0.010*MEO2 + 0.017*MECO3 + 0.156*RO2N + 1.031*R2O2 + 0.003*CO + 0.071*HCHO + 0.403*CCHO + 0.250*RCHO + 0.452*ACET + 0.100*MEK + 0.123*PRD2 + 0.022*TBUO	-1.2	4.29E-12	6.82E-12	139
ALK5 + OH = 0.678*RO2R + 0.303*RO2N + 0.945*R2O2 + 0.021*HCHO + 0.106*CCHO + 0.240*RCHO + 0.100*ACET + 0.095*MEK + 0.379*PRD2 + 0.019*MECO3 + 0.002*CO	-3.5	9.07E-12	1.10E-11	58
OLE1 + OH = 0.976 RO2R + 0.001 MEO2 + 0.023 RO2N + 0.024 R2O2 + 0.954 HCHO + 0.805 CCHO + 0.162 RCHO + 0.006 ACET + 0.004 PRD2 + 0.004 MACR + 0.003 MVK + 0.001 IPRD	-17.5	2.71E-11	5.20E-12	-495
OLE2 + OH = 0.922 RO2R + 0.078 RO2N + 0.028 R2O2 + 0.551 HCHO + 0.001 CO + 0.374 CCHO + 0.144 RCHO + 0.544 ACET + 0.0049 MACR + 0.061 MEK + 0.051 IPRD	-4.7	6.11E-11	1.78E-11	-370
ARO1 + OH = 0.174 HO2 + 0.467 RO2R + 0.298 OH + 0.061 RO2N + 0.228 GLY + 0.145 MGLY + 0.174 CRES + 0.053 BALD + 0.174 AFG1 + 0.200 AFG2 + 0.298 AFG3	-7.1	5.71E-12	2.33E-12	-269
ARO2 + OH = 0.130 HO2 + 0.547 RO2R + 0.228 OH + 0.095 RO2N + 0.023 PRD2 + 0.137 GLY + 0.278 MGLY + 0.064 BA CL + 0.130 CRES + 0.046 BALD + 0.202 AFG1 + 0.180 AFG2 + 0.324 AFG3	-19.1	2.08E-11	2.08E-11	--

^aRate constant calculated for temperature of 300 K by

^bUnits of k(300) and A are [cm³ molec⁻¹ s⁻¹]

^cUnits of E_a are [cm³ mol⁻¹ s⁻¹] and units of R are [kcal mol⁻¹ deg⁻¹]

3.3.2 Ozone model results for Episode 1 (E1)

Temperature and ozone concentration maps are presented in Figure 3-7. The ozone response shown is for the Revised mechanism with all of the described changes. During E1 in summer 2000, coastal regions and the SF Bay area had low levels of ozone due to clean onshore flow, while the eastern side of the Central Valley and southern Sierras have comparatively elevated levels of ozone (Fujita et al., 2005).

The third panel of Figure 3-7 compares predicted ozone concentrations using the Revised and Default versions of the chemical mechanism and emissions. The top row of Figure 3-7 shows model predictions at 10 am. These results are presented because anthropogenic VOC reactivity peaks in the morning hours when atmospheric mixing height is relatively low and emissions are increasing. Slight ozone increases are observed in Sonoma County and the northern part of the Central Valley. A negative ozone response using the updated chemical mechanism is apparent in the southern part of the Central Valley. The magnitude and spatial extent of the negative ozone response increase throughout the day. The bottom row of Figure 3-7 shows model predictions at 4 pm, corresponding to typical inland peak ozone timing during the 2-week simulation. Ozone decreases are more widespread than ozone increases at this time of day. The negative ozone responses at 4 pm are co-located with high ozone areas directly over, or just downwind of areas with high anthropogenic VOC emissions. The largest ozone decrease is about 1.2 ppb at 4 pm downwind of Bakersfield. The ozone response does not appear to be sensitive to the changes encompassed in the Revised mechanism, but further simulations were performed to determine if any specific changes in the Revised mechanism were of opposing sensitivity, e.g. cancelling each other out.

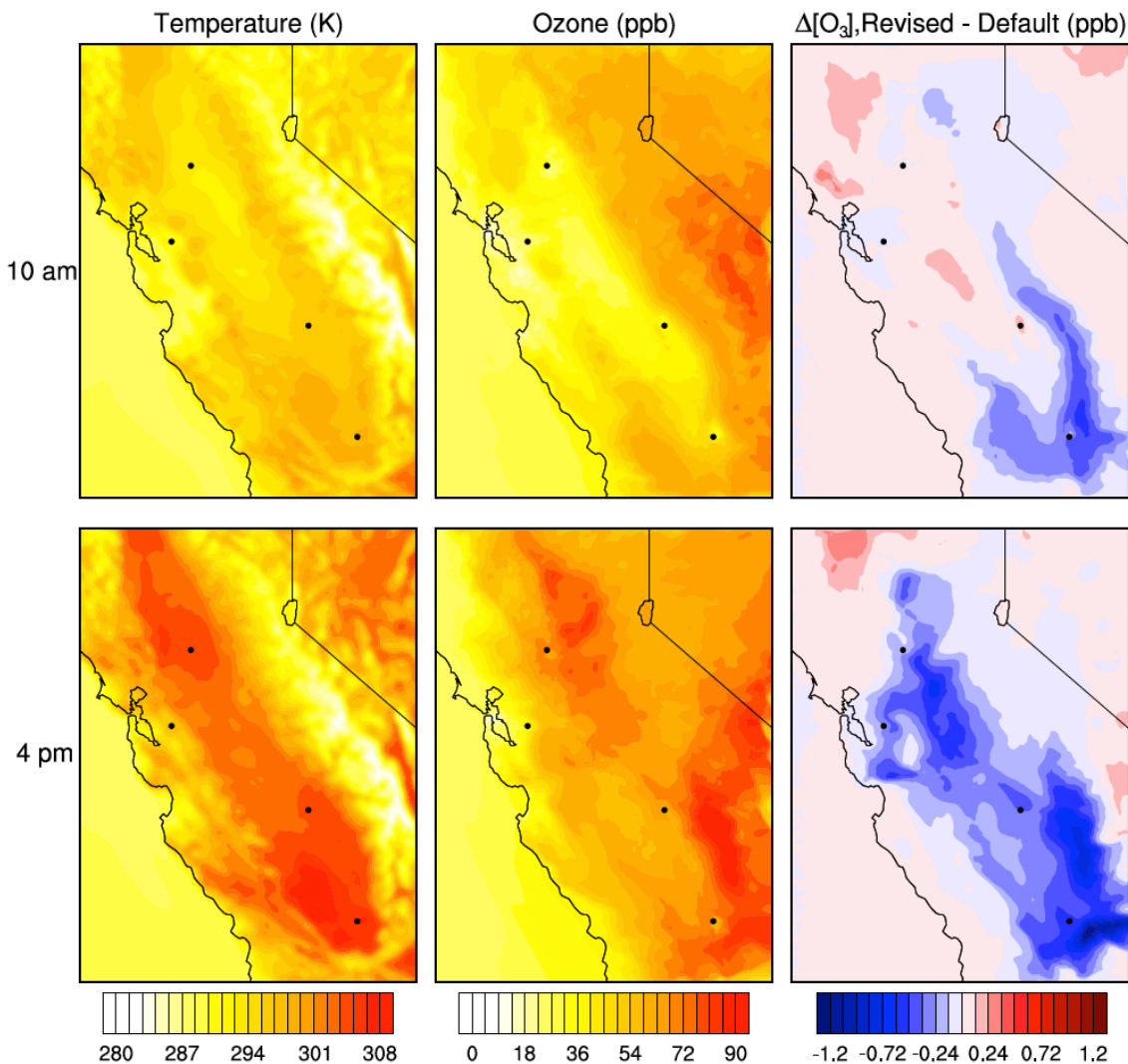


Figure 3-7. Temperature, default ozone concentrations, and the ozone response for Revised mechanism (E1)

Episode 1, average weekday temperature, the difference between the Revised mechanism and emissions and the Default mechanism and emissions, at 10 am and 4 pm.

To better understand the effect of the Revised mechanism and emissions on model results, intermediate simulations were performed, with the grouped changes altered in a stepwise fashion. The ozone response to the stepwise changes is presented in Figure 3-8 to determine the relative importance of the various changes made. The leftmost column shows the ozone response to introducing new species (MTBE, ETOH, PACET, UPOH, and AMIN). The 10 am response at Bakersfield shows a small increase in ozone in the area with the densest anthropogenic emissions. However, the area surrounding Bakersfield, as well as the Sierra foothills show decreases in ozone. These areas of negative ozone response are collocated with relatively high ozone levels for this time of day. The ozone levels in these regions build up throughout the day, and without sufficient anthropogenic NO emissions to remove ozone at night by titration, stay high overnight relative to the more populated areas. Introducing the new species results in widespread lower peak ozone concentrations at 4 pm.

The second column of Figure 3-8 shows the ozone response to changing the definitions of what remains in the lumped alkanes. A slight ozone increase is observed over almost the entire domain. A large ozone response was not expected, as the OH-reaction rate coefficients and the IR values changed little compared to other species, and alkanes are much less reactive than olefins and aromatics. The largest increase is 0.08 ppb at 4 pm south of Sacramento. The ozone response to altered lumped olefin definitions is presented in the third column of Figure 3-8. At 10 am, the Sierra Nevada and southern San Joaquin Valley show a slight decrease in ozone, while the rest of the domain sees ozone increases. By 4 pm, the negative ozone response spread throughout the San Joaquin Valley. The last panel of Figure 3-8 shows the ozone response of the altered lumped aromatic definitions. Ozone decreases are widespread at 10 am, and while 4 pm still shows decreases, the spatial extent of the decreases has diminished. Creating new species and updating the OLE and ARO lumped species definitions, all have effects on ozone concentrations that are of similar magnitude, but vary in sign. Thus there are offsetting effects, on ozone in the revisions that were made to the mechanism in the morning. However, in the afternoon, significant for peak ozone analysis, the revisions appear to have similar small responses in Central Valley.

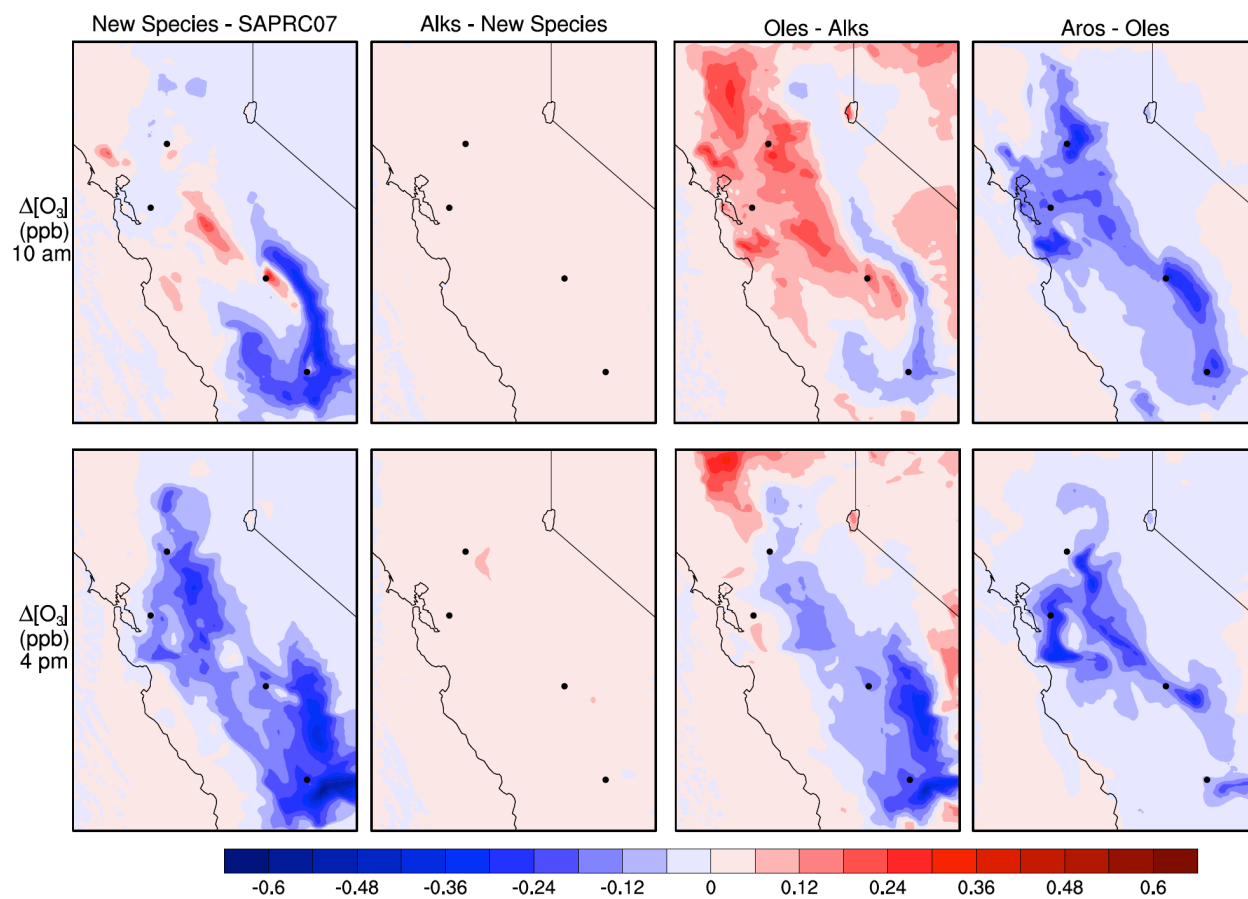


Figure 3-8. Ozone response due to step-wise changes made to the SAPRC07 mechanism
Weekday average at 10 am and 4 pm.

3.3.3 Episode 2 (E2) results

Temperature, predicted ozone concentrations, and the ozone responses for E2 are shown in Figure 3-9. Note that the scale of all color bars extends to higher levels compared to E1 results in Figure 3-7. The meteorology during E2 was driven by a high pressure over the Great Basin that caused stagnant conditions allowing for high temperatures and ozone accumulation. Similar anthropogenic emissions led to an ozone peak > 40 ppb higher in E2 than in E1. The most elevated ozone concentrations are downwind of Fresno and Bakersfield. Elevated ozone levels also extend along the coast south of the SF Bay area in the E2 simulation.

The Revised mechanism ozone response (Revised – Default), shown in the last panel of Figure 3-9, has a spatial pattern similar to the response in E1. Given higher baseline ozone levels, the magnitude of the change in ozone due to chemical mechanism revisions is larger during E2, up to a 1.8 ppb decrease occurs at 4 pm. The spatial extent of the region with ozone decreases is also larger, now including areas in and due east of the SF Bay area. The ozone decrease in Livermore and the surrounding area is of the same magnitude as the reductions downwind of Fresno and Bakersfield. The results indicate that the Revised mechanism reduces reactivity of the VOC emissions as compared to the Default mechanism. Thus, areas of central California with high anthropogenic emissions, the Revised mechanism predicts slightly lower peak ozone concentrations than the standard SAPRC07 mechanism, more so for times and locations where meteorology is conducive to ozone accumulation.

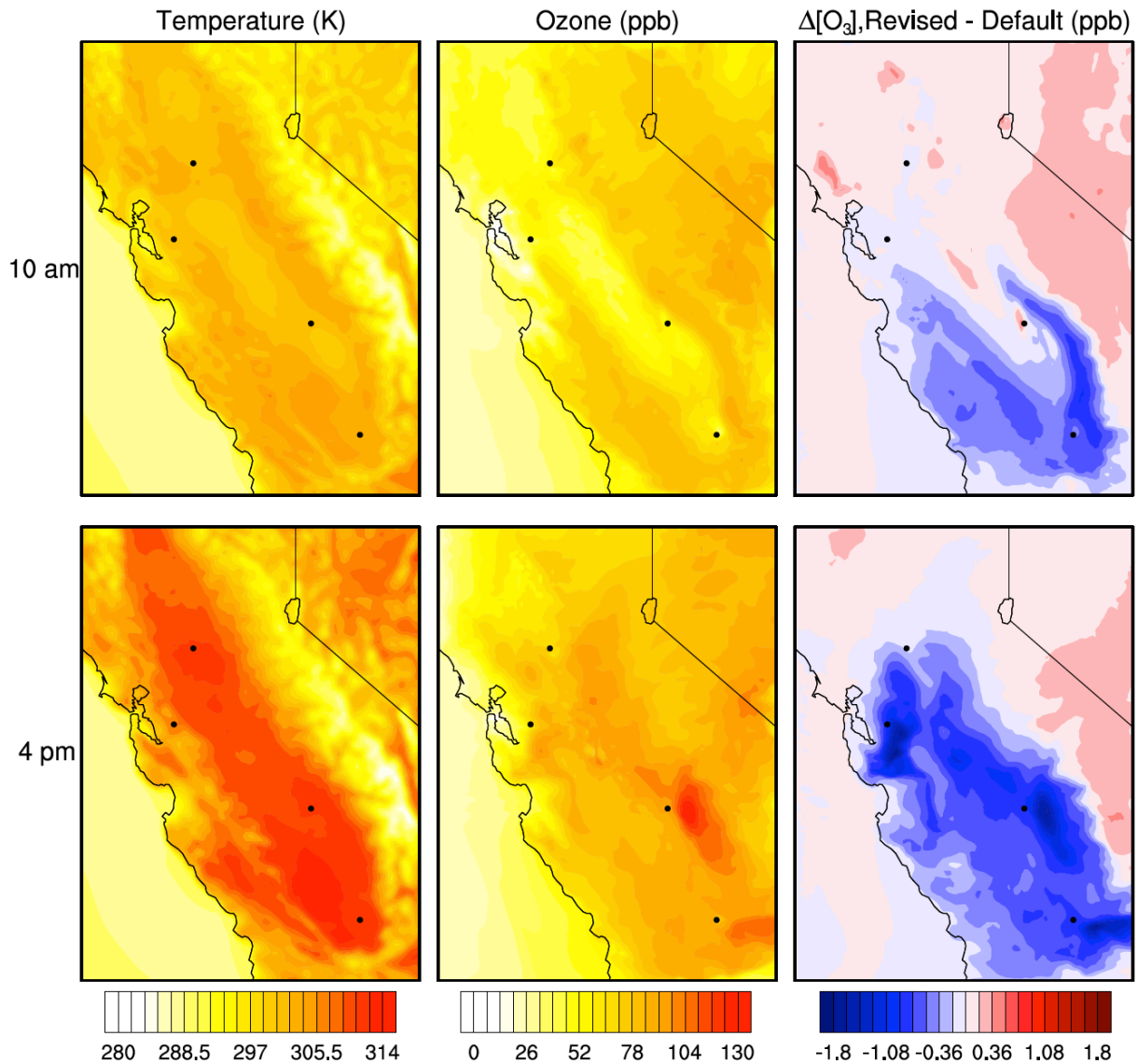


Figure 3-9. Temperature, default ozone concentrations, and the ozone response for Revised mechanism (E2)

Revised mechanism and emissions and the Default mechanism and emissions, at 10 am and 4 pm.

3.3.4 VOC concentration and OH-reactivity analysis

Simulated OH-reactivity statistics for the Default and Revised mechanisms are presented for four sites in Table 3.11. The OH radical concentration is higher at all times and sites, likely because the overall k_{OH} for VOC was lowered with the new lumped species definitions. Analogously, each of the VOC reactivity metrics decreased (with one exception, morning Fresno VOC + OH· IRR barely increased). Total VOC reactivity has also decreased at each site with use of the Revised mechanism.

Table 3-11. Comparison of Default and Revised OH-reactivity statistics

	Livermore				Sacramento			
	Morning		Afternoon		Morning		Afternoon	
	Default	Revised	Default	Revised	Default	Revised	Default	Revised
O3 (ppb)	18.3	18.3	62.2	61.5	39.9	39.9	61.9	61.8
OH (ppb)	2.80E-05	2.91E-05	2.93E-04	3.00E-04	4.88E-05	5.12E-05	4.73E-04	4.82E-04
VOC + OH IRR (ppb/h)	0.46	0.43	4.09	3.87	0.70	0.68	1.90	1.86
VOC Reactivity (1/s)	3.94	3.49	3.47	3.19	3.57	3.32	1.05	1.01
Total Reactivity (1/s)	11.82	11.36	9.78	9.44	7.51	7.22	3.30	3.25
	Fresno				Bakersfield			
	Morning		Afternoon		Morning		Afternoon	
	Default	Revised	Default	Revised	Default	Revised	Default	Revised
O3 (ppb)	46.9	46.8	105.0	104.0	21.9	21.9	62.8	62.0
OH (ppb)	6.52E-05	6.87E-05	6.93E-04	7.14E-04	3.20E-05	3.32E-05	2.97E-04	3.04E-04
VOC + OH IRR (ppb/h)	1.54	1.55	5.96	5.82	0.43	0.40	4.58	4.36
VOC Reactivity (1/s)	5.36	5.13	2.13	2.01	3.08	2.76	3.72	3.42
Total Reactivity (1/s)	12.00	11.72	5.49	5.33	9.48	9.15	10.55	10.19

The percent contribution of the four major VOC groups (anthropogenic VOC, oxidized VOC, aromatics, and biogenic VOC) to total reactivity in Fresno in the morning and afternoon is shown in Figure 3-10. AVOC, OVOC, and BVOC contribute more to reactivity in the morning, when there are fresh emissions and secondary VOC have not had time to accumulate. It is of note that the Revised mechanism results in an increased apportionment to OVOC in concert with a reduced apportionment to AVOC) due to the creation of the new oxidized species. It is also of note that there is a slight increase in apportionment (and IRR) of OH-reactivity attributed to NO₂ (NO₂ + OH· → HNO₃).

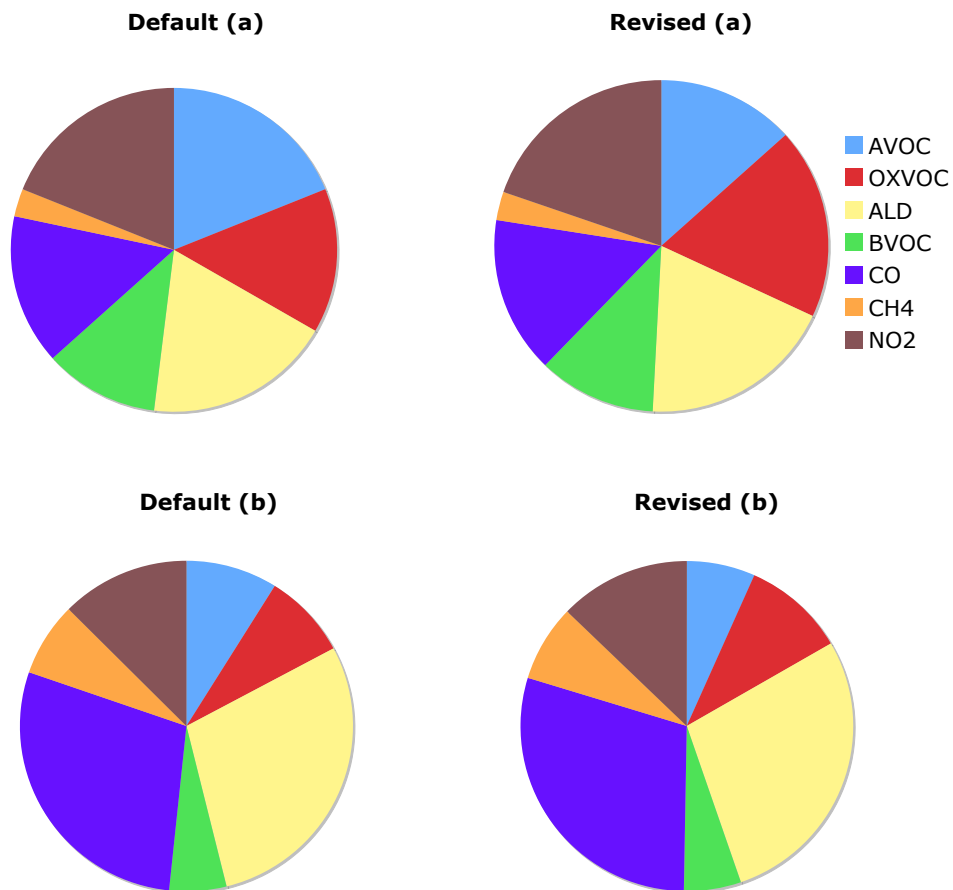


Figure 3-10. Percent contribution to $R_{OH, total}$ for the Default and Revised mechanisms
 Example for Fresno: morning (a), 6-8 am, and afternoon (b), 1-3 pm.

3.4 Discussion

As is typical in air quality modeling studies, measured 1-hour maximum ozone values in the Central Valley are under-predicted in the model simulations. Updating the chemical mechanism from SAPRC99 to SAPRC07A lowered simulated ozone concentrations further (Chapter 2), increasing negative model bias in these regions. Updating emissions and VOC lumped species definitions as described in this chapter, further adds to the negative bias in model predictions. However, the changes in predicted ozone concentrations resulting from mechanism revisions described in this chapter are generally small. The improvements to the chemical mechanism described here are also essential as an enabling step for better describing the temperature dependence of VOC reactions and their oxidation products. This is the focus of research to be described in Chapter 4.

Improving the description of atmospheric chemistry in air quality models will allow the research community to quantify and diagnose reasons for bias in ozone predictions, as well as highlighting more clearly possible errors in the VOC emission inventory. Measures of overall OH-reactivity can be used to compare ground-based VOC measurements to modeled

concentrations. Steiner et al. (2008) found predicted VOC reactivity to be a factor of 2 to 3 times lower than measured values in Fresno. The updates considered here lowered OH-reactivity further, suggesting that there is a VOC emission source that is missing or underestimated. Steiner et al. (2008) suggest that a source emitting both NO_x and VOC, such as industrial processes or motor vehicle emissions, is underestimated, and that oxidized biogenic emissions from crops, currently not represented in the emissions, may play a role. Another recent study suggests that VOC emissions from livestock feed (e.g. corn silage), which are not represented in the current emission inventory, have an ozone-forming potential that is higher than that of VOC emissions from light-duty motor vehicles in the San Joaquin Valley (Howard et al., 2010).

Correctly describing the atmospheric reactions of VOC emissions and their oxidation products will also be helpful in the context of studying the effects of climate change on air quality. In particular, it appears various temperature dependencies in the atmospheric chemistry of VOC are either ignored or incorrectly modeled in current chemical mechanisms. In the following chapter, VOC oxidation reactions in the chemical mechanism are further refined to add missing temperature-dependent chemistry in describing the oxidation products that form and react as a result of VOC emissions to the atmosphere.

Chapter 4: Improved representation of the temperature dependence of VOC oxidation reactions for air quality modeling

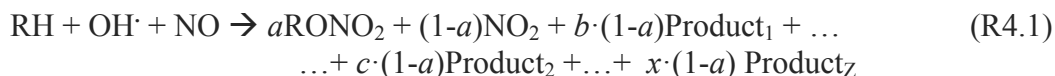
4.1 Introduction

4.1.1 Motivation

Ozone concentrations are strongly correlated to temperature, as shown by multiple observational studies across the United States (Sillman and Samson, 1995; Bloomer et al., 2007; Camalier et al., 2007; Steiner et al., 2010). For typical summer temperatures, ozone concentration increases linearly with temperature, and the extent of the increase can be defined by a site-specific slope, m_{O_3-T} . Bloomer et al. (2007) describe this slope as the “climate change penalty factor,” as the higher temperatures expected with climate change will make ozone control even more difficult. Using a box model, Sillman and Samson (1995) found many factors that contribute to the positive m_{O_3-T} , including water vapor and biogenic emissions that increase with temperature, increases in photolysis rates (due to insolation increase correlated with high temperatures), and most importantly, temperature-dependent reaction rate coefficients. Anthropogenic emissions and stagnant meteorological conditions were not considered in the Sillman and Samson (1995) analysis, and it was suggested these factors could be responsible for the unexplained portion of the observed O_3 -temperature correlations, as their models did not predict slopes as steep as the measured m_{O_3-T} . The stagnant meteorology theory is supported by two studies (Vukovich, 1995; Vukovich and Sherwell, 2003) that verified a negative relationship between wind speed and ozone measurements. Additionally, Jacob et al. (1993) show “that regional stagnation, rather than high temperature, is the primary forcing factor for the occurrence of high- O_3 episodes.” However, a recent study indicates that increases in anthropogenic emissions with temperature do contribute to m_{O_3-T} (Steiner et al., 2010). While the effects of climate change on ozone air quality have been studied by numerous investigators (Steiner et al., 2006; Kleeman, 2008; Nolte et al., 2008; Wu et al., 2008; Zhang et al., 2008; Jacob and Winner, 2009; Liao et al., 2009; Millstein and Harley, 2009), little progress has been made beyond the 1995 Sillman and Samson analysis in assessing the sensitivity of possible contributors to the climate change penalty factor in box-model simulations.

Most of the known ozone-temperature effects mentioned above can be evaluated using air quality models (AQM). For instance, the meteorological models that drive an AQM typically include predictions of water vapor, wind speeds (that help define stagnation events), and temperature (that drive biogenic emissions and the rates of chemical reactions). The rate coefficients for pertinent atmospheric reactions are defined as part of the chemical reaction mechanism, such as SAPRC07 (Carter, 2010a). Sillman and Samson (1995) found that the negative temperature dependence of the PAN decomposition rate, which releases NO_2 and a radical, was the most important chemical factor in modeling m_{O_3-T} . Another study finds that “50% of the observed increase of O_3 with temperature might be explained by the enhancement in the chemical processes” (Olszyna et al., 1997). Chemical mechanisms used in air quality models

already include parameterizations of the temperature dependence of many relevant reaction rates. In contrast, however, current mechanisms used for air quality modeling typically specify VOC oxidation product yields using temperature-*independent* branching ratios. Current methods of condensing VOC oxidation schemes in chemical mechanisms do not allow temperature-dependent reaction rate coefficients for important intermediate species, such as peroxy (RO_2^\cdot) and alkoxy (RO^\cdot) radicals. Figure 1-1 shows how RO_2^\cdot and RO^\cdot fit into the overall VOC degradation scheme, and Figure 4-1 shows the chemical schematic relevant for the work in this chapter, most of which has previously been condensed into one chemical reaction step per VOC, or reactive hydrocarbon (RH), for modeling purposes:



where z is the number of products that result from RO^\cdot reaction via the competing processes of isomerization, reaction with O_2 , and unimolecular decomposition. RH can represent alkane, olefin, and aromatic species. Current mechanisms used in air quality models treat the coefficients a, b, c, \dots , and x , as constants. Values for the various product yield parameters appearing in (R4.1) have typically been estimated assuming a nominal temperature of 300 K. Whenever actual temperatures depart from the 300 K assumption, variations in organic nitrate (RONO_2) and alkoxy radical reaction product yields will occur in the real atmosphere, but air quality models fail to capture these effects. Therefore, models may be unable to describe correctly the effects of spatial and temporal variations in temperature on air quality. Relevant sources of temperature variability can arise due to contrasts between day and night, surface and aloft, coastal and inland, and day-to-day differences in weather. Also climate change may systematically shift the distribution of prevailing temperatures in the future. In this chapter, a new chemical mechanism for use in air quality modeling is developed, which allows for varying, temperature-dependent hydrocarbon oxidation product yields. In addition to the $\text{RH} + \text{OH}$ reactions, temperature-dependent product yields are created for $\text{RH} + \text{O}_3$ and $\text{RH} + \text{NO}_3$ reactions.

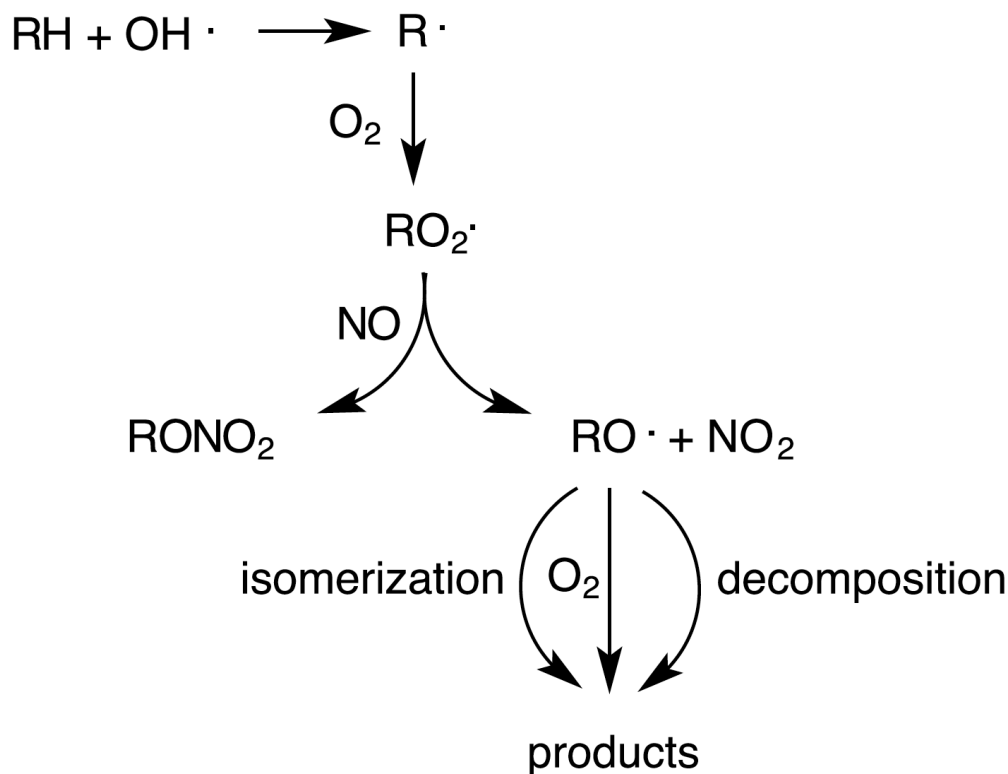


Figure 4-1: Schematic for VOC degradation in the atmosphere

RH represents any hydrocarbon. H-abstraction or OH-addition (to a carbon with a carbon-carbon double bond) leads to formation of R \cdot . Olefin and aromatic reaction with NO $_3$ also leads to R \cdot .

The RO $_2 \cdot$ radical that forms as an initial (generic) product of VOC oxidation reacts with NO to form either an alkoxy radical (RO \cdot) and NO $_2$, or an organic nitrate (RONO $_2$).



In the SAPRC mechanism, the yield of RONO $_2$, relative to NO \rightarrow NO $_2$ conversion via reaction (R4.2), is represented using parameter a in (R4.1) and is specified for each lumped hydrocarbon reaction. The specified values of a increase with carbon number of the hydrocarbons being modeled, but are invariant with temperature in SAPRC. In reality the yield of RONO $_2$ should decrease significantly with increasing temperature. Altering RONO $_2$ yields has the potential to affect ozone concentrations as its formation is a chain-terminating step, suppressing radical concentrations and NO $_x$, both of which are necessary components for ozone formation. However, as organic nitrates are thermally unstable at high temperatures, they can be a source of NO $_x$ downwind if temperatures increase (e.g., later in the day or further inland where it may be warmer). Implementation of temperature-dependent RONO $_2$ formation in an AQM could be of particular importance in central California, as current models generally overestimate ozone for the cooler coastal areas, and underestimate ozone in the Central Valley where it is often much warmer during summer months (Jin et al., 2010).

The temperature dependence of alkoxy radical (RO[•]) reactions (reaction with O₂, isomerization, and unimolecular decomposition) is added to the reaction mechanism as part of the research reported in this chapter. Each competing pathway results in different oxidized organic products. Furthermore, isomerization and decomposition pathways lead to extra NO→NO₂ conversions compared to RO[•] reaction with O₂. The kinetics of unimolecular decomposition processes have especially strong temperature dependence, and lead to chain branching (i.e., increasing the radical population) when they occur. Also the resulting fragmentation of the parent hydrocarbon increases volatility of the products, which can act to offset the vapor pressure effects of adding oxygenated functional groups. The relative yields of each alkoxy radical reaction product (multiple products form for each pathway) are described for each oxidation reaction as the coefficients *b, c, ..., x* in (R4.1).

The objectives of this research are to add these missing temperature dependencies in the SAPRC mechanism, and to evaluate the effects of temperature on air quality model predictions made using the updated mechanism. Missing temperature-dependent branching of RO[•] and RO₂[•] reactions were introduced for nine explicit and twelve lumped VOC species reactions in the SAPRC07A chemical mechanism. The sensitivity of model predictions to these changes in the chemical mechanism was studied using the Community Multiscale Air Quality (CMAQ) model applied to central California. The effects on longer-lived nitrogenous species (NO_z) are investigated, as well as VOC and ozone concentrations. Data from field measurement campaigns reporting NO₂ and NO_z speciation (i.e., separate values for NO₂, peroxyacyl nitrates, alkyl nitrates, nitric acid), which have not been used previously to evaluate air quality model predictions, and the effects of temperature on air quality, are used to diagnose model performance and provide recommendations to improve the nitrate representation in the SAPRC mechanism. Further background on relevant atmospheric chemistry and the chemical mechanism used for air quality modeling is provided below, as well as motivation for an easily alterable chemical mechanism.

Additionally, a temperature-dependent emission sensitivity study is conducted. Traditionally, air quality model emissions are created for a specific air pollution episode to capture emission timing and spatial distribution, as well as day-of-week emission differences. While mobile-source tailpipe VOC emissions have been shown to be largely independent of temperature (Welstand et al., 2003), Rubin et al. (2006) found that evaporative emissions increase with temperature. Information from Rubin et al. is used to model the effect of varying evaporative emissions on photochemical air quality in central California.

Finally, including the newly defined temperature dependences of both the chemical mechanism and vehicle-related evaporative emissions, a 2× pre-industrial CO₂ temperature perturbation scenario is assessed, as feedback effects of future climate change on air quality will be affected by the temperature sensitivity of the underlying chemical mechanism and emissions.

4.1.2 Background

An updated VOC lumping strategy was presented in Chapter 3, allowing for a more realistic representation of VOC emissions and chemistry in the atmosphere. This was accomplished using a similar number of lumped species to maintain comparable levels of chemical detail and

computational demand as in the existing mechanism. Prior to species reduction by VOC lumping, reactions for each VOC are condensed to achieve the computational efficiency needed for regional air quality modeling. To illustrate the VOC reaction parameterizations used in SAPRC, the reaction steps involved in n-butane oxidation are shown in Figure 4-2. To reduce the number of reactions, the many reactions shown in Figure 4-2 are described by one condensed reaction. This allows effective removal of most of the intermediate radical species and associated radical chemistry. The overall temperature dependence of the reaction is limited to that of the initial reaction step, which is H-abstraction by the OH radical in the case of n-butane (Figure 4-2).

The temperature dependence of the initial reaction step is represented in SAPRC and other mechanisms. However other important details are lost because oxidation product yields are held constant. In reality, because the intermediate reaction rate coefficients for alkyl peroxy radicals ($\text{RO}_2\cdot$) and alkoxy radicals ($\text{RO}\cdot$) depend on temperature, the resulting product yields should also change with temperature. Current treatment in the SAPRC mechanism assumes fixed product yields, calculated using underlying rate coefficient values specified at 300 K. None of the current mechanisms (SAPRC, CB5, RACM) commonly used for air quality modeling include temperature-dependent yields for VOC oxidation products.

While the Master Chemical Mechanism (MCM; Jenkin et al., 1997) does capture the temperature dependence of alkoxy radical reactions, it does so at prohibitive cost in terms of computational efficiency. There is minimal VOC lumping or condensation in MCM, resulting in a mechanism with about 17,000 reactions. This system of reactions is much too computationally intensive for most present-day computing systems for use with 3-dimensional models. The Caltech Atmospheric Chemistry Mechanism (CACM; Griffin et al., 2002) includes temperature-dependent organic nitrate yields, but at the expense of other chemical detail and generality of the mechanism. The surrogate species approach, in which only one species defines the chemistry of each lumped VOC group, is used for VOC lumping in CACM. The lumped species developed in Chapter 3 for the SAPRC mechanism represent all species emitted in quantities greater than 5% for the group on a molar basis, and in the work reported in the chapter, each of these species reactions with OH is factored in when expressing temperature-dependent organic nitrate and other product yields.

Ozone predictions have been a major focus of air quality model evaluations, but model evaluations that consider only ozone can be misleading due to possible compensating errors. A deeper evaluation must consider the accuracy of model predictions for NO_x and NO_z species and VOC as well. This is of particular importance in evaluating efforts to reduce either VOC or NO_x emissions that are being undertaken for ozone control. The NO_x species include two short-lived (< 1 hour) reactive oxides of nitrogen, nitrogen oxide (NO) and nitrogen dioxide (NO_2). Longer-lived nitrogenous species, that can act as a reservoir for nitrogen oxides, are referred to as the NO_z species and include nitric acid (HNO_3), organic nitrates (RONO_2), and peroxyacetylnitrate (PAN) and its analogues.

For this study, RONO_2 concentrations are of particular interest because its yield is directly altered by temperature-dependent VOC reaction chemistry. Altering model treatment for any of the nitrogenous species has the potential to impact the others. Von Kuhlmann et al. (2004) found that both NO_x and O_3 concentrations were sensitive to nitrate yield. In their global modeling, a doubling of isoprene nitrate yield caused NO_x concentration increases and decreases (in different geographic regions) of up to 30 and 20%, respectively. Ozone decreases were more common and concentrations were lower by 30% in some areas.

While model predictions of NO_2 are often compared with ambient measurements, this study evaluates predictions of NO_z speciation. Measurement details are presented in section 4.2.5. Model NO_z validation is important because the chemical mechanism description of RONO_2 is highly uncertain. Of the NO_z species, RONO_2 concentrations have the most variation in model simulations using different chemical mechanisms (Luecken et al., 1999). RONO_2 is known to be

an important reservoir for NO_x as ambient measurements at two sites in California show that it makes up a significant portion of NO_z , 10 to 50% (Day et al., 2003). Perring et al. (2009) find that RONO_2 comprises 12 to 20% of NO_z in the eastern US.

As VOC measurements have become more dependable and widespread, increased attention to model performance has followed (Steiner et al., 2008; Luecken et al., 2012). Steiner et al. (2008) compared VOC reactivity determined in an air quality model using SAPRC99 to VOC reactivity calculated from measured concentrations of VOC and NO_2 . Luecken et al. (2012) found for the eastern half of the US that formaldehyde and acetaldehyde in the atmosphere are mainly due to photochemical production. The CMAQ model using the SAPRC mechanism underpredicted these compounds by as much as 50% in some areas. Model performance for VOC is explored here using an improved chemical mechanism applied to modeling air quality in central California.

The need for a mechanism generation system that includes the capability for alternate lumping strategies (as developed in Chapter 3) and specification of variable reaction product yields is emphasized by the recently observed issue of winter season high-ozone events. To study high-ozone conditions observed during winter months in the Upper Green River Basin of Wyoming, the SAPRC mechanism was rederived with lumped species representative of the local VOC mix, and with product yields specified for a temperature of 265 K rather than 300 K (Carter and Seinfeld, 2012). Hourly average ozone measurements above 140 ppb are recorded in this region (Schnell et al., 2009), and exceedance of the 8-hour ozone standard occurs regularly in winter (since monitoring began) due to stagnant meteorological conditions and high VOC and NO_x emissions associated with natural gas extraction (Environ, 2010). A similar wintertime ozone problem has been reported for the Uinta Basin in Utah (Carter and Seinfeld, 2012). It is unclear how widespread the issue is because there are few ozone monitors located in such remote areas. However, Schnell et al. (2009) speculate that winter ozone events occur around fossil fuel extraction sites with similar meteorological conditions, which includes other areas in the Western US, Canada, Russia, Kazakhstan, Mongolia, and China. Natural gas extraction is expected to increase in many areas of the world (Mohr and Evans, 2011). Further model-based analyses of winter season air quality will require a mechanism with easily alterable lumped species representation, as well as temperature-dependent oxidation product yields for VOC reactions. Currently, only the SAPRC mechanism developer (Carter) has the ability to alter the mechanism for a different assumed temperature than 300 K. The ability to rederive the mechanism at a specific temperature is useful and may be necessary for retuning the model to work for specific applications. This chapter provides a general solution to the problem of correctly describing temperature-dependent chemistry. A mechanism and AQM are altered to allow VOC oxidation products to change with temperature. I explore the implications of capturing the effects of spatially and temporally-varying temperature fields on air quality model predictions.

4.2 Methods

4.2.1 Temperature-dependent VOC oxidation products

Reaction rate coefficients for $\text{VOC} + \text{OH}^\cdot$ reactions have been experimentally determined for approximately 750 of the thousands of known VOC (Meylan and Howard, 2003). However, most of these studies do not report on the relative importance of subsequent reaction pathways, each of

which can lead to different oxidation products. Very few alkyl peroxy and alkoxy radical rate coefficients have been investigated. Various structure-reactivity correlations, also called structure-activity relationships (SARs), have been developed using the available data, such that reaction coefficients can be estimated for all VOC + OH[•], alkyl peroxy, and alkoxy radical reaction pathways for use in research studies. Alkyl peroxy and alkoxy radicals can also result from VOC reaction with NO₃ and O₃, the temperature-dependence of these radicals is also considered.

Initiation

For alkanes and alcohols, oxidation is initiated by reaction with the OH radical, and proceeds by H-abstraction. H-abstraction from a C-H bond creates an alkyl radical (R[•]) that quickly reacts with oxygen to form an alkyl peroxy radical (RO₂[•]). Figure 4-2 shows the two reaction pathways in which H-abstraction occurs for n-butane. The generalized reactions, where R equals an arbitrary alkyl group, are summarized more simply below.



H-abstraction from the -OH group in an alcohol leads to direct formation of an alkoxy radical, as shown below.



Atkinson (1986 and 1987) developed, and subsequently updated (Kwok and Atkinson, 1995), SARs to estimate reaction rate coefficients for VOC with OH radical. The rate coefficient is calculated based on the molecular context of each carbon atom from which hydrogen atoms can be abstracted. Carbon atoms are classified as primary, secondary, or tertiary, depending on the number of other carbon atoms to which they are directly bonded. Additional substituent factors capture effects relating to molecular structures associated with the neighboring carbon atoms. The reaction rate for H-abstraction from an O-H bond is calculated similarly using an SAR. Calculation details and parameters defining the rate coefficients used in this research are presented in Table 4-1.

Table 4-1. Temperature-dependent structure activity relationship

Used to calculate rate coefficients for hydrogen-abstraction from a VOC by OH radical, from Kwok and Atkinson (1995)

$k(G)$: rate constant calculation for H-abstraction from group G	k^a for group G ($\text{cm}^3 \text{ molecule}^{-1} \text{ s}^{-1}$)
$k(\text{CH}_3\text{-X}) = k_{\text{prim}}F(X)$	$k_{\text{prim}} = (4.49 \times 10^{-18})T^2 \exp(-320/T)$
$k(\text{X-CH}_2\text{-Y}) = k_{\text{sec}}F(X)F(Y)$	$k_{\text{sec}} = (4.50 \times 10^{-18})T^2 \exp(253/T)$
$k\left(\begin{array}{c} \text{X} \\ \diagdown \\ \text{CH} \\ \diagup \\ \text{Y} \end{array} - \text{Z}\right) = k_{\text{tert}}F(X)F(Y)F(Z)$	$k_{\text{tert}} = (2.12 \times 10^{-18})T^2 \exp(-696/T)$
$k(\text{OH-X}) = k_{\text{OH}}F(X)$	$k_{\text{OH}} = (2.12 \times 10^{-18})T^2 \exp(-85/T)$

^aT = temperature in K

Substituent factors are specified in the form, $F(X) = e^{\text{Ex}/T}$. Substituent factors for molecules including an -OH functional group have been updated (Bethel et al., 2001). Table 4-2 shows the substituent factors used in this research. The overall VOC + OH· rate constant is the sum of every possible H-abstraction rate constant, e.g. for n-butane,

$$k_{\text{butane, total}} = 2k_{\text{prim}}F(-\text{CH}_2-) + 2k_{\text{sec}}F(-\text{CH}_3)F(-\text{CH}_2-) \quad (\text{E4.1})$$

Table 4-2. Substituent factor parameters for VOC

Information used to calculate $F(X)$, substituent factor for H-abstraction by OH radical, and $F_{\text{isom}}(X)$, substituent factor for alkoxy radical isomerization

Substituent Factors			
X	E_X	$F(X)^a$	$F_{\text{isom}}(X)^b$
-CH ₃	0	1.0	1.0
-CH ₂	61.7	1.23	1.3
-CH	61.7	1.23	1.3
-C	61.7	1.23	1.3
=O	645	8.6	16.4
-C=O	-85.7	0.75	0.7
-CHC=O	406	3.9	5.9
5-member ring	-133	0.64	0.6
6-, 7-, and 8-member rings	0	1.0	1.0
-OH ^c	317	2.9	4.0
-COH ^c	285	2.6	3.5

^a $F(X) = \exp(E_X/T)$, shown at 300 K

^b $F_{\text{isom}}(X) = (\exp(E_X/T))^{1.3}$, shown at 300 K

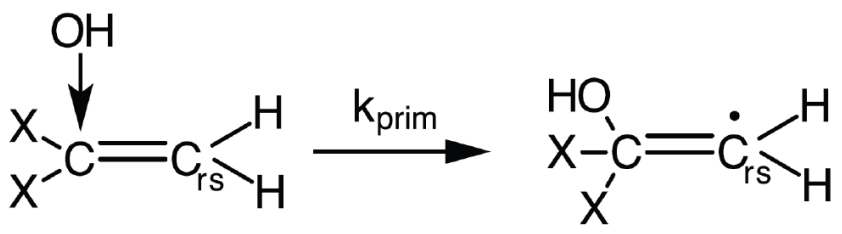
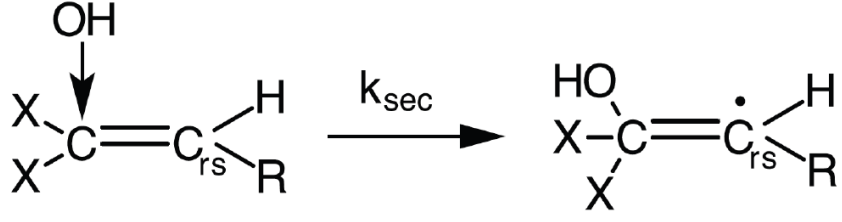
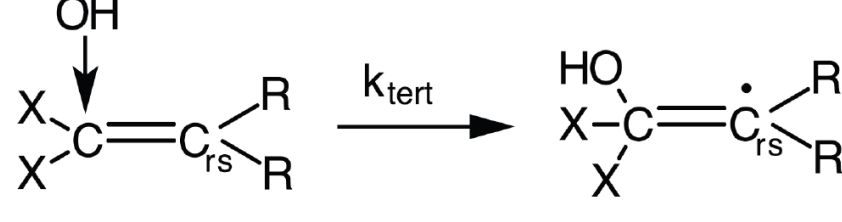
^c values from Bethel et al. (2001), all others from Kwok and Atkinson (1995)

H-abstraction can occur for alkene + OH[•] reactions, but for a C=C double bond, OH-addition is the dominant reaction pathway, resulting in a hydroxyalkyl radical. A site-specific description of OH-addition to carbon-carbon double bonds, based on a structure-activity relationship developed by Peeters et al. (2007), is used for the alkenes in this research. Unlike the SAR to calculate alkane rate coefficients, the SAR for site-specific OH-addition to alkenes is temperature-*independent*, and was determined based on experimental results at 298 K, as summarized in Table 4-3. The procedure for polyalkenes is similar; examples and values can be found in Peeters et al. (2007). The resulting hydroxyalkyl radical (see Table 4-3) reacts quickly with O₂ to form a hydroxyalkyl peroxy radical, analogous to the alkyl peroxy radicals formed from alkane + OH[•] reactions.

For alkene radicals which can undergo unimolecular isomerization, of which only isoprene and 3-methyl-butene have significant yields, a 25% isomerization rate is assumed, based on values defined for isoprene in the MCM v3.2 (available at <http://mcm.leeds.ac.uk/MCM/roots.htm>).

Table 4-3. Mechanism and SAR parameters for OH· addition to alkenes

Used to calculate rate coefficients for species that contain one or more C=C double bonds. These radical site (rs) specific parameters are used to determine the relative importance of each OH-addition pathway.
Developed by Peeters et al. (2007)

OH addition to alkene	SAR parameter ($10^{-11} \text{ cm}^3 \text{ molecule}^{-1} \text{ s}^{-1}$)
	.45
	3.0
	5.5

Alkene and terpene initiation reactions with NO_3 radical and O_3 are not altered from the Base SAPRC07 mechanism, because the SAR for these initiation pathways have not been updated.

Organic peroxy radicals

In the presence of NO_x , organic nitrate (RONO_2) formation competes with NO to NO_2 conversion, which happens in parallel with alkoxy radical ($\text{RO}\cdot$) formation, as described in reactions R4.2 and R4.3. Both of these reaction pathways are theorized to proceed via a common intermediate, peroxy alkyl nitrite (ROONO), and nitrate formation occurs when ROONO is able to isomerize (Zhang et al., 2004). Experimental results show that nitrate yield is a function of temperature, pressure, and molecular structure. However, the current treatment in the SAPRC mechanisms only accounts for differences in molecular structure, and the RONO_2 yield at 300K and 1 atmosphere is used exclusively.

Two methods to constrain nitrate formation based on temperature, pressure, and molecular structure have been developed independently and result in similar nitrate yields (Carter and Atkinson, 1989; Zhang et al., 2004). The nitrate yield calculation method of Carter and Atkinson (1989) with the revised parameters presented in Carter (2000) is used in this study for all relevant

peroxy radicals. The effect of differences among molecules has been described in Carter's parameterization by the number of carbon atoms as well as the order of the carbon atom where the radical center is located. Nitrate yields decrease with temperature and increase with pressure and carbon number. Maximum nitrate yield occurs for radicals on a secondary carbon. Equations to calculate the organic nitrate yield from a secondary alkyl peroxy radical (Y_{sec}) are shown below.

$$Y_{sec} = (k_N/k_R)/[1 + (k_N/k_R)] \quad (E4.2)$$

where,

$$k_N/k_R = \left(\frac{R_0 \cdot M \cdot (T/300)^{-m_0}}{R_{\infty}^{300} \cdot (T/300)^{-m_{\infty}}} \right) F^Z \quad (E4.3a)$$

$$Z = \left\{ 1 + \left[\log \left(\frac{R_0 \cdot M \cdot (T/300)^{-m_0}}{R_{\infty}^{300} \cdot (T/300)^{-m_{\infty}}} \right) \right]^2 \right\}^{-1} \quad (E4.3b)$$

and

$$R_0 = \alpha \cdot e^{\beta C_n} \quad (E4.3c)$$

In the above equations, k_N/k_R represents the rate constant ratio for nitrate formation to radical formation, M is the total gas molecule density in molecules/cm³, and the empirical parameters, obtained using a non-linear fitting procedure, were determined by Carter (2000) as follows:

$$\alpha = 3.94 \cdot 10^{-22} \text{ cm}^3 \text{ molecule}^{-1}, \beta = 0.705, R_{\infty}^{300} = 0.380, m_0 = 2.15, m_{\infty} = 6.36, F = 0.745$$

A reduction of 1.5 in the assumed number of carbon atoms is used to calculate nitrate yield with the above equations for all non-secondary and/or substituted peroxy radicals (Carter, 2000).

Alkoxy radicals

While organic nitrate formation is a sink for radicals, the competing reaction, formation of alkoxy radicals and NO₂, is a chain-propagating step that enhances ozone production. Alkoxy radicals transform quickly in the atmosphere by reaction with oxygen, isomerization, or thermal decomposition (as seen for n-butane oxidation, Figure 4-2). Thousands of these intermediate radicals are formed in the atmosphere, and few have been studied in the laboratory, so structure-activity relationships (SAR) for alkoxy radical rate constants have been developed (Atkinson, 1997; Atkinson, 2007).

Reaction with oxygen

Reaction with O₂ results in a carbonyl (aldehyde or ketone) and a hydroperoxyl radical (HO₂·). Atkinson (2007) recommended a reaction rate coefficient for both primary (RCH₂O·) and secondary (RCH(O·)R') radicals:

$$k_{O_2} = 2.5 \times 10^{-14} e^{-300/T} \text{ cm}^3 \text{ molecule}^{-1} \text{ s}^{-1} \quad (\text{E4.4})$$

This is a second order reaction, but the isomerization and decomposition reactions described below are first-order reactions. In order to compare these reaction rate coefficients, a pseudo-first order loss rate is calculated. The pseudo-first-order loss rate for VOC reaction with O₂ is calculated by multiplying the reaction rate coefficient by the O₂ gas molecule density.

Isomerization

Isomerization (molecular structure rearrangement) of alkoxy radicals involves a hydrogen atom transfer from a carbon atom to an oxygen atom. This type of isomerization can only occur in molecules with a minimum of four carbons between the oxygen atom and an abstractable hydrogen, through a 6-member transition state, and results in a 4-hydroxyalkyl radical. Two examples of this type of isomerization are shown in Figure 4-2. The rate of isomerization increases with the order of the carbon from which the hydrogen is abstracted (e.g. H-abstraction via isomerization from a primary carbon is slower than from a tertiary carbon), and also increases with temperature. Similar to H-abstraction in a VOC + OH[•] reaction, the neighbors of the carbon from which the H-atom is abstracted are taken into account using substituent factors.

Table 4-4. Temperature-dependent structure activity relationship

Used to calculate rate coefficients for hydrogen-abstraction by isomerization, from Atkinson (2007)

$k_{\text{isom}}(\text{G})$: isomerization rate constant calculation for H-abstraction from group G	k_{isom}^a for group G (s ⁻¹)
$k_{\text{isom}}(\text{CH}_3\text{-X}) = k_{\text{isom/prim}} F_{\text{isom}}(\text{X})$	$k_{\text{isom/prim}} = (1.2 \times 10^{11}) \exp(-3825/T)$ $= 3.5 \times 10^5$ at 300 K
$k_{\text{isom}}(\text{X-CH}_2\text{-Y}) = k_{\text{isom/sec}} F_{\text{isom}}(\text{X}) F_{\text{isom}}(\text{Y})$	$k_{\text{isom/sec}} = (8.0 \times 10^{10}) \exp(-3010/T)$ $= 3.5 \times 10^6$ at 300 K
$k_{\text{isom}} \left(\begin{array}{c} \text{X} \\ \diagdown \\ \text{C} \\ \diagup \\ \text{Y} \end{array} \text{CH-Z} \right) = k_{\text{isom/tert}} F_{\text{isom}}(\text{X}) F_{\text{isom}}(\text{Y}) F_{\text{isom}}(\text{Z})$	$k_{\text{isom/tert}} = (4.0 \times 10^{-10}) \exp(-2440/T)$ $= 1.2 \times 10^7$ at 300 K

^aT = temperature in K

Atkinson (2007) recommended substituent factors estimated based on the H-abstraction substituent factors, $F_{\text{isom}}(\text{X}) = [F(\text{X})]^{1.3}$. $F_{\text{isom}}(\text{X})$ and $F(\text{X})$ values at 298 K are presented in Table 4-2. The formulas used to calculate the rate coefficients for the two isomerization examples in the butane oxidation example shown in Figure 4-2 are presented in order below.

$$k_{\text{isom-1}} = k_{\text{isom/prim}} F_{\text{isom}}(-\text{CH}_2-) \quad (\text{E4.5A})$$

$$k_{\text{isom-2}} = k_{\text{isom/sec}} F_{\text{isom}}(-\text{CH}_2-) F_{\text{isom}}(-\text{OH}) \quad (\text{E4.5B})$$

After the first isomerization occurs, the resulting 1,4-hydroxyalkyl radical reacts quickly with O₂ to form a 1,4-hydroxyperoxy radical. This resulting peroxy radical is treated as described in the section above titled “organic peroxy radicals.” For example, temperature-dependent organic nitrate formation versus 1,4-hydroxyalkoxy radical formation is determined, and then the potential 1,4 hydroxyalkoxy radical reaction pathways are determined (e.g. the relative rates of O₂, isomerization, and decomposition). In general, the second isomerization dominates over reaction with O₂ or decomposition because H-atom abstraction (via isomerization) from a carbon with an OH group attached is predicted to be faster than the initial isomerization. Notice in Table 4-2 that the substituent factor for (-OH) is about three times higher than that of the non-substituted groups (e.g., -CH₂-).

Decomposition

Decomposition of an alkoxy radical results in formation of a carbonyl and a radical. The equations from Atkinson (2007) used to describe the rate of decomposition of an alkoxy radical are shown below.

$$k_{\text{decomp}} = A \cdot n \cdot e^{-E_d/RT} \quad (\text{E4.6a})$$

$$E_d = a + b(\Delta H) \quad (\text{E4.6b})$$

where n is the reaction path degeneracy, and the pre-exponential factor, $A = 5 \times 10^{13} \text{ sec}^{-1}$, was determined based on experimental results and theoretical calculations. Reaction path degeneracy is normally one. It is greater than one only if there is more than one possible identical leaving radical (i.e. for branched molecules.) The Arrhenius activation energy E_d is dependent on properties of the leaving radical (reflected in parameter a), the heat of reaction (ΔH), and an empirical constant ($b=0.4$). Values for a used in this study are shown in Table 4-5. Decreasing a values correlate with increasing rates of decomposition for similar alkoxy radicals. The heat of reaction is calculated by the difference in enthalpies of formation between the alkoxy radical and the two products. Enthalpies of formation were obtained using a group-additivity method (Stein and Brown, 2005). Where enthalpies of formation cannot be calculated (i.e. a numerical value has not been assigned), the reaction rate is calculated in accordance with the method of Vereecken and Peeters (2009), which only takes into account properties of the two carbon atoms involved in the bond scission.

Table 4-5. Parameter used for estimating alkoxy radical decomposition rate

As given in Atkinson (2007)

Leaving Radical	a (kJ/mol)
Methyl	54
Ethyl	41
1-Propyl	40
General RC·H ₂	40
2-Propyl	35
General R ₂ C·H	34
t-Butyl	30
General R ₃ C·	30
RC·HOH	28
RC·HOH	22
R ₂ C·OH	20

4.2.2 SAPRC mechanism

The temperature dependencies described above were applied to each of the 28 VOC oxidation reactions shown in Table 4-6. Each of the VOC oxidation reactions has the same overall rate coefficient as defined in the revised chemical mechanism presented in Chapter 3. Most of these reaction rate coefficients were already temperature-dependent, but now for these 28 reactions organic nitrate yield changes with temperature and pressure. For most of the reactions, other temperature-dependent product yields, resulting from varying rates of alkoxy radical reaction with O₂, isomerization, and decomposition, change as well. The shaded reactions in Table 4-6 indicate only temperature and pressure-dependent nitrate yields are updated.

The aromatic species (BENZ, ARO1, and ARO2) only include temperature-dependent organic nitrate formation, which is standard even for the highly detailed master chemical mechanism (MCM), as the chemistry of these species is not as well understood as alkane, alcohol, and olefin chemistry. In the case of the MVK + OH and ISOP + NO₃ reactions, temperature-dependent stoichiometric coefficients were not created, because the only temperature-dependent pathway is first-generation nitrate formation. To account for temperature-dependent nitrate formation in these equations, a separate reaction is created for nitrate formation alone and the rate coefficients are allowed to vary as shown in Table 4-6.

Table 4-6. Reactions in which temperature-dependent products are included

(shaded gray reactions have temperature-dependent nitrate formation only)

Reaction & Products	k(300) ^a
MVK + OH = RO2N	yON4*2.0E-11
MVK + OH = 0.3*RO2R + 0.7*MECO3 + 0.7*R2O2 + 0.3*HCHO + 0.7*RCHO + 0.3*MGLY	(1-yON4)*2.0E-11
ISOP + NO3 = RO2N + XNE	yON5*3.0E-12
ISOP + NO3 = 0.8*RO2R + 0.2*NO2 + 0.2*R2O2 + 0.2*IPRD + 0.8*RNO3IN	(1-yON5)*3.0E-12
MACR + OH = .480*RO2R + .5*MACO3 + .02*RO2N + .337*CO + .143*HCHO + .337*MEK + .143*MGLY	2.84E-11
MACR + NO3 = .480*RO2R + .5*MACO3 + .02*RO2N + .480*CO + .48*ONA + .02*XNE + .5*HNO3	3.54E-15
MEK + OH = .103*RO2R + .504*MECO3 + .342*RCO3 + .053*RO2N + 1.15*R2O2 + .342*HCHO + .504*CCHO + .103*RCHO	1.20E-12
AFG3 + OH = .568*RO2R + .117*MECO3 + .206*MACO3 + .117*R2O2 + .109*RO2N + .225*CO + .225*GLY + .117*MGLY + .437*IPRD + .124*AFG1 + .124*AFG2 # 9.35e-11;	9.35E-11
IPRD + OH = .734*RO2R + .204*MACO3 + .046*RO2N + .437*CO + .0156*HO2 + .165*HCHO + .013*CCHO + .184*RCHO + .119*MEK + .366*PRD2 + .119*GLY + .058*MGLY + .016*AFG1 + .008*IPRD # 6.19e-11;	6.19E-11
IPRD + NO3 = .731*RO2R + .039*R2O2 + .179*MACO3 + .049*RO2N + .049*XNE + .731*RNO3 + .039*NO2 + .179*HNO3 + .212*HCHO + .014*RCHO + .025*GLY + .014*MGLY + .025*MEK + .518*CO	1.00E-13
PRD2 + OH = .296*HO2 + .529*RO2R + .094*R2O2 + .015*MECO3 + .052*RCO3 + .101*RO2N + .272*HCHO + .114*CCHO + .643*RCHO + .168*MEK + .242*PRD2	1.55E-11
ETOH + OH = .889*HO2 + .109*RO2R + .001*RO2N + .147*HCHO + .925*CCHO	3.21E-12
MTBE + OH = .731*RO2R + .177*MEO2 + .014*TBUO + .391*R2O2 + .078*RO2N + .215*HCHO + .008*ACET + .723*MEK + .177*PRD2	2.95E-12
PACET + OH = .441*RO2R + .494*RCO3 + .548*R2O2 + .065*RO2N + .012*CO + .001*HCHO + .041*CCHO + .050*RCHO + .348*MEK + .497*AACD + .009*PACD + .002*MGLY	3.40E-12
UPOH + OH = .912*HO2 + .086*RO2R + .002*RO2N + .085*HCHO + .202*CCHO + .072*RCHO + .569*ACET + .142*MEK	9.05E-12
ALK2 + OH = .942*RO2R + .020*R2O2 + .014*MEO2 + .044*RO2N + .020*HCHO + .035*CCHO + .240*RCHO + .682*ACET	1.11E-12
ALK3 + OH = .635*RO2R + 0.672*R2O2 + .019*MEO2 + .266*TBUO + .080*RO2N + .060*HCHO + .447*CCHO + .120*RCHO + .053*ACET + .287*MEK	2.30E-01

cont. on next page

cont. from previous page

Reaction & Products	k(300) ^a
ALK4 + OH = .768*RO2R + 1.074*R2O2 + .006*MEO2 + .033*TBUO + .020*MECO3 + .003*RCO3 + .170*RO2N + .079*HCHO + .406*CCHO + .265*RCHO + .460*ACET + .080*MEK + .126*PRD2 + .045*CO	4.29E-12
ALK5 + OH = .641*RO2R + 1.126*R2O2 + .003*MEO2 + .019*MECO3 + .002*RCO3 + .144*RO2N + .050*HCHO + .124*CCHO + .283*RCHO + .324*PRD2 + .090*MEK + .089*ACET + .002*MGLY + .014*CO	8.24E-12
OLE1 + OH = .966*RO2R + .047*R2O2 + .002*MEO2 + .032*RO2N + .873*HCHO + .756*CCHO + .149*RCHO + .015*ACET + .039*MEK + .018*PRD2 + .008*MACR + .004*MVK	2.71E-11
OLE1 + NO3 = .925*RO2R + .066*RO2N + .117*R2O2 + .009*HCHO + .024*CCHO + .011*RCHO + .033*ACET + .098*RNO3 + .767*ONA + .061*ONB + .061*XNE + .009*NO2	1.06E-14
OLE2 + OH = .948*RO2R + .011*R2O2 + .001*MACO3 + .050*RO2N + .549*HCHO + .393*CCHO + .133*RCHO + .577*ACET + .058*MEK + .003*PRD2 + 0.001*CO + .083*MACR + .003*MVK + .024*IPRD	6.11E-11
OLE2 + NO3 = .161*RO2R + .880*R2O2 + .090*RO2N + .124*HCHO + .776*CCHO + .394*RCHO + .061*ACET + .042*MEK + .035*MACR + .018*IPRD + .002*MVK + .044*RNO3 + .115*ONA + .093*XNE + .749*NO2	1.56E-12
ISOP + OH = .935*RO2R + .003*R2O2 + .065*RO2N + .726*HCHO + .265*MACR + .460*MVK + .209*IPRD	9.96E-11
BENZ + OH = .57*HO2 + .116*OH + .290*RO2R + .024*RO2N + .29*GLY + .57*CRES + .029*AFG1 + .261*AFG2 + .116*AFG3	1.22E-12
ARO1 + OH = .174*HO2 + .298*OH + .467*RO2R + .061*RO2N + .041*PRD2 + .228*GLY + .145*MGLY + .174*CRES + .052*BALD + .174*AFG1 + .199*AFG2 + 0.29798*AFG3	5.71E-12
ARO2 + OH = .130*HO2 + .227*OH + .547*RO2R + .096*RO2N + .023*PRD2 + .137*GLY + .278*MGLY + .064*BACL + .130*CRES + .046*BALD + .202*AFG1 + .188*AFG2 + .324*AFG3	2.08E-11
TERP + OH = .761*RO2R + .038*RCO3 + .373*R2O2 + .201*RO2N + + .001*CO + .262*HCHO + .525*RCHO + .029*ACET + .010*MEK + .250*PRD2 + .0126*MGLY + .010*BACL + .001*MVK + .002*IPRD	7.97E-11
TERP + O3 = .052*HO2 + .585*OH + .085*RO2R + .694*R2O2 + .126*MECO3 + .138*RCO3 + .194*RO2N + .154*HCHO + .155*RCHO + .114*ACET + .004*MEK + .409*PRD2 + .107*FACD + .043*PACD + .074*BACL + .001*MACR + .183*CO	6.99E-17
TERP + NO3 = .136*RO2R + 1.350*R2O2 + .011*RCO3 + .408*RO2N + .044*HCHO + .453*RCHO + .137*ACET + .001*MGLY + .001*MVK + 0.137*RNO3 + .002*ONA + .405*XNE + .445*NO2 + .020*CO	6.55E-12

^aUnits of k(300) are [cm³ molec⁻¹ s⁻¹]

To determine total predicted nitrate and to compare with measurements, additional mechanism revisions were necessary. The SAPRC species RNO_3 , which is used to represent reactive nitrate, or nitrate with an OH^\cdot reaction rate coefficient (k_{OH}) higher than $5 \times 10^{-13} \text{ cm}^3 \text{ molec}^{-1} \text{ s}^{-1}$ (Carter, 2000), is the species formed in the $\text{VOC} + \text{OH}^\cdot$ reactions shown in Table 4-6. However, there is another model species, XN, that accounts for lost nitrogen (mainly produced by VOC reactions with the nitrate radical). Lost nitrogen includes (1) low reactivity nitrate products ($k_{\text{OH}} < 5 \times 10^{-13} \text{ cm}^3 \text{ molec}^{-1} \text{ s}^{-1}$, calculated using the Kwok and Atkinson (1995) structure-activity method), (2) nitrate species that represented in the mechanism as a different lumped species, and (3) nitrate species with more than one $-\text{ONO}_2$ group. Since nitrate predictions are not generally analyzed in modeling studies, the XN species is not included in the standard CMAQ implementation, and furthermore cannot be used in its present form because only a portion is reactive. For the model simulations in this chapter, the XN species is altered to only include extra nitrate. Only two “unreactive” nitrate species, 1-hydroxy-2-propanone nitrate and nitromethyl formate, were found to contribute to the XN species, so these were added in the updated mechanism as separate species, with species names ONA and ONB, respectively. Another species was added (RNO3IN) in order to account for nitrate formation from the reaction of isoprene with NO_3 . SAPRC07 treated this species as IPRD (lumped isoprene product), but that species could not be used unambiguously for nitrate accounting. Each of these three species and their associated reactions are shown in Table 4-7; reaction products and parameters from the MCM (Jenkin et al., 1997) were used. The $\text{RNO3IN} + \text{OH}$ reaction was altered similarly to the $\text{MVK} + \text{OH}$ and $\text{ISOP} + \text{NO}_3$ reactions described above to account for temperature and pressure-dependent nitrate formation. The deposition velocity of the RNO_3 species is equal to that of PAN in the standard SAPRC driven CMAQ model. The same deposition velocity is added for XN, ONA, ONB, and RNO3IN for the simulations in this chapter. In this chapter, RNO_3 always refers to the model species, and RONO_2 refers to total nitrate, $\text{RONO}_2 + \text{XN} + \text{ONA} + \text{ONB} + \text{RNO3IN}$.

Table 4-7. Species added to SAPRC07 to account for organic nitrate

Reaction & Products	k^a
$\text{ONA} + \text{OH} = .784 \cdot \text{RO2R} + .784 \cdot \text{R2O2} + 1.568 \cdot \text{HCHO} + .216 \cdot \text{MGLY} + \text{NO}_2$	$1.33\text{E}-13$
$\text{ONA} = \text{MECO}_3 + \text{HCHO} + \text{NO}_2$	photolysis
$\text{ONB} + \text{OH} = \text{R2O2} + \text{HNO}_3 + \text{HCHO} + \text{NO}_2$	$1.93\text{E}-11$
$\text{ONB} + \text{NO}_3 = \text{R2O2} + \text{HNO}_3 + \text{HCHO} + \text{NO}_2$	$3.80\text{E}-15$
$\text{ONB} = \text{CO} + \text{HCHO} + \text{NO}_2 + \text{HO}_2$	photolysis
$\text{RNO3IN} + \text{OH} = \text{RO2N} + \text{XNE} \# 4.54\text{e}-11;$	$y_{\text{ON}} \cdot 4.5\text{E}-11$
$\text{RNO3IN} + \text{OH} = 0.345 \cdot \text{R2O2} + 0.345 \cdot \text{IPRD} + 0.345 \cdot \text{NO}_2 + 0.655 \cdot \text{ONA}$ + $0.645 \cdot \text{GLY} + 0.645 \cdot \text{RO2R}$	$(1 - y_{\text{ON}}) \cdot 4.5\text{E}-11$
$\text{RNO3IN} = \text{ONA} + 2 \cdot \text{CO} + 2 \cdot \text{HO}_2 \# 1.0 / \langle \text{MACR_SAPRC07} \rangle;$	photolysis

^aWhere given, units of k are $[\text{cm}^3 \text{ molec}^{-1} \text{ s}^{-1}]$, all reported are temperature-independent

4.2.3 Air quality model

Chemistry is defined in the CMAQ model with a suite of chemical mechanism text files. These files describe the species and reactions, rate coefficients, product yields, diffusion coefficients,

and deposition velocities of selected species (CMAQ documentation). Product yields per mole of precursor reacting, otherwise known as stoichiometric coefficients, at 300 K and 1 atm pressure are defined in a text file which is referenced as a look-up table by the modeling system at each time step (multiple times per model-hour). Direct calculation of temperature- and pressure-dependent product yields, using the formulas described above, within CMAQ at each time step was found to be too computationally intensive. Therefore a preprocessor was developed to produce another mechanism definition file, with stoichiometric coefficients for all of the VOC reactions, pre-calculated at small intervals of temperature and pressure over the relevant ranges of values. A look-up table method was implemented in my revised version of CMAQ, in which the four values on either side of the temperature and pressure are pulled, and the temperature and pressure-dependent stoichiometric coefficients are calculated using bilinear interpolation.

For the MVK + OH, ISOP + NO₃, and RNO₃IN + OH reactions, variable rate coefficients dependent on temperature and pressure are used to account for varying nitrate yield. This method of accounting for temperature-dependent organic nitrate formation can only be used to account for first-order organic nitrate formation, but saves model computational time as compared to using a look-up table for each product. The reaction rate coefficients are scaled in the CMAQ code in each model cell time step such that each VOC oxidation reaction has the same overall rate, but the rate of nitrate formation compared to other product formation now changes with temperature and pressure.

4.2.4 Temperature-dependent emissions

As shown in Figure 3-3 for the summer 2000 Central California Ozone Study emissions (developed by CARB), motor vehicle emissions were modeled as being identical Monday through Thursday, but included differences in traffic timing and volume on Friday, Saturday, and Sunday. (Differences between the Friday and the Monday through Thursday motor vehicles emissions are difficult to discern in Figure 3-3, but the differences include slightly higher emissions throughout the morning, and a slightly lower evening emission peak.) Model emissions for area sources account for weekday-weekend differences in activity patterns. However, the potential impact of variability in anthropogenic VOC emissions due to day-to-day temperature differences was not considered in the 2-week simulations presented in Chapters 2 and 3 of this dissertation or in a longer four-month study using the same emissions (Jin et al., 2010).

Rubin et al. (2006) employ a chemical mass balance approach using VOC measurements from Granite Bay, CA, to quantify the rate of evaporative emission increase due to increases in ambient air temperatures. A 6.5% increase in gasoline evaporative emissions per degree Celsius was reported for the summer of 2001. In order to include this temperature-dependency in the emissions underlying the model simulations reported in this chapter, the 15-day (July 22 through August 5, 2000) average hourly temperature was determined for each ground-level grid cell. The molar percent of evaporative gasoline emissions for each VOC species was determined in Chapter 3. Rubin et al. (2006) used the Granite Bay data to infer hourly percent contribution to headspace vapor – from 7% in morning to a peak of 22% at 3 pm. These results were used to perturb average VOC evaporative gasoline emissions for each grid cell-hour; both motor vehicle and area emission input files are altered. The overall sum of VOC emissions in each grid cell is the same if summed over the 15-day AQM input data, but emissions in cells with temperatures

lower than the average hourly temperature are lower while emissions in cells with temperatures higher than the hourly temperature are higher.

4.2.5 Air quality model simulations

The CMAQ simulations in this chapter use the meteorology, emissions, and boundary and initial conditions described in Chapter 3. First, simulations with new temperature-dependent stoichiometric coefficients (referred to as the SCT simulations) are compared to the updated SAPRC07 mechanism with stoichiometric coefficients at 300 K (Base simulations). Model simulations are compared to see the effects of including temperature-dependent VOC oxidation product yields over a wide range of summertime conditions (including diurnal, day-to-day, and coastal/inland differences in temperature). In a further step, evaporative emissions are perturbed and model simulations performed using the SCT mechanism (these simulations are referred to as SCT_EV). Although 13 day simulations are performed, from July 24 through August 5 (July 22 and 23 are considered spin-up), the results presented in this chapter center around two days, one representing a low-temperature summer day and the other representing a high-temperature summer day.

Lastly, I reevaluate climate change impacts on ozone air quality. The temperature and water vapor perturbations described in Chapter 2 were applied to a larger study domain used in this chapter, as shown in Figure 4-3. Future (2050) anthropogenic VOC and NO_x emissions are first scaled by predicted increases in population by county (California Department of Finance, 2013). Forecast of emission factors, accounting for future advancements in emissions control technology, used by Steiner et al. (2006) were also applied here. CO and VOC emissions, mostly associated with light-duty vehicles as shown in Chapter, are expected to decrease for each automobile. An 80% reduction, or a scaling factor of 0.2, is extrapolated based on past success of previous emission reduction strategies, and is applied to CO and anthropogenic VOC. The scaling factor for NO_x is estimated to be twice this value (i.e., 0.4), due to a predicted increase in diesel engine emission contributions, from which NO_x is harder to control (Steiner et al., 2006). Simulations using both the Base and SCT mechanism with temperature-dependent evaporative emissions are compared to assess air quality differences due to the improved description of temperature dependencies in the revised model.

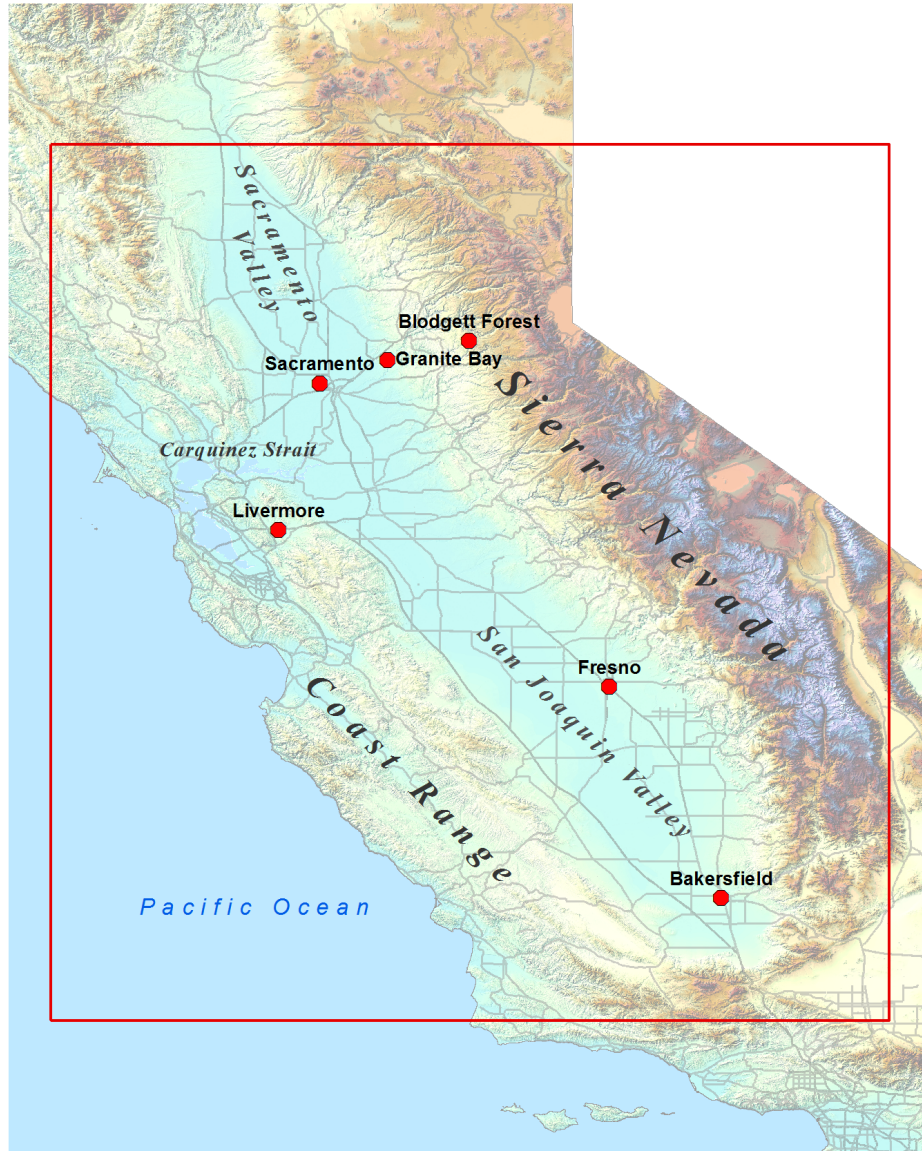


Figure 4-3. Central California model domain outlined with red box

4.2.6 Ambient measurements: NO_2 , NO_z , and ozone

A new approach developed at UC Berkeley uses a thermal dissociation laser-induced fluorescence (TD-LIF) instrument to measure NO_2 and NO_z , the sum of longer-lived NO_2 reservoir species (Day et al., 2002). In the summer of 2001 (July 19 to Sept 15), the TD-LIF instrument was deployed to measure NO_2 and NO_z (HNO_3 , total peroxy nitrates, and total organic nitrates) at Granite Bay, CA (38.74° N , 121.20° W , 277 m altitude) and at the Blodgett Forest Research Station (38.88° N , 120.62° W , 1315 m altitude), shown on the map in Figure 4-3. Granite Bay is on the eastern edge of the Sacramento area, and measurements here are heavily influenced by anthropogenic emissions. Blodgett Forest is a rural site located in the Sierra

Nevada mountains in a ponderosa pine plantation. Ozone was measured at each of the sites during the same time periods (Murphy et al., 2006).

Measured data from these sites have been extensively studied and reported (Day et al., 2003; Cleary et al., 2005; Murphy et al., 2006; Cleary et al., 2007; Murphy et al., 2007; Day et al., 2008; Day et al., 2009). With the new technology, Day et al. (2003) found that alkyl and multifunctional nitrates are an important component of NO_z , and are most likely the source of the “missing NO_y ” identified in several field measurement campaigns (e.g. Williams et al., 1997; Patz et al. 2000; Zellweger et al., 2000; Hayden et al., 2003). Where NO_y includes all nitrogenous species: NO , NO_2 , HNO_3 , RONO_2 , PAN and its analogues, HONO, N_2O_5 , and NO_3 (Day et al., 2003).

The measured NO_z speciation has been compared to Lagrangian model results centered at Blodgett Forest, using Granite Bay data to inform estimation of appropriate values for initial conditions (Perez et al., 2009). However, these California NO_z data have not been used to evaluate 3-d model results, as is done in this chapter. I compare overall diurnal trends in observed and modeled NO_z relationships, because the field data were collected during the summer of 2001, whereas the CMAQ model simulations are for summer 2000.

4.3 Results

4.3.1 Chemical mechanism

Temperature-dependent oxidation product yields were calculated for each VOC species tracked in the air quality model. For the lumped species, the stoichiometric coefficients were calculated based on a weighted average of parameters for relevant species used to define the lumped group (see Table 3-3 for definitions). The resulting mechanism is called the SCT mechanism. Table 4-8 shows temperature-dependent stoichiometric coefficients for the n-butane + OH^\cdot reaction at three temperatures and two pressures. n-Butane accounts for 59% of the ALK3 lumped species in the SAPRC mechanism. Organic nitrate yield increases as temperature decreases, so increased nitrate yield would be expected in cool conditions, as occur at high elevations. However, nitrate yield decreases with decreasing pressure, which offsets the temperature effect on nitrate yield. For instance, the nitrate yield for the n-butane + OH^\cdot reaction at 300 K and 0.9 atm is only 5% percent higher than the yield at 310 K and 1 atm, but is 12% higher at 300 K and the same pressure. The nitrate yield for n-butane is among the lowest described in the mechanism, as nitrate yield increases with carbon number.

Table 4-8. Stoichiometric coefficients for n-butane + OH· reaction

Values given at two pressures and three temperatures

	0.9 atmosphere P			1 atmosphere P		
	290 K	300 K	310 K	290 K	300 K	310 K
NO → RNO ₃	0.087	0.078	0.070	0.091	0.083	0.076
NO → NO ₂	1.22	1.37	1.51	1.20	1.34	1.48
MEO ₂	0.02	0.03	0.04	0.02	0.03	0.04
CCHO	0.417	0.664	0.910	0.394	0.622	0.856
RCHO	0.130	0.150	0.172	0.129	0.148	0.168
MEK	0.575	0.441	0.305	0.584	0.460	0.330
HO ₂	0.895	0.892	0.885	0.892	0.888	0.882

Figure 4-4 shows the nitrate yield at 1 atmosphere for a range of hydrocarbons. The nitrate yield and its temperature dependence increases with carbon number, so the temperature-dependent product yields will be proportionally more affected for larger organic molecules. Temperature-dependent nitrate yields for secondary alkyl peroxy radicals (e.g. 2-butylperoxy) are shown in Figure 4-4. As described in the methods section above, primary, tertiary, or substituted alkyl peroxy radicals are estimated have lower yields, calculated using a reduced carbon number.

The NO → NO₂ conversion process competes with nitrate formation (see Figure 4-1), so the response as a function of temperature is always opposite to that of nitrate formation. The total yield of other products, MEO₂, CCHO, RCHO, MEK, and HO₂· in the case of n-butane + OH· scales with NO → NO₂ conversion. However, these stoichiometric coefficients are also dependent on the competition between alkoxy radical reaction with O₂, isomerization, and decomposition. The resulting temperature-dependent stoichiometric coefficients shown in Table 4-9 are predominantly controlled by the competing reaction pathways of the 2-butoxy radical, as ~80% of H-abstraction takes place from secondary (interior) carbons of n-butane.

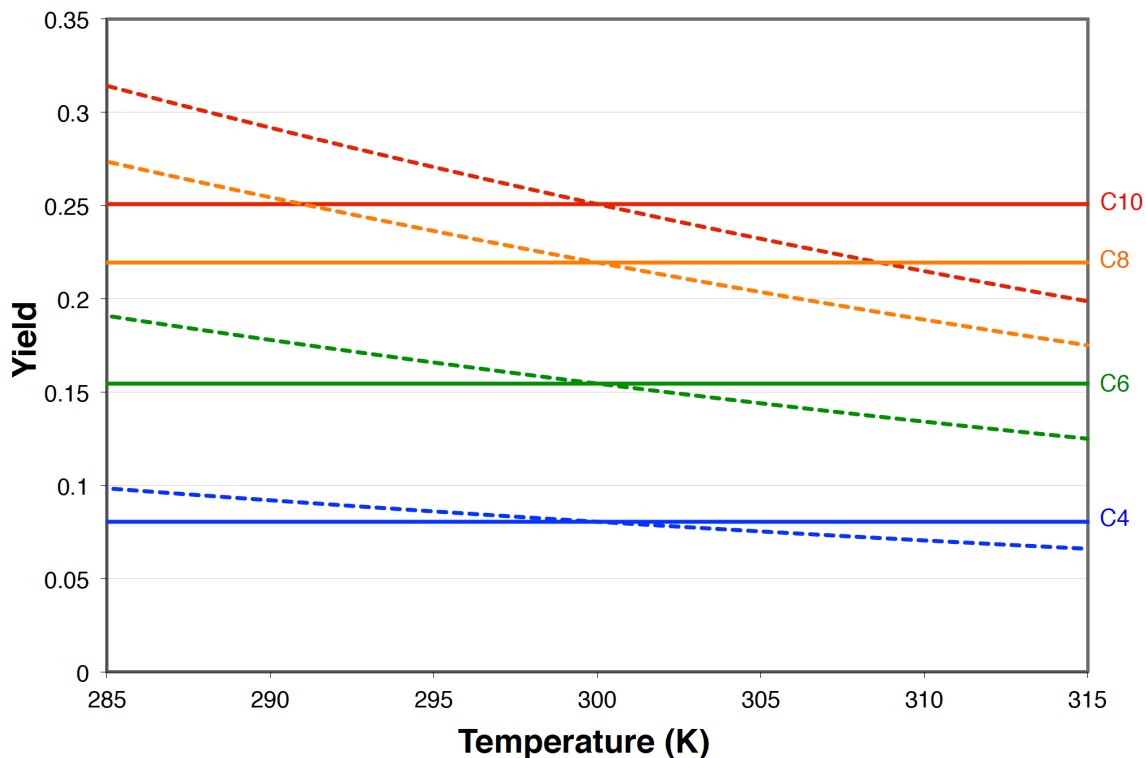


Figure 4-4. Nitrate yield for VOC of different carbon number

Solid line represents the nitrate yield at 300 K and 1 atm, that which is used in the Base SAPRC mechanism.

The dotted lines show the temperature-dependent nitrate yields at 1 atm used in the SCT mechanism developed in this chapter. Values shown are for secondary alkyl peroxy radicals, and are slightly reduced (e.g. calculated with reduced carbon number) for primary, tertiary, and substituted peroxy radicals.

Figure 4-5 shows the 2-butoxy radical reactions and products. The reaction rate coefficients of the decomposition pathways increase with temperature at a faster rate than that of reaction with O_2 . A plot showing these reaction rate coefficients as a function of temperature is presented in Figure 4-6. The relative yield of MEK, formed via 2-butoxy radical reaction with O_2 , decreases as temperature increases. Conversely, the relative yields of MEO₂ (methyl peroxy radical), RCHO (C_3^+ aldehyde), and CCHO (acetaldehyde) increase as the butoxy radical decomposition reactions that form them speed up with increasing temperature.

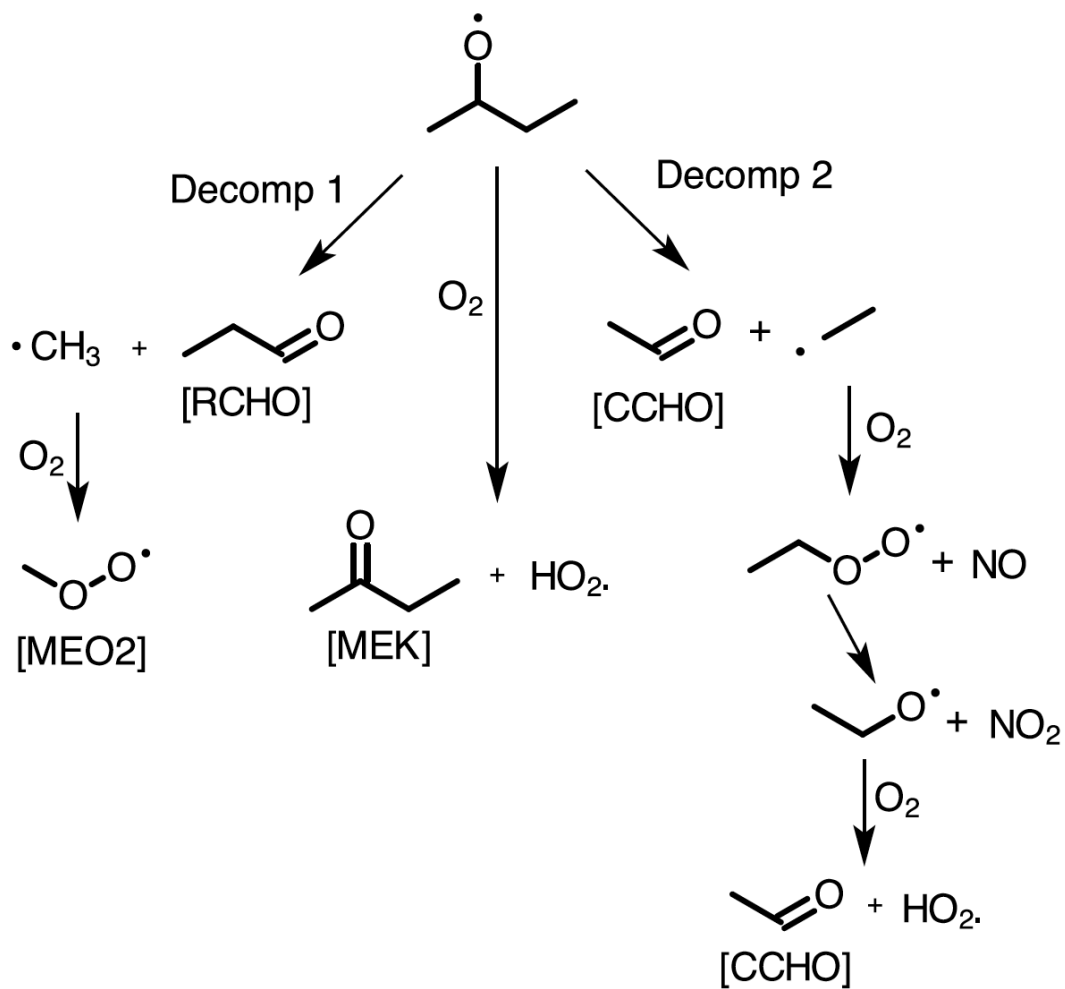


Figure 4-5. Atmospheric reactions for 2-butoxy radical in the presence of NO
 SAPRC species names shown in brackets. Pathways that account for less than 1% of n-butane oxidation are not shown.

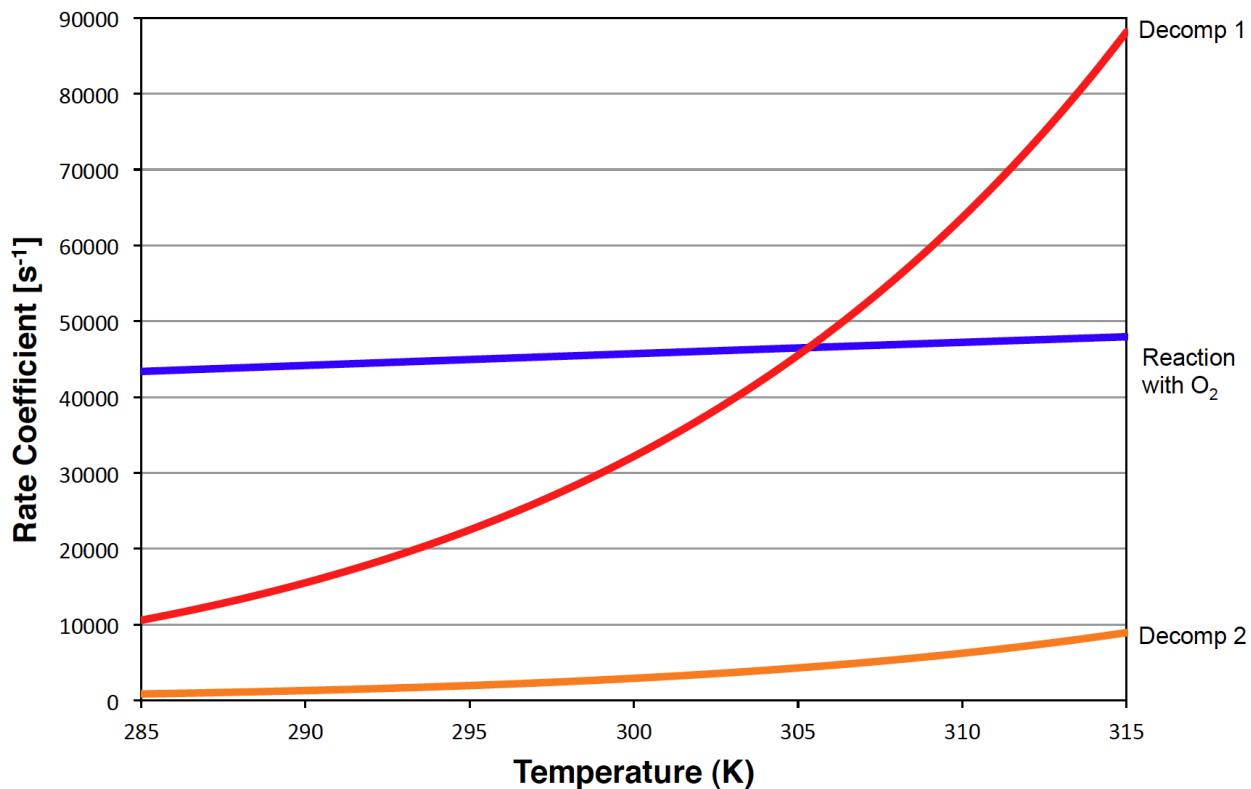


Figure 4-6. Dependence of reaction rate coefficients for 2-butoxy radical on temperature. Rate coefficient shown for reaction with O₂ is pseudo-first-order radical loss rate at 1 atm. The 2-butoxy radical cannot isomerize, so no rate coefficient for that process is shown.

The reaction pathways of the less common 1-butoxy radical are shown in Figure 4-7. The relevant reactions, isomerization and reaction with O₂, both form RCHO. Note that in SAPRC substituted aldehydes are represented using RCHO (C₃⁺ aldehyde), just as substituted nitrates are represented as RNO₃. Figure 4-8 shows that the reaction rate coefficient for isomerization increases with temperature at a much faster rate relative to that of reaction with O₂. This serves to further enhance NO → NO₂ conversion with increasing temperature in the modified SCT mechanism.

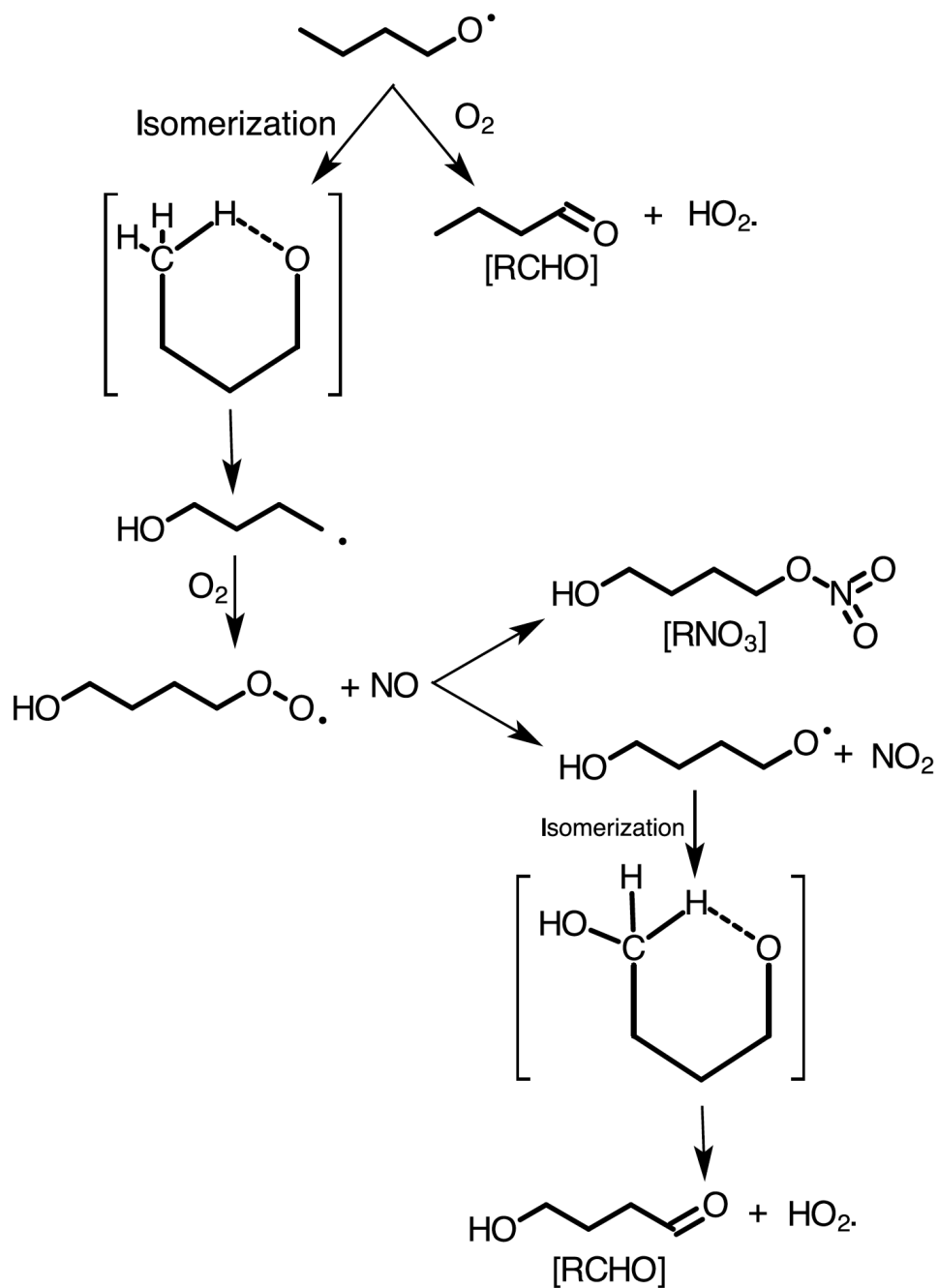


Figure 4-7. Atmospheric reactions for 1-butoxy radical in the presence of NO
 SAPRC species names shown in brackets. Pathways that account for less than 1% of n-butane oxidation are not shown.

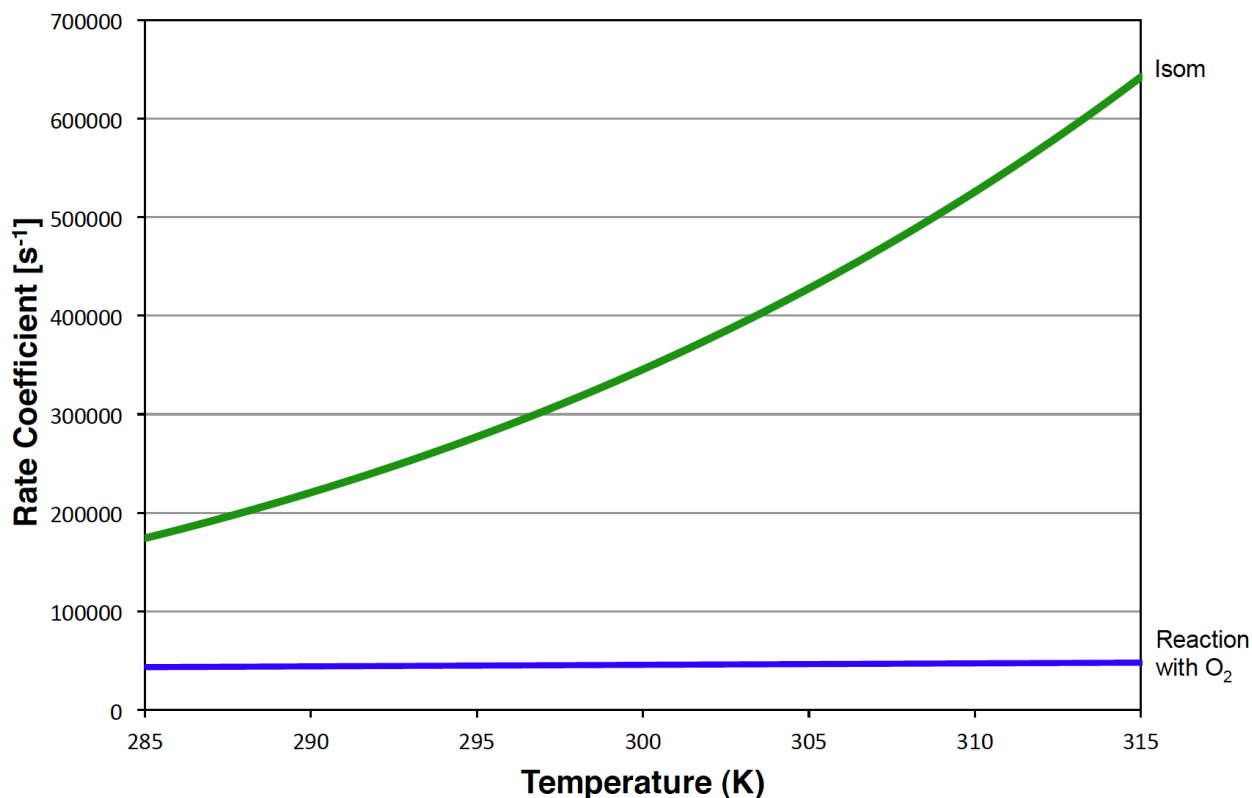


Figure 4-8. Temperature-dependent reaction rate coefficients for 1-butoxy radical

Rate coefficient shown for reaction with O₂ is pseudo-first-order radical loss rate at 1 atm.

The n-butane + OH[•] example presented above provides an illustration of the effects of temperature-dependent radical reaction chemistry; the temperature dependencies of product yields for other VOC have also been modeled in this work, and show similar trends. Generally, for larger alkoxy radicals, reaction with O₂ is insignificant compared to isomerization. However, for larger molecules, decomposition and isomerization often compete, resulting in temperature effects similar to those for n-butane. Table 4-9 shows the change in product yields going from 290 to 310 K. RO₂N, the operator that forms RNO₃, decreases with increasing temperature (as per E4.2 and E4.3 and shown graphically for selected carbon numbers in Table 4-4) for all RO₂[•] radicals. Larger rates of decrease with increasing temperature are correlated with larger molecules (higher carbon number). The sum of product yields of the remaining species responds in the opposite direction, but these yields are also dependent on the RO[•] reaction rate coefficients. Aldehyde (HCHO, CCHO, and RCHO) and acetone (ACET) are generally products of decomposition, and their yields increase with temperature for most reactions. In general the reaction rate coefficients for unimolecular decomposition of branched RO[•] radicals increase faster than the reaction rate coefficients for RO[•] radical isomerization. Yields of MEK and PRD2 (C₅ and higher ketones), the main products of isomerization for larger RO[•] radicals, either show an insignificant increase (because total yield of all non RO₂N species increases), or a decrease in yield with temperature. Aldehydes are generally much more reactive than ketones of similar size

(Kwok and Atkinson, 1995). The structure of a ketone implies that the carbon with the oxygen double bond does not have a hydrogen available for abstraction. This increase in relative yield of more reactive aldehydes to less reactive ketones with increasing temperature is an additional temperature effect that is generally not accounted for in current climate change/air quality model simulations.

Table 4-9. Difference in stoichiometric coefficients due to temperature increase

“0” indicates there is no change, whereas “--” indicates product not formed for specified reaction.

Reaction	Stoichiometric Coefficient(310 K) - Stoichiometric Coefficient(290 K)								
	RO2N	RO2R	R2O2	HCHO	CCHO	RCHO	ACET	MEK	PRD2
MACR + OH	-0.005	0.005	--	0.008	--	--	--	-0.003	--
MACR + NO3	-0.005	0.005	--	--	--	--	--	--	--
MEK + OH	-0.010	-0.057	0.127	0.071	-0.004	-0.057	--	--	--
AFG3 + OH	-0.031	0.025	0.005	--	--	--	--	--	--
IPRD + OH	-0.012	0.012	--	0.004	0.002	0.002	--	0.002	0.003
IPRD + NO3	-0.013	0.006	0.007	0.003	--	0.003	--	0.003	--
PRD2 + OH	-0.026	0.012	0.024	-0.004	0.010	0.052	--	-0.012	-0.005
ISOP + OH	-0.017	0.017	0.001	0.014	--	--	--	--	--
BENZ + OH	-0.007	0.007	--	--	--	--	--	--	--
ETOH + OH	-1.5E-04	0.013	--	0.080	-0.040	--	--	--	--
MTBE + OH	-0.002	9.0E-05	0.002	2.0E-04	--	--	9.0E-05	0	0.002
PACET + OH	-0.017	0.008	0.010	1.0E-05	2.0E-04	0.001	--	0.001	--
UPOH + OH	0.000	0.017	--	0.025	0.021	-0.003	-0.010	-0.012	0.012
ALK2 + OH	-0.011	-0.014	0.032	0.032	0.057	-0.009	-0.037	--	--
ALK3 + OH	-0.017	0.012	0.208	0.030	0.315	0.012	0.025	-0.161	--
ALK4 + OH	-0.041	0.025	0.110	0.030	0.061	0.030	0.005	-0.026	--
ALK5 + OH	-0.071	0.063	0.246	0.028	0.062	0.083	0.009	-0.011	-0.012
OLE1 + OH	-0.008	0.007	-0.002	0.064	0.057	0.001	2.5E-04	-0.047	-0.004
OLE1 + NO3	-0.017	0.008	0.038	0.008	0.021	0.010	0.003	--	--
OLE2 + OH	-0.013	0.012	0.002	0.005	0.008	0.004	0.006	4.9E-04	-0.002
OLE2 + NO3	-0.025	-0.024	0.046	0.007	0.037	0.024	0.001	0.003	--
ARO1 + OH	-0.017	0.017	--	--	--	--	--	--	0.002
ARO2 + OH	-0.028	0.028	--	--	--	--	--	--	0.001
TERP + OH	-0.051	0.049	0.046	0.019	--	0.038	0.011	0.001	0.012
TERP + O3	-0.047	0.010	0.137	0.049	--	0.032	0.034	0	0
TERP + NO3	-0.096	0.054	0.229	0.031	--	0.064	0.055	--	--

4.3.2 Organic nitrate

The first two columns of Figure 4-9 show temperature and RONO₂ concentration (RONO₂ = the sum of RNO₃, RNO₃IN, ONA, ONB, and XN) for two model days during the year 2000 simulations at 4 pm. Julian day 209 (JD209; Thursday July 27) had the lowest peak

temperatures, never exceeding 306 K (33°C), while JD214 (Tuesday August 1) had temperatures reaching as high as 315 K (42°C).

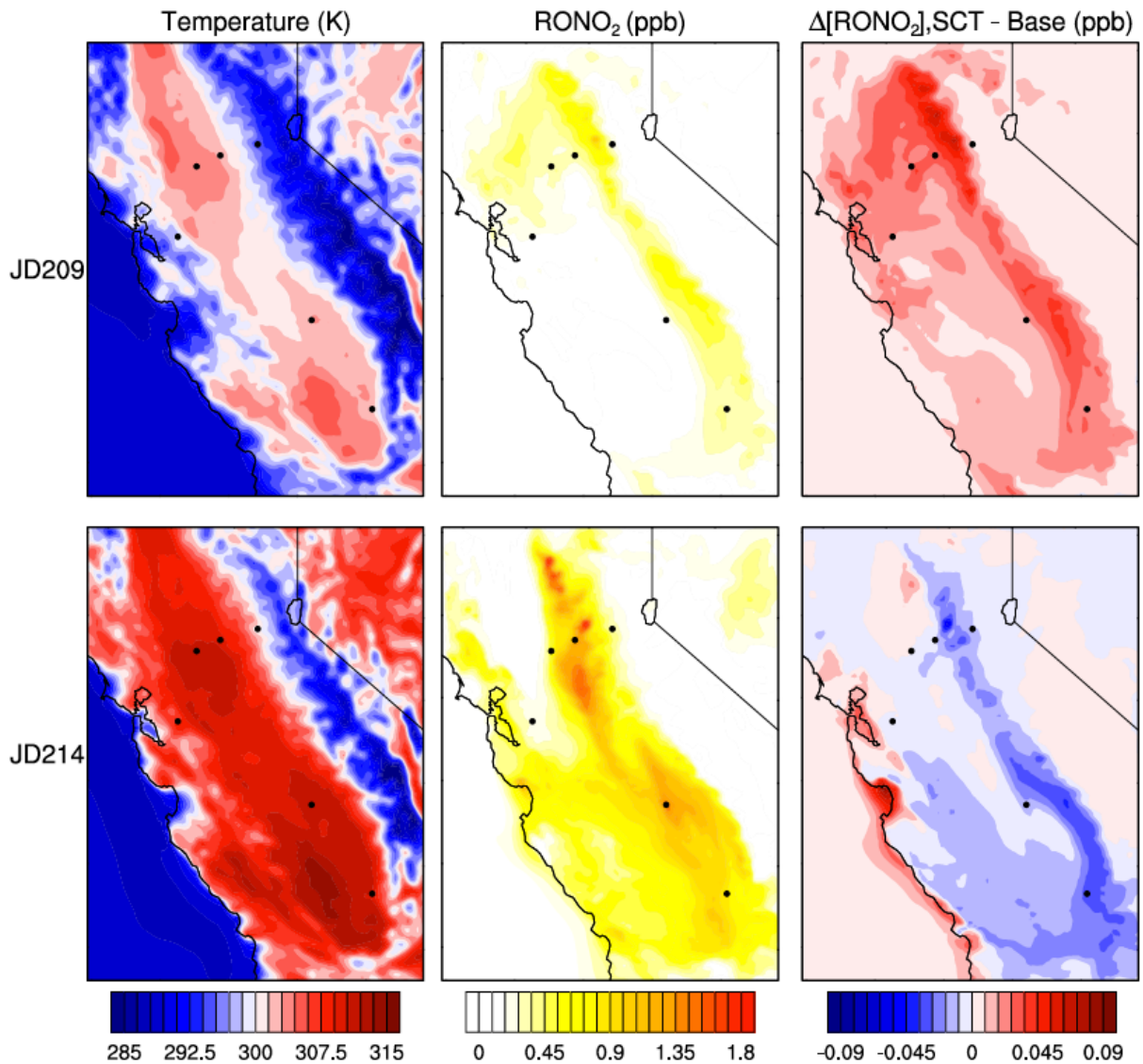


Figure 4-9. Temperature, RONO₂ concentration, and the change in RONO₂ concentration with use of the SCT mechanism

For two different days (Julian days 209 and 214) at 4 pm. Cooler JD209 shows increases in RONO₂ concentration and warm JD214 shows increases along the coast, and decreases at warmer inland locations.

Areas of elevated RONO₂ correlate with areas of high biogenic emissions (see Fig. 3-2 for emissions map). Accordingly, the hotter JD214 has much higher levels of RONO₂ than JD209, as biogenic emissions increase exponentially with temperature. For days on which temperature did not exceed 310 K anywhere in the model domain, the peak RONO₂ concentration was always

below 2 ppb; the peak for JD209 was 1.3 ppb. For days on which temperature exceeded 310 K, peak RONO₂ concentrations were above 2 ppb. The peak during JD214 is 2.4 ppb, but concentrations up to 3.5 ppb were predicted on other days in the 13-day modeling period. RONO₂ concentration peaks are predicted downwind of Sacramento, up into the Sierra Nevada foothills, generally downwind of an area with both high anthropogenic and biogenic emissions. These results are within the range of measured values, as RONO₂ above 3 ppb, and even up to 5.5 ppb have been reported at Granite Bay (Day et al., 2003) and in La Porte, TX (Rosen et al., 2004).

The differences in RONO₂ due to use of the temperature-dependent SCT mechanism are shown in the third column of Figure 4-9. During JD209 there are very few cell-hours where the temperature is over 300 K. Because organic nitrate yield is set to its value at 300 K in the base mechanism, and nitrate yields increase with decreasing temperature in the SCT mechanism, RONO₂ increases across the entire domain for JD209. For JD214, the hottest day in the simulation, RONO₂ decreases in comparison with the base mechanism. However, along the coast where conditions remained relatively cool, predicted RONO₂ decreased on this "hot" day as well.

Average RONO₂ for the six cities shown in Figure 4-3 are summarized in Table 4-10. For each site the daily average RONO₂ concentration is much higher on JD214 than JD209. The concentration of model species ONA, ONB, and RNO₃IN only increase with use of the SCT mechanism (although ONB concentrations are an order of magnitude less than ONA). These species are the result of NO₃ radical reactions that are relevant at night, when temperatures in these simulations are always below 300 K, while the RNO₃ model species is formed photochemically throughout the day. The minimum and maximum differences in RNO₃, the most relevant nitrate species whose formation competes with ozone production, due to use of the SCT mechanism are shown in Table 4-9. All sites have negative minimums and positive maximums both days, indicating the diurnal temperature variation at all sites is strong enough to change direction of not only RNO₃ formation, but also concentration.

The XN species, which represents the additional -ONO₂ of multifunctional nitrates, is not considered reactive in the mechanism, but must be recorded for RONO₂ accounting (to compare with thermal dissociation measurements). XN accounted for over 20% of RONO₂ on a daily average basis, at each of the sites reported in Table 4-10. In a modeling study focusing on isoprene nitrates, Perring et al. (2009) estimate that less than 5% of RONO₂ would be dinitrates, an estimate much lower than the XN concentrations reported for these simulations. This study shows higher XN concentrations for two possible reasons. In both studies, XN does not react but is removed from the atmosphere via dry deposition. Perring et al. (2009) assume a higher deposition rate (that of HNO₃ rather than PAN, which is about three times higher on average for the simulations performed in this dissertation), which will result in lower atmospheric concentrations. Additionally, Perring et al. (2009) find that over 50% of organic nitrates are formed directly from isoprene oxidation, and isoprene nitrate chemistry is explicit in their study. The only source of XN in their model is due to further reactions of isoprene nitrates. In the SAPRC mechanism, isoprene nitrates are lumped with RNO₃. Much of the XN is created from recycled RNO₃, which is represented by a surrogate species with an effective carbon number of 6.5, while isoprene has only 5 carbons. Thus, the SAPRC mechanism recycles more nitrate (>10% more at 300 K) than the mechanism used by Perring et al. (2009).

Table 4-10. Selected nitrate descriptors for six central California sites and two days

RONO₂ is the sum of all nitrate species, RNO₃ is the main photochemically produced nitrate species, XN accounts for multifunctional nitrate, averages are daily and for the Base mechanism simulations. Ozone data also presented, max(O₃) is the daily maximum ozone for the Base mechanism simulations. The min(ΔRNO₃) and max(ΔRNO₃) represent the minimum and maximum change in RNO₃ with use of the SCT mechanism as compared to the Base mechanism; min(ΔO₃) and max(ΔO₃) are calculated similarly.

Model Parameter	Units	Livermore		Fresno		Bakersfield	
		JD209	JD214	JD209	JD214	JD209	JD214
avg RONO ₂	ppt	194	374	325	797	252	919
min(ΔRNO ₃)	ppt	-0.3	-21.0	0.0	-40.3	0.0	-34.2
max(ΔRNO ₃)	ppt	35.7	4.9	20.6	8.8	13.8	12.2
avg XN	% RONO ₂	20.7%	24.7%	32.7%	41.4%	26.5%	33.1%
max(O ₃)	ppb	68.9	84.1	82.6	113.0	69.6	106.8
min(ΔO ₃)	ppb	-0.74	-0.04	-0.46	-0.05	-0.50	-0.07
max(ΔO ₃)	ppb	0.06	0.16	0.03	0.44	0.11	0.34
		Sacramento		Granite Bay		Blodgett Forest	
		JD209	JD214	JD209	JD214	JD209	JD214
avg RONO ₂	ppt	239	532	357	656	350	432
min(ΔRNO ₃)	ppt	0.0	-21.0	0.0	-30.1	0.0	-35.7
max(ΔRNO ₃)	ppt	20.5	1.0	25.6	4.7	17.4	3.3
avg XN	% RONO ₂	34.1%	32.3%	33.7%	31.1%	23.1%	27.5%
max(O ₃)	ppb	65.9	72.6	74.7	77.9	78.8	87.5
min(ΔO ₃)	ppb	-0.31	-0.01	-0.36	-0.03	-0.23	-0.04
max(ΔO ₃)	ppb	0.10	0.14	0.06	0.24	0.07	0.34

Modeled species concentrations on JD209 are compared to measurements in Figure 4-10. The hourly 5th and 95th percentile NO₂ and NO_z measurements taken in Granite Bay during the summer of 2001 (July 19 to Sept 15), are presented as the shaded curves to show the range of measured values. The dotted line is the measurement median, and the solid and dashed lines are the base and SCT mechanism simulations, respectively. This time series shows that for the cooler JD209, the SCT mechanism causes a very small increase in RONO₂ at Granite Bay, which nudges the model simulations slightly closer to the range of daytime measured values. Small decreases in the other NO_z species, HNO₃ and PAN, follow accordingly but are negligible. NO_x increases are colocated with RONO₂ increases across the domain, so the decrease in HNO₃ and PAN is attributed to the reduction in radical propagation (supported by colocated HO_x reduction) due to more RONO₂ formation.

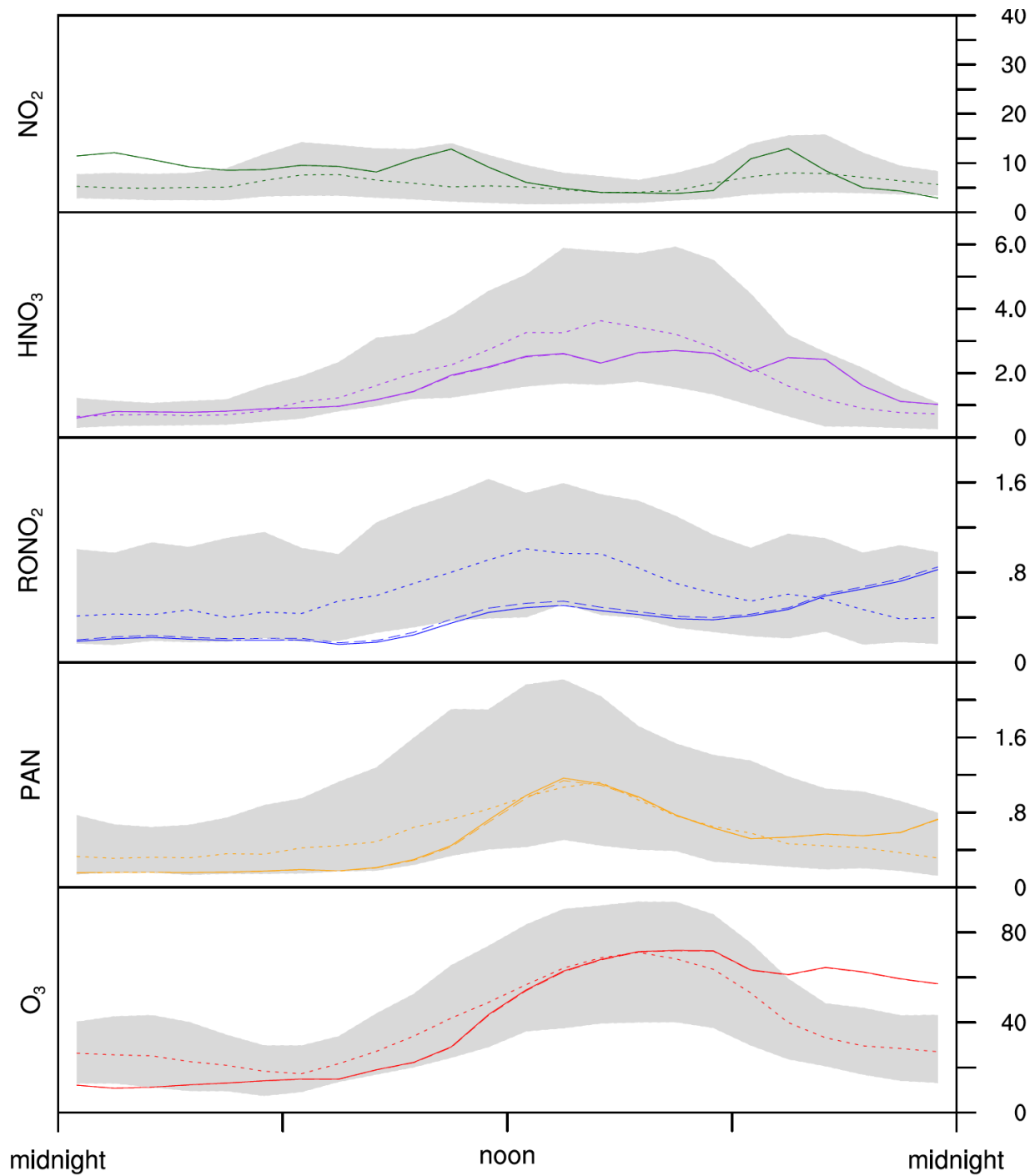


Figure 4-10. Pollutant concentrations (ppb) at Granite Bay for Julian day 209
 Range (5-95th percentile) of measured values denoted by gray shading, dotted line is median of the measurements, solid line is modeled using Base mechanism and dashed line is modeled using SCT mechanism. Base and SCT concentration predictions are often indistinguishable.

To further evaluate model performance, the same measured values are presented in Figure 4-11 with the hourly minimum, median, and maximum at Granite Bay. More variance is seen in the 13 model simulation days than in the 5th to 95th percentile range over 48 days of measurements from the summer of 2001. The two sharp peaks of NO₂ indicate transport of an emission plume. This, and the model NO₂ rising later than the measured NO₂ indicate that while the magnitude of emissions in Sacramento area may be correct, they may be distributed incorrectly by time of day and/or by location. It is possible that the inventory developers (staff at the California Air Resources Board) scaled an earlier emission inventory, but did not account for higher population growth in the suburbs as compared to the city center.

The steep increase in RONO₂ and PAN seen in the evening for the maximum model values (and to a lesser extent the median values), is likely attributable to a more rapid decrease in planetary boundary layer height than what occurred in reality. However, Figure 4-12 shows a similar plot for Blodgett Forest, and the steady afternoon increase in RONO₂ (exceeding measured values more so than for other NO_z species), suggests that a removal mechanism is missing or misrepresented. Use of the SCT mechanism in place of the Base mechanism has an inconsequential effect on predicted ozone and NO_z species at the Granite Bay and Blodgett Forest sites.

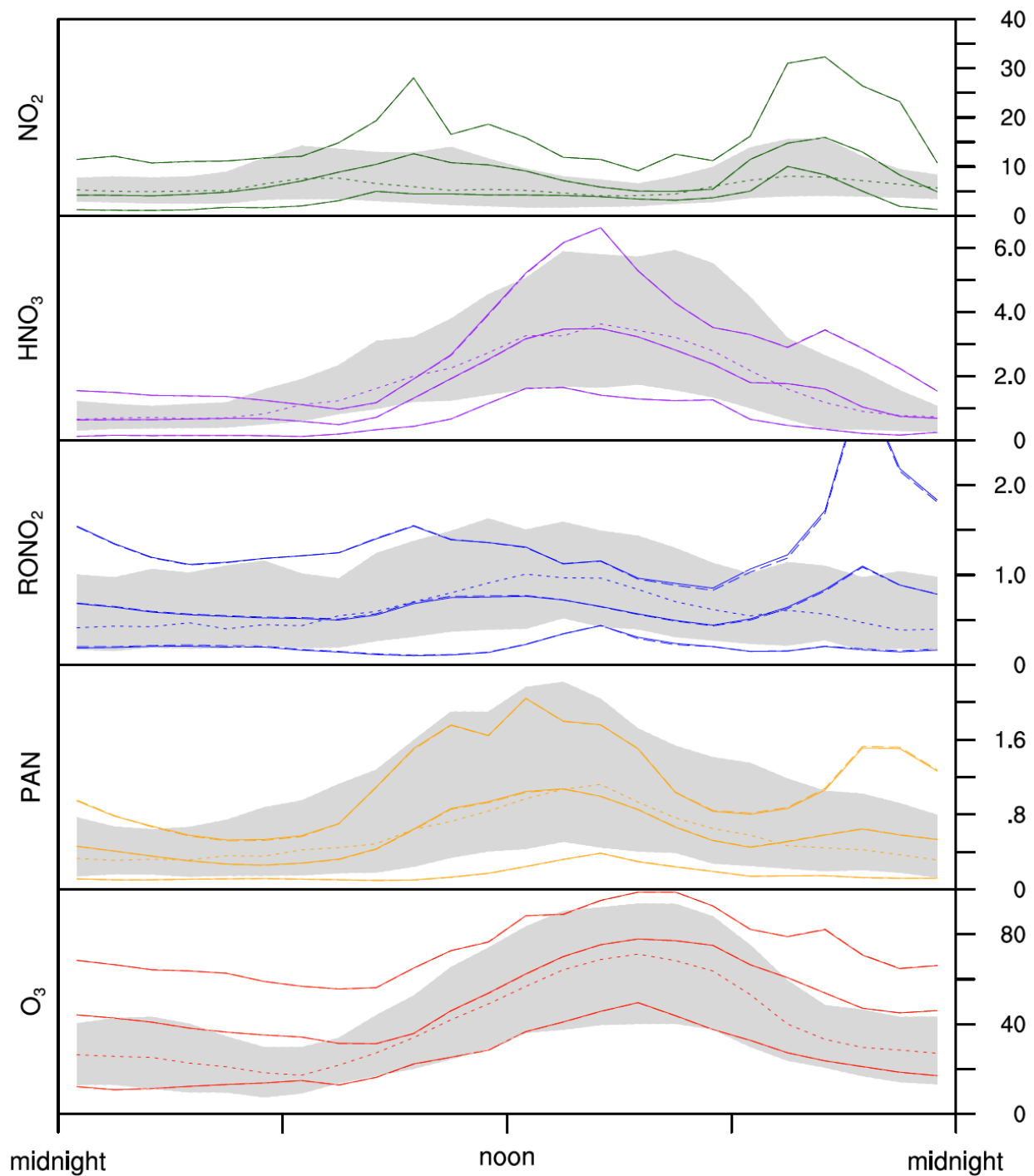


Figure 4-11 Pollutant concentrations (ppb) at Granite Bay

Range (5-95th percentile) of measured values denoted by gray shading. Dotted line is measurement median, solid lines are modeled using Base mechanism and dashed lines are modeled using SCT mechanism (minimum, median, and maximum hourly values), The two sets of model predictions are often indistinguishable.

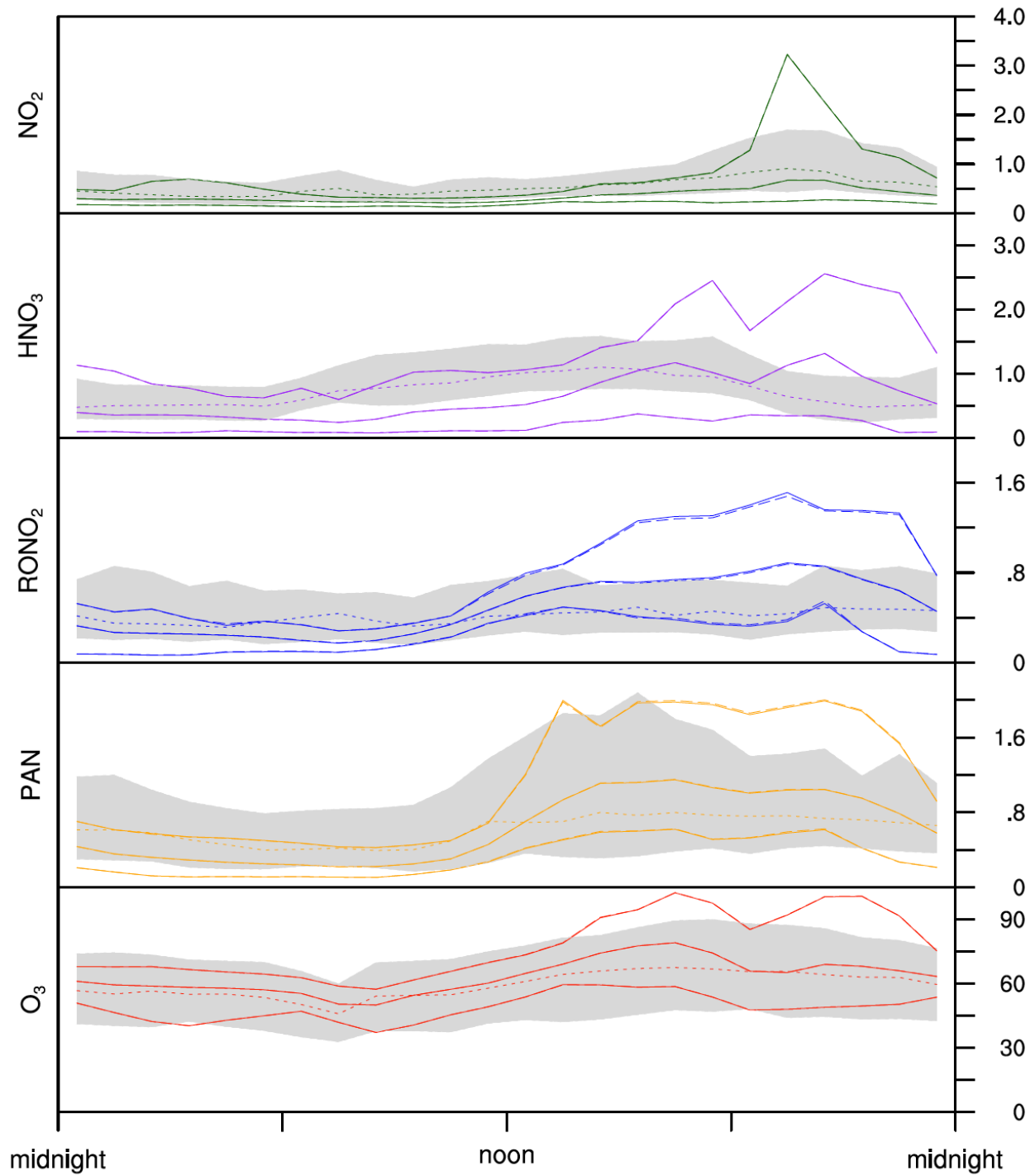


Figure 4-12 Pollutant concentrations (ppb) at Blodgett Forest

Range (5-95th percentile) denoted by gray shading. Dotted line is measurement median, solid lines are modeled using Base mechanism and dashed lines are modeled using SCT mechanism (minimum, median, and maximum hourly values). Base and SCT concentrations often overlap.

Figure 4-13, which presents daily integrated reaction rates, shows that isoprene and terpene precursors were responsible for much of the RONO_2 at Granite Bay, upwind of Blodgett Forest, and almost all of the RONO_2 at Blodgett Forest. It is likely that RNO_3 as defined in the SAPRC mechanism is an imperfect representation for isoprene and terpene nitrates. RNO_3 is represented using 6 alkyl and multifunctional nitrates, but none of these has a carbon-carbon double bond, as isoprene and terpene nitrates do. Horowitz et al. (2007) found that 70% of isoprene nitrate chemical loss is through reaction with O_3 , which is not accounted for in the SAPRC mechanism. Better afternoon and evening RONO_2 model-measurement agreement may result if isoprene and terpene nitrates are separated from the RNO_3 model species.

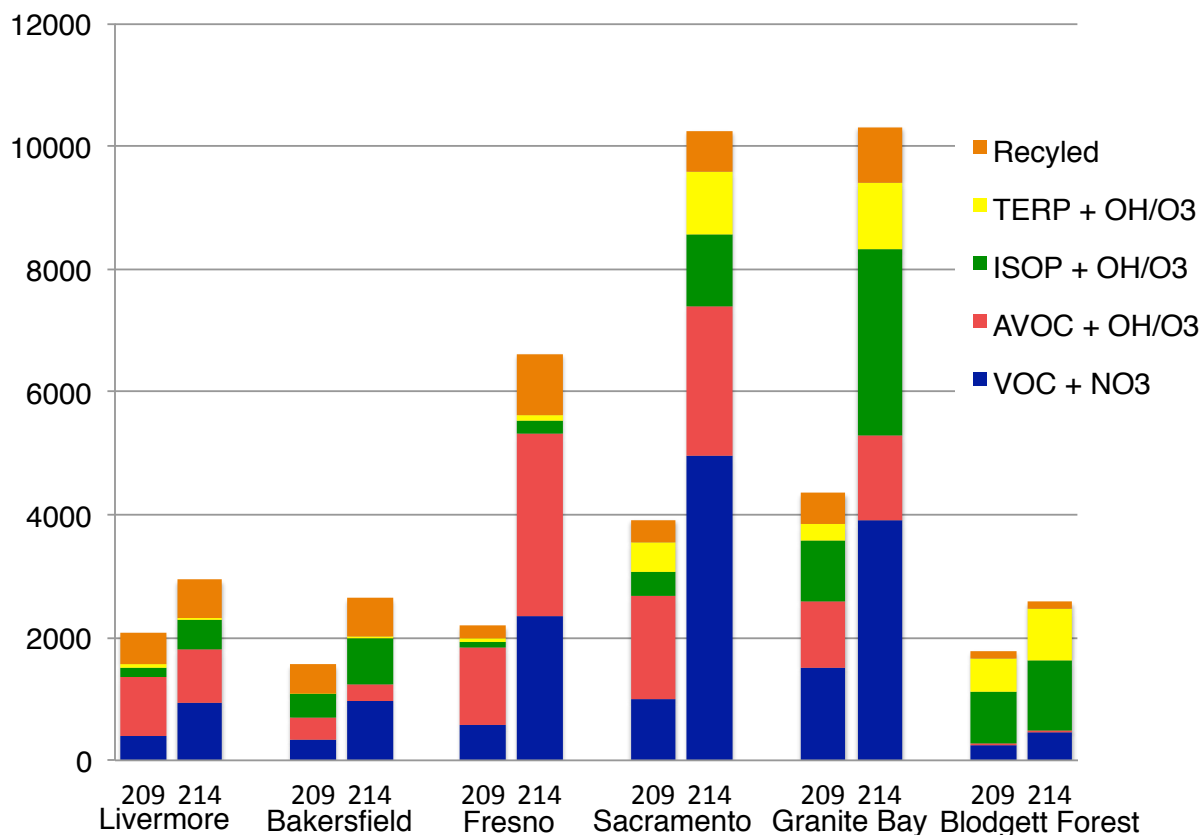


Figure 4-13. Nitrate formation rates attributed to different reactions (ppb/day)
 Julian days 209 (cooler) and 214 (hotter) shown. Integrated reaction rates show relative importance of various reactions.

Adding temperature-dependent evaporative emissions has very little effect on RONO_2 . Smaller, lower carbon number, VOC are enriched in headspace vapors and these don't contribute significantly to organic nitrate. Note, however, that the very small changes in predictions are in opposite directions for the two limiting weather days (i.e., coolest and hottest days). For JD209, organic nitrate increases due to use of SCT (nitrate yield increases with decreasing temperature),

but evaporative emissions decrease due to the lower prevailing temperatures, leading to a slight decrease in RONO_2 . The opposite is true for JD214.

4.3.3 Secondary VOC

In developing the temperature-dependent SCT version of the chemical mechanism, the yield of aldehydes was found to increase with increasing temperature. Figure 4-14 shows that changes in aldehyde concentration due to use of the SCT mechanism follow accordingly. The Base mechanism is based on estimated product yields at 300 K, so JD209, with temperatures mostly below 300 K, shows larger decreases in aldehyde concentrations. Small increases in aldehydes do occur in the Central Valley in the late afternoon when temperatures rose to 306 K in some locations. During JD214, one of the hottest simulation days, aldehyde concentrations increase throughout most of the domain. Along the coast, where temperatures remained cool, predicted aldehyde concentrations decreased.

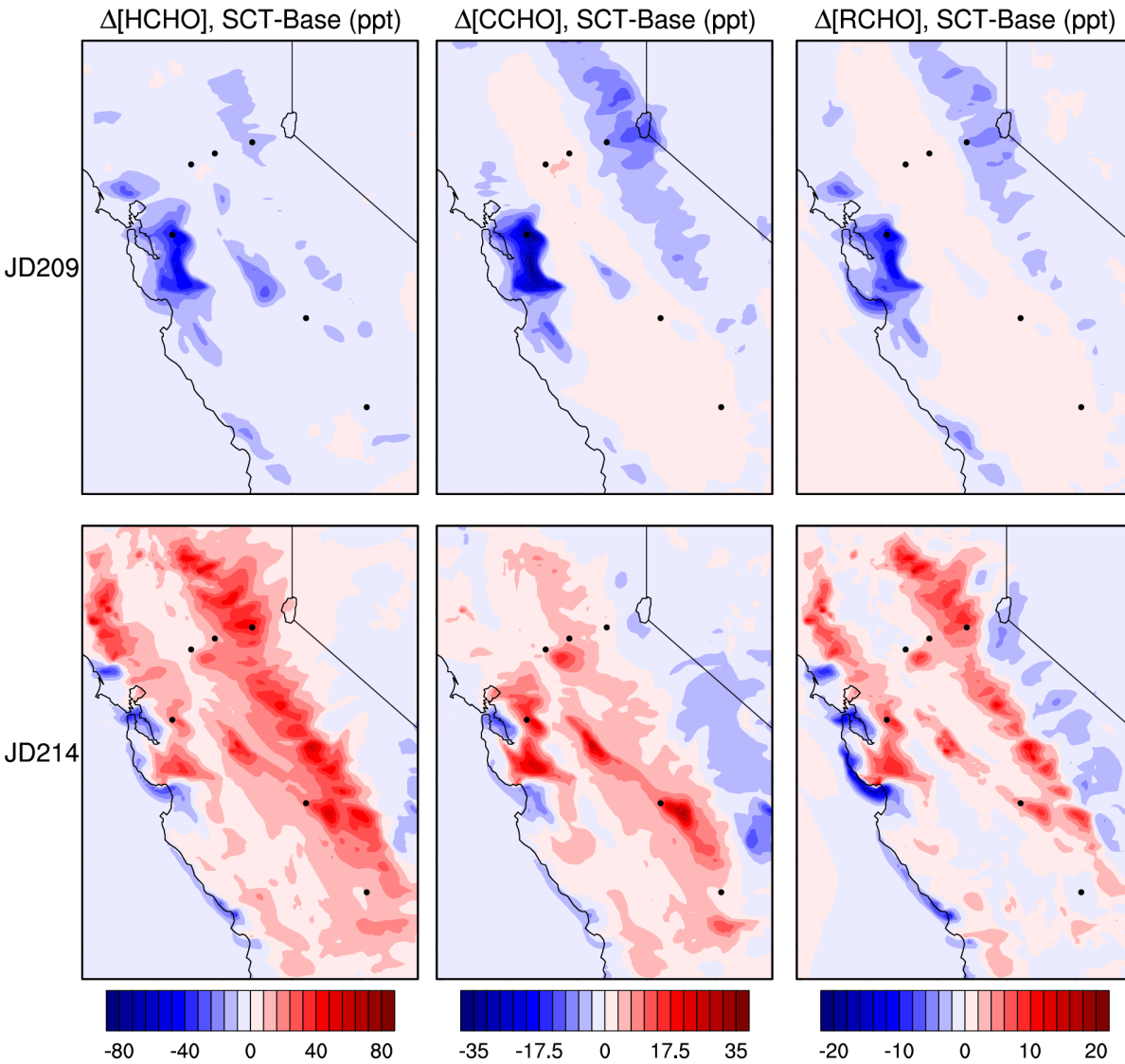


Figure 4-14 Change in aldehyde concentration with use of the SCT mechanism

For Julian days 209 and 214 at 4 pm. Cooler JD209 shows mostly decreases in RONO_2 concentration, warmer JD214 shows decreases along the coast, and increases for the warmer inland areas.

Figure 4-15 shows the change in aldehydes with use of the SCT mechanism and temperature-dependent evaporative emissions. For each ground-level grid cell, evaporative emissions decrease for temperatures below the average, and increase when temperatures are above average. As these are days represent bounding case examples from the simulations, all the grid cells over land had temperatures below average for JD209, and above average for JD214. This serves to amplify the major effects of the SCT mechanism for aldehydes: aldehyde concentrations on JD209 are lower because both emissions and aldehyde yields are reduced under cooler conditions. Similarly, higher emissions on JD214 lead to further increases in predicted aldehyde concentrations on hotter days.

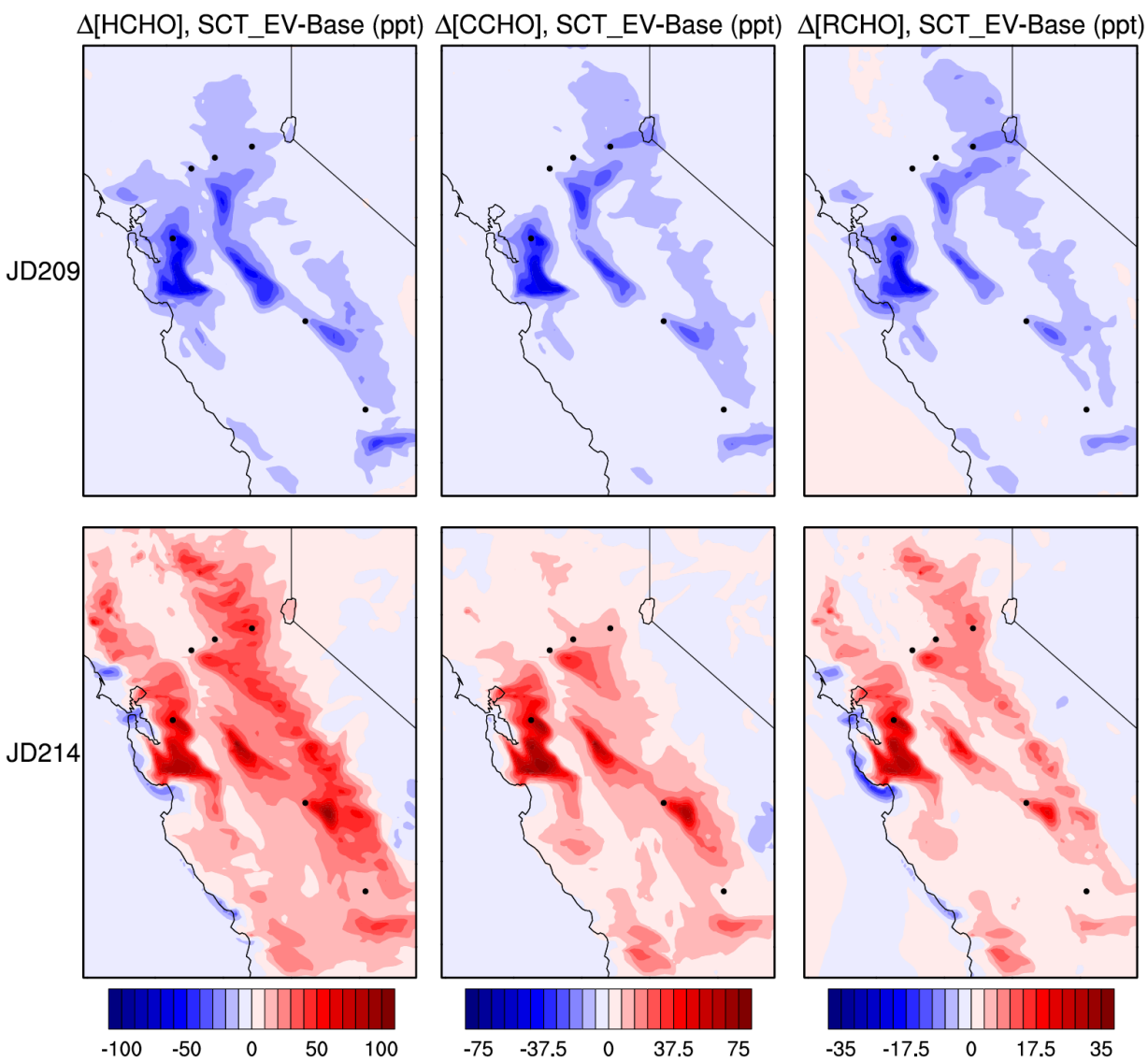


Figure 4-15 Change in aldehyde concentration due to use of temperature-dependent evaporative emissions

For Julian days 209 and 214 at 4 pm. Changes that result from use of SCT mechanism are amplified; VOC reactivity increases with both changes.

On a percentage basis, the CCHO and RCHO species change more than HCHO with the use of the SCT temperature-dependent mechanism and emissions. CCHO decreases of as much as 7% and RCHO decreases of as much as 10% are calculated along the coast during JD209. On the other hand, increases of up to 5 and 7% for CCHO and RCHO, respectively, are calculated downwind of the Bay Area and in the Central Valley for JD214.

Figures 4-16 and 4-17 show similar plots for the ketones. Figure 4-16 shows that use of the SCT mechanism leads to decreases in ACET and increases in MEK and PRD2, as expected for temperatures below 300 K. For JD214, along the coast and in the Central Valley, the expected

response is evident: ACET concentrations increase in areas where temperatures exceed 300 K, and MEK and PRD2 decrease. Because JD214 is a hot day, biogenic emissions are much higher than on JD209. The changes in the eastern Central Valley and in the southern Sierra Nevada are controlled by terpene emissions. For the TERP group, nitrate yields are high enough and temperature dependence is steep enough that it overshadows the temperature dependence of the alkoxy radical reactions. It follows that the terpene emissions in the foothills and the Sierra Nevada, which are largely cooler than 300 K at most hours, cause an increase in RNO_3 and thus a decrease in PRD2. Although the SCT mechanism results in a relative decrease of PRD2, the yield is high (almost 0.25 at 300 K). The $\text{PRD2} + \text{OH}^\cdot$ reaction becomes important for this region of elevated terpene emissions as well, leading to a relative increase in MEK as the yield for this species decreases with temperature (and the reactions are taking place at temperatures less than 300 K).

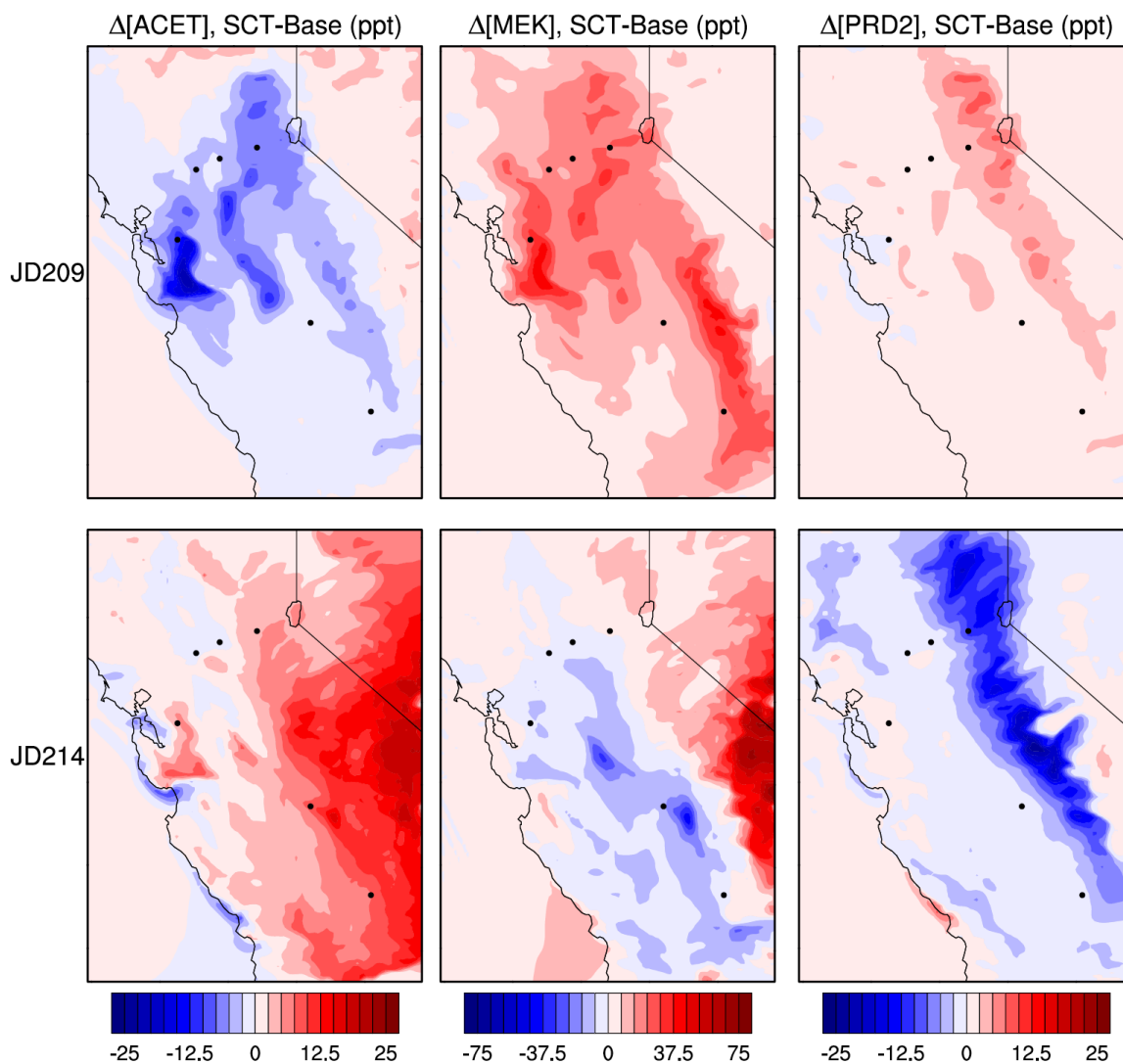


Figure 4-16. Change in ketone concentration with use of the SCT mechanism

For Julian days 209 and 214 at 4 pm. Acetone concentrations follow aldehyde emissions as expected. Higher ketone (MEK and PRD2) have expected opposite response of aldehydes since they are formed by isomerization or reaction with O_2 rather than decomposition of precursor alkoxy radicals.

The added effect of temperature-dependent evaporative emissions is shown in Figure 4-17. For JD209 which has below-average temperatures, the effect of reduced emissions more than quadruples the reduction in acetone, and reduces the increases seen in ketones due to use of the SCT mechanism. While MEK still shows increases, the effect is reversed for much of the domain for the PRD2 species. Similar but opposite effects are seen for the Bay Area and Central Valley, but the Sierra Nevada remains unaffected because this sparsely populated area has very low anthropogenic (evaporative) emissions.

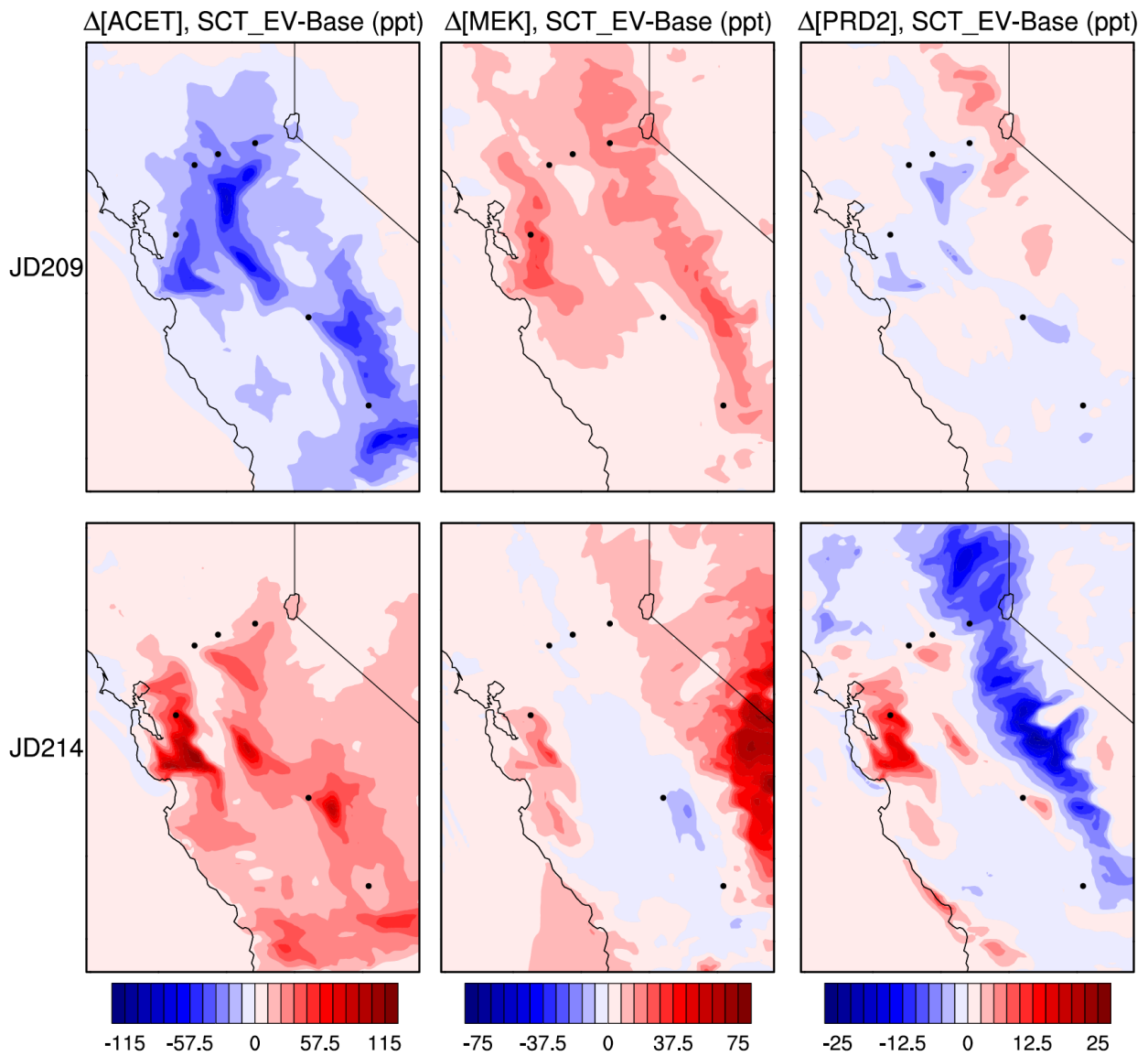


Figure 4-17. Change in ketone concentration due to use of temperature-dependent evaporative emissions

For Julian days 209 and 214 at 4 pm. Acetone (ACET) concentrations follow aldehyde emissions as expected; changes that result from use of SCT mechanism are amplified. MEK and PRD2 are affected in the opposite way.

The change in ACET is the most significant for the ketones. For the cool JD209 episode, decreases of around 3% are seen in the Bakersfield and Sacramento regions. There is up to a 3% increase in ACET for the JD214 episode downwind of the Bay Area. For MEK and PRD2, the SCT mechanism and the temperature-dependent evaporative emissions nudge concentrations in different directions.

Overall, switching to the temperature-dependent SCT mechanism and inclusion of day-specific temperature effects on evaporative emissions decrease domain reactivity on cooler days, and

increase it on warmer days. This is likely to result in increased m_{O_3-T} , and greater sensitivity of photochemical air pollution problems to climate change.

4.3.4 Ozone air quality

Use of the SCT mechanism results in an increase of $NO \rightarrow NO_2$ conversions with temperature, as well as increases in the more reactive secondary organic reaction products. The effects on ozone concentrations are shown in Figure 4-18. On the cooler day with temperatures rarely over 300 K, ozone decreases relative to the base mechanism. Modeled ozone levels increase on the hotter day. The magnitude of the ozone changes isn't large, typically $\sim \pm 1$ pbb or less, but it is slightly amplified when temperature-dependent evaporative emissions are included in the simulations. The compounded changes in ozone concentrations for these simulations are shown in Figure 4-19.

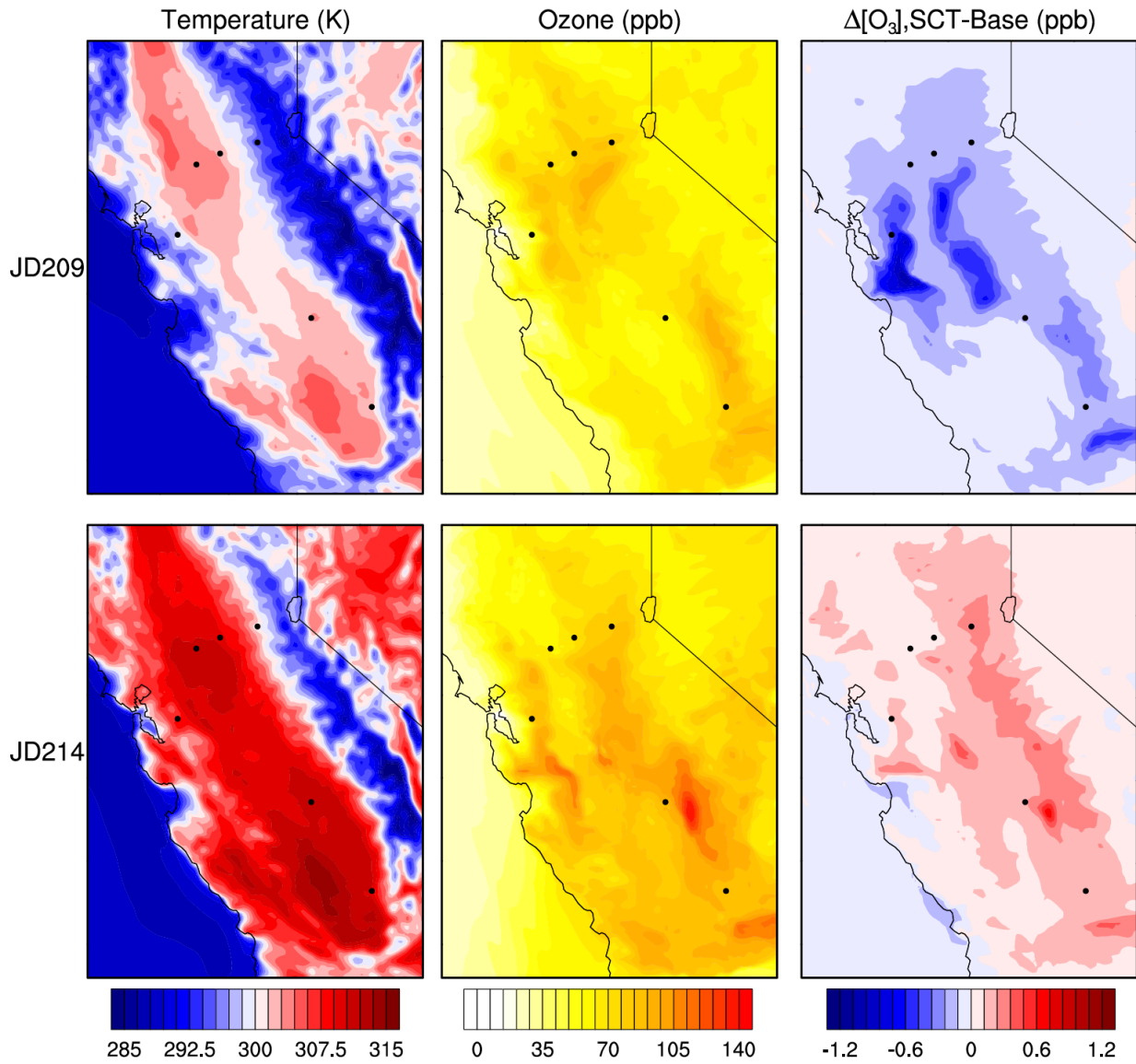


Figure 4-18. Temperature, O₃ concentration, and the change in O₃ concentration with use of the SCT mechanism

For Julian days 209 and 214 at 4 pm. Cooler JD209 shows decreases in O₃ concentration and warmer JD214 shows decreases for inland areas.

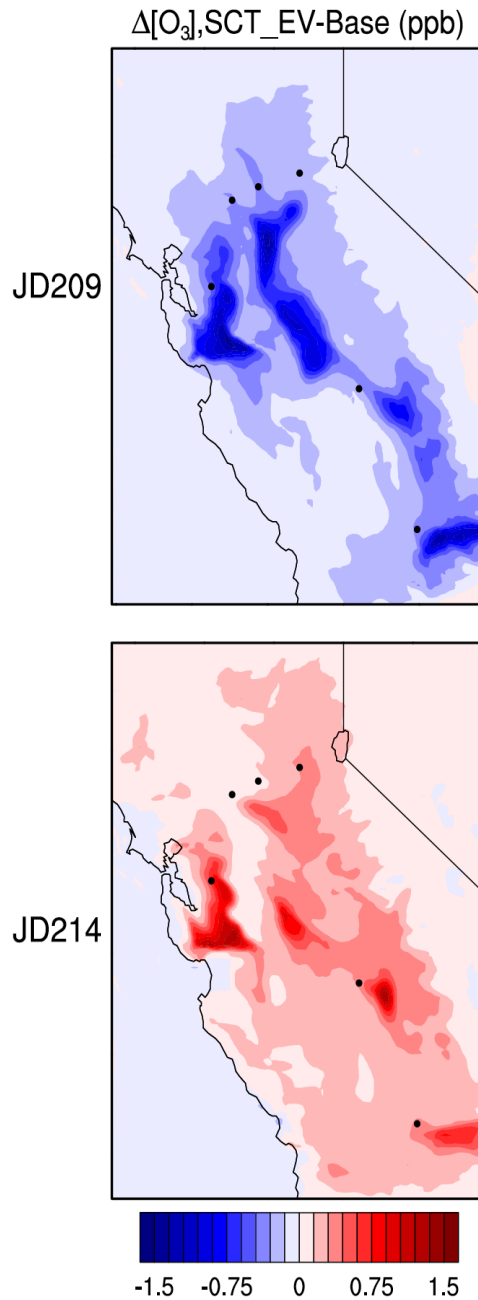


Figure 4-19. Change in O_3 concentration due to use of temperature-dependent evaporative emissions

For Julian days 209 and 214 at 4 pm. Changes that result from use of SCT mechanism are amplified due to extra $\text{NO} \rightarrow \text{NO}_2$ conversion and increased reactivity with temperature.

The minimum and maximum ozone differences shown for the six sites in Table 4-9 indicate that each of the site-specific $m_{\text{O}_3\text{-T}}$ increase with use of the SCT mechanism and temperature-dependent evaporative emissions. The model results presented here are likely to remain on the conservative side in estimating temperature effects on air quality. While variations in evaporative

VOC emissions from gasoline are now included in the analysis, the temperature dependencies of various area source emissions have not been modeled. For instance, VOC emissions from silage (fermented corn used as cattle feed), has been shown to be an important contributor to VOC emissions and ozone formation in the Central Valley (Hu et al., 2012). Ethanol emissions from silage have been shown to increase exponentially with increasing temperature (Montes et al., 2010). Other temperature-dependent emission source terms are likely to exist, and their inclusion in the model should act to increase m_{O_3-T} further.

4.3.5 Ozone air quality in 2050

The temperature-dependent changes in emissions and atmospheric chemistry included above lead to a slight increase in modeled m_{O_3-T} , which is sometimes referred to as a climate change penalty factor for air quality. In this section, the effects of using the SCT mechanism, which was shown to slightly increase m_{O_3-T} as compared to the Base mechanism for the 13-day summer 2000 simulations, is assessed in the same domain for year 2050 climate-change simulations.

Temperature and water vapor perturbations for the model domain are shown in Figure 4-20 (derived from a global 2× pre-industrial CO₂ scenario, downscaled using a regional climate model for California by Snyder et al., 2002). Related increases in biogenic emissions, and forecast changes in anthropogenic NO_x emissions due to offsetting effects of population growth and advances in emissions control technology are shown in Figure 4-21. The emission factors applied to each county to forecast anthropogenic emissions in 2050 are listed in Table 4-11. On a relative basis, population in the Central Valley is expected to increase more than in the rest of the domain. Kern, Madera, and Sutter counties all have forecasted slight increases in NO_x emissions in 2050 relative to the 2000. None of the counties in the domain are forecast to see increases in VOC emissions.

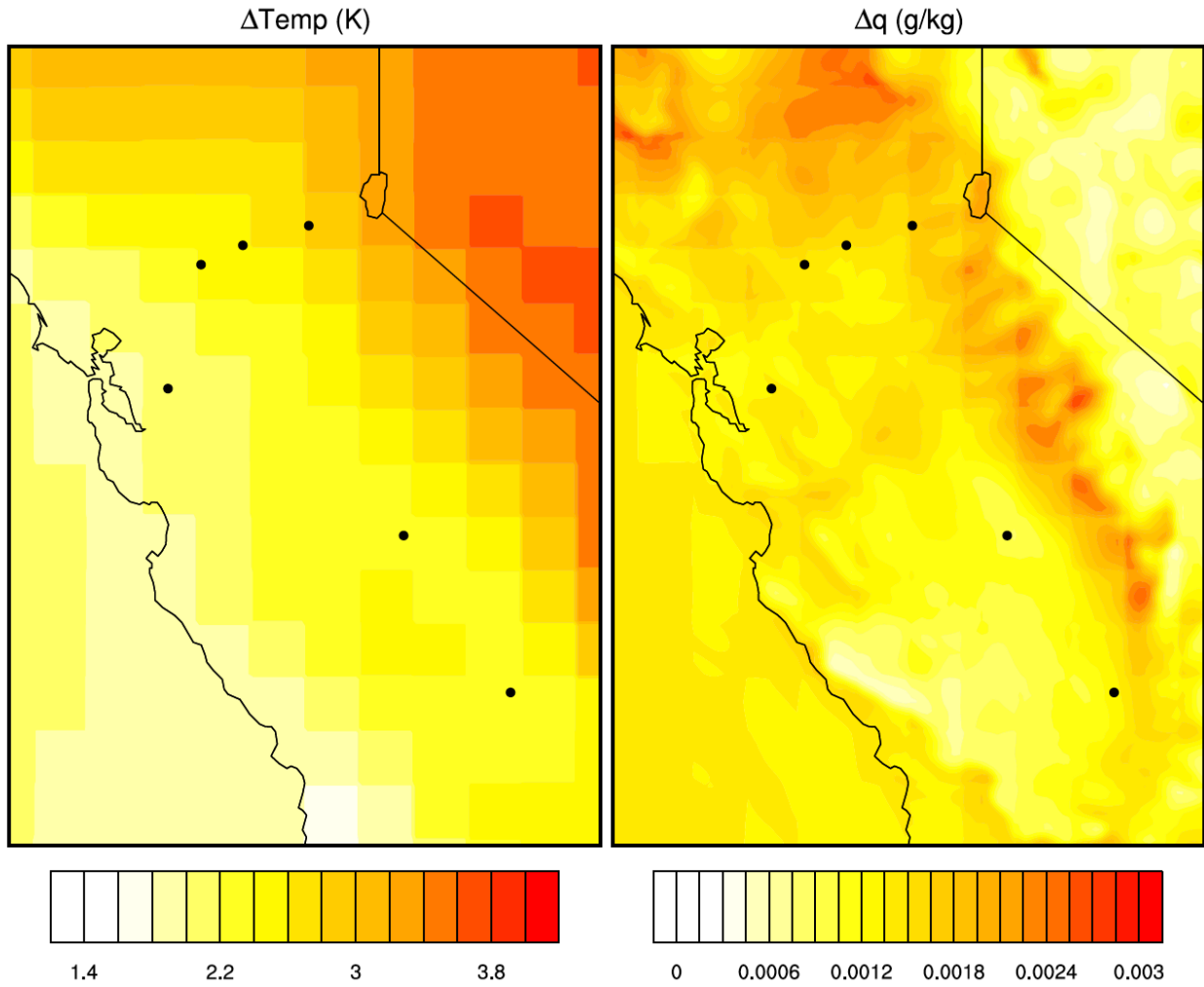


Figure 4-20. Temperature and water vapor perturbations for the year 2050, JD209 at 4 pm

Table 4-11. Emission scaling factors by county for 2050 anthropogenic emissions relative to year 2000

Basin & County	Population Growth Factor	Anthropogenic VOC/CO Scaling Factor	NOx Scaling Factor	Basin & County	Population Growth Factor	Anthropogenic VOC/CO Scaling Factor	NOx Scaling Factor
<u>San Francisco Bay Area</u>				<u>Mountain Counties</u>			
Alameda	1.17	0.23	0.47	Amador	1.28	0.26	0.51
Contra Costa	1.57	0.31	0.63	Calaveras	1.48	0.30	0.59
Marin	1.07	0.21	0.43	El Dorado	1.81	0.36	0.72
Napa	1.49	0.30	0.60	Mariposa	1.34	0.27	0.54
Solano	1.50	0.30	0.60	Nevada	1.53	0.31	0.61
San Mateo	1.27	0.25	0.51	Plumas	0.94	0.19	0.38
San Francisco	1.17	0.23	0.47	Sierra	1.02	0.20	0.41
Santa Clara	1.28	0.26	0.51	Tuolumne	1.13	0.23	0.45
<u>San Joaquin Valley</u>				<u>North Central Coast</u>			
Fresno	1.89	0.38	0.76	Monterey	1.35	0.27	0.54
Kern	2.81	0.56	1.12	San Benito	1.54	0.31	0.62
Kings	2.01	0.40	0.80	Santa Cruz	1.19	0.24	0.48
Madera	2.63	0.53	1.05	<u>South Central Coast</u>			
Merced	2.36	0.47	0.94	San Luis Obispo	1.37	0.27	0.55
San Joaquin	2.45	0.49	0.98	Santa Barbara	1.27	0.25	0.51
Stanislaus	1.93	0.39	0.77	<u>Great Basin Valleys</u>			
Tulare	2.13	0.43	0.85	Alpine	0.95	0.19	0.38
<u>Sacramento Valley</u>				Mono	1.48	0.30	0.59
Colusa	1.95	0.39	0.78	<u>Lake County</u>			
Glenn	1.44	0.29	0.57	Lake	1.81	0.36	0.73
Yuba	2.39	0.48	0.96	<u>Counties on edge of model domain</u>			
Sutter	2.69	0.54	1.08	Inyo	1.28	0.26	0.51
Yolo	1.76	0.35	0.70	Lassen	1.23	0.25	0.49
Butte	1.64	0.33	0.66	Los Angeles	1.20	0.24	0.48
Placer	2.20	0.44	0.88	Mendocino	1.16	0.23	0.46
Sonoma	1.31	0.26	0.52	Tehama	1.76	0.35	0.70
Sacramento	1.69	0.34	0.67	Trinity	1.40	0.28	0.56
				Ventura	1.32	0.26	0.53

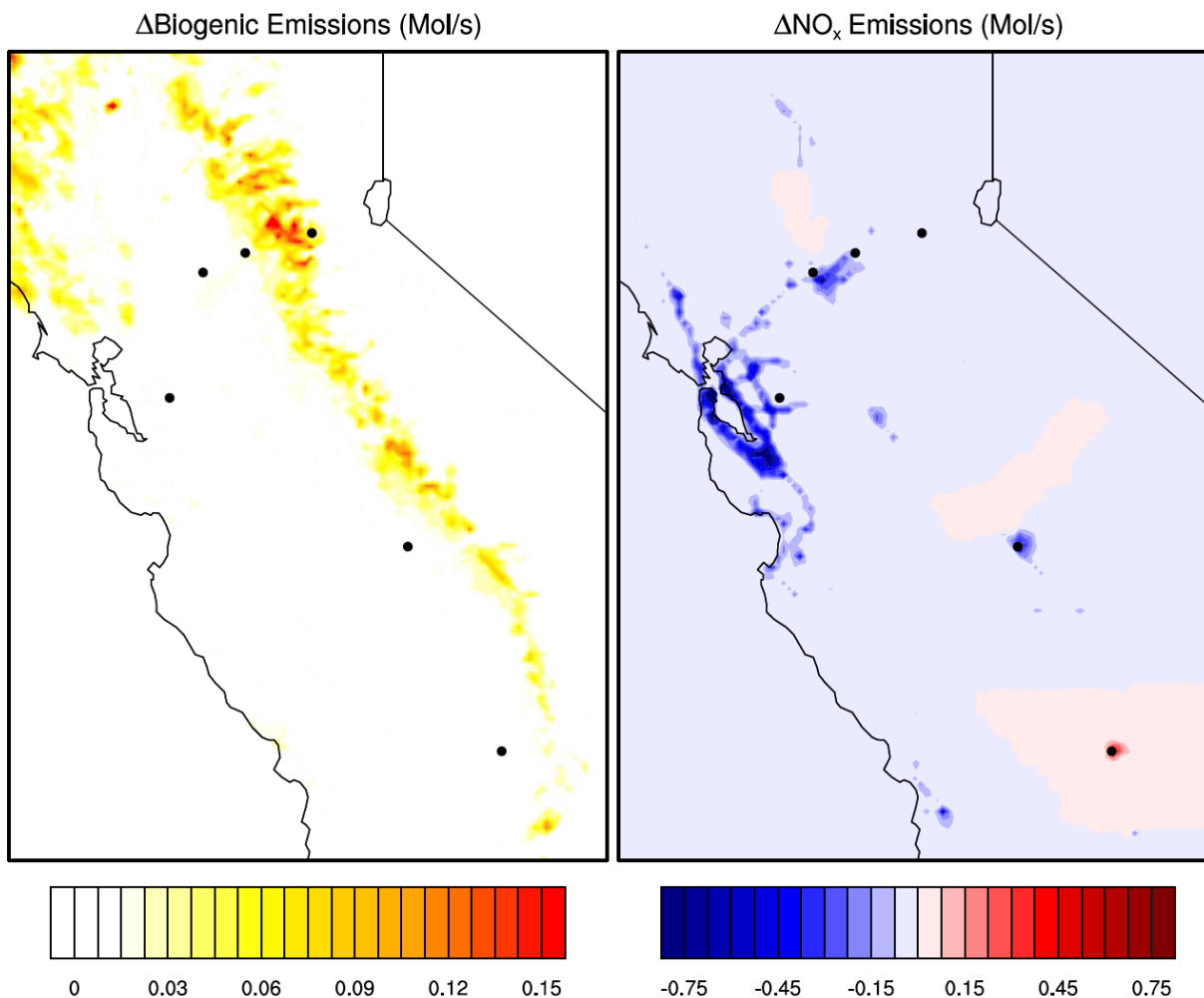


Figure 4-21. Biogenic and anthropogenic emission perturbations for the year 2050 at 4 pm ($Emissions_{2050} - Emissions_{2000}$) shown for JD209. Note, there are only increases in biogenic emissions (accounting for temperature increase). The NO_x emission perturbation (accounting for both population increase and assumed advances in emission control technology; see values in Table 4-10), shows three counties with increased emissions, but decreased emissions throughout the rest of the domain.

The first panel of Figure 4-22 shows the change in ozone expected using the Base mechanism between 2000 and 2050. Widespread ozone decreases are expected to occur, with the exception of the Bay Area, which may see ozone increases. This outcome is broadly consistent with results from Steiner et al. (2006), although population estimates have been updated, and the newer SAPRC07 mechanism has been implemented as part of the Base model. The second panel shows a similar plot, using the SCT mechanism and including temperature-dependent evaporative emissions. The evaporative emissions were adjusted using the scaling factors in Table 4-10, and then perturbed to account for effects of forecast increases in temperature.

The difference between the changes shown in the first two panels is shown in the third panel of Figure 4-22, to assess differences in ozone sensitivity between models. The updated mechanism and modeling developed in my research show larger ozone increases in the Bay Area and smaller ozone decreases throughout the rest of the domain. All of these changes are undesirable from an air quality management perspective, and may slightly raise the bar in terms of the emission reductions needed to meet air quality standards in the future. While previous modeling efforts appear to have missed a portion of the underlying temperature sensitivity of ozone air pollution in assessing possible climate change impacts, the effects on ozone concentration for these central California simulations are small (less than 1 ppb for maximum hourly ozone concentrations). As was the case for the year 2000 Base simulations, estimates of the evaporative emission effects are likely to be conservative as some species are not included in the current inventory. Inclusion of these temperature-dependent VOC species may increase the temperature effects described for ozone concentrations. However, coastal impacts of climate change are less certain and may nudge the system towards lower ozone, due to the possibility of stronger sea breezes and local cooling in coastal areas, driven by a larger temperature contrast between marine and inland areas.

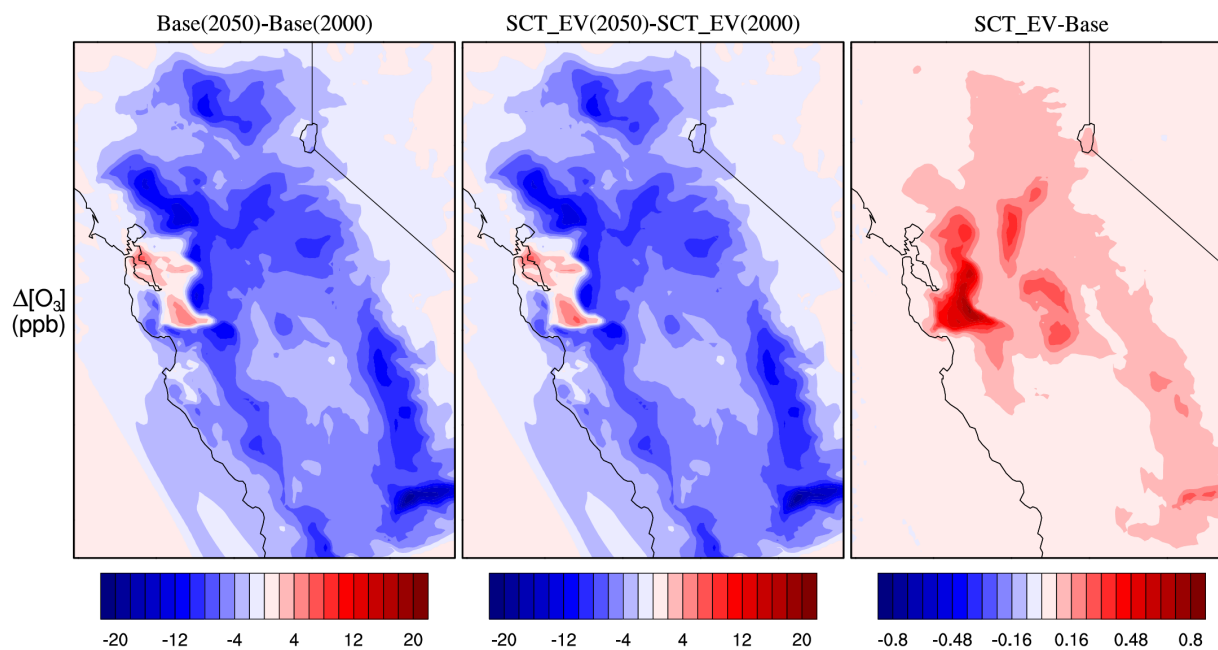


Figure 4-22. Change in O₃ from 2000 to 2050

For Julian days 209 at 4 pm. Change with Base mechanism, change with SCT and temperature-dependent evaporative emissions, and the increase in sensitivity due to use of SCT mechanism and altered emissions.

4.4 Discussion

In this chapter, a chemical mechanism was developed to allow temperature-dependent VOC oxidation products in an air quality model. In doing so, alkoxy radical structure-activity

relationships were updated for the base SAPRC mechanism as well. Additional changes were made to the mechanism to allow appropriate organic nitrate accounting. The additional species, ONA, RNO3IN, and XN, were determined to be important sources of nitrate, while ONB formation is small enough to lump with XN without significantly altering nitrate speciation. It is further recommended to remove isoprene and terpene nitrates from the RNO₃ group as they have a much higher reactivity and lower multifunctional nitrate yield than the lumped RNO₃ species. This step was not taken for the SCT mechanism simulations presented in this chapter, but it is expected to improve the comparisons between modeled and measured nitrate at the Granite Bay and Blodgett Forest sites.

The temperature-dependent RO₂· reactions allow that NO → NO₂ conversions, associated with increased reactivity, increase with temperature (as nitrate yields decrease). Similarly, the temperature-dependent RO· reactions further increase reactivity as the yields of higher reactivity aldehydes to lower reactivity ketones increase with temperature. The addition of temperature-dependent evaporative emissions slightly amplifies these effects. Slightly increased ozone sensitivity to temperature in a year 2000 simulation and a year 2050 climate change simulation follow. These are expected to be conservative estimates, as other known temperature-dependent emissions have not been included, but for these simulations the changes in ozone concentration are minor.

Chapter 5: Conclusions

5.1 Summary of research findings

The research presented in this dissertation explores the sensitivity of air quality model predictions to changes in the description of atmospheric chemical processes for central California during a summer 2000 tropospheric ozone episode. The major focus of the efforts presented in this research include (1) updating an air quality model to use a current (SAPRC07) rather than an out-of-date mechanism (SAPRC99), (2) improving the representation of lumped groups of volatile organic compounds, and (3) adding missing effects of variations in temperature and pressure on atmospheric reaction rates and oxidation product yields. Changes to the chemical mechanism are incorporated in a 3-D photochemical air quality model. A summer 2000 central California air pollution episode is evaluated, and then the mechanism changes are evaluated through the lens of climate change in the same domain. The final improved mechanism that is a major product of this research is used to reassess effects of climate change on air quality.

The first step of this research, described in Chapter 2, was to modernize a widely used air quality model (CMAQ) to include the SAPRC07 chemical mechanism. This new mechanism incorporates many new reactions and kinetic parameters based on results of atmospheric chemistry research published since 2000. SAPRC07 was published in 2010 but has not yet been used much in air quality research and planning studies. In Chapter 2, the CS07A mechanism, a more highly condensed version of SAPRC07 that was designed to be computationally competitive with other currently used mechanisms, was implemented in CMAQ and model performance was assessed. Mechanism changes required development of new initial condition, boundary condition, and emission files. These mechanism changes include the introduction of benzene and acetylene as explicit species (previously these species were awkwardly lumped with other dissimilar hydrocarbons), and the combination of phenol and cresol model species. The most highly condensed version of the new mechanism, CS07A, requires additional merging of emitted species.

Use of CS07A in place of the SAPRC99 mechanism results in widespread decreases in predicted ozone concentrations in central California. Ozone decreases of up to 25 ppb in hourly maximum ozone were seen in the model simulations using the new chemical mechanism. Model sensitivity to individual reaction rates was investigated, and it was found that a 19% increase in the rate coefficient for the reaction $\text{OH} \cdot + \text{NO}_2 \rightarrow \text{HNO}_3$ in SAPRC07 is responsible for most of the ozone decrease. The additional condensation of VOC chemistry in CS07A, intended to improve computational efficiency, is found to cause decreases in ozone concentration of a similar magnitude. Use of CS07A increases modeling error for ozone, including both peak hourly and 8-hour average values.

Although widespread ozone decreases were found in the CS07A simulations, the sensitivity to predicted ozone to VOC emission reductions is *increased*. A 20% reduction in VOC leads to a greater decrease in ozone concentration in the CS07A simulations. Greater NO_x disbenefit (with 20% reduction in NO_x emissions) is found in the Central Valley using the CS07A mechanism, but little difference in NO_x effects between mechanisms is apparent in the Bay Area.

The evaluation of a new chemical mechanism in Chapter 2 reinforces the importance of correctly representing rate parameters for the key reactions involved in atmospheric chemistry. A key study (Mollner et al., 2010) used new experimental techniques to determine $\text{OH} \cdot + \text{NO}_2 \rightarrow \text{HNO}_3$ reaction parameters with high precision and greater generality compared to previous studies. These updated kinetic parameters are used in Chapters 3 and 4. Additionally, use of the most highly condensed mechanism (CS07A) was not deemed appropriate for the remainder of the dissertation, as use of the condensed mechanism led to unexpected divergence in model predictions from the reference mechanism (SAPRC07). These decisions remove two of the largest causes of changes to model predictions in moving to the new mechanism.

With the computing power currently available to support air quality modeling, regional-scale simulations are forced to use significantly condensed descriptions of the atmospheric chemistry of the thousands of VOC that are present in the real atmosphere. In the SAPRC mechanism, the assigned composition profiles of lumped VOC species are defined based on ambient air measurements of speciated hydrocarbon concentrations made during the mid-1980s. In Chapter 3 of this dissertation, the definitions of the lumped VOC species are updated in this chapter using current emission inventory data and source-specific speciation profiles from the peer-reviewed literature. Revisions are needed in light of the major changes in fuels and consumer product formulations that have occurred since the 1980s, as well as changes in the relative importance of different emission source categories.

Oxygenated organic species including alcohols, ethers, and esters now comprise a large portion of the emissions assigned to the lumped alkane species groups, but such species have not been included in the corresponding definitions of lumped species properties. Also ambient measurements of organic gas concentrations rarely include the oxygenated species, focusing instead on traditional measurements of non-methane hydrocarbons. This treatment makes it impossible to evaluate model predictions for lumped organic species, since the model predictions typically include contributions from many unmeasured species. Separate new model species were introduced in this research for tracking oxygenated organics, including ethanol, methyl-tert butyl ether, propyl acetate, lumped amines, and C_3^+ alcohols, so that the lumped alkane species can truly be used to represent the concentrations and reactions of alkanes. Updated descriptions of the hydrocarbon mixtures appropriate for the lumped olefin and aromatic species in the mechanism led to decreased reactivity for these species groups, as measured by k_{OH} . Policy-driven efforts to reduce VOC reactivity in these highly reactive species groups are now represented in the kinetic and mechanistic parameters used to define the properties of these lumped species. Most of the new lumped species definitions show much better agreement with measured VOC speciation than the old definitions still used in SAPRC. The updated lumped species definitions result in peak ozone concentration decreases of up to 1.8 ppb. Compared to the major mechanism update assessed in Chapter 2 (changes of up to 25 ppb ozone), these effects are negligible and not widespread. The updated lumped species definitions are also essential for my research on adding missing temperature and pressure effects on atmospheric reaction rates to the chemical mechanism.

In Chapter 4, the chemical reaction mechanism was rederived to include temperature-dependent rates for reactions of $\text{RO} \cdot$ and $\text{RO}_2 \cdot$ radicals. Additional changes were made to the mechanism to allow for an appropriate accounting of organic nitrate, in order to make comparisons of model

predictions with TD-LIF measurements made in recent field studies in Granite Bay and Blodgett Forest, CA. Mechanism improvements of this kind are needed to reproduce more accurately the observed diurnal, day-to-day, and spatial differences in air quality that are due to meteorological factors. Also assessments of the effects of climate change on air quality require an accurate description of many of the same factors such as temperature effects on chemical reaction rates and oxidation product yields.

The temperature-dependent $\text{RO}_2 + \text{NO}$ reactions allow for $\text{NO} \rightarrow \text{NO}_2$ conversions, that are associated with increased reactivity, to increase with temperature (at the same time, organic nitrate yields decrease). Similarly, including temperature-dependent RO^\cdot reactions further increases reactivity at higher temperatures, as the yields of reactive aldehydes increase. The inclusion of previously unmodeled temperature dependence in evaporative emissions associated with gasoline use slightly amplifies these effects. Increased ozone sensitivity to temperature differences in both year 2000 and 2050 simulations follows. Although in the expected direction, ozone responses to the updated mechanism are small, never exceeding $\sim \pm 1.5$ ppb for an hourly ozone concentration.

5.2 Recommendation for future research

In this dissertation, modeling efforts, such as the meteorological model and emission estimates, were based on results of the summer 2000 Central California Ozone Study (CCOS), and were used to explore air quality model sensitivities to chemical mechanism updates. Measurements and meteorological modeling for the 2010 California Research at the Nexus of Air Quality and Climate Change (CalNex) Study will provide an updated basis for a next wave of research (Ryerson et al. 2013). To accelerate progress in the understanding of atmospheric chemistry, CCOS research efforts should be considered when designing and conducting CalNex simulations.

Further SAPRC mechanism and emission inventory improvements are recommended based on the research described in this dissertation. It is recommended to remove isoprene and terpene nitrates from the SAPRC RNO_3 group as they have a much higher reactivity and lower multifunctional nitrate yield than the lumped RNO_3 species. This change is expected to improve the comparisons between modeled and measured nitrate. New lumped species definitions should be prepared using current emission inventories. It is likely that VOC associated with area sources will play a larger role in the VOC lumped species definitions as Warneke et al. (2012) find that VOC in the Los Angeles basin, presumed to be gasoline-dominated, decreased by a factor of two from 2002 to 2010. The expected increased in importance of area emissions in the VOC inventory compared to motor vehicle emissions points to the importance of identifying and quantifying emissions in the Central Valley related to animal husbandry.

Montes et al. (2010) find ethanol emissions from silage to increase exponentially with temperature. Forty-five other oxygenated VOC have been identified in silage (Hafner et al., 2013) of which some others likely exhibit some temperature-dependence. Hu et al. (2012) show in a central California AQM that silage has the second largest ozone forming potential as a VOC

emission source, but emissions included are assumed to be temperature-*independent*. These and other temperature-dependent emission source terms should be included in future assessments. In addition to silage, other relevant (but currently unmodeled) temperature effects on emissions to consider include power plant emissions operating under peak demand versus normal summer days, and effects of temperature on cold start and running emissions (from vehicles due to increased air conditioner use), fuel economy changes, etc.

Finally, the sensitivity of secondary organic aerosols to use of the SCT mechanism should be investigated. Current SOA parameterization in CMAQ includes dependence on RO₂ originating from aromatic, isoprene, and terpenes. Choi et al. (2006) found that while ozone concentrations were not very sensitive to an overestimation of VOC emissions from surface coatings, secondary organic aerosol concentrations showed substantial sensitivity. My research is relevant to, but did not formally address, the effects of mechanism revisions on SOA formation.

There are many further opportunities for improved simulations of the linkages between climate change and air quality as well. Greenhouse gas emission control laws such as AB32 should help to inform future air quality modeling efforts. A scoping plan update for post-2020 planning will be focused on six areas: 1) transportation, fuels, and infrastructure; 2) energy generation, transmission, and efficiency; 3) waste; 4) water; 5) agriculture; and 6) natural resources GHG emission efforts (<http://www.arb.ca.gov/cc/scopingplan/scopingplan.htm>). The GHG emission control efforts in the transportation arena are the most likely to affect air quality. Biofuels have been widely studied as a substitute for petrochemicals. Suitable alternatives have been proposed, but it is unknown what replacements will eventually emerge. As possibilities are presented, atmospheric effects should be explored to avoid potential pitfalls. UC Berkeley researchers have developed a drop-in gasoline replacement through a fermentation process that produces the 5-carbon alcohols: 3-methyl-2-buten-1-ol, 3-methyl-3-buten-1-ol, and 3-methyl-butan-1-ol (<http://www.lbl.gov/tt/techs/lbnl2392.html>). Theoretically, this mixture could replace 20% of gasoline, but the effects on air quality have not been investigated. These types of investigations are more easily pursued with the updated mechanism presented in this dissertation.

Other potential air quality sensitivities that should be investigated in future coupled climate change-air quality assessments include pollution inflow at the Western (Pacific Ocean) boundary and effects on meteorology. In my research, temperature and water vapor were perturbed, but other changes in wind fields, planetary boundary layer heights, and the frequency of stagnation events were not modeled. A coupled climate-chemistry model would allow for representation of aerosol feedbacks and more realistic assessments of the effects of an altered climate. Inclusion of the mechanism and temperature-dependent emissions developed in this dissertation will help to provide more accurate assessments of air quality sensitivity to climate change. Past assessments systematically understate the effects of temperature increases on air quality.

References

- Ainsworth EA, Yendrek CR, Sitch S, Collins WJ, Emberson LD, 2012. The effects of tropospheric ozone on net primary productivity and implications for climate change. *The Annual Review of Plant Biology* **63**, 637-691. doi:10.1146/annurev-arplant-042110-103829
- American Lung Association, State of the Air: 2012 Report. Available for download at: <http://www.stateoftheair.org/2013/assets/ala-sota-2013.pdf>
- Anfossi D, Sandroni S, Viarengo S, 1991. Tropospheric ozone in the nineteenth century? The Moncalieri Series. *Journal of Geophysical Research* **96** (D9), 17349-17352. doi:10.1029/91JD01474
- Aris RM, Christian D, Hearne PQ, Kerr K, Finkbeiner WE, Balmes JR, 1993. Ozone-induced airway inflammation in human subjects as determined by airway lavage and biopsy. *American Review of Respiratory Disease* **148** (5), 1363-1372.
- Atkinson R, 1986. Estimations of OH radical rate constants from H-atom abstraction from C-H and O-H bonds over the temperature range 250-1000 K. *International Journal of Chemical Kinetics* **18**, 555-568. doi:10.1016/1352-2310(95)00069-B
- Atkinson R, 1987. Structure-activity relationship for the estimation of rate constants for the gas-phase reactions of OH radicals with organic compounds. *International Journal of Chemical Kinetics* **19**, 799-828. doi:10.1002/kin.550190903
- Atkinson R, 1997. Atmospheric reactions of alkoxy and beta-hydroxyalkoxy radicals. *International Journal of Chemical Kinetics* **29**, 99-111. doi:10.1002/(SICI)1097-4601(1997)29:2<99::AID-KIN3>3.0.CO;2-F
- Atkinson R, 2000. Atmospheric chemistry of VOC and NO_x. *Atmospheric Environment* **34**, 2063-2101. doi:10.1016/S1352-2310(99)00460-4
- Atkinson R, 2007. Rate constants for the atmospheric reactions of alkoxy radicals: An updated estimation method. *Atmospheric Environment* **41**, 8468-8485. doi:10.1016/j.atmosenv.2007.07.002
- Ausset P, Bannery F, Del Monte M, Lefevre RA, 1998. Recording of pre-industrial atmospheric environment by ancient crusts on stone monuments. *Atmospheric Environment* **32** (16), 2859-2863. doi: 10.1016/S1352-2310(98)00063-6
- Avery RJ, 2006. Reactivity-based VOC control for solvent products: More efficient ozone reduction strategies. *Environmental Science & Technology* **40**, 4845-4850. doi:10.1021/es060296u
- Bell ML, Davis DL, 2001. Reassessment of the lethal London fog of 1952: novel indicators of acute and chronic consequences of acute exposure to air pollution. *Environmental Health Perspectives* **109** (Suppl 3), 389-394.
- Bell ML, Peng RD, Dominici F, 2006. The exposure-response curve for ozone and risk of mortality and the adequacy of current ozone regulations. *Environmental Health Perspectives* **114** (4), 532-536. doi:10.1289/ehp.8816

- Bethel HL, Atkinson R, and Arey J, 2001. Kinetics and products of the reactions of selected diols with the OH radical. *International Journal of Chemical Kinetics* **33** (5), 310-316.
doi:10.1002/kin.1025
- Blomberg A, Mudway IS, Nordenhall C, Hendenstrom H, Kelly FJ, Frew AJ, Holgate ST, Sandstrom T, 1999. Ozone-induced lung function decrements do not correlate with early inflammatory or antioxidant responses. *European Respiratory Journal* **13** (6), 1418-1428.
- Bloomer BJ, Stehr JW, Piety CA, Salawitch RJ, Dickerson RR, 2009. Observed relationships of ozone air pollution with temperature and emissions. *Geophysical Research Letters* **36**, L09803. doi:10.1029/2009GL037308
- Brienes M, 1976. Smog comes to Los Angeles. *Southern California Quarterly* **58** (4), 515-532.
- Brimblecombe P. The big smoke: a history of air pollution in London since medieval times. London: Methuen, 1987.
- Brown SG, Main HH, 2002. *PAMS Data Validation for the Northeast States 2000-2001*, Final Report for Northeast States for Coordinated Air Use Management: STI-902071-2205-FR, Sonoma Technology, Inc.
- Byun D, Schere KL, 2006. Review of the governing equations, computational algorithms, and other components of the Models-3 Community Multiscale Air Quality (CMAQ) modeling system. *Applied Mechanics Reviews* **59**, 51-77.
- Cai C, Kelly JT, Avise JC, Kaduwela AP, Stockwell WR, 2011. Photochemical modeling in California with two chemical mechanisms: Model intercomparison and response to emission reductions. *Journal of the Air & Waste Management Association* **61**, 559-572.
doi:10.3155/1047-3289.61.5.559
- California Department of Finance, 2013. Report P-1 (County): State and County Total Population Projections, 2010-2060. Sacramento, California.
- Camalier L, Cox L, Dolwick P, 2007. The effects of meteorology on ozone in urban areas and their use in assessing ozone trends. *Atmospheric Environment* **41**, 7127-7137.
doi:10.1016/j.atmosenv.2007.04.061
- CARB, 1990. Code of Regulations. Reformulated gasoline: proposed phase 1 specifications. Available at <http://www.arb.ca.gov/fuels/gasoline/Carfg1/carfg1.htm>. Accessed November, 2010.
- CARB, 2000. The California Reformulated Gasoline phase 3 amendments, Final regulation order, Title 13, California code of regulations. Available at <http://www.arb.ca.gov/regact/carfg3/carfg3.htm>. Accessed November, 2010.
- CARB, 2005. Regulation for reducing the ozone formed from aerosol coating product emissions. Article 3 in *The California Consumer Products Regulations*, 79-129. Available at <http://www.arb.ca.gov/consprod/regs/regs.htm>. Accessed November, 2010.
- CARB, 2009a. The California Almanac of Emissions and Air Quality, 2009 Edition. Available at <http://www.arb.ca.gov/aqd/almanac/almanac09/almanac09.htm>. Accessed November, 2010.

- CARB, 2009b. Almanac emission projection data. Available at <http://www.arb.ca.gov/app/emsinv/emssumcat.php>. Accessed November, 2010.
- CARB, 2010. Speciation profiles used in ARB modeling. Available at http://arb.ca.gov/ei/speciate/profphp00/orgprof_list.php. Accessed November, 2010.
- Cardelino CA, Chameides WL, 1990. Natural hydrocarbons, urbanization, and urban ozone. *Journal of Geophysical Research* **95** (D9), 13971-13979. doi:10.1029/JD095iD09p13971
- Carter WPL, Atkinson R, 1989. Alkyl nitrate formation from the atmospheric photooxidation of alkanes; a revised estimation method. *Journal of Atmospheric Chemistry* **8**, 165-173. doi:10.1007/BF00053721
- Carter WPL, Winer AM, Darnall KR, Pitts Jr JN, 1979. Smog chamber studies of temperature effects in photochemical smog. *Environmental Science & Technology* **13** (9), 1094-1100. doi:10.1021/es60157a006
- Carter WPL, 1994. Development of ozone reactivity scales for volatile organic compounds, *Journal of the Air & Waste Management Association* **44**, 881-899.
- Carter WPL, 2000. Documentation of the SAPRC-99 chemical mechanism for VOC reactivity assessment. Report to the California Air Resources Board. College of Engineering, Center for Environmental Research and Technology, University of California at Riverside, CA. Contracts 92-329 and 95-308. Available at <http://www.cert.ucr.edu/~carter/reactdat.htm>
- Carter WPL, 2009. Peer Review of the SARPRC-07 Chemical Mechanism: Response to Reviewers' Comments. Prepared for California Air Resources Board, Contract 07-730. Available at <http://www.arb.ca.gov/research/reactivity/3-25-2009/carter-resp-rev3.pdf>, accessed August, 2013.
- Carter WPL, 2010a. Development of the SAPRC-07 chemical mechanism. *Atmospheric Environment* **44**, 5324-5335. doi:10.1016/j.atmosenv.2010.01.026
- Carter WPL, 2010b. "Development of the SAPRC-07 Chemical Mechanism and Updated Ozone Reactivity Scales," Revised report to the California Air Resources Board Contracts No. 03E318, 06E408, and 07E730, January 27. Available at <http://www.cert.ucr.edu/~carter/SAPRC>
- Carter WPL, 2010c. Development of a condensed SAPRC-07 chemical mechanism. *Atmospheric Environment* **44**, 5336-5345. doi:10.1016/j.atmosenv.2010.01.024
- Carter WPL, Seinfeld JH, 2012. Winter ozone formation and VOC incremental reactivities in the Upper Green River Basin of Wyoming, *Atmospheric Environment* **50**, 255-266. doi: 10.1016/j.atmosenv.2011.12.025
- Chen S, Ren X, Mao J, Chen Z, Brune WH, Lefer B, Rappenglueck B, Flynn J, Olson J, Crawford JH, 2010. A comparison of chemical mechanisms based on TRAMP-2006 field data. *Atmospheric Environment* **44**, 4116-4125. doi:10.1016/j.atmosenv.2009.05.027
- Chevron Products Co., Richmond, CA, 1998. Diesel fuels - Technical review. Figure 4-2, pg. 26.

- Choi Y-J, Calabrese RV, Ehrman SH, Dickerson RR, Stehr, JW, 2006. A combined approach for the evaluation of a volatile organic compound emissions inventory. *Journal of the Air & Waste Management Association* **56**, 169-178. doi:10.1080/10473289.2006.10464446
- Cleary PA, Murphy JG, Wooldridge PJ, Day DA, Millet DB, McKay M, Goldstein AH, Cohen RC, 2005. Observations of total alkyl nitrates within the Sacramento urban plume. *Atmospheric Chemistry and Physics Discussions* **5**, 4801-4843. doi:10.5194/acpd-5-4801-2005
- Cleary PA, Wooldridge PJ, Millet DB, McKay M, Goldstein AH, Cohen RC, 2007. Observations of total peroxy nitrates and aldehydes: measurement interpretation and inference of OH radical concentrations. *Atmospheric Chemistry and Physics* **7**, 1947-1960. doi:10.5194/acp-7-1947-2007
- Crounse JK, Paulot F, Kjaergaard HG, Wennberg PO, 2011. Peroxy radical isomerization in the oxidation of isoprene. *Physical Chemistry Chemical Physics* **13**, 13607-13613. doi:10.1039/c1cp21330j
- Dabdub D, Seinfeld JH, 1994. Numerical advective schemes used in air quality models – Sequential and parallel implementation. *Atmospheric Environment* **28** (20), 3369-3385. doi:10.1016/1352-2310(94)00124-4
- Day DA, Wooldridge PJ, Dillon MB, Thornton JA, Cohen RC, 2002. A thermal dissociation laser-induced fluorescence instrument for in situ detection of NO₂, peroxy nitrates, alkyl nitrates, and HNO₃. *Journal of Geophysical Research* **107** (D6), 4046. doi:10.1029/2001JD000779
- Day DA, Dillon MB, Wooldridge PJ, Thornton JA, Rosen RS, Wood EC, Cohen RC, 2003. On alkyl nitrates, O₃, and the “missing NO_y.” *Journal of Geophysical Research* **108** (D16), 4501. doi:10.1029/2003JD003685
- Day DA, Wooldridge PJ, Cohen RC, 2008. Observations of the effects of temperature on atmospheric HNO₃, ΣANs, ΣPNs, and NO_x: evidence for a temperature-dependent HO_x source. *Atmospheric Chemistry and Physics* **8**, 1867-1879. doi:10.5194/acp-8-1867-2008
- Day DA, Farmer DK, Goldstein AH, Wooldridge PJ, Minejima C, Cohen RC, 2009. Observations of NO_x, ΣPNs, ΣANs, and HNO₃ at a rural site in the California Sierra Nevada mountains: summertime diurnal cycles. *Atmospheric Chemistry and Physics* **9**, 4879-4896. doi:10.5194/acp-9-4879-2009
- Devlin RB, Duncan KE, Jardim M, Schmitt MT, Rappold AG, Diaz-Sanchez D, 2012. Controlled exposure of healthy young volunteers to ozone causes cardiovascular effects. *Circulation* **126**, 104-111. doi: 10.1161/CIRCULATIONAHA.112.094359
- Dewey SH, 2000. Don't Breathe the Air: Air Pollution and U.S. Environmental Politics, 1945-1970. College Station: Texas A&M University Press.
- Environ, 2010. Final Report: A Conceptual Model of Winter Ozone Episodes in Southwest Wyoming. Novato, CA.

- Faraji M, Kimura Y, McDonald-Buller E, Allen D, 2008. Comparison of the Carbon Bond and SAPRC photochemical mechanisms under conditions relevant to southeast Texas. *Atmospheric Environment* **42**, 5821-5836.
- Fujita EM, Watson JG, Chow JC, Magliano KL, 1995. Receptor model and emissions inventory source apportionments of non-methane organic gases in California's San Joaquin valley and San Francisco bay area, *Atmospheric Environment* **29**, 3019-3035. doi:10.1016/1352-2310(95)00122-F
- Fujita EM, Lu Z, Sheet G, Harshfeld G, Zielinska B, 1997. Determination of mobile source emission fraction using ambient field measurements. Prepared for Coordinating Research Council, Atlanta, GA, Desert Research Institute Reno, NV.
- Fujita EM, Campbell DE, Snorraddottir T, 2005. Central California Ozone Study (CCOS) Data Validation, Final Report. California Air Resources Board, Sacramento.
- Georgopoulos PG, 1995. Regulatory ozone modeling: Status, directions, and research needs. *Environmental Health Perspectives* **103** (Suppl 2), 107-132.
- Gery MW, Whitten GZ, Killus JP, Dodge MC, 1989. A photochemical kinetics mechanism for urban and regional scale computer modeling. *Journal of Geophysical Research* **94** (D10), 12925–12956. doi:10.1029/JD094iD10p12925
- Goliff WS, Stockwell WR, Lawson CV, 2013. The regional atmospheric chemistry mechanism, version 2. *Atmospheric Environment* **68**, 174-185. doi:10.1016/j.atmosenv.2012.11.038
- Grell GA, Dudhia J, Stauffer DR, 1995. A description of the fifth generation Penn State/NCAR Mesoscale Model (MM5). NCAR Tech. Note NCAR/TN-39811A, 122 pp. Available at <http://www.mmm.ucar.edu/mm5/doc1.html>
- Griffin RJ, Dabdub D, Seinfeld JH, 2002. Secondary organic aerosol: 1. Atmospheric chemical mechanism for production of molecular constituents. *Journal of Geophysical Research* **107** (D17), 4332. doi:10.1029/2001JD000541
- Guenther AB, Zimmerman PR, Harley PC, Monson RK, Fall R, 1993. Isoprene and monoterpene emission rate variability - Model evaluations and sensitivity analyses, *Journal of Geophysical Research* **98** (D7), 12609-12617. doi:10.1029/93JD00527
- Haagen-Smit AJ, 1952. Chemistry and physiology of Los Angeles smog. *Industrial and Engineering Chemistry* **44** (6), 1342-1346.
- Haagen-Smit AJ, Fox MM, 1954. Photochemical ozone formation with hydrocarbons and automobile exhaust. *Air Repair* **4** (3), 105-136.
- Hafner SD, Howard C, Muck RE, Franco RB, Montes F, Green PG, Mitloehner F, Trabue SL, Rotz CA, 2013. Emission of volatile organic compounds from silage: Compounds, sources, and implications. *Atmospheric Environment* **77**, 827-839. doi:10.1016/j.atmosenv.2013.04.076
- Hanna SR, Lu Z, Frey HC, Wheeler N, Vukovich J, Arunachalam S, Fernau M, Hansen DA, 2001. Uncertainties in predicted ozone concentrations due to input uncertainties for the

- UAM-V photochemical grid model applies to the July 1995 OTAG domain. *Atmospheric Environment* **35**, 891-903. doi:10.1016/S1352-2310(00)00367-8
- Harley RA, Coulter-Burke SC, Yeung TS, 2000. Relating liquid fuel and headspace vapor composition for California reformulated gasoline samples containing ethanol. *Environmental Science & Technology* **34**, 4088–4094. doi:10.1021/es0009875
- Harley RA, Kean AJ, 2004. Chemical composition of vehicle-related volatile organic compound emissions in central California. Final report to CARB, Contract 00-14CCOS. Available at <http://www.arb.ca.gov/airways/ccos/ccos.htm>. Accessed November, 2010.
- Harley RA, Brown NJ, Tonse SR, Jin L, 2006. A seasonal perspective on regional air quality in central California: Phase I final report for San Joaquin Valley wide Air Pollution Study Agency and the California Air Resources Board, Department of Civil and Environmental Engineering, University of California, Berkeley.
- Hartman DL, 1994. *Global Physical Climatology*. San Diego: Academic Press.
- Hayden KL, Anlauf KG, Hastie DR, Bottenheim JW, 2003. Partitioning of reactive atmospheric nitrogen oxides at an elevated site in southern Quebec, Canada. *Journal of Geophysical Research* **108** (D19), 4603. doi:10.1029/2002JD003188
- Heo G, Kimura Y, McDonald-Buller E, Carter WPL, Yarwood G, Allen DT, 2010. Modeling alkene chemistry using condensed mechanisms for conditions relevant to southeast Texas, USA. *Atmospheric Environment* **44**, 5365-5374. doi:10.1016/j.atmosenv.2009.10.001
- Horowitz HW, Fiore AM, Milly GP, Cohen RC, Perring A, Wooldridge PJ, Hess PG, Emmons LK, Lamarque J-F, 2007. Observational constraints on the chemistry of isoprene nitrates over the eastern United States. *Journal of Geophysical Research* **112**, D12S08. doi:10.1029/2006JD007747
- Howard CJ, Kumar A, Malkina I, Mitloehner F, Green PG, Flocchini RG, Kleeman MJ, 2010. Reactive organic gas emissions from livestock feed contribute significantly to ozone production in central California. *Environmental Science & Technology* **44**, 2309-2314. doi:10.1021/es902864u
- Hu J, Howard CJ, Mitloehner F, Green PG, Kleeman MJ, 2012. Mobile source and livestock feed contributions to regional ozone formation in central California. *Environmental Science & Technology* **46**, 2781–2789. doi:10.1021/es203369p
- IPCC, 2007. Summary for Policymakers. In *Climate Change 2007: The Physical Science Basis. Contribution of Working Group I to the Fourth Assessment Report of the Intergovernmental Panel on Climate Change*; Solomon S, Qin D, Manning M, Chen Z, Marquis M, Avery KB, Tignor M, Miller HL, Editors. New York: Cambridge University Press.
- Isaacman G, Wilson KR, Chan AWH, Worton DR, Kimmel JR, Nah T, Hohaus T, Gonin M, Kroll JH, Worsnop DR, Goldstein AH, 2012. Improved resolution of hydrocarbon structures and constitutional isomers in complex mixtures using gas chromatography-vacuum ultraviolet-mass spectrometry. *Analytical Chemistry* **84**, 2335-2342. doi:10.1021/ac2030464

- IUPAC, 2006. Evaluated Kinetic and Photochemical Data. IUPAC Subcommittee on Gas Kinetic Data and Evaluation for Atmospheric Chemistry. Available at <http://www.iupac-kinetic.ch.cam.ac.uk/>
- Jacob DJ, Logan JA, Gardner GM, Yevich RM, Spivakovsky CM, Wofsy SC, Sillman S, Prather MJ, 1993. Factors regulating ozone over the United States and its export to the global atmosphere. *Journal of Geophysical Research* **98** (D8), 14817-14826. doi: 10.1029/98JD01224
- Jacob DJ, Winner DA, 2009. Effect of climate change on air quality. *Atmospheric Environment* **43**, 51-63. doi:10.1016/j.atmosenv.2008.09.051
- Jeffries HE, Sexton KG, Arnold JR, Kale TL, 1989. Validation testing of new mechanisms with outdoor chamber data. Volume 2: Analysis of VOC data for the CB4 and CAL photochemical mechanisms, Final Report, EPA-600/3-89-010b.
- Jeffries HE, Tonnesen S, 1994. A comparison of two photochemical reaction mechanisms using mass balance and process analysis. *Atmospheric Environment* **28** (18), 2991-3003. doi:10.1016/1352-2310(94)90345-X
- Jenkin ME, Saunders SM, Pilling MJ, 1997. The tropospheric degradation of volatile organic compounds: a protocol for mechanism development. *Atmospheric Environment* **31**, 81-104. doi:10.1016/S1352-2310(96)00105-7
- Jimenez P, Baldasano JM, Dabdub D, 2003. Comparison of photochemical mechanisms for air quality modeling. *Atmospheric Environment* **37**, 4179-4194. doi:10.1016/S1352-2310(03)00567-3
- Jin L, Tonse S, Cohan D, Mao X, Harley RA, Brown NJ, 2008. Sensitivity analysis of ozone formation and transport for a Central California air pollution episode. *Environmental Science & Technology* **42**, 3683-3689.
- Jin L, Brown NJ, Harley RA, Bao J, Michelson SA, Wilczak JM, 2010. Seasonal versus episodic performance evaluation for an Eulerian photochemical air quality model. *Journal of Geophysical Research* **115**, D09302. doi:10.1029/2009JD012680
- Kirchstetter TW, Singer BC, Harley RA, Kendall GR, Hesson JM, 1999. Impact of California reformulated gasoline on motor vehicle emissions. 2. Volatile organic compound speciation and reactivity. *Environmental Science & Technology* **33**, 329-336. doi:10.1021/es980374g
- Kleeman MJ, 2008. A preliminary assessment of the sensitivity of air quality in California to global change. *Climatic Change* **87** (Suppl 1), S273-S292. doi:10.1007/s10584-007-9351-3
- Kotkin J, Frey WH, 2007. The Third California: The Golden State's New Frontier. Research Brief. Washington, DC: The Brookings Institute.
- Kwok ESC, Atkinson R, 1995. Estimation of hydroxyl radical reaction rate constants for gas phase organic compounds using a structure-reactivity relationship: An update. *Atmospheric Environment* **29**, 1685-1695. doi:10.1016/1352-2310(95)00069-B

- Lefohn AS, Shadwick D, Oltmans SJ, 2010. Characterizing changes in surface ozone levels in metropolitan and rural areas in the United States for 1980-2008 and 1994-2008. *Atmospheric Environment* **44**, 5199-5210. doi:10.1016/j.atmosenv.2010.08.049
- Li J, Zhang H, Ying Q, 2012. Comparison of the SAPRC07 and SAPRC99 photochemical mechanisms during a high ozone episode in Texas: Differences in concentrations, OH budget and relative response factors. *Atmospheric Environment* **54**, 25-35. doi:10.1016/j.atmosenv.2012.02.034
- Liao K-J, Tagaris E, Manomaiphiboon K, Wang C, Woo J-H, Amar P, He S, Russell AG, 2009. Quantification of the impact of climate uncertainty on regional air quality. *Atmospheric Chemistry and Physics* **9**, 865-878.
- Logan JA, 1989. Ozone in rural areas of the United States. *Journal of Geophysical Research* **94** (D6), 8511-8532. doi:10.1029/98JD01224
- Lonneman WA, 1986. Comparison of 0600-0900 AM hydrocarbon compositions obtained from 29 cities, Proceedings APCA/U.S. EPA Symposium on Measurements of Toxic Air Pollutants, Raleigh, NC.
- Luecken DJ, Tonnesen GS, Sickles JE II, 1999. Differences in NO_y speciation predicted by three photochemical mechanisms. *Atmospheric Environment* **33**, 1073-1084. doi:10.1016/S1352-2310(98)00319-7
- Luecken DJ, Phillips S, Sarwar G, Jang C, 2008. Effects of using the CB05 vs. SAPRC99 vs. CB4 chemical mechanism on model predictions: Ozone and gas-phase photochemical precursor concentrations. *Atmospheric Environment* **42**, 5805-5820. doi:10.1016/j.atmosenv.2007.08.056
- Luecken DJ, Hutzell WT, Strum ML, Pouliot GA, 2012. Regional sources of atmospheric formaldehyde and acetaldehyde and implications for atmospheric modeling. *Atmospheric Environment* **47**, 477-490. doi:10.1016/j.atmosenv.2011.10.005
- Madronich S, Calvert JG, 1990. Permutation reactions of organic peroxy radicals in the troposphere. *Journal of Geophysical Research* **95** (D5), 5697-5717. doi:10.1029/JD095iD05p05697
- Marr LC, Noblet GS, Harley RA, 2002. Formation of photochemical air pollution in central California 2. Impact of revised emissions on Eulerian model predictions. *Journal of Geophysical Research* **107** (D6), 4048. doi:10.1029/2001JD000690
- Martien PT, Harley RA, 2006. Adjoint sensitivity analysis for a three-dimensional photochemical model: application to Southern California. *Environmental Science & Technology* **40**, 4200-4210. doi:10.1021/es051026z
- McRae GJ, Goodin WR, Seinfeld JH, 1982. Numerical solution of the atmospheric diffusion equation for chemically reacting flows. *Journal of Computational Physics* **45**, 1-42.
- Meylan WM, Howard PH, 2003. A review of quantitative structure-activity relationship method for the prediction of atmospheric oxidation of organic chemicals. *Environmental Toxicology and Chemistry*, **22** (8), 1724-1732. doi:10.1897/01-275

- Michelson SA, Djalalova IV, Bao J-W, 2010. Evaluation of the summertime low-level winds simulated by MM5 in the Central Valley of California. *Journal of Applied Meteorology and Climatology* **49**, 2231-2245. doi:10.1175/2010JAMC2295.1
- Millstein DE, Harley RA, 2009. Impact of climate change on photochemical air pollution in Southern California. *Atmospheric Chemistry and Physics* **9**, 3745-3754.
- Mohr SH, Evans GM, 2011. Long term forecasting of natural gas production. *Energy Policy* **39**, 5550-5560. doi:10.1016/j.enpol.2011.04.066
- Mollner AK, Valluvadasan S, Feng L, Sprague MK, Okumura M, Milligan DB, Bloss WJ, Sander SP, Martien PT, Harley RA, McCoy AB, Carter WPL, 2010. Rate of gas phase Association of hydroxyl radical and nitrogen dioxide. *Science* **330**, 646-649. doi:10.1126/science.1193030
- Montes F, Hafner SD, Rotz CA, Mitloehner FM, 2010. Temperature and air velocity effects on ethanol emission from corn silage with the characteristics of an exposed silo face. *Atmospheric Environment* **44**, 1987-1995. doi:10.1016/j.atmosenv.2010.02.037
- Murphy JG, Day DA, Cleary PA, Wooldridge PJ, Cohen RC, 2006. Observations of the diurnal and seasonal trends in nitrogen dioxides in the western Sierra Nevada. *Atmospheric Chemistry and Physics* **6**, 5321-5338. doi:10.5194/acp-6-5321-2006
- Murphy JG, Day DA, Cleary PA, Wooldridge PJ, Millet DB, Goldstein AH, Cohen RC, 2007. The weekend effect within and downwind of Sacramento – Part 1: Observations of ozone, nitrogen oxides, and VOC reactivity. *Atmospheric Chemistry and Physics* **7**, 5327-5339. doi:10.5194/acp-7-5327-2007
- NASA, 2006. Chemical kinetics and photochemical data for use in atmospheric studies, Evaluation Number 15. JPL Publication 06-2. Jet Propulsion Laboratory, Pasadena, California. Available at http://jpldataeval.jpl.nasa.gov/previous_evaluations.html
- NASA, 2011. Chemical kinetics and photochemical data for use in atmospheric studies, Evaluation Number 17. JPL Publication 10-6. Jet Propulsion Laboratory, Pasadena, California. Available at <http://jpldataeval.jpl.nasa.gov/>
- Nemery B, Hoet PHM, Nemmar A, 2001. The Meuse Valley fog of 1930: an air pollution disaster. *The Lancet* **357** (9257), 704-708. doi:10.1016/S0140-6736(00)04135-0
- Newchurch MJ, Ayoub MA, Oltmans S, Johnson B, Schmidlin FJ, 2003. Vertical distribution of ozone at four sites in the United States. *Journal of Geophysical Research* **108** (D1), 4031. doi:10.1029/2002JD002059
- Nolte CG, Gilliland AB, Hogrefe C, Mickley LJ, 2008. Linking global to regional models to assess future climate impacts on surface ozone levels in the United States. *Journal of Geophysical Research* **113**, D14307. doi:10.1029/2007JD008497
- Olszyna KJ, Luria M, Meagher JF, 1997. The correlation of temperature and rural ozone levels in southeastern U.S.A. *Atmospheric Environment* **31** (18), 3011-3022. doi:10.1016/S1352-2310(97)00097-6

- Patz H-W, Corsmeier U, Glaser K, Vogt U, Kalthoff N, Klemp D, Kolahgar B, Lerner A, Neining B, Schmitz T, Schultz MG, Slemr J, Volz-Thomas A, 2000. Measurements of trace gases and photolysis frequencies during SLOPE96 and a coarse estimate of the local OH concentration from HNO₃ formation. *Journal of Geophysical Research* **105** (D1), 1563–1583. doi:10.1029/1999JD900918
- Paulot F, Crouse JD, Kjaergaard HG, Kroll JH, Seinfeld JH, Wennberg PO, 2009. Isoprene photooxidation: new insights into the production of acids and organic nitrates. *Atmospheric Chemistry and Physics* **9**, 1479-1501. doi:10.5194/acp-9-1479-2009
- Peeters J, Boullart V, Pultau S, Vandenberg S, and Vereecken L, 2007. Structure-activity relationship for the addition of OH to (poly)alkenes: Site-specific and total rate constants. *Journal of Physical Chemistry A* **111**, 1618-1631. doi:10.1021/jp066973o
- Peeters J, Müller J-F, 2010. HO_x radical regeneration in isoprene oxidation via peroxy radical isomerisations. 2: experimental evidence and global impact. *Physical Chemistry Chemical Physics* **12**, 14227-14235. doi:10.1039/C0CP00811G
- Perez IM, LaFranchi BW, Cohen RC, 2009. Nitrogen oxide chemistry in an urban plume: investigation of the chemistry of peroxy and multifunctional organic nitrates with a Lagrangian model. *Atmospheric Chemistry and Physics Discussions* **9**, 27099-27165.
- Perring AE, Bertram TH, Wooldridge PJ, Fried A, Heikes BG, Dibb J, Crouse JD, Wennberg PO, Blake NJ, Brune WH, Singh HB, Cohen RC, 2009. Airborne observations of total RONO₂: new constraints on the yield and lifetime of isoprene nitrates. *Atmospheric Chemistry and Physics* **9**, 1451-1463. doi:10.5194/acp-9-1451-2009
- Portney PR, Stavins RN, editors, 2000. *Public Policies for Environmental Protection*. Washington DC: RFF Press Book.
- Reich PB, Amundson RG, 1985. Ambient levels of ozone reduce net photosynthesis in tree and crop species. *Science* **230** (4725), 566-570. doi:10.1126/science.230.4725.566
- Renewable Fuel Association, 2010. Ethanol industry statistics. Available at <http://www.ethanolrfa.org/pages/statistics>, accessed November, 2010.
- Rosen RS, Wood EC, Wooldridge PJ, Thornton JA, Day DA, Kuster W, Williams WJ, Jobson BT, Cohen RC, 2004. Observations of total alkyl nitrates during Texas Air Quality Study 2000: Implications for O₃ and alkyl nitrate photochemistry. *Journal of Geophysical Research* **109**, D07303. doi:10.1029/2003JD004227
- Rubin JI, Kean AJ, Harley RA, Millet DB, Goldstein AH, 2006. Temperature dependence of volatile organic compound evaporative emissions from motor vehicles. *Journal of Geophysical Research* **111**, D03305. doi:10.1029/2005JD006458
- Russell A, Dennis R, 2000. NARSTO critical review of photochemical models and modeling. *Atmospheric Environment* **34**, 2283-2324. doi:10.1016/S1352-2310(99)00468-9
- Ryerson TB, Andrews AE, Angevine WM, Bates TS, Brock CA, Cairns B, Cohen RC, Cooper OR, de Gouw JA, Fehsenfeld FC, Ferrare RA, Fischer ML, Flagan RC, Goldstein AH, Hair JW, Hardesty RM, Hostetler CA, Jimenez JL, Langford AO, McCauley E, McKeen SA,

- Molina LT, Nenes A, Oltmans SJ, Parrish DD, Pererson JR, Pierce RB, Prather K, Quinn PK, Seinfeld JH, Senff CJ, Sorooshian A, Stutz J, Surratt JD, Trainer M, Volkamer R, Williams EJ, Wofsy SC, 2013. The 2010 California research at the nexus of air quality and climate change (CalNex) field study. *Journal of Geophysical Research* **118**, 5830-5866. doi:10.1002/jgrd.50331
- Sarwar G, Luecken D, Yarwood G, Whiten GZ, Carter WPL, 2008. Impact of an updated Carbon Bond Mechanism on predictions for the CMAQ Modeling System: preliminary assessment. *Journal of Applied Meteorology and Climatology* **47**, 3-14. doi:10.1175/2007JAMC1393.1
- Sarwar G, Godowitch J, Henderson B, Fahey K, Pouliot G, Hutzell WT, Mathur R, Kang D, Goliff WS, Stockwell WR, 2013. A comparison of atmospheric composition using the Carbon Bond and Regional Atmospheric Chemistry Mechanisms. *Atmospheric Chemistry and Physics Discussions* **13**, 6923–6969. doi:10.5194/acpd-13-6923-2013
- Saunders SM, Jenkin ME, Derwent D, Pilling MJ, 2003. Protocol for the development of the Master Chemical Mechanism, MCM v3 (Part A): tropospheric degradation of non-aromatic volatile organic compounds. *Atmospheric Chemistry and Physics* **3**, 161–180. doi:10.5194/acp-3-161-2003
- Schauer JJ, Kleeman MJ, Cass GR, Simoneit BRT, 1999. Measurement of emissions from air pollution sources. 2. C₁ through C₃₀ organic compounds from medium duty diesel trucks. *Environmental Science and Technology* **33**, 1578-1587. doi:10.1021/es980081n
- Schauer JJ, Kleeman MJ, Cass GR, Simoneit BRT, 2002. Measurement of emissions from air pollution sources. 5. C₁ through C₃₂ organic compounds from gasoline-powered motor vehicles. *Environmental Science and Technology* **36**, 1169-1180. doi:10.1021/es0108077
- Schnell RC, Oltmans SJ, Neely RR, Endres MS, Molenaar JV, White AB, 2009. Rapid photochemical production of ozone at high concentrations in a rural site during winter. *Nature Geoscience* **2**, 120-122. doi:10.1038/NGEO415
- Scott KI, Benjamin MT, 2003. Development of a biogenic volatile organic compounds emission inventory for the SCOS97–NARSTO domain, *Atmospheric Environment* **37** (S2), 39-49. doi:10.1016/S1352-2310(03)00381-9
- Shearer SM, Harley RA, Jin L, Brown NJ, 2011. Comparison of SAPRC99 and SAPRC07 mechanisms in photochemical modeling for central California. *Atmospheric Environment* **46**, 205-216. doi:10.1016/j.atmosenv.2011.09.079
- Shönbein CF, 1851. On some secondary physiological effects produced by atmospheric electricity. *Medico-Chirurgical Transactions* **34**, 205-220.
- Sillman S, 1999. The relationship between ozone, NO_x, and hydrocarbons in urban and polluted rural environments. *Atmospheric Environment* **33**, 1821-1845.
- Sillman S, Samson PJ, 1995. Impact of temperature on oxidant photochemistry in urban, polluted rural and remote environments, *Journal of Geophysical Research* **100** (D6), 11497-11508. doi:10.1029/94JD02146

- Sitch S, Cox PM, Collins WJ, Huntingford C, 2007. Indirect radiative forcing of climate change through effects on the land-carbon sink. *Nature* **448**, 791-794. doi: 10.1038/nature06059
- Snyder MA, Bell JL, Sloan LC, Duffy PB, Govindasamy B, 2002. Climate responses to a doubling of atmospheric carbon dioxide for a climatically vulnerable region. *Geophysical Research Letters* **29**, 1514. doi:10.1029/2001GL014431
- Stavrakou T, Peeters J, Müller J-F, 2010. Improved global modelling of HOx recycling in isoprene oxidation: evaluation against the GABRIEL and INTEX-A aircraft campaign measurements. *Atmospheric Chemistry and Physics* **10**, 9863-9878. doi:10.5194/acp-10-9863-2010
- Stein SE, Brown RL, 2005. "Structures and Properties Group Additivity Model" in NIST Chemistry WebBook, NIST Standard Reference Database Number 69, Eds. PJ Linstrom and WG Mallard, National Institute of Standards and Technology, Gaithersburg MD, 20899, <http://webbook.nist.gov/chemistry/grp-add/> (retrieved August, 2012).
- Steiner AL, Tonse S, Cohen RC, Goldstein AH, Harley RA, 2006. Influence of future climate and emissions on regional air quality in California. *Journal of Geophysical Research* **111** (D18303). doi:10.1029/2005JD006935
- Steiner AL, Cohen RC, Harley RA, Tonse S, Millet DB, Schade GW, Goldstein AG, 2008. VOC reactivity in central California: comparing an air quality model to ground-based measurements. *Atmospheric Chemistry and Physics* **8**, 351-368. doi:10.5194/acp-8-351-2008
- Steiner AL, Davis AJ, Sillman S, Owen RC, Michalak AM, Fiore AM, 2010. Observed suppression of ozone formation at extremely high temperatures due to chemical and biophysical feedbacks. *Proceedings of the National Academy of Sciences* **107** (46), 19685-19690. doi:10.1073/pnas.1008336107
- Stockwell WR, Kirchner F, Kuhn M, Seefeld S, 1997. A new mechanism for regional atmospheric chemistry modeling. *Journal of Geophysical Research* **102** (D22), 25847-25879. doi:10.1029/97JD00849
- Thurston GD, Ito K, 1999. Epidemiological studies of ozone exposure effects, p 485-510 in *Air Pollution and Health*, editors Holgate ST, Samet JM, Koren HS, Maynard RL, San Diego: Academic Press.
- Tonse SR, Brown NJ, 2007. Parallel efficiency analysis and performance improvement of CMAQ V4.5 on a Beowulf Linux cluster. Lawrence Berkeley National Laboratory. Report prepared for California Energy Commission. LBNL Report No. 62896.
- Tonse SR, Brown NJ, Harley RA, Jin L, 2008. A process-analysis based study of the ozone weekend effect. *Atmospheric Environment* **42**, 7728-7736. doi:10.1016/j.atmosenv.2008.05.061
- USDA NASS (United States Department of Agriculture and National Agricultural Statistics Service), 2009. Census of Agriculture - 2007. Available at <http://www.agcensus.usda.gov/Publications/2007/index.php>

- USEPA (United States Environmental Protection Agency), 2008. Regulatory determinations support document for selected contaminants from the second drinking water contaminant candidate list (CCL 2). Chapter 13: MTBE. EPA Report 815-R-08-012.
- USEPA (United States Environmental Protection Agency), 2012. National Ambient Air Quality Standards. Available at <http://www.epa.gov/air/criteria.html>
- USEPA (United States Environmental Protection Agency), 2013. State Implementation Plan Status and Information. Available at <http://www.epa.gov/air/urbanair/sipstatus/index.html>
- Van Dingenen R, Dentener FJ, Raes F, Krol MC, Emberson L, Cofala J, 2009. The global impact of ozone on agricultural crop yields under current and future air quality legislation. *Atmospheric Environment* **43**, 604-618. doi:10.1016/j.atmosenv.2008.10.033
- Velasco E, Lamb B, Westberg H, Allwine E, Sosa G, Arriaga-Colina JL, Jobson BT, Alexander ML, Prazeller P, Knighton WB, Rogers TM, Grutter M, Herndon SC, Kolb CE, Zavala M, de Foy B, Volkamer R, Molina LT, Molina MJ, 2007. Distribution, magnitudes, reactivities, ratios and diurnal patterns of volatile organic compounds in the Valley of Mexico during MCMA 2002 & 2003 field campaigns. *Atmospheric Chemistry and Physics* **7**, 329–353. <http://www.atmos-chem-phys.net/7/329/2007/>
- Vereecken L, Peeters J, 2009. Decomposition of substituted alkoxy radicals – part 1: a generalized structure-activity relationship for reaction barrier heights. *Physical Chemistry Chemical Physics* **11**, 9062-9074. doi:10.1039/b909712k
- Vingarzan R, 2004. A review of surface ozone background levels and trends. *Atmospheric Environment* **38**, 3431-3442. doi:10.1016/j.atmosenv.2004.03.030
- Volz A, Kley D, 1988. Evaluation of the Montsouris series of ozone measurements made in the nineteenth century. *Nature* **332**, 240-242. doi:10.1038/332240a0
- von Kuhlmann R, Lawrence MG, Poschl U, Crutzen PJ, 2004. Sensitivities in global scale modeling of isoprene, 2004. *Atmospheric Chemistry and Physics* **4**, 1–17. doi:10.5194/acp-4-1-2004
- Vukovich FM, 1995. Regional-scale boundary layer ozone variations in the eastern United States and their association with meteorological variations. *Atmospheric Environment* **17**, 2259-2273. doi:10.1016/1352-2310(95)00146-P
- Vukovich FM, Sherwell J, 2003. An examination of the relationship between certain meteorological parameters and surface ozone variations in the Baltimore-Washington corridor. *Atmospheric Environment* **37**, 971-981. doi:10.1016/S1352-2310(02)00994-9
- Wark K, Warner CF, Davis WT, 1998. *Air Pollution: Its Origin and Control*, 3rd Edition. Upper Saddle River: Prentice Hall.
- Warneke C, de Gouw JA, Holloway JS, Peishl J, Ryerson TB, Atlas E, Blake D, Trainer M, Parrish DD, 2012. Multiyear trends in volatile organic compounds in Los Angeles, California: Five decades of decreasing emissions. *Journal of Geophysical Research* **117**, D00V17. doi: 10.1029/2012JD017899

- Wayne WS, Wehrle PF, Carroll RE, 1967. Oxidant air pollution and athletic performance. *The Journal of the American Medical Association* **199** (12), 151-154.
- Weaver CP, Liang X-Z, Zhu J, Adams PJ, Amar P, Avise J, Caughey M, Chen J, Cohen RC, Cooter E, Dawson JP, Gilliam R, Gilliland A, Goldstein AH, Grambsch A, Grano D, Guenther A, Gustafson WI, Harley RA, He S, Hemming B, Hogrefe C, Huang H-C, Hunt SW, Jacob DJ, Kinney PL, Kunkel K, Lamarque J-F, Lamb B, Larkin NK, Leung LR, Liao KJ, Lin JT, Lynn BH, Manomaiphiboon K, Mass C, McKenzie D, Mickley LJ, O'Neill SM, Nolte C, Pandis SN, Racherla PN, Rosenzweig C, Russell AG, Salathe E, Steiner AL, Tagaris E, Tao Z, Tonse S, Wiedinmyer C, Williams A, Winner DA, Woo J-H, Wu S, Wuebbles DJ, 2009. A preliminary synthesis of modeled climate change impacts on US regional ozone concentrations. *Bulletin of the American Meteorological Society* **90**, 1843–1863. doi:10.1175/2009BAMS2568.1
- Welstand JS, Haskew HH, Gunst RF, Bevilacqua OM, 2003. Evaluation of the effects of air conditioning operation and associated environmental conditions on vehicle emissions and fuel economy, SAE Technical Paper Series 2003-01-2247, Society of Automotive Engineers: Warrendale, Pa.
- Wilkins ET, 1954. Air pollution aspects of the London fog of December 1952. *Journal of the Royal Meteorological Society* **80** (344), 267-271. doi:10.1002/qj.49708034420
- Williams EJ, Roberts JM, Baumann S, Bertman SB, Bertman S, Buhr S, Norton B, Fehsenfeld FC, 1997. Variations in NO_y composition at Idaho Hill, Colorado. *Journal of Geophysical Research* **102** (D5), 6297-6314. doi:10.1029/96JD03252
- Wittig VE, Ainsworth EA, Long SP, 2007. To what extent do current and projected increases in surface ozone affect photosynthesis and stomatal conductance of trees? A meta-analytic review of the last 3 decades of experiments. *Plant, Cell & Environment* **30** (9), 1150-1162. doi:10.1111/j.1365-3040.2007.01717.x
- Wittig VE, Ainsworth EA, Naidu SL, Karnosky DF, Long SP, 2009. Quantifying the impact of current and future tropospheric ozone on tree biomass, growth, physiology and biochemistry: a quantitative meta-analysis. *Global Change Biology* **15** (2), 396-424. doi:10.1111/j.1365-2486.2008.01774.x
- World Health Organization, 2000, Air quality guidelines for Europe. WHO Regional Publications, European Series, No 91. Copenhagen.
- Wu S, Mickley LJ, Leibensperger EM, Jacob DJ, Rind D, Streets DG, 2008. Effects of 2000-2050 global change on ozone air quality in the United States. *Journal of Geophysical Research* **113**, D06302. doi:10.1029/2007JD008917
- Yarwood G, Rao S, Yocke M, Whitten GZ, 2005. Updates to the Carbon Bond chemical mechanism: CB05. Final Report to the US EPA, RT-0400674. Available at http://www.camx.com/publ/pdfs/CB05_Final_Report_120805.pdf.
- Zellweger C, Ammann M, Buchmann B, Hofer P, Lugauer M, Ruttimann R, Streit N, Weingartner E, Baltensperger U, 2000. Summertime NO_y speciation at the Jungfraujoch,

3580 m above sea level, Switzerland. *Journal of Geophysical Research* **105** (D5), 6655–6667. doi:10.1029/1999JD901126

Zhang J, Dransfield T, Donahue NM, 2004. On the mechanism for nitrate formation via the peroxy radical + NO reaction. *Journal of Physical Chemistry A* **108**, 9082-9095. doi:10.1021/jp048096x

Zhang Y, Hu X-M, Leung LR, Gustafson Jr WI, 2008. Impacts of regional climate change on biogenic emissions and air quality. *Journal of Geophysical Research* **113**, D18310. doi:10.1029/2008JD009965

Appendix



Figure A-1. Map of central California counties

Modeling domain shown using solid red rectangle. Chapter 3 emissions respecified based on county-level data.

Table A-1. County level VOC emissions, tons organic gas (TOG) from year 2000 CARB emission estimates.

Tons per day (daily year 2000 average) from anthropogenic sources estimated by CARB (2009b). Data used to create Revised chemical mechanism and emissions in Chapter 3.

Basin & County	Off-Road		On Road		Total Diesel	Consumer Products	Animal Waste Decomposition	Architectural		Consumer		Thinning and Cleanup Solvents	Non-Methyl Bromide Pesticides	Methyl Bromide Pesticides
	Gas	Gas	Gas	Gas				Coatings - Oil Based	Coatings - Water Based	Aerosol Coatings	Aerosols/ Aerosol			
<u>San Francisco Bay Area</u>														
Alameda	12.2051	50.2184	7.2508	11.7071	10.0998	2.6655	1.8171	1.2976	0.7430	0.0578	0.0232			
Contra Costa	10.7963	34.2498	5.0210	7.6857	9.2152	1.7545	1.1961	0.8500	0.4890	0.1381	0.0128			
Marin	6.6128	9.9375	1.1136	2.0351	9.8814	0.4555	0.3105	0.2275	0.1269	0.0160	0.0071			
Napa	3.5588	7.3786	0.8867	1.0184	8.1543	0.2291	0.1561	0.1132	0.0639	0.0931	0.1110			
Solano	7.0179	14.5013	3.2167	3.2096	5.0574	0.7282	0.4964	0.3484	0.2030	0.3844	0.0301			
San Mateo	7.3167	26.1897	2.8009	5.8192	2.8882	1.3038	0.8889	0.6506	0.3634	0.0556	0.0116			
San Francisco	7.8671	20.3836	5.1332	6.3389	1.6284	1.4329	0.9767	0.7063	0.3993	0.0143	0.0038			
Santa Clara	13.5676	59.5670	6.5240	13.7593	8.8405	3.1052	2.1171	1.5326	0.8656	0.2070	0.0939			
<u>San Joaquin Valley</u>														
Fresno	9.8566	28.3415	9.1029	6.5844	136.9593	1.4727	1.0045	0.7031	0.4106	6.1316	0.9714			
Kern	6.1494	26.4730	14.3559	5.4727	52.8630	1.2184	0.8309	0.5771	0.3396	5.8562	0.9905			
Kings	0.8209	4.3372	2.1683	1.0740	47.8901	0.2386	0.1626	0.1072	0.0665	1.4249	0.0679			
Madera	3.4784	5.5835	1.9211	1.0551	31.8015	0.2282	0.1554	0.1064	0.0636	0.6794	0.0328			
Merced	2.0642	9.7036	4.4466	1.7060	105.6451	0.3873	0.2642	0.1834	0.1080	2.1746	0.8568			
San Joaquin	9.7889	21.9697	9.2803	4.6118	59.4131	1.0428	0.7112	0.4868	0.2909	1.4760	0.4560			
Stanislaus	4.2662	17.3412	4.3556	3.6863	151.9388	0.8274	0.5637	0.3873	0.2306	1.4270	0.3793			
Tulare	5.0665	15.5821	4.3566	3.0348	163.7691	0.6776	0.4622	0.3242	0.1889	2.0478	0.5733			
<u>Sacramento Valley</u>														
Colusa	0.7593	1.0766	0.9780	0.1611	9.3836	0.0347	0.0236	0.0167	0.0097	0.6552	0.0026			
Glenn	0.6261	1.5720	0.9240	0.2250	15.2766	0.0487	0.0335	0.0240	0.0136	0.6042	0.0637			
Yuba	2.7033	2.7288	0.5878	0.4918	8.0465	0.1104	0.0752	0.0562	0.0307	0.2968	0.0191			
Sutter	0.7656	3.6035	1.4624	0.6538	2.3232	0.1457	0.0996	0.0693	0.0408	1.0476	0.1809			
Yolo	2.3826	6.8457	1.9519	1.3955	4.1506	0.3022	0.2070	0.1450	0.0835	0.8854	0.0638			
Butte	3.9322	10.2200	1.9962	1.7032	4.7781	0.3734	0.2548	0.1812	0.1042	0.7536	0.0686			
Placer	8.0453	11.1168	2.1447	2.0580	6.4327	0.4382	0.3022	0.2052	0.1205	0.1794	0.0067			
Sonoma	6.7487	22.3468	2.7025	3.7395	31.5339	0.8460	0.5770	0.4115	0.2359	0.4002	0.1970			
Sacramento	12.3668	43.4974	5.7340	10.1354	19.3150	2.2192	1.5182	1.0429	0.6148	0.3723	0.0333			

Table A-2. VOC weight percent in gasoline, separated by SAPRC07 species

Original data from Harley and Kean (2004). Used to create new lumped VOC species in Chapter 3.

Group & Compound	Sacramento 2001 Liquid Gasoline	Sacramento 2001 Headspace Vapors	Caldecott 1999 1999 Tunnel Emissions	Caldecott 2001 2001 Tunnel Emissions
Alkanes				
ALK1				
Ethane	0	0	0.88	1.03
ALK2				
Propane	0.0183	0.64	0.19	0.17
2,2-dimethylpropane	0.0078	0.06	-	-
2-methyl-2-propanol	0.0046	0	-	-
ALK3				
MTBE	10.5669	15.97	3.74	3.79
2,2-dimethylbutane	0.9615	1.81	1.56	0.9
Butane	0.8893	8.9	1.68	1.43
Ethanol	0.8622	1.22	-	-
2-methylpropane	0.1737	2.43	0.22	0.29
2,2-dimethylpentane	0.1147	0.08	-	-
3,3-Dimethylpentane	0.1132	0.06	-	-
ALK4				
2-methylbutane	7.5069	29.82	10.72	8.55
2-methylpentane	3.5513	4.68	3.04	4.14
Pentane	2.8296	8.52	2.85	2.72
Methylcyclopentane	2.7609	2.4	2.54	2.4
3-methylpentane	2.1913	2.59	2.43	2.26
224-triMe-pentane	1.9274	0.65	3.54	2.75
Hexane	1.9026	1.82	1.45	1.32
Heptane	1.6101	0.51	0.98	0.8
2,3-dimethylbutane	1.1369	1.64	-	-
233-triMe-pentane	0.9690	0.18	-	-
234-triMe-pentane	0.9494	0.18	1.58	1.07
2,4-dimethylpentane	0.7323	0.48	-	-
Cyclopentane	0.5164	0.98	0.52	0.76
TAME	0.4164	0.16	-	-
225-trimethylhexane	0.3790	0.05	-	-
113-triMeCyPentane	0.1354	0.04	-	-
223-triMe-pentane	0.1140	0.03	-	-
113-t4-tetraMeCyPent	0.1097		-	-
244-trimethylhexane	0.0808	0.01	-	-
3,3-dimethylhexane	0.0554	0.01	-	-
2,2-dimethylhexane	0.0481	0.01	-	-
3,3-dimethylheptane	0.0381	0	-	-
223-Trimethylbutane	0.0362	0.02	-	-
4,4-dimethylheptane	0.0248	0	-	-
2,2-dimethylheptane	0.0181	0	-	-
112-triMeCyPentane	0.0058	0	-	-
1,1-diMecyclopentane	0.0023	0	0.67	0.98

Table A-2. (continued)

Group & Compound	Sacramento	Sacramento	Caldecott 1999	Caldecott 2001
	2001 Liquid Gasoline	2001 Headspace Vapors	1999 Tunnel Emissions	2001 Tunnel Emissions
ALK5				
3-methylhexane	1.8991	0.79	1.34	2.25
Methylcyclohexane	1.7756	0.56	0.67	0.98
2,3-dimethylpentane	1.7083	0.8	0.54	1.19
Cyclohexane	1.6121	1.02	0.52	0.98
2-methylhexane	1.4939	0.66	0.59	1.89
2-Methylheptane	0.8474	0.13	0.23	0.39
3-methylheptane	0.8389	0.12	0.5	0.36
1C3-diMecyclopentane	0.6786	0.31	-	-
Octane	0.6452	0.07	1.01	0.3
1T2-diMecyclopentane	0.6252	0.27	-	-
1T3-diMecyclopentane	0.5777	0.27	-	-
2,4-dimethylhexane	0.4218	0.09	-	-
2-Me-3-Et-pentane	0.4214	0.07	-	-
2,5-dimethylhexane	0.3805	0.08	0.31	0.65
4-Methylheptane	0.3798	0.06	-	-
Ethylcyclopentane	0.3601	0.1	-	-
3-methyloctane	0.3480	0	-	-
3,5-dimethylheptane	0.3080	0.03	-	-
Nonane	0.2801	0.01	0.17	0.25
2-methyloctane	0.2767	0	-	-
1C3-diMecyclohexane	0.2563	0.04	-	-
4-methyloctane	0.2333	0	-	-
4-methylnonane	0.2310	0	-	-
1T2C4-triMeCyPentane	0.2196	0.05	-	-
2,6-dimethylheptane	0.2164	0.02	-	-
Ethylcyclohexane	0.2144	0.02	-	-
1T3-diMecyclohexane	0.1849	0.02	-	-
1MeC3EtCyclopentane	0.1652	0.02	-	-
1MeC3Etcyclohexane	0.1519	0	-	-
1-M-t-3-Et Cycpentane	0.1454	0.02	-	-
1T2C3-triMeCyPentane	0.1444	0.03	-	-
3-ethylpentane	0.1326	0.05	-	-
1C3T5-triMeCyhexane	0.1258	0	-	-
Decane	0.1191	0	-	0.24
1Me-1EtCyclopentane	0.1186	0.02	-	-
2-methylnonane	0.1153	0	-	-
1T2-diMecyclohexane	0.1148	0.01	-	-
3-methylnonane	0.1096	0	-	-
2,3-dimethylheptane	0.1022	0.01	-	-
235-trimethylhexane	0.0961	0.01	-	-
3-ethylheptane	0.0919	0	-	-
3,4-dimethylheptane	0.0662	0.01	-	-

ALK5 cont. on next page

Table A-2. (continued)

Group & Compound	Sacramento	Sacramento	Caldecott 1999	Caldecott 2001
	2001 Liquid Gasoline	2001 Headspace Vapors	1999 Tunnel Emissions	2001 Tunnel Emissions
<i>ALK5 cont.</i>				
255-triMe-heptane	0.0657	0	-	-
1C2-diMecyclohexane	0.0607	0.01	-	-
223-triMethylheptane	0.0606	0	-	-
1Me-C2EtCyclopentane	0.0602	0.01	-	-
1C4-diMecyclohexane	0.0579	0.01	-	-
2,4-dimethylheptane	0.0568	0	-	-
Undecane	0.0541	0	0.05	0.22
225-triMe-heptane	0.0518	0	-	-
Propylcyclohexane	0.0484	0	-	-
2-Me-3-Et-heptane	0.0473	0	-	-
1-M-t2-PropCyHexane	0.0470	0	-	-
4-ethylheptane	0.0467	0	-	-
4-ethyloctane	0.0461	0	-	-
2,2-dimethyloctane	0.0454	0	-	-
113-triMecyclohexane	0.0439	0	-	-
236-triMe-heptane	0.0410	0	-	-
2,3-dimethyloctane	0.0370	0	-	-
244-triMe-heptane	0.0359	0	-	-
2,6-dimethylnonane	0.0336	0	-	-
223-trimethylhexane	0.0336	0	-	-
1MeT4Etcyclohexane	0.0328	0	-	-
1,1-diMecyclohexane	0.0325	0.01	-	-
3-methyldecane	0.0315	0	-	-
1C2T3-triMeCyhexane	0.0252	0	-	-
4,4-dimethyloctane	0.0219	0	-	-
Propylcyclopentane	0.0214	0	-	-
2,6-dimethyloctane	0.0210	0	-	-
245-triMe-heptane	0.0201	0	-	-
2-methyldecane	0.0200	0	-	-
224-triMe-heptane	0.0200	0	-	-
Dodecane	0.0179	0	0.03	0.06
246-triMe-heptane	0.0166	0	-	-
sec-Bu-Cyclohexane	0.0162	0	-	-
Cis-hydrindane	0.0149	0	-	-
1MeC4EtCyclohexane	0.0115	0	-	-
1C2T3-triMeCyPentane	0.0114	0	-	-
3-Me-4-Et-hexane	0.0070	0	-	-
2,6-diMe-hendecane	0.0063	0	-	-
2MePropylCyclohexane	0.0057	0	-	-
2,5-dimethylheptane	0.0044	0	-	-
2,6,10triM-hendecane	0.0044	0	-	-
iso-Bu-Cyclohexane	0.0040	0	-	-

ALK5 cont. on next page

Table A-2. (continued)

Group & Compound	Sacramento 2001 Liquid Gasoline	Sacramento 2001 Headspace Vapors	Caldecott 1999 1999 Tunnel Emissions	Caldecott 2001 2001 Tunnel Emissions
<u>ALK5 cont.</u>				
1C2C3-triMeCypentane	0.0034	0	-	-
1C2C4-triMeCyPentane	0.0034	0	-	-
2,6,10triMe-dodecane	0.0026	0	-	-
335-triMe-heptane	0.0002	0	-	-
2,3-Dimethylhexane	0	0	0.51	0.29
Other Alkanes	0.3272	-	1.97	2.42
Olefins				
ETHE (ethene)	0	0	6.89	5.85
<u>OLE1</u>				
1-pentene	0.1051	0.38	0.16	0.21
4-M-1-Heptene	0.0504		-	-
4-methyl-1-pentene	0.0405	0.04	0.02	0.1
1-hexene	0.0388	0.04	0.13	0.16
3-methyl-1-butene	0.0308	0.15	0.13	0.1
1-Heptene	0.0162	0.01	-	-
5-Me-1-hexene	0.0085	0	-	-
44-diMe-1-pentene	0.0083	0	-	-
1-butene	0.0077	0.09	1.53	1.58
Nonenes	0.0041	0	-	-
1-Octene	0.0033	0	-	-
3,3-dimethylbutene	0.0022	0	-	-
3-Me-1-hexene	0.0017	0	-	-
Propene	0.0008	0	4.3	3.84
33-DiMe-1-pentene	0.0005	0	-	-
<u>OLE2</u>				
2-methyl-2-butene	0.4083	1.11	0.01	0.34
trans-2-pentene	0.256	0.75	0.2	0.25
2-methyl-2-pentene	0.2275	0.22	-	-
2-methyl-1-butene	0.1745	0.61	0.02	0.22
Cis-2-pentene	0.1267	0.36	0.14	0.16
T-4Me-2-pentene	0.1267	0.17	-	-
C-2-m-3-heptene	0.1264	0	-	-
Trans-2-hexene	0.1183	0.12	-	-
1-Me-cyclopentene	0.0926	0.05	-	-
T-3Me-2-pentene	0.0876	0.08	-	-
2-Me-1-pentene	0.077	0.09	0	0.09
Cis-3-hexene	0.0668	0.07	-	-
C-3Me-2-pentene	0.058	0.06	-	-
Cyclopentene	0.0568	0.13	-	-
3-Et-2-pentene	0.0555	0.03	-	-
Cis-2-hexene	0.0506	0.05	-	-
2-Methyl-2-heptene	0.0428	0	-	-
<i>OLE2 cont. on next page</i>				

Table A-2. (continued)

Group & Compound	Sacramento	Sacramento	Caldecott 1999	Caldecott 2001
	2001 Liquid Gasoline	2001 Headspace Vapors	1999 Tunnel Emissions	2001 Tunnel Emissions
OLE2 cont.				
2,3dimethyl-2-butene	0.039	0.03	-	-
Indene	0.0334	0	-	-
Octadiene A	0.0316	0	-	-
3-Me-cyclopentene	0.0287	0.02	-	-
Trans-2-butene	0.0286	0.27	0.28	0.34
2-Me-2-hexene	0.0282	0.02	-	-
C-4Me-2-pentene	0.0267	0.04	-	-
Cis-2-butene	0.0244	0.21	0.31	0.38
2-Et-1-butene	0.0207	0.03	-	-
3-Me-c3-hexene	0.0205	0.01	-	-
Trans-2-heptene	0.0156	0.01	-	-
1-Me-cyclopentadiene	0.0148	0.02	-	-
C2-Octene	0.0141	0	-	-
2-Me-1-hexene	0.0128	0.01	-	-
2-Me-t3-hexene	0.0123	0.01	-	-
3-Me-t3-hexene	0.0123	0.01	-	-
2-Me-1,3-butadiene	0.0123	0.04	-	-
2-methylpropene	0.0118	0.14	-	-
T-1,3-pentadiene	0.0115	0.03	-	-
T3-Heptene	0.0087	0	-	-
23-diMe-1-pentene	0.007	0	-	-
Cyclopentadiene	0.0069	0.02	-	-
C-1,3-pentadiene	0.0047	0.01	-	-
24-dime-1-pentene	0.0036	0	-	-
44-diMe-c2-pentene	0.0029	0	-	-
T-2-T-4-hexadiene	0.0026	0	-	-
2,3dimethyl-1-butene	0.0016	0	-	-
c-6-M-2-Heptene	0.0016	0	-	-
1,4-pentadiene	0.0006	0	-	-
1,3-butadiene	0	0	0.71	0.48
Styrene	0	0	0.3	0.39
Other Alkenes	0.1262	0.04	0.95	3.32
Aromatics				
BENZ (benzene)	0.5388	0.35	4.07	3.38
ARO1				
Toluene	7.8443	1.6	9.93	9.36
Ethylbenzene	1.5225	0.11	1.42	1.15
Propylbenzene	0.5107	0	0.26	0.23
Cumene	0.1069	0	0.1	0.12
Butylbenzene	0.0877	0	0.62	0.3
Isobutylbenzene	0.0693	0	-	-
Sec-butylbenzene	0.0589	0	0.33	0.02
acetophenone	0	0	0.005	0.009

ARO1 cont. on next page

Table A-2. (continued)

Group & Compound	Sacramento	Sacramento	Caldecott 1999	Caldecott 2001
	2001 Liquid Gasoline	2001 Headspace Vapors	1999 Tunnel Emissions	2001 Tunnel Emissions
ARO2				
m-Xylene	5.0386	0.32	6.27	4.76
124-TriMe-benzene	2.7962	0	2.41	1.43
o-Xylene	2.3618	0.12	1.14	1.93
1-Me-3-Et-benzene	1.7024	0	0.76	1.9
p-Xylene	1.4461	0.1	-	-
135-triMe-benzene	0.8509	0	0.55	0.69
1-Me-4-Et-benzene	0.7503	0	0.45	0.24
1-Me-2-Et-benzene	0.5864	0	0.16	0.37
123-triMe-benzene	0.5626	0	0.63	0.62
1,2-diethylbenzene	0.3649	0	-	-
12-diMe4Et-benzene	0.3299	0	-	-
1-Me-3-Pr-benzene	0.3124	0	-	-
Indan	0.282	0	-	-
14-diMe2Et-benzene	0.2619	0	-	-
1235-tetMe-benzene	0.2274	0	-	-
13-diMe4Et-benzene	0.2111	0	-	-
1-Me-4-Pr-benzene	0.1925	0	-	-
1245-tetMe-benzene	0.1772	0	-	-
2-Methylindane	0.1472	0	-	-
Naphthalene	0.1279	0	-	-
1,3-diethylbenzene	0.126	0	-	-
1-Me-2-Pr-benzene	0.1042	0	-	-
1-Methylindane	0.0962	0	-	-
12-diMe3Et-benzene	0.0938	0	-	-
2-Methylnaphthalene	0.086	0	-	-
m-Cymene	0.0816	0	-	-
1234-tetMe-benzene	0.0704	0	-	-
C-11 Aromatic E	0.0553	0	-	-
1-Methylnaphthalene	0.0401	0	-	-
12-diMe-3Pr-benzene	0.0368	0	-	-
Tetralin	0.0326	0	-	-
1-Me-3Bu-benzene	0.0326	0	-	-
125-triMe-3Etbenzene	0.0308	0	-	-
12-diMe-4Pr-benzene	0.0304	0	-	-
1-Phenyl-2Me butane	0.0296	0	-	-
1-Me35diEt-benzene	0.0289	0	-	-
Dimethylindane B	0.0269	0	-	-
p-Cymene	0.0264	0	-	-
13-diMe2Et-benzene	0.0262	0	-	-
Dimethylindane F	0.025	0	-	-
123-triMe-5Etbenzene	0.0236	0	-	-
124-triMe-5Etbenzene	0.0213	0	-	-

ARO2 cont. on next page

Table A-2. (continued)

Group & Compound	Sacramento 2001 Liquid Gasoline	Sacramento 2001 Headspace Vapors	Caldecott 1999 1999 Tunnel Emissions	Caldecott 2001 2001 Tunnel Emissions
<u>ARO2 cont.</u>				
Dimethylindane G	0.0198	0	-	-
o-Cymene	0.0192	0	-	-
Dimethylindane E	0.0189	0	-	-
Dimethylindane C	0.0151	0	-	-
Pentamethylbenzene	0.0144	0	-	-
C-11 Aromatic K	0.0138	0	-	-
135-triMe-2Etbenzene	0.0134	0	-	-
13-DiMe-naphthalene	0.0129	0	-	-
C-11 Indane H	0.0116	0	-	-
Dimethylindane A	0.0112	0	-	-
123-triMe4Et-benzene	0.0096	0	-	-
16-DiMe-naphthalene	0.006	0	-	-
C-10 Alkenylbenzenes	0.0058	0	-	-
23-DiMe-naphthalene	0.0057	0	-	-
1-Phenyl-3Me butane	0.0044	0	-	-
1-Ethyl-naphthalene	0.0032	0	-	-
C-12 Aromatic F	0.0031	0	-	-
12-DiMe-naphthalene	0.0029	0	-	-
26-DiMe-naphthalene	0.0019	0	-	-
2-Ethyl-naphthalene	0.0017	0	-	-
124-triMe-3Etbenzene	0.0014	0	-	-
Other Aromatics	-	-	1.38	0.89
Carbonyls				
<u>RCHO</u>				
propanal	0	0	0.047	0.067
butanal	0	0	0.033	0.044
pentanal	0	0	0.02	0.027
isopentanal	0	0	0.019	0.033
hexanal	0	0	0.012	0.021
heptanal	0	0	0.006	0.013
<u>BALD</u>				
benzaldehyde	0	0	0.281	0.343
m-tolualdehyde	0	0	0.199	0.268
p-tolualdehyde	0	0	0.109	0.151
o-tolualdehyde	0	0	0.086	0.108
2,5-dimethylbenzaldehyde	0	0	0.07	0.104
2,4-dimethylbenzaldehyde	0	0	0.047	0.06
2,4,6-trimethylbenzaldehyde	0	0	0.024	0.025
<u>MEK</u>				
2-butanone (MEK)	0	0	0.032	0.049
2-pentanone	0	0	0.023	0.034

Table A-2. (continued)

Group & Compound	Sacramento 2001 Liquid Gasoline	Sacramento 2001 Headspace Vapors	Caldecott 1999 1999 Tunnel Emissions	Caldecott 2001 2001 Tunnel Emissions
<u>MACR</u>				
methacrolein	0	0	0.094	0.1
acrolein	0	0	0.059	0.129
<u>BACL</u>				
biacetyl	0	0	0.007	0.008
<u>PRD2</u>				
4-me-2-pentanone(MIBK)	0	0	0.028	0.026
<u>IPRD</u>				
crotonaldehyde	0	0	0.062	0.058
<u>HCHO</u> - formaldehyde	0	0	1.755	2.379
<u>CCHO</u> - acetaldehyde	0	0	0.468	0.512
<u>ACET</u> - acetone	0	0	0.23	0.37
<u>MGLY</u> - methyl glyoxal	0	0	0.043	0.05
<u>GLY</u> - glyoxal	0	0	0.005	0.009
Alkynes				
<u>ACYE</u> - Acetylene	0	0	3.16	2.74
Unclassified	1.3293	-	-	-

Table A-3. Redistribution of area emissions from SAPRC07 to SCCOS, motor vehicle redistribution has the same multipliers for each county

Data used to create emissions for Revised mechanism in Chapter 3.

Basin & County	County Average Multiplier for Area Emissions (%*species)					
	ETOH (from ALK3)	MTBE (from ALK3)	PACET (from ALK3)	AMIN (from ALK5)	UPOH (from ALK4)	UPOH (from ALK5)
<u>San Francisco Bay Area</u>						
Alameda	0.585	0.114	0.023	0.090	0.291	0.564
Contra Costa	0.554	0.137	0.029	0.111	0.248	0.500
Marin	0.473	0.190	0.070	0.256	0.189	0.282
Napa	0.492	0.167	0.095	0.346	0.224	0.237
Solano	0.512	0.170	0.030	0.120	0.189	0.412
San Mateo	0.559	0.135	0.013	0.051	0.245	0.552
San Francisco	0.557	0.137	0.007	0.028	0.239	0.570
Santa Clara	0.590	0.111	0.018	0.070	0.294	0.584
<u>San Joaquin Valley</u>						
Fresno	0.660	0.047	0.163	0.665	0.570	0.181
Kern	0.672	0.049	0.104	0.499	0.504	0.295
Kings	0.700	0.015	0.216	0.841	0.823	0.106
Madera	0.612	0.081	0.182	0.677	0.454	0.121
Merced	0.674	0.018	0.229	0.847	0.804	0.084
San Joaquin	0.595	0.092	0.138	0.522	0.393	0.224
Stanislaus	0.668	0.026	0.232	0.814	0.746	0.109
Tulare	0.663	0.029	0.234	0.831	0.727	0.087
<u>Sacramento Valley</u>						
Colusa	0.670	0.055	0.168	0.759	0.524	0.079
Glenn	0.676	0.034	0.204	0.825	0.674	0.073
Yuba	0.516	0.159	0.117	0.450	0.237	0.152
Sutter	0.682	0.055	0.041	0.257	0.387	0.428
Yolo	0.611	0.107	0.046	0.221	0.274	0.403
Butte	0.553	0.145	0.043	0.190	0.213	0.366
Placer	0.438	0.223	0.044	0.167	0.139	0.279
Sonoma	0.581	0.103	0.119	0.438	0.361	0.284
Sacramento	0.582	0.116	0.045	0.174	0.295	0.483
<u>Mountain Counties</u>						
Amador	0.5358	0.1310	0.17644	0.6043	0.3305	0.1068
Calaveras	0.3389	0.2881	0.08168	0.2866	0.1033	0.0841
El Dorado	0.4068	0.2460	0.02580	0.0963	0.1156	0.3009
Maiposa	0.4414	0.2023	0.15886	0.5387	0.2103	0.0368
Nevada	0.3913	0.2561	0.03595	0.1324	0.1110	0.2557
Plumas	0.3176	0.3045	0.07552	0.2650	0.0903	0.0720
Sierra	0.2351	0.3676	0.05549	0.1935	0.0504	0.0200
Tuolumne	0.3123	0.3108	0.05771	0.2049	0.0810	0.1061
<u>North Central Coast</u>						
Monterey	0.4997	0.0915	0.08029	0.3259	0.3153	0.2786
San Benito	0.6579	0.0315	0.22150	0.7841	0.7059	0.1210
Santa Cruz	0.4902	0.0886	0.01748	0.0696	0.2916	0.5004

Table A-3. (continued)

Basin & County	County Average Multiplier for Area Emissions (%*species)					
	ETOH (from ALK3)	MTBE (from ALK3)	PACET (from ALK3)	AMIN (from ALK5)	UPOH (from ALK4)	UPOH (from ALK5)
<u>South Central Coast</u>						
San Luis Obispo	0.5540	0.1172	0.11679	0.4424	0.3168	0.2354
Santa Barbara	0.5499	0.1043	0.05407	0.2263	0.2892	0.3895
<u>Great Basin Valleys</u>						
Alpine	0.3762	0.2536	0.13097	0.4460	0.1473	0.0229
Mono	0.4586	0.1946	0.12339	0.4301	0.2062	0.1364
<u>Lake County</u>						
Lake	0.2910	0.3320	0.02487	0.0913	0.0565	0.1435
<u>Counties on edge of model domain</u>						
Inyo	0.4256	0.2181	0.12625	0.4362	0.1799	0.0907
Lassen	0.5227	0.1361	0.18066	0.6165	0.3208	0.0833
Los Angeles	0.5625	0.1337	0.00153	0.0060	0.2303	0.6086
Mendocino	0.4775	0.1777	0.10064	0.3652	0.2123	0.2026
Tehama	0.6214	0.0550	0.21681	0.7487	0.5792	0.1085
Trinity	0.2857	0.3308	0.05156	0.1823	0.0678	0.0904
Ventura	0.4677	0.1331	0.00499	0.0199	0.1993	0.4797